

Abstract

CAO, SHUFEN. A Novel Hybrid Scheme for Large-Eddy Simulation of Turbulent Combustion Based on the One-Dimensional Turbulence Model. (Under the direction of Dr. Tarek Echekki).

A hybrid numerical scheme based on Large-Eddy Simulation (LES) and the One-Dimensional Turbulence (ODT) model for turbulent combustion is developed and validated. The ODT model resolves, both temporally and spatially, subgrid scale processes such as mixing, molecular transport, and chemistry. This model addresses the limitations of traditional models in representing strong local and transient phenomena such as ignition or extinction and processes strongly dependent on cross-correlations of different scalars.

The ODT model formulation and numerical implementation involves the treatment of different processes governing the transport and chemistry for scalars and momentum through a combination of stochastic and deterministic solutions, which are implemented in parallel on the ODT domains. These domains are embedded in the LES computational domain. The ODT-based and the LES solutions provide a coupled set of solutions for scalars and momentum with redundancy in the way these quantities can be computed. The key processes included in the proposed formulation are: molecular processes consisting of reaction and diffusion, turbulent stirring, and filtered convection. In the present study, turbulent stirring is represented by random, instantaneous rearrangements of the fields of transported variables along a one-dimensional line via ‘triplet maps’, which emulate the rotational folding effects of turbulent eddies. Molecular diffusion and chemistry are solved deterministically through finite-difference solutions of the unsteady reaction-diffusion transport equation along the 1D

domain. A novel method to incorporate 3D convection in ODT, denoted as ‘node convection’ combined with ‘intra-node relaxation’, is implemented. The Smagorinsky model is used as a subgrid stress closure model for LES. The coupling of LES and ODT is accomplished spatially by interpolating velocity information from LES to ODT and temporally at each LES time step.

The problem of non-homogeneous autoignition in isotropic turbulence is used to validate the proposed model. This problem offers a stringent test for the proposed model because it exhibits different modes of combustion (from ignition kernels to premixed and non-premixed flames) and a complex coupling between turbulent transport and molecular processes, diffusion and reaction, under highly transient conditions. The validation is carried out in comparison of the LES-ODT results with results from Direct Numerical Simulation (DNS). Both low and high turbulence conditions are considered, with three Lewis number cases carried out for the high turbulence condition. Both volume-averaged statistics and mixture fraction-conditioned statistics show that LES-ODT is able to accurately predict not only the flame ignition and extinction, kernel propagation, transition between different burning modes, but also the turbulence and Lewis number effects. LES-ODT simulation results are in excellent agreement with DNS results. This is achieved with a significantly reduced computational cost compared to DNS.

A Novel Hybrid Scheme for Large-Eddy Simulation of Turbulent Combustion Based on the One-Dimensional Turbulence Model

by

Shufen Cao

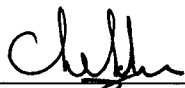
A dissertation submitted to the Graduate Faculty of
North Carolina State University
In partial fulfillment of the
Requirements for the degree of
Doctor of Philosophy

Aerospace Engineering

Raleigh, NC

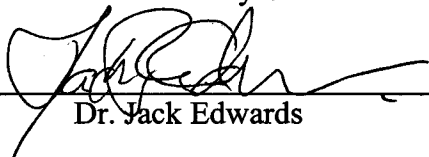
2006

Approved by:

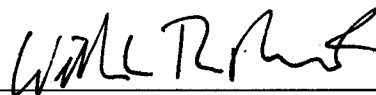


Dr. Tarek Echehki

Chair of the Advisory Committee



Dr. Jack Edwards



Dr. William Roberts



Dr. Alina Cherkock

Dedication

This Ph.D. thesis is dedicated to my father, Buzhong Cao, and to my mother, Guirong Liu.

Biography

Shufen Cao was born on September 12th, 1979 in Datong, China. She obtained her Bachelor of Science degree in Thermal Engineering from Chongqing University in July 2000. To further her study, she joined Tufts University in September 2001 and obtained a Master of Science degree in Mechanical Engineering in August 2003. Immediately after her graduation from Tufts University, she started her graduate work at North Carolina State University towards a Doctor of Philosophy degree in Aerospace Engineering.

Acknowledgments

First and foremost, I would like to thank Dr. Tarek Echehki for serving as my Ph.D. dissertation advisor. His brilliant technical insight, guidance, and constant support have made this work truly enjoyable. His patience and understanding are always with me, for this I am extremely grateful. I would also like to thank Dr. William Roberts for serving as a committee member and the instructor of two combustion classes I took. His knowledge has benefited me tremendously on the understanding of combustion. Great thanks extend to Dr. Jack Edwards and Dr. Alina Chertock for serving on my Ph.D. committee.

Furthermore, I would like to thank Professor Christopher Rutland and Dr. Scott Mason, who kindly provided their DNS code, which provided a starting point for my DNS and LES work. I would like to express my appreciation to our group members Bhargav Ranganath and Hemanth Kolera-Gokula for their great help and valuable suggestions on this research work.

Finally, I would like to thank all of my friends and family. Special thanks to Yuee Feng and Xinhui Lou, my roommates and best friends, for their continued support and for making my life at NC State so memorable. Yuee has accompanied me through the most difficult time of my life. Lots of amazing things that have happened to me in the past three years would have not happened if it was not for her. I would like to extend my special thanks to my wonderful husband for his love and support. In addition to providing me his intelligent suggestions to this work, he has made my life truly precious.

This work was supported by the U.S. Air Force Office of Scientific Research under a research grant F49620-03-1-0023, monitored by Dr. Julian Tishkoff.

Table of Contents

List of Tables	ix
List of Figures.....	x
Chapter 1 Introduction.....	1
1.1 Background.....	1
1.2 Motivation.....	3
1.3 LES of Turbulent Combustion.....	5
1.3.1 Flamelet Models	8
1.3.2 Conditional Moment Closure.....	11
1.3.3 Transported Filtered Density Function Approach	12
1.3.4 The Linear-Eddy Model.....	14
1.3.5 The One-Dimensional Turbulence Model	16
1.4 Objectives	18
1.5 Outline	19
Chapter 2 Autoignition in Non-Homogeneous Mixtures: DNS Formulation and Numerical Implementation	21
2.1 Objectives	21
2.2 Non-Homogeneous Autoignition in Isotropic Turbulence	22
2.3 Reaction Mechanism.....	24
2.4 The Governing Equations	28
2.5 Numerical Implementation	34
2.5.1 Spatial Discretization	35
2.5.2 Spatial Differentiation.....	36
2.5.3 Solution to the Governing Equations.....	37
2.5.4 Numerical Integration Procedure.....	38
2.6 Conclusions.....	39
Chapter 3 DNS of Autoignition in Non-Homogenous Mixtures: Conditional Statistical Results	40
3.1 Objectives	40
3.2 Initialization of the Flow Field	40
3.2.1 Initialization of the Vector Field.....	40
3.2.2 Initialization of the Scalar Field.....	43
3.3 Boundary Conditions	47
3.4 Simulation Parameters	47
3.5 Data Post-Processing Using Conditional Moment Closure Approach	50
3.6 Past Research on DNS of Autoignition	52
3.7 Simulation Results of the Present Study.....	53
3.7.1 Conditional Means of Scalars.....	54
3.7.2 Conditional Co-Variance	63
3.7.3 Conditional Variances.....	68
3.7.4 The Progress Variable as a Second Conditioning Variable.....	75

3.8 Conclusions.....	82
Chapter 4 LES-ODT Formulation and Numerical Implementation	85
4.1 Objectives	85
4.2 Model Strategy.....	86
4.3 The Governing Equations	87
4.3.1 LES Governing Equations	87
4.3.2 ODT Governing Equations	89
4.4 The Representation of Turbulent Transport in ODT	90
4.4.1 The Triplet Map	91
4.4.2 The Pressure-Scrambling Model	94
4.4.3 The Eddy Rate Distribution	99
4.4.4 Sampling the Distribution.....	101
4.5 The Molecular Diffusion and Reaction Processes in ODT.....	104
4.6 The Convection Process in ODT	105
4.7 Operations for LES-ODT Coupling.....	106
4.7.1 Interpolation.....	106
4.7.2 Filtering.....	109
4.8 Numerical Implementation of Large-Eddy Simulation	109
4.9 Numerical Implementation on ODT Elements	111
4.9.1 Implementation of the Turbulent Transport.....	114
4.9.2 Implementation of Molecular Diffusion and Reaction	116
4.9.3 Implementation of Convection	116
4.10 Numerical Coupling of LES and ODT	121
4.10.1 Solution Algorithm	121
4.10.2 Coupling Procedure	122
4.11 Conclusions.....	124
Chapter 5 LES-ODT Simulation Conditions: Autoignition in Non-Homogeneous Mixtures.....	127
5.1 Objectives	127
5.2 The Governing Equations for Autoignition	128
5.2.1 LES Equations	128
5.2.2 ODT Equations	129
5.3 Initialization of the LES-ODT Flow Field.....	130
5.4 Boundary Conditions	130
5.5 Simulation Conditions	131
5.6 Simulation Parameters	133
5.7 Data Post-Processing	135
5.7.1 Volume-Averaged Statistics	136
5.7.2 Conditional Statistics	136
5.8 Conclusions.....	137
Chapter 6 LES-ODT Model Validation: Autoignition in Non-Homogeneous Mixtures – Volume-Averaged Statistics	139

6.1 Objectives	139
6.2 Extent of Scalar Mixedness	139
6.3 Volume-Averaged Means	141
6.4 Volume-Averaged RMS	146
6.5 Conclusions.....	147
Chapter 7 LES-ODT Model Validation: Autoignition in Non-Homogeneous Mixtures – Conditional Statistics	149
7.1 Objectives	149
7.2 Case with the Low Turbulence Intensity	150
7.2.1 Conditional Means of the Temperature	150
7.2.2 Conditional Means of the Mass Fractions	152
7.2.3 Conditional Means of the Reaction Rate	154
7.2.4 Conditional RMS of the Temperature and the Mass Fractions	157
7.3 Case with the High Turbulence Intensity	161
7.3.1 Conditional Means of the Temperature	161
7.3.2 Conditional Means of the Fuel Mass Fraction.....	166
7.3.3 Conditional Means of the Oxidizer Mass Fraction.....	170
7.3.4 Conditional Means of the Reaction Rate	174
7.3.5 Conditional RMS of the Temperature	178
7.3.6 Conditional RMS of the Fuel Mass Fraction.....	182
7.3.7 Conditional RMS of the Oxidizer Mass Fraction	186
7.4 Conclusions.....	190
Chapter 8 Conclusions and Recommendations for Future Work.....	192
8.1 Introduction.....	192
8.2 Conclusions.....	192
8.2.1 DNS results.....	192
8.2.2 LES-ODT Model Formulation	194
8.2.3 LES-ODT Coupling.....	195
8.2.4 LES-ODT Model Validation Using Volume-Averaged Statistics.....	196
8.2.5 LES-ODT Model Validation Using Conditional Statistics	196
8.3 Recommendations for Future Work	197
8.3.1 LES SGS Closure	197
8.3.2 LES-ODT Coupling.....	198
8.3.3 Chemistry Representation.....	198
8.3.4 Application to Other Types of Flows	199
References.....	200
Appendices	206
Appendix A Fractional Method for Solution of DNS Momentum Equations.....	207
Appendix B Solution to DNS Energy and Species Equations.....	211

List of Tables

Table 3-1	Common parameters for DNS simulation of non-homogeneous autoignition in isotropic turbulence.....	49
Table 3-2	Specific parameters for DNS simulation of non-homogeneous autoignition in isotropic turbulence.....	50
Table 5-1	Common parameters for LES-ODT simulation of non-homogeneous autoignition in isotropic turbulence	134
Table 5-2	Specific parameters for LES-ODT simulation of non-homogeneous autoignition in isotropic turbulence	135

List of Figures

Figure 2-1	Three-dimensional computational domain	35
Figure 2-2	Two-dimensional computational grid in xy-plane.....	36
Figure 2-3	Flow chart of the numerical solution procedure	38
Figure 3-1	Initial mixture fraction field.....	44
Figure 3-2	DNS conditional means of the scalar dissipation rate for different cases.....	56
Figure 3-3	DNS conditional means of the temperature for different cases	57
Figure 3-4	DNS conditional means of the fuel mass fraction for different cases.....	58
Figure 3-5	DNS conditional means of the oxidizer mass fraction for different cases.....	59
Figure 3-6	DNS conditional means of the reaction rate for different cases	62
Figure 3-7	DNS conditional RMS of the scalar dissipation rate for different cases	64
Figure 3-8	DNS conditional RMS of the temperature for different cases.....	65
Figure 3-9	DNS conditional RMS of the fuel mass fraction for different cases	66
Figure 3-10	DNS conditional RMS of the oxidizer mass fraction for different cases	67
Figure 3-11	Conditional profiles of the variance of the temperature and the dissipation rate for pure mixing	69
Figure 3-12	The correlation coefficient between the temperature, T , and the scalar dissipation rate, χ , for the homogeneous burning case at different times	70
Figure 3-13	DNS conditional profiles of the variance of the temperature and the dissipation rate	72
Figure 3-14	DNS conditional profiles of the variance of the fuel mass fraction and the dissipation rate	73
Figure 3-15	DNS conditional profiles of the variance of the oxidizer mass fraction and the dissipation rate	74
Figure 3-16	Scatter plot of the fuel mass fraction at different times vs. the reaction progress variable, c , for a range of mixture fractions between 0.495 and 0.505	77
Figure 3-17	Scatter plot of the reaction rate at different times vs. the reaction progress variable, c , for a range of mixture fractions between 0.495 and 0.505.....	79
Figure 3-18	Scatter plot of the fuel mass fraction at different times vs. the reaction progress variable, c , for a range of mixture fractions between 0.595 and 0.605	80
Figure 3-19	Scatter plot of the reaction rate at different times vs. the reaction progress variable, c , for a range of mixture fractions between 0.595 and 0.605.....	81
Figure 4-1	Schematic layout of the ODT elements in x - y plane.....	87
Figure 4-2	The triplet mapping procedure.....	93
Figure 4-3	The discrete triplet map with $ke = 9$. Dashed line: original line segment; Dotted line: line after triplet mapping.....	94
Figure 4-4	Tri-linear interpolation.....	108
Figure 4-5	Implementation of ODT simulations in parallel processes.....	113
Figure 4-6	The turbulent stirring process	115

Figure 4-7	Schematic show of the node convection.....	121
Figure 4-8	Solution algorithm of LES and ODT	122
Figure 4-9	Coupling of LES and ODT	123
Figure 5-1	Turbulence energy spectrum plotted as a function of wave numbers.....	132
Figure 6-1	Comparison between LES-ODT and DNS for the extent of scalar mixedness as a function of time.....	140
Figure 6-2	Comparison between LES-ODT and DNS for volume-averaged means of the progress variable as a function of time	142
Figure 6-3	Comparison between LES-ODT and DNS for volume-averaged means of the reaction rate as a function of time.....	143
Figure 6-4	Comparison between LES-ODT and DNS for volume-averaged means of the temperature as a function of time.....	144
Figure 6-5	Comparison between LES-ODT and DNS for volume-averaged means of the fuel mass fraction as a function of time	144
Figure 6-6	Comparison between LES-ODT and DNS for volume-averaged means of the oxidizer mass fraction as a function of time	145
Figure 6-7	Comparison between LES-ODT and DNS for volume-averaged RMS of the temperature as a function of time.....	146
Figure 6-8	Comparison between LES-ODT and DNS for volume-averaged RMS of the fuel mass fraction as a function of time	146
Figure 6-9	Comparison between LES-ODT and DNS for volume-averaged RMS of the oxidizer mass fraction as a function of time	147
Figure 7-1	Comparison of conditional means of the temperature between LES-ODT and DNS at different times for the low turbulence case with $Le = 1$	151
Figure 7-2	Comparison of conditional means of the fuel mass fraction between LES-ODT and DNS at different times for the low turbulence case with $Le = 1$	153
Figure 7-3	Comparison of conditional means of the oxidizer mass fraction between LES-ODT and DNS at different times for the low turbulence case with $Le = 1$	154
Figure 7-4	Comparison of conditional means of the reaction rate between LES-ODT and DNS at different times for the low turbulence case with $Le = 1$	156
Figure 7-5	Comparison of conditional RMS of the temperature between LES-ODT and DNS at different times for the low turbulence case with $Le = 1$	158
Figure 7-6	Comparison of conditional RMS of the fuel mass fraction between LES-ODT and DNS at different times for the low turbulence case with $Le = 1$	159
Figure 7-7	Comparison of conditional RMS of the oxidizer mass fraction between LES-ODT and DNS at different times for the low turbulence case with $Le = 1$	160
Figure 7-8	Comparison of conditional means of the temperature between LES-ODT and DNS at different times for the high turbulence case with $Le = 0.5$	163
Figure 7-9	Comparison of conditional means of the temperature between LES-ODT and DNS at different times for the high turbulence case with $Le = 1.0$	164
Figure 7-10	Comparison of conditional means of the temperature between LES-ODT and DNS at different times for the high turbulence case with $Le = 2.0$	165

Figure 7-11	Comparison of conditional means of the fuel mass fraction between LES-ODT and DNS at different times for the high turbulence case with $Le = 0.5$	167
Figure 7-12	Comparison of conditional means of the fuel mass fraction between LES-ODT and DNS at different times for the high turbulence case with $Le = 1.0$	168
Figure 7-13	Comparison of conditional means of the fuel mass fraction between LES-ODT and DNS at different times for the high turbulence case with $Le = 2.0$	169
Figure 7-14	Comparison of conditional means of the oxidizer mass fraction between LES-ODT and DNS at different times for the high turbulence case with $Le = 0.5$	171
Figure 7-15	Comparison of conditional means of the oxidizer mass fraction between LES-ODT and DNS at different times for the high turbulence case with $Le = 1.0$	172
Figure 7-16	Comparison of conditional means of the oxidizer mass fraction between LES-ODT and DNS at different times for the high turbulence case with $Le = 2.0$	173
Figure 7-17	Comparison of conditional means of the reaction rate between LES-ODT and DNS at different times for the high turbulence case with $Le = 0.5$	175
Figure 7-18	Comparison of conditional means of the reaction rate between LES-ODT and DNS at different times for the high turbulence case with $Le = 1.0$	176
Figure 7-19	Comparison of conditional means of the reaction rate between LES-ODT and DNS at different times for the high turbulence case with $Le = 2.0$	177
Figure 7-20	Comparison of conditional RMS of the temperature between LES-ODT and DNS at different times for the high turbulence case with $Le = 0.5$	179
Figure 7-21	Comparison of conditional RMS of the temperature between LES-ODT and DNS at different times for the high turbulence case with $Le = 1.0$	180
Figure 7-22	Comparison of conditional RMS of the temperature between LES-ODT and DNS at different times for the high turbulence case with $Le = 2.0$	181
Figure 7-23	Comparison of conditional RMS of the fuel mass fraction between LES-ODT and DNS for the high turbulence case with $Le = 0.5$	183
Figure 7-24	Comparison of conditional RMS of the fuel mass fraction between LES-ODT and DNS for the high turbulence case with $Le = 1.0$	184
Figure 7-25	Comparison of conditional RMS of the fuel mass fraction between LES-ODT and DNS for the high turbulence case with $Le = 2.0$	185
Figure 7-26	Comparison of conditional RMS of the oxidizer mass fraction between LES-ODT and DNS for the high turbulence case with $Le = 0.5$	187
Figure 7-27	Comparison of conditional RMS of the oxidizer mass fraction between LES-ODT and DNS for the high turbulence case with $Le = 1.0$	188
Figure 7-28	Comparison of conditional RMS of the oxidizer mass fraction between LES-ODT and DNS for the high turbulence case with $Le = 2.0$	189

Chapter 1 Introduction

1.1 Background

Combustion and its control are of vital importance in the history of humanity. In prehistoric times, our ancestors discovered fire and used it to warm themselves, cook their food, and provide protections from predators. The discovery of fire was a start of human civilization. With rapid development of science and technology, combustion has become a separate field for study. It impacts our daily life with or without our notice. The heat for our home comes directly from combustion of coal, oil, or gas, or indirectly through electricity generated by burning fossil fuels. Moreover, many industrial processes rely heavily on combustion.

A combustion process involves mixing and burning of a mixture of a fuel and an oxidizer resulting in heat release. Based on the types of the fluid flow, a combustion process can be categorized as laminar and turbulent. While applications of laminar combustion are restricted to candles, lighters, and some domestic furnaces, turbulent combustion is encountered in most practical devices such as internal combustion engines or aircraft engines, industrial burners, and furnaces. Computational Fluid Dynamics (CFD) provides us useful ways to solve the governing equations for the turbulent combustion problems. The first definitive work of importance in CFD may be attributed to Richardson (1910), who introduced point iterative schemes for numerically solving Laplace's equation and the biharmonic equation in an address to the Royal Society of London (Tannehill *et al.*, 1997).

Nowadays, a variety of numerical methods have been developed and applied to a broad variety of fluid physics, including combustion. Computational approaches within the continuum limit of reacting flows can be divided into three categories based on the resolved scales in the flow.

The first category is the Direct Numerical Simulation (DNS) of the transport equations for scalars and momentum (Poinsot and Veynante, 2001) in which all (temporal and spatial) scales are resolved on the computational grid. DNS can provide complete information regarding the 3D turbulent flow field that is often difficult to obtain experimentally. Thus, DNS results can greatly enhance our understanding of turbulence flows and can be used to assist the development and improvement of turbulence models. However, in DNS, the number of grid points needed to capture the physics of the flow increases exponentially as the problem size increases and the computational work is disproportionately weighted to the small scales. A fine-grained resolution of the reacting flow field also requires very small time steps to accurately capture physics associated with chemistry and transport. Furthermore, as turbulence Reynolds number becomes high, the Kolmogorov length scale, which expresses the size of the smallest turbulent structures, becomes very small and the number of numerical grids to solve the problem increases dramatically. Due to the prohibitive numerical costs, DNS is limited to applications with relatively low Reynolds numbers and simple geometries.

The second approach is known as the ‘Reynolds Averaged Navier-Stokes’ (RANS) technique (Poinsot and Veynante, 2001). In this approach, the mean values of all quantities in

the flow field are obtained by solving the averaged governing equations for scalars and momentum. The mean values correspond to either time averages for statistically stationary mean flows or ensemble averages. The averaging process results in loss of unresolved details associated with the spatial and temporal resolution of the physics; these details are to be represented through closure terms in the governing equations. Compared to DNS, the numerical cost of RANS is reduced, but only lower moments of transported quantities are solved.

The third category is the Large-Eddy Simulation (LES) approach (Poinsot and Veynante, 2001). Motivated by the limitations of RANS and DNS approaches, Deardorff (1974) proposed the LES approach. In LES, the three-dimensional unsteady turbulent motions in larger scales are explicitly computed while the effects of the motions in smaller scales are modeled using subgrid closure models. Although LES is more expensive than RANS in the aspect of computational cost, it is more accurate and reliable for flows that exhibit significant unsteadiness in large scales. Compared with DNS, the computational cost of LES is much cheaper because the LES grid is coarser than the DNS grid. Therefore, LES can be applied to high-Reynolds-number flows in which DNS becomes inapplicable. Recently, LES has been implemented to study engineering flows involving combustion (see for example, Sankaran *et al.*, 2003).

1.2 Motivation

Simulating turbulent combustion processes is a challenging task because:

- Combustion by itself is a complex chemical process involving heat release and a large number of species.
- Turbulence by itself is a complex phenomenon and processes of transport occur along a wide range of length and time scales. This range increases with turbulent intensity as well as the complexity and the size of the flow geometry.
- In turbulent combustion, turbulence increases the volumetric combustion rate and modifies the chemistry process through the balance of chemistry and transport; therefore, flame structures are also modified by turbulence. On the other hand, the heat release from the combustion process has a large effect on the turbulent flows. It can either contribute to the dissipation of turbulence through increased viscosity or to the baroclinic generation of vorticity. The two-way interactions between chemistry and turbulence are very complicated and the descriptions of turbulent combustion remain open questions.

The prediction of turbulent reacting or mixing flows offers additional challenges. Processes of combustion in localized reaction-diffusion structures (i.e. flames) may extend the range of time and length scales required to resolve the physics. More importantly, these small scale processes may play an important role in defining the dynamics of the larger scales. The equations governing the transport of species or their phases, energy, and other potential scalars offer additional non-linearities due especially to reaction source terms.

Traditional theories emphasized the convenience of treating turbulent processes from a statistical perspective: a complex unsteady flow may be statistically steady and an averaged

approach to the governing equations may result in formulations of the flow that are similar to their laminar counterparts. More recent theories of turbulent flows have emphasized the role of large scales in determining the rate of transport of momentum and scalars and the universality of the role of smaller scales. From this emphasis, important strategies have been adopted to address the multi-scale nature of turbulent flows. Large-Eddy Simulation (LES) represents one promising strategy to address this nature.

1.3 LES of Turbulent Combustion

In this section, we discuss some important strategies adopted to address the closure for chemistry and transport in turbulent combustion. The bulk of the discussion is based on LES models for non-premixed combustion to illustrate the limitations of existing models and motivate our proposed strategy. Similar challenges exist for premixed combustion as well, and at least two models, the Filtered Density Function (FDF) approach and the Linear-Eddy Model (LEM) can be used to model turbulent premixed flames. Much progress in LES of turbulent combustion has been made over the past decade or so. LES has been broadly applied in various combustion problems such as the predictions of pollutants (Eggenpieler and Menon, 2004) and engine combustion (Haworth and Jansen, 2000; Moin, 2002).

In LES, the governing equations are generated through a low-pass spatial filtering process. Below the filter scales, the unresolved contributions are modeled and closure terms have to be represented. These terms concern primarily non-linear contributions in the original unfiltered equations. The same constraints are present for averaging operations of these

equations as applied in RANS. Thus, the similar closure problem encountered in RANS is also present in LES. Among the non-linear contributions to the transport equations of scalars and momentum, two closure issues are most prominent. The first is related to Subgrid scale (SGS) transport of momentum, the so-called SGS stress, or scalars (SGS fluxes). The traditional approach to LES closure of SGS scalars or fluxes is based on gradient diffusion type approximations such as the Smagorinsky model (Smagorinsky, 1963) and the dynamic model (Germano, 1991). Those gradient diffusion types of models rely on deriving the closure information for unresolved physics using resolved scales. These models have serious limitations for turbulent mixing and combustion. One limitation is that the non-unity Lewis, Prandtl, and Schmidt number effects may not be adequately modeled with gradient diffusion. Moreover, counter-gradient diffusion has been observed in computational and experimental studies (Poinsot *et al.* 1996; Veynante *et al.*, 1997; Caldeira-Pires and Heitor, 2001) when heat release is present.

Another important challenge in the LES of turbulent combustion is the modeling of source terms of chemistry or radiation. These terms are generally non-linear and display a myriad of time scales associated with different rates of a complex mechanism, which can involve thousands of reactions and hundreds of species for practical fuels. Even more critical in the modeling of these source terms is their tight coupling with molecular transport mechanisms, such as diffusion. From this coupling, thin structures such as flames that characterize the combustion process can impose even stringer requirements on the spatial resolution to resolve these structures. This coupling is also modulated by the temporally

evolving flow field. Large scale mixing increases the number of interfaces separating reactants and products (in premixed flames) or the fuel and the oxidizer (in non-premixed flames) and affects scalar gradients in the flow field, thus directly affects the rates of molecular transport processes and their coupling with chemistry.

While large scale mixing is expected to be coupled with small scale mixing and chemistry for a wide range of practical combustion problems, reasonable assumptions can be made to attempt to decouple, at least partially, these processes. The validity of the assumption will depend on the conditions in a particular regime in which combustion occurs. The Eddy-Dissipation Concept (EDC) or the Eddy Break-Up (EBU) model is among the earlier approaches based on the comparison of rates of mixing versus rates of chemistry. Recently, more sophisticated approaches have been demonstrated with reasonable success using the Reynolds-Averaged Navier-Stokes (RANS) approach and have been extended to LES. Among these are the Flamelet model, the Conditional Moment Closure (CMC) model, and the transported Filtered Density Function (FDF) model. A principal assumption for flamelet and CMC approaches is that reactive scalars can be represented through ‘transport’ equations in phase space or sample space in terms of quantities that can be transported in physical space. A typical quantity used in both flamelets and CMC is the mixture fraction. The transport of a passive scalar in physical space reduces the number of scalar transport equations and eliminates requirements for the description of source terms in the transport equations. But, such parameterization also involves assumptions about the combustion mode

(e.g. non-premixed) or the combustion regime (e.g. flamelet or distributed reaction), which can not be met uniformly in space or time.

Structure-based approaches in physical space, such as the Linear-Eddy Model (LEM) and the One-Dimensional Turbulence (ODT) model, are design to overcome inherent assumptions about the combustion mode or regime. More importantly, they address the coupling between turbulent transport, chemistry and molecular transport with reasonable fidelity. In LEM and ODT, the coupling of mixing and chemistry is predicted at all scales by resolving the turbulent advection, molecular transport, and chemistry in one-dimension in physical space. A brief review of those models is included below.

1.3.1 Flamelet Models

The basic idea of flamelet modeling is to assume that chemical timescales are short enough so that reactions occur in a thin layer around stoichiometric mixture on a scale smaller than the small scales of turbulence (Pitsch, 2006). With this assumption, a small instantaneous flame element embedded in a turbulent flow has the structure of a laminar flame. The advantage of flamelet modeling is that it takes into account for the finite-rate chemistry effect. There are basically two strategies in flamelet modeling depending on the parameter used in the flamelet library.

The first strategy is to use the scalar dissipation rate for parameterization. The steady flamelet modeling approach, in which the flame structure is assumed to be in steady state, has been applied to simulations of experimental configurations by Kempf *et al.* (2003) and

Raman and Pitsch (2005a). However, the steady flamelet model is inaccurate when chemistry is slow. Thus, transient flamelet models have been proposed and applied in LES of turbulent combustion. Pitsch and Steiner (2000) have used the Lagrangian flamelet model (LFM) in LES for a piloted methane/air diffusion flame, in which the unsteady flamelet equations are solved and coupled with LES solutions to provide the filtered scalar quantities using a presumed filtered probability density function of the mixture fraction. Another version of the transient flamelet approach proposed by Pitsch (2002) is the Eulerian flamelet model, in which the flamelet equations are solved in the Eulerian form and the resolved fluctuations of the scalar dissipation rate are considered. The disadvantage of transient flamelet modeling is that the scalar dissipation rate has to be properly determined.

Although the flamelet approach using the scalar dissipation rate as a parameter in the flamelet library has advantages in dealing with the finite-rate chemistry effect, it has an inherent weakness in predicting flame extinction and reignition due to the fact that solutions to the transport equations are not unique for one scalar dissipation rate value. Therefore, researchers (Pierce and Moin, 2004) suggested a second parameter for the flamelet model based on the progress variable.

In the second category of flamelet models, the reaction progress variable is used to replace the scalar dissipation rate for parameterization, which offers the advantage to better describe local extinction and reignition. The transport equation is solved for the filtered progress variable and the filtered chemical source term is closed with the flamelet library and the presumed joint filtered probability density function of the mixture fraction and the

reaction progress variable. Pierce and Moin (2004) applied this model to a non-premixed dump combustor using a delta-function for the presumed filtered probability density function. The results show that the progress variable approach is able to capture the unsteady, lifted flame dynamics observed in the experiments and the model significantly outperforms the steady laminar flamelet model. However, Ihme *et al.* (2005) found that the steady-state assumption of the flamelet solutions, especially during reignition at the low scalar dissipation rate, is inaccurate. An extension of the model to an unsteady flamelet library formulation has been addressed by Pitsch and Ihme (2005) as a new development of the model.

While using the progress variable to parameterize the flamelet library offers an improved description of the flame extinction and reignition, it imposes another challenge because the joint filtered probability density function (FPDF) of the mixture fraction and the reaction progress variable needs to be provided. The delta and beta functions for the FPDF have been investigated and further improvement needs to be addressed.

As we attempt to predict more complex combustion phenomena, refinements in flamelet approaches involve the addition of additional variables to parameterize reactive scalars' response to transport. With additional variables, more closure models are needed, with potentially increased uncertainty about model accuracy or physical predictions. The problem is further complicated by the fact that when more than a single stream of fluid are present.

1.3.2 Conditional Moment Closure

The conditional Moment Closure (CMC) approach was independently developed by Klimenko (1990) and Bilger (1993) in a RANS context. The basic idea is to derive, close, and solve exact balance equations for the mixture fraction-conditioned means of reactive scalars. Kim and Pitsch (2005) developed CMC model for LES because the mixture fraction-conditioned balance equations are difficult to solve in LES. Navarro-Martinez *et al.* (2005) successfully applied the LES-CMC approach to a non-premixed, piloted, turbulent jet diffusion flame. The results show good predictions of the variance of major and intermediate species and improved predictions of the conditional mass fractions over RANS-CMC simulation (Roomina and Bilger, 2001).

However, there are a number of limitations for the CMC approach. First, CMC provides an approximate closure of chemical source terms because the mean chemical source terms are assumed to be dependent on the conditional mean values only (Chen, 2004). Second, because CMC solves for conditional average equations that have many similar features to the transient flamelet model, it shares similar challenges facing the transient flamelet modeling approach, such as the determination of the scalar dissipation rate and limitations in the prediction of strong finite-rate chemistry effects such as flame extinction and reignition (Chen, 2004). Refinements to these models to predict these effects involve either adding transport equations for higher moments of the scalars or using additional conditioning variables. These refinements, as in the case of the flamelet approach, require additional closure models and add substantial computational cost.

1.3.3 Transported Filtered Density Function Approach

The transported Filtered Density Function (FDF) method was originally introduced by Pope (1990). This method has been demonstrated capable of modeling turbulent combustion with strong finite-rate chemistry effects, such as local extinction and reignition (Chen, 2004). However, because the transport equation is based on one-point one-time information, the molecular mixing, depending on multipoint information, has to be modeled. This is a severe restriction for the model to be applied to turbulent combustion, in which the turbulent mixing can be as important as the details of chemistry (Pitsch, 2006). Moreover, the joint scalar FDF transport equation can not be solved by finite volume or finite difference method and is usually represented by the equivalent system of notional particles. Because the accuracy of the model scales with the square root of the number of notional particles, a large number of particles is required per cell (Pitsch, 2006). Thus, computational cost becomes a major challenge in applying FDF in LES. Muradoglu *et al.* (1999) proposed a hybrid scheme, in which energy equation is solved using the transport equation but the chemical source term is obtained through the joint PDF. Zhang and Haworth (2004) have provided an appropriate algorithm for unsteady RANS; but for LES, it needs more work (Pitsch, 2006).

Despite its potential computational cost, there are inherently a number of advantages of the FDF approach compared to the flamelet and CMC approaches. The FDF methodology does not implicitly assume a given mode of combustion or a parameterization in the sample space of reactive scalars. Therefore, the principal challenge to FDF approaches is related to the mixing models.

Summary

The above three types of models provide improved predictions of the finite-rate chemistry effects in turbulent combustion compared to the traditional EDC and EBU models. However, with the exception of the FDF approach, these models offer limited predictions in the study of a class of problems including strong local or transient phenomena such as ignition or extinction events, processes that are strongly dependent on cross-correlations of different scalars such as soot radiation, and problems involving transition of burning modes during simulations. In FDF methods, predictions of important finite-rate chemistry effects in combustion, such as extinction and re-ignition, largely depend on the mixing model used.

Furthermore, representing the physics of turbulent mixing and chemical reaction is directly related to model accuracy in the turbulent combustion process. Because scalar mixing process involves interactions of turbulent advection and micro-processes such as viscous dissipation at scales smaller than Kolmogorov scales, a model that can distinguish those processes at the smallest scales of the flow is essential. Although direct numerical simulation can provide us detailed information in both space and time, it becomes computationally unaffordable as the problem size increases. Therefore, it is necessary to develop new modeling approaches that are spatially and temporally resolved. To reduce the computational requirement of the spatial and temporal resolution, the new modeling approaches are low-dimensional.

1.3.4 The Linear-Eddy Model

The Linear-Eddy Model (LEM), which was originally proposed by Kerstein (1988), addresses the difficulty in adequately predicting turbulent mixing-reaction coupling at all scales by spatially and temporally resolving the turbulent advection, molecular transport, and chemistry in one-dimension in physical space. A key advantage of LEM over other traditional models is that turbulent stirring and molecular diffusion, two primary physical mechanisms that govern the scalar mixing process, are treated distinctively. The molecular diffusion and chemical reaction are implemented by the numerical time integration of the reaction-diffusion equation along the 1D domain. The turbulent advection is treated stochastically by random, instantaneous rearrangements of the scalar field, which is accomplished using triplet mapping. The triplet mapping emulates the strain and rotational folding effects of turbulent eddies.

In the LEM proposed by Kerstein (1988), a block inversion model is used to represent turbulent convection and Fickian diffusion is used to represent molecular processes. One limitation of this model is the discontinuity of fluid motions inherent in the stochastic process representing convection. Kerstein (1989, 1990) applied this model to turbulent shear layers and consequently generalized it to axi-symmetric flows. Kerstein (1991, 1992a, and 1992b) used the LEM to study the microstructure of diffusive scalar mixing fields, the structure of turbulent jet diffusion flames, and finite-rate chemistry and multi-stream mixing. In those applications, the turbulent convection is represented by the triplet mapping method, which is more advanced than the block inversion method because it is measure preserving and

continuous. McMurtry *et al.* (1993) used LEM to predict the evolution of a decaying scalar field in homogeneous turbulent flows over a wide range of Reynolds and Schmidt numbers. The results show overall good agreement with direct numerical simulation results. Goldin and Menon (1996) applied LEM to steady-state turbulent combustion. The model constructs the single point joint scalar probability density function (PDF) from LEM simulations and has been applied to a turbulent jet diffusion flame. All of the above applications use the LEM as a stand alone model.

LEM as a sub-grid closure is first applied by McMurtry *et al.* (1992) to hydrogen-air combustion. Later, Menon *et al.* (1993) studied LES-LEM for both turbulent premixed and non-premixed combustion flows. The splicing method is employed to transport the subgrid scalar information across LES cell boundaries. Zimberg *et al.* (1998) studied coupled turbulent mixing, soot chemistry, and radiation effects using coupled LES-LEM and results demonstrate that LEM can capture the interaction between turbulent mixing and radiative cooling in high soot regions. Sone *et al.* (2001) used LES to simulate fuel-air mixing in the internal combustion engine, in which LEM is used as the subgrid closure to LES. Good agreement is demonstrated with DNS/LES and experimental studies.

LEM also have some limitations. In LEM, the frequency and the eddy size distribution of the stirring events are prescribed by a predefined energy spectrum and flow properties are specified empirically by assigning parameters that govern the random event sequence. Therefore, there is no provision for feedback of local flow properties to the random process governing subsequent events. Furthermore, LEM is a mixing model and the

turbulence information of the velocity field is not represented at small scales. For flows whose turbulence properties known empirically, this approach has been proven useful; however, for general flows, we need a more advanced model.

1.3.5 The One-Dimensional Turbulence Model

A more recent and robust refinement of the LEM approach is the One-Dimensional Turbulence (ODT) model, which was also developed by Kerstein (1999a). ODT is a method for simulating, with full spatial and temporal resolution, the turbulent transport and dynamic fluctuations in velocity and fluid properties that one might measure along a one-dimensional (1D) line of sight through an actual 3D turbulent flow (Schmidt *et al.*, 2003).

ODT is an outgrowth of LEM and both of them treat the turbulent advection and molecular diffusion similarly. However, distinct from LEM, a mixing model, ODT is a self-contained turbulence model in that it not only solves for scalars but also velocity vectors at subgrid scales, which provide information about the shear field, thereby a mechanism for driving the turbulence. Therefore, ODT is a more advanced model compared to LEM in that it is a methodology for fully resolved simulations of pure mixing, chemical reaction, and related scalar processes in turbulence. Another advantage of ODT over LEM is that the distribution function in ODT is not predetermined, rather it advances in time and is computed based on the turbulent kinetic energy. Furthermore, ODT has an advantage of allowing affordable simulation of high Reynolds number turbulent flows over a full range of dynamically relevant length scales. Thus, ODT is a more robust and advanced model than

LEM and it provides a sound representation of turbulent advection, molecular diffusion, and chemical reaction. ODT can be either a stand-alone model or a subgrid closure model for LES. In our research work, we will focus on the performance of ODT as a subgrid model for LES.

Considerable progress has been achieved in the development of ODT model since it was proposed. Kerstein (1999a) has implemented ODT to compute statistical properties of velocity and scalar fields in shear and buoyant stratified flows. This study illustrated the extension of the application of ODT capability for inertia-driven as well as buoyancy-driven flows. For buoyancy-driven flows with no applied shear, important features of double-diffusion convection (Kerstein 1999b) and associated properties are reproduced with ODT. The computed fluxes across heat-salt and salt-sugar interfaces reproduced the experimental observation of a variable regime in a single flow realization, which has not previously been achieved computationally or experimentally. Accordingly, it is verified that ODT can be used to decouple multi-component diffusion effects, applied shear, property variation, and related flow and fluid properties that happen in many technological and naturally turbulent combustion processes. Kerstein (2001) developed the vector formulation of ODT and applied it to free shear flows. The formulation is able to capture the free shear flow structure, energetics, and fluctuation properties. Schmidt *et al.* (2003) developed a near-wall LES closure model based on a modified form of ODT. In this formulation, finely resolved ODT lines are embedded within each wall-adjacent LES cell.

The simulation by Echehki *et al.* (2001) of turbulent hydrogen-air flames is the first implementation of ODT for reacting flows. The results obtained using ODT show reasonable agreement with experimental statistics of thermo-chemical scalars. Moreover, ODT predictions and measurements of differential-diffusion effects show that those effects are important in the near-field and decrease as moving to downstream.

Summary

LEM and ODT for LES of turbulent combustion resolve both temporally and spatially subgrid scale processes such as mixing, molecular transport, and chemistry. They address the limitations of the first class of modeling approaches, thus offer better predictions of turbulent combustion. Most importantly, ODT is a more robust than LEM because it resolves not only the scalar but also the vector field as well. Furthermore, ODT offers better predictions of turbulence because the distribution of turbulent eddies is not prescribed, but computed instantaneously based on the kinetic energy of the flow field.

1.4 Objectives

The goal of this thesis is to develop an innovative hybrid scheme, Large-Eddy Simulation and One-Dimensional Turbulence (LES-ODT) model, and to validate the scheme by performing simulations of non-homogeneous autoignition in isotropic turbulence and comparing the results with the direct numerical simulation results. We have chosen non-homogeneous autoignition in isotropic turbulence for simulation because it is a complex

process involving interactions of chemical reactions, molecular diffusion, and turbulent transport. Moreover, it is a transient process. Both LES-ODT and direct numerical simulations are carried out on a three-dimensional computation domain with equal length in each direction. Periodic boundary conditions are imposed in all three directions. A random mixture fraction field is initialized using the von Karman-Pao Spectrum (Hinze, 1975). The reaction mechanism is simplified to single step, second order, and irreversible. We implement the concept of Conditional Moment Closure (CMC) and present the statistics of the numerical simulations in terms of the averages and variances to study the burning modes and the flame propagation phenomenon. We also explore conditioning using a second variable, a progress variable for the direct numerical simulations.

1.5 Outline

The remainder of this dissertation is organized as follows. Chapter 2 presents the DNS approach of studying the autoignition. Chapter 3 discusses the statistical description of the flow field and the DNS results. This discussion serves to motivate the complexity of the problem of autoignition in non-homogeneous mixtures and to highlight the potential challenge to its study using LES. The LES-ODT model formulation and numerical implementation of the model are the main emphasis of Chapter 4. Moreover, the coupling of LES with ODT is addressed in Chapter 4. Chapter 5 addresses the simulation conditions and parameters for LES-ODT simulation of non-homogeneous autoignition in isotropic turbulence. Chapter 6 presents the volume-averaged statistical results from LES-ODT

simulations and the results are compared that from DNS. Chapter 7 presents the mixture fraction-conditioned statistical results from LES-ODT simulations and the results are also compared with that from DNS. Chapter 8 is the last chapter, in which conclusions and recommendations for future work are addressed.

Chapter 2 Autoignition in Non-Homogeneous Mixtures: DNS

Formulation and Numerical Implementation

2.1 Objectives

We have discussed in Chapter 1 some principal challenges encountered in modeling turbulent combustion. The different remedies proposed within the context of the flamelet and the CMC approaches addressed key assumptions of the modeling process by reducing the solution of thermo-chemical scalars in the phase space. These assumptions are specific to the mode of combustion (e.g. premixed vs. non-premixed), the dominant chemistry (e.g. strained flamelets vs. ignition), or the combustion regime (flamelet vs. distributed reaction). While these assumptions can be made for a large class of problems, they clearly have their limitations in general. Another challenge is the prescription of the mixing mechanism, which is also a constraint for FDF models. In flamelet and CMC models, the mixing process is modeled through a presumed PDF shape to account for fluctuations of pertinent scalars. However, in many conditions, the actual PDF shape is not known *a priori*.

The principal limitations of existing modeling approaches are illustrated here using a canonical problem of importance in practical combustion: the problem of autoignition in non-homogeneous mixtures. The same problem will be used to validate our proposed LES-ODT model; and therefore, it will illustrate the proposed model versatility to address evolving chemistry, combustion modes, and even combustion regimes. The discussion will emphasize

the salient features of statistics exhibited by the simple canonical problem, such as autoignition in non-homogeneous mixtures.

In this chapter, the non-homogeneous autoignition in isotropic turbulence is studied using direct numerical simulation (DNS). The present DNS is based on the numerical solution of non-dimensional transport equations for total mass, momentum, energy, and reactants' mass fractions. The principal assumptions include ideal gas behavior, constant transport coefficients, and negligible radiation, Soret, and Dufour effect. The following discussion is organized as follows. First, the reaction mechanism is discussed. Second, the governing equations of turbulent combustion are presented. Third, the numerical implementation and solution procedures for the governing equations are examined.

2.2 Non-Homogeneous Autoignition in Isotropic Turbulence

Autoignition in non-homogeneous mixtures is a complex process, because it involves interactions of chemical reactions, molecular diffusion, and turbulent transport. For example, in a non-homogeneous mixture, the rate of chemistry competes with the rates of turbulent mixing and diffusion. Since autoignition occurs in discrete kernels where conditions for the onset of chemistry are favorable (e.g. low dissipation rate, right temperature and mixture composition), the details of this competition eventually determines the volumetric rates of heat release or even the fate of the reacting mixture. Another important characteristic of autoignition is that, it is a transient process. During this process, the dominant chemical reactions, the mode of chemistry or the combustion regime can evolve in time.

Autoignition in turbulent flows is important in many practical applications such as diesel and aircraft jet engines. In these applications, autoignition competes with the mixing process for fuel, oxidizer or burnt products. The competition between mixing and chemistry results in different regimes for autoignition and the subsequent combustion process. When mixing is very rapid, autoignition occurs in a relatively homogeneous mixture; although non-homogeneities in the temperature field can result from the presence of physical boundaries such as walls. When mixing is very slow, autoignition is initiated at the interface between the fuel and the oxidizer streams, and may occur primarily in a non-premixed combustion mode. This ‘diffusive burning’ regime has long been the standard model for Diesel engine combustion.

Recent observations in Diesel engines (Dec, 1997) show that autoignition occurs primarily in a stratified mixture, and evolves through propagation and mixing to the remaining regions of the non-homogeneous mixture. Therefore, the autoignition process generally will involve both mixing and propagation of ignition fronts. Echehki and Chen (2002) carried out simulations in a stratified mixture. In this study, the mixture contains a random field of fuel and oxidizer regions (or ‘blobs’) and the mixture fraction varies between zero and one. The results show that the ignition is initiated in lean premixed mixtures and propagates into richer mixtures. They also show that as the kernels of flames expand into richer mixtures, diffusion flames form along the stoichiometric isocontours. Echehki and Chen (2003) further investigated the coupling between chemistry and the unsteady scalar dissipation rate in 2D non-homogeneous autoignition. Because of this

coupling, the balance between radical production and dissipation determines the success or failure of a kernel to ignite. Details of the coupling effects are documented in Echekki and Chen (2003). Therefore, the simulations by Echekki and Chen (2003) illustrate the importance of propagation and the presence of different modes of combustion to the autoignition process.

In the present study, we will investigate the important statistical features of autoignition in non-homogeneous mixtures using DNS in a simplified mixture and flow configurations. The conditions considered here share similar features to the general problem of autoignition in stratified mixtures. The present study will address only the features that are in common with more practical fuels and configurations, including the transient nature of autoignition, the presence of different modes of burning, combustion off stoichiometric conditions, and the presence of propagation as an integral mechanism for the autoignition process.

2.3 Reaction Mechanism

In the present study, we implemented a simple chemistry model in which the chemistry is characterized by the single-step, second-order, and irreversible reaction mechanism with an Arrhenius dependence on temperature. This is a standard simplification in ignition works, justifiable when the activation energy is high, that the fuel and oxidant concentrations do not change appreciably (Mastorakos *et al.*, 1997b). Although the current reaction mechanism is simplified, it is sufficient for us to study the transient nature and the

presence of burning modes. In the following discussion, the development for the simplified chemistry model is included.

A one-step chemical reaction for a general system can be written as the following equation by Kuo (1986)



where ν_i' is the stoichiometric coefficient of species i as a reactant, ν_i'' is the stoichiometric coefficient of species i as a product, M_i is the chemical symbol for species i , and N is the total number of species in the reaction.

The law of mass action, which is confirmed by numerous experiments, states that the rate of reaction is proportional to the products of the concentrations of the reactants (Kuo, 1986)

$$RR = k \prod_{i=1}^N (C_i)^{\nu_i'} , \quad (2-2)$$

where k is the reaction rate constant and C_i is the concentration of the reacting chemical species. Therefore, the rates of change for the chemical components during reaction are

$$\frac{dC_i}{dt} = (\nu_i'' - \nu_i') k \prod_{i=1}^N (C_i)^{\nu_i'} . \quad (2-3)$$

For a given reaction, k is the function of the temperature only and is given by the Arrhenius law

$$k = BT^{\alpha} \exp\left(-\frac{E_a}{R_u T}\right), \quad (2-4)$$

where B is the collision frequency factor, T is the temperature, α is the temperature exponent, and E_a is the activation energy.

For ideal gases

$$C_i = \frac{p_i}{R_u T}, \quad (2-5)$$

where p_i is the partial pressure of the chemical species i . The mass of species i per unit volume, ρ_i is

$$\rho_i = \left(\frac{p_i}{R_u T} \right) W_i, \quad (2-6)$$

where R_u is the universal gas constant and W_i represents the molecular weight of species i .

Combining Eq. (2-5) with (2-6), we can get

$$C_i = \frac{\rho_i}{W_i} = \frac{\rho Y_i}{W_i}. \quad (2-7)$$

Substituting Eqs. (2-4) and (2-7) into (2-3) and using ω_i to express the rates of change for the chemical species i in units of mass per volume yeild

$$\omega_i = W_i (v_i'' - v_i') B T^\alpha \exp\left(-\frac{E_a}{R_u T}\right) \prod_{m=1}^N \left(\frac{\rho Y_m}{W_m}\right)^{v_m'}. \quad (2-8)$$

In the present work, the chemistry is represented by one single step, second-order, and irreversible reaction between a fuel F and an oxidizer O with equal molecular weight. We also assume that the reaction forms a single product P , which has the same molecular weight as that of the fuel and the oxidizer ($W_P = W_O = W_F$). Thus, the reaction is simplified to



where

$$\begin{array}{ccc} \nu'_F = 1 & \nu'_O = 1 & \nu'_P = 0 \\ \nu''_F = 0 & \nu''_O = 0 & \nu''_P = 1 \end{array} \quad (2-10)$$

Moreover, we neglect the term T^α compared to the exponential term in (2-8). Therefore, Eq. (2-8) gives us

$$\omega_p = -\omega_F = -\omega_O = \omega, \quad (2-11)$$

where

$$\omega = \frac{B}{W} \rho^3 Y_F Y_O \exp\left(\frac{-E_a}{R_u T}\right). \quad (2-12)$$

From Eq. (2-9), the mixture fraction at any given time and location can be expressed as

$$Z = Y_F + \frac{1}{2} Y_P, \quad (2-13)$$

where Y_p is the mass fraction of the product and it can be expressed as

$$Y_p = 1 - Y_F - Y_O. \quad (2-14)$$

Substituting Eq. (2-14) into (2-13) yields

$$Z = \frac{1}{2}(1 + Y_F - Y_O). \quad (2-15)$$

In the present autoignition problem, Y_F and Y_O equal to 0.5 at stoichiometric conditions. Thus, the stoichiometric the mixture fraction value is 0.5. Therefore, lean premixed flames exist at conditions under which mixture fraction value is lower than 0.5 and rich premixed flames sit at places where the mixture fraction value is higher than 0.5. Diffusion flames are formed at the stoichiometric mixture fraction of 0.5.

2.4 The Governing Equations

The governing equations for continuity, conservation of momentum, conservation of energy, and conservation of species, and the equation of state (Mason, 2000) are presented in this section. The governing equations are simplified based on the following assumptions (Mason, 2000): 1) ideal gas behavior for all species, 2) Newtonian fluid, 3) negligible body forces, 4) zero bulk viscosity, 5) constant and equal specific heat C_p for all species, 6) Fourier's law for molecular heat conduction, 7) constant thermal conductivity λ , 8) negligible Soret and Dufour effects and thermal radiation, 9) Fick's law for mass diffusion and equal mass diffusivities D for all species, and 10) constant dynamic viscosity.

Continuity:

$$\frac{\partial \rho}{\partial t} + \frac{\partial \rho u_i}{\partial x_i} = 0, \quad (2-16)$$

where ρ is the density.

Conservation of Momentum:

$$\rho \left(\frac{\partial u_i}{\partial t} + u_j \frac{\partial u_i}{\partial x_j} \right) = -\frac{\partial P}{\partial x_i} + \mu \frac{\partial^2 u_i}{\partial x_j \partial x_j} + \frac{1}{3} \mu \frac{\partial}{\partial x_i} \left(\frac{\partial u_j}{\partial x_j} \right), \quad (2-17)$$

where μ is the dynamic viscosity and P is the pressure.

Conservation of Energy:

Multiple forms exist for the energy conservation equation. Here, the conservation of energy for a reacting flow is written in terms of temperature T .

$$\rho C_p \left(\frac{\partial T}{\partial t} + u_i \frac{\partial T}{\partial x_i} \right) = \frac{DP}{Dt} + \lambda \frac{\partial^2 T}{\partial x_i \partial x_i} + \tau_{ij} \frac{\partial u_i}{\partial x_j} - \sum_{k=1}^N \omega_k \Delta h_{f,k}^\circ, \quad (2-18)$$

where C_p is the specific heat, $\frac{DP}{Dt}$ is the substantial derivative of pressure, λ is the thermal

conductivity, ω_k is the reaction rate for species k , $\Delta h_{f,k}^\circ$ is the standard enthalpy of

formation per unit mass for species k , where τ_{ij} is

$$\tau_{ij} = \mu \left(\frac{\partial u_i}{\partial x_j} + \frac{\partial u_j}{\partial x_i} \right) - \frac{2}{3} \mu \left(\delta_{ij} \frac{\partial u_k}{\partial x_k} \right). \quad (2-19)$$

Use the relation provided in Eq. (2-11), the last term in the conservation of energy equation is reduced to

$$- \sum_{k=1}^N \omega_k \Delta h_{f,k}^\circ = \omega \left(\Delta h_{f,F}^\circ + \Delta h_{f,O}^\circ - \Delta h_{f,P}^\circ \right), \quad (2-20)$$

where ω is given in (2-12). Following Mason (2000), assume

$$\Delta h_{f,F}^\circ + \Delta h_{f,O}^\circ - \Delta h_{f,P}^\circ = C_p (T_{ad} - T_{ref}), \quad (2-21)$$

where T_{ad} is the adiabatic flame temperature and T_{ref} is the reference temperature. Eq. (2-18)

now becomes

$$\rho C_p \left(\frac{\partial T}{\partial t} + u_i \frac{\partial T}{\partial x_i} \right) = \frac{DP}{Dt} + \lambda \frac{\partial^2 T}{\partial x_i \partial x_i} + \tau_{ij} \frac{\partial u_i}{\partial x_j} + \omega C_p (T_{ad} - T_{ref}). \quad (2-22)$$

Conservation of Species:

For flows involving chemistry, the species conservation equation for species k is

$$\rho \left(\frac{\partial Y_k}{\partial t} + u_i \frac{\partial Y_k}{\partial x_i} \right) = \frac{\partial}{\partial x_i} \left(\rho D \frac{\partial Y_k}{\partial x_i} \right) + \omega_k, \quad (2-23)$$

where D is the mass diffusivity. Assuming ρD is constant for all species, Eq. (2-23) can be further simplified to

$$\rho \left(\frac{\partial Y_k}{\partial t} + u_i \frac{\partial Y_k}{\partial x_i} \right) = \rho D \frac{\partial^2 Y_k}{\partial x_i \partial x_i} + \omega_k. \quad (2-24)$$

In the present study, only three species are present. We only need to solve species conservation equations for the fuel and the oxidizer and the mass fraction of product can be found from Eq. (2-14). From Eq. (2-11), we know $\omega_F = \omega_O = -\omega$ and ω is given in Eq. (2-12). Therefore, the conservation equations for the fuel and the oxidizer are the same

$$\rho \left(\frac{\partial Y_k}{\partial t} + u_i \frac{\partial Y_k}{\partial x_i} \right) = \rho D \frac{\partial^2 Y_k}{\partial x_i \partial x_i} - \omega, \quad (2-25)$$

where $k = F$ or O .

Equation of State:

All the species are assumed to behave as ideal gases, thus the equation of state for all the species is

$$PW = \rho R_u T. \quad (2-26)$$

Following the non-dimensionalization and low-Mach number assumption in Mason (2000), the above governing equations can be written as

Continuity:

$$\frac{\partial \rho}{\partial t} + \frac{\partial \rho u_i}{\partial x_i} = 0 \quad (2-27)$$

Conservation of Momentum:

$$\frac{\partial u_i}{\partial t} + u_j \frac{\partial u_i}{\partial x_j} = -\frac{1}{\rho} \frac{\partial P}{\partial x_i} + \frac{1}{\rho Re} \frac{\partial^2 u_i}{\partial x_j \partial x_j} + \frac{1}{3\rho Re} \frac{\partial}{\partial x_i} \left(\frac{\partial u_j}{\partial x_j} \right) \quad (2-28)$$

Conservation of Energy:

$$\frac{\partial T}{\partial t} + u_i \frac{\partial T}{\partial x_i} = \frac{1}{\rho Pr Re} \frac{\partial^2 T}{\partial x_i \partial x_i} + \omega \quad (2-29)$$

Conservation of Fuel:

$$\frac{\partial Y_F}{\partial t} + u_i \frac{\partial Y_F}{\partial x_i} = \frac{1}{\rho Le Pr Re} \frac{\partial^2 Y_F}{\partial x_i \partial x_i} - \omega \quad (2-30)$$

Conservation of Oxidizer:

$$\frac{\partial Y_o}{\partial t} + u_i \frac{\partial Y_o}{\partial x_i} = \frac{1}{\rho Le Pr Re} \frac{\partial^2 Y_o}{\partial x_i \partial x_i} - \omega \quad (2-31)$$

Reaction Rate:

$$\omega = Da \rho Y_F Y_o \exp \left[\frac{-\beta(1-T)}{1-\alpha(1-T)} \right] \quad (2-32)$$

Equation of State:

$$\rho \left[T \left(\frac{\alpha}{1-\alpha} \right) + 1 \right] = P_0 \quad (2-33)$$

In Eqs. (2-27)–(2-33), the following scaling is applied:

$$\begin{aligned} x_i &= \frac{(x_i)_d}{L_{ref}} & u_i &= \frac{(u_i)_d}{U_{ref}} & \rho &= \frac{\rho_d}{\rho_{ref}} \\ t &= \frac{t_d U_{ref}}{L_{ref}} & P &= \frac{P_d}{\rho_{ref} \frac{R_u}{W} T_{ref}} & T &= \frac{T_d - T_{ref}}{T_{ad} - T_{ref}} \end{aligned} \quad (2-34)$$

The subscript ‘*d*’ in (2-34) denotes the dimensional quantity and the subscript ‘*ref*’ denotes a reference value. The subscript ‘*ad*’ represents adiabatic mixture conditions. The non-dimensional parameters in Eqs. (2-27) to (2-33) are

The Mach Number:

$$Ma = \frac{U_{ref}}{\left(\gamma \frac{R_u}{W} T_{ref} \right)}, \quad (2-35)$$

where γ is the ratio of specific heats.

The Reynolds Number:

$$Re = \frac{\rho_{ref} L_{ref} U_{ref}}{\mu} \quad (2-36)$$

The Prandtl Number:

$$Pr = \frac{C_p \mu}{\lambda} \quad (2-37)$$

The Lewis Number:

$$Le = \frac{\lambda}{\rho_{ref} C_p D} \quad (2-38)$$

The Non-dimensional Temperature Rise:

$$\alpha = \frac{T_{ad} - T_{ref}}{T_{ad}} \quad (2-39)$$

The Non-dimensional Activation Energy:

$$\beta = \frac{E_a \alpha}{R_u T_{ad}} \quad (2-40)$$

The Damköhler Number:

$$Da = \frac{L_{ref} / U_{ref}}{\left[\frac{B}{W} \rho_{ref} \exp\left(-\beta / \alpha\right) \right]^{-1}} \quad (2-41)$$

With the low-Mach number approximation, density changes due to heat release are allowed, but acoustic waves are not.

Note that P in the momentum equation denotes the first-order pressure $P^{(1)}$ in the low-Mach number expansion of pressure $P = P^{(0)} + \varepsilon P^{(1)} + \varepsilon^2 P^{(2)} + \dots$ in terms of the parameter $\varepsilon = \gamma Ma^2$. The first order pressure $P^{(0)}$ is assumed to be constant. Moreover, the viscous dissipation term $\tau_{ij} \frac{\partial u_i}{\partial x_j}$ is removed from the energy equation because it is of order of ε and $\varepsilon \ll 1$.

The non-dimensional governing Eqs. (2-27)-(2-31) represent a complete system with unknowns including u, v, w, P, T, Y_F , and Y_O . The numerical solution procedure for the system of equations will be discussed in the following section.

2.5 Numerical Implementation

The DNS code is based on the formulation by Mason (2000). Non-staggered uniform grids are used in the formulation. A third-order Runge-Kutta method is used to integrate the system of equations in time. A fully consistent fractional-step method is used for the solution of the momentum equation. The pressure in the momentum equation is solved using the Poisson's equation. Linearly implicit variation of third-order Runge-Kutta scheme is used to integrate the energy and the species equations. Spatial derivatives are computed using the fifth-order explicit finite-difference schemes.

2.5.1 Spatial Discretization

A schematic of the three-dimensional computational domain is given in Figure 2-1. The non-dimensional domain length in each direction is the same and is denoted by L in the figure. The boundary and initial conditions for all the variables are presented in Chapter 3. The computational domain is discretized using uniform non-staggered grids in all directions. One advantage of using non-staggered grids is that all the dependent variables are located at the same position. Therefore, momentum cells are collocated with the continuity cells and this eliminates the need for cell boundary interpolation. The result is that the code is computationally more efficient than using staggered grids.

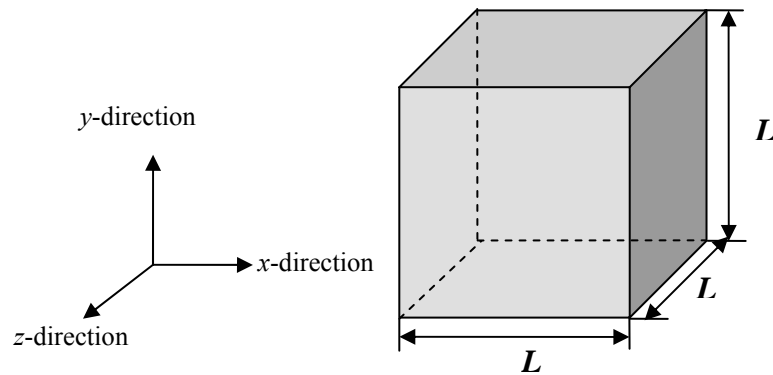


Figure 2-1 Three-dimensional computational domain

Figure 2-2 shows the two-dimensional grid geometry in the xy -plane. Grids are uniform in both x and y directions. Solutions for dependent variables $u, v, w, P, T, Y_F,$ and Y_O at nodes denoted by ‘•’ in Figure 2-2 are obtained. Each node is associated with a continuity cell of width and height ΔL for which the continuity and

transport equations are solved. In the present study, simulations are in three dimensions. In each direction, x , y , and z , the grid spacing is

$$\Delta L = \frac{L}{N-1}, \quad (2-42)$$

where N is the total number of nodes in each direction.

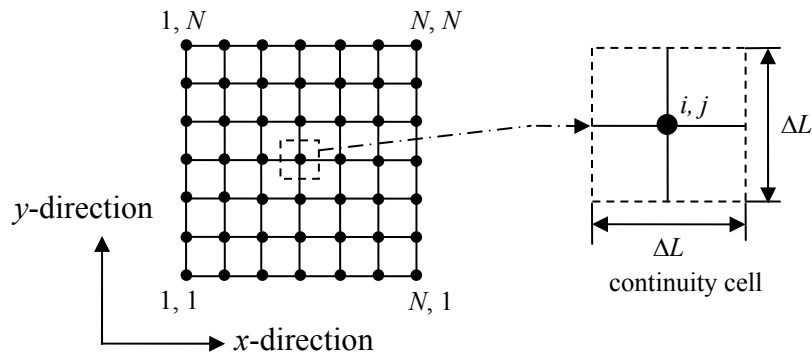


Figure 2-2 Two-dimensional computational grid in xy-plane

2.5.2 Spatial Differentiation

The explicit finite difference scheme is used for spatial differentiation. In the present implementation, the order of spatial derivatives can be specified in a range of 3 to 11 as a user input. Fifth order is used in the present study. The stencils for derivatives in all three directions are pre-computed. This is done by using Taylor series and solving the system of linear algebraic equations for the coefficients. The linear system is solved using a simple Gauss elimination procedure. The truncation error matrix is subject to a singularity for operators with high orders of accuracy. Mason (2000) used the singular value decomposition (SVD) method to check the singularity of each truncation error matrix for every operator.

The major advantage of using explicit finite difference scheme is that it offers the flexibility for exploring the issue of operator consistency in the solution to the Poisson's equation for pressure.

2.5.3 Solution to the Governing Equations

Details of solving the momentum equations can be found in Mason (2000) and Appendix A, which is included for completion. Here, we are just highlighting the major steps. The momentum equation is integrated using the fractional-step method following Mason (2000). First, an intermediate velocity field is generated by integrating the convection and diffusion terms in the momentum equation. Second, the pressure is solved using the Poisson's equation. Third, the new velocity field is obtained by correcting the intermediate velocity vectors using the gradients of pressure.

Details of solving the energy and species equations can be found in Mason (2000) and Appendix B, which is included for completion. The energy and species equations are integrated in time using a linearly implicit variation of the third-order Runge-Kutta scheme used to integrate the momentum equation. While the convection and the diffusion terms are integrated in the same way as in the momentum equation, the reaction rate term is integrated implicitly for stability due to the fact that it is usually large. Crank-Nicolson scheme is used to integrate the reaction rate term.

2.5.4 Numerical Integration Procedure

At each Runge-Kutta sub-step within each time step, the governing equations are solved in an order that is listed in Figure 2-3. First, the reaction rate term is computed using the most recent values of the temperature, the density, and the species mass fraction. Second, the energy and species equations are integrated. The reaction rate term is integrated using the linearly implicit scheme. Third, the density is obtained from the equation of state. Finally, the momentum equation is integrated in three steps. The first step is to integrate the convection and diffusion terms to obtain the intermediate velocity field; the second step is to solve the Poisson's equation for pressure; the third step is to update the velocity field.

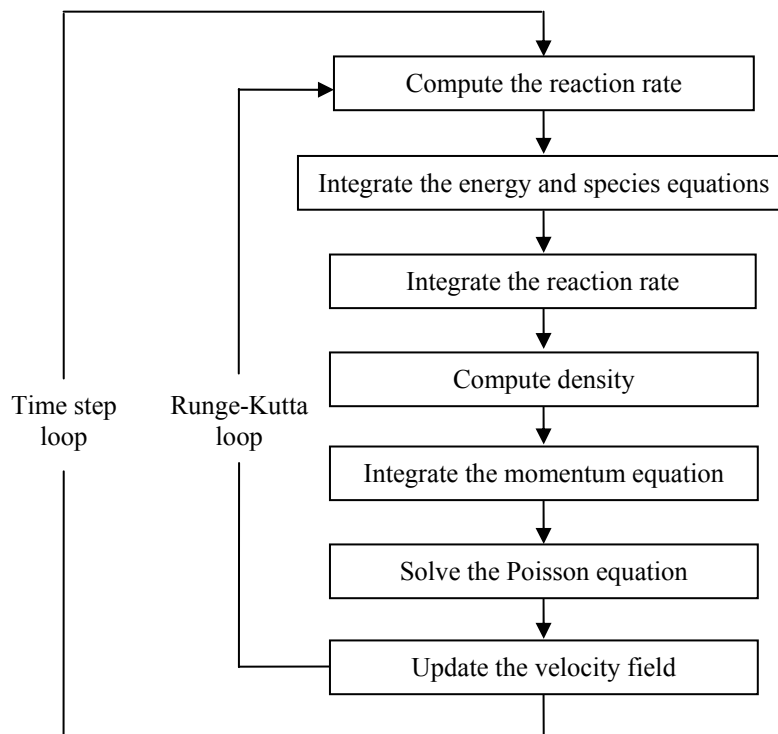


Figure 2-3 Flow chart of the numerical solution procedure

2.6 Conclusions

In this chapter, we have identified non-homogeneous autoignition in isotropic turbulence as the problem for the present study and developed the chemistry model for the autoignition problem. The governing equations including continuity, conservation of momentum, conservation of energy, and conservation of species are presented and the numerical implementation of the equations is outlined. The direct numerical simulation results are included in the next chapter.

Chapter 3 DNS of Autoignition in Non-Homogenous Mixtures: Conditional Statistical Results

3.1 Objectives

The goal of this chapter is to present the statistical results of 3D direct numerical simulation of the non-homogeneous autoignition in isotropic turbulence based on the governing equations in Chapter 2. The non-homogeneous autoignition is simulated for two turbulence conditions, one with low turbulence intensity and the other with high turbulence intensity. For high turbulence conditions, three cases with Lewis numbers equal to 0.5, 1.0, and 2.0 are studied. The following discussion of this chapter is organized as follows. First, initial conditions are presented in section 3.2, followed by a discussion of the boundary conditions (section 3.3), and the simulation parameters (section 3.4). A discussion of the statistical quantities obtained from the simulations is presented in section 3.5. Results based on these statistics are presented and discussed in sections 3.5-3.7.

3.2 Initialization of the Flow Field

3.2.1 Initialization of the Vector Field

The initialization of the turbulent velocity field to an isotropic state is performed in the associated Fourier space based on the random distribution of the turbulent kinetic energy.

The analytical relation between the distribution of the turbulent kinetic energy and the wave number is described by the von Karman with Pao (Hinze, 1975) correction for near-dissipation scales and it is given in the following form

$$E(k) = A \frac{\left(\overline{u_{turb}^2}\right)^5}{\varepsilon_d} \frac{(k/k_e)^4}{\left[1 + (k/k_e)^2\right]^{17/6}} \cdot \exp\left(-\frac{3}{2}\alpha(k/k_d)^{4/3}\right), \quad (3-1)$$

where $A = 1.5$ and $\alpha = 1.5$. In Eq. (3-1), both u_{turb} , which is the root mean square velocity, and ε_d , which is the dissipation number, are user-input parameters. Also in Eq. (3-1), k_e is the wave number of the most energetic scale and it represents the peak of the turbulent kinetic energy distribution; k_d is the wave number corresponding to the Kolmogorov dissipation scale and it represents the maximum level of dissipation.

The initialization of the velocity field in the Fourier space using the von Karman-Pao spectrum must satisfy the continuity condition

$$\underline{\tilde{u}} = \tilde{u}_i \underline{e}_i = \alpha(\underline{k}) \underline{e}'_1 + \beta(\underline{k}) \underline{e}'_2, \quad (3-2)$$

where \underline{e}_i is the computation vector basis and \underline{e}'_i is any vector basis having \underline{e}'_3 parallel to \underline{k} . The complex components α and β in general are random in amplitude and phase and having the following form

$$\alpha = \sqrt{\frac{E(k)}{4\pi k^2}} e^{i\theta_1} \cos \phi, \quad (3-3)$$

$$\beta = \sqrt{\frac{E(k)}{4\pi k^2}} e^{i\theta_2} \sin \phi, \quad (3-4)$$

where θ_1 , θ_2 , and ϕ are the phases of the turbulent velocity components in the Fourier space. They are uncorrelated and are uniformly distributed random numbers on the interval $(0, 2\pi)$ given as

$$\theta_1 = 2\pi(\text{Rand}_1 - 0.5), \quad (3-5)$$

$$\theta_2 = 2\pi(\text{Rand}_2 - 0.5), \quad (3-6)$$

$$\phi = 2\pi(\text{Rand}_3 - 0.5). \quad (3-7)$$

To complete the formulation of the initial velocity field in the Fourier space, we need to relate the basis \underline{e}'_i to the computational basis \underline{e}_i . Any basis subject to the constraint

$$k\underline{e}'_3 = k_1\underline{e}_1 + k_2\underline{e}_2 + k_3\underline{e}_3, \quad (3-8)$$

works because rotations about \underline{e}'_3 are absorbed into the random phase ϕ . We can choose arbitrarily a basis having

$$\underline{e}'_1 \cdot \underline{e}_3 = 0, \quad (3-9)$$

which leads us to the solution for \underline{e}'_i

$$\sqrt{k_1^2 + k_2^2} \underline{e}'_1 = k_2\underline{e}_1 - k_1\underline{e}_2, \quad (3-10)$$

$$k\sqrt{k_1^2 + k_2^2} \underline{e}'_2 = k_1k_3\underline{e}_1 + k_2k_3\underline{e}_2 - (k_1^2 + k_2^2)\underline{e}_3, \quad (3-11)$$

where k_1 , k_2 , and k_3 are wave numbers in x , y , and z directions, respectively, and are given in the following expression

$$k_1 = k_2 = k_3 = \begin{cases} (i-1) \cdot 2\pi/L & \text{for } 1 \leq i \leq N/2+1 \\ (N-i+1) \cdot 2\pi/L & \text{for } N/2+1 \leq i \leq N \end{cases}. \quad (3-12)$$

In Eq. (3-11), k is the following

$$k = \sqrt{k_1^2 + k_2^2 + k_3^2}. \quad (3-13)$$

By solving Eqs. (3-10) and (3-11), we get

$$\tilde{\mathbf{u}} = \left(\frac{\alpha k k_2 + \beta k_1 k_3}{k \sqrt{k_1^2 + k_2^2}} \right) \mathbf{e}_1 + \left(\frac{\beta k_2 k_3 - \alpha k k_1}{k \sqrt{k_1^2 + k_2^2}} \right) \mathbf{e}_2 - \left(\frac{\beta \sqrt{k_1^2 + k_2^2}}{k} \right) \mathbf{e}_3. \quad (3-14)$$

The inverse FFT transfers the values of the turbulent velocities in the Fourier space back to the real, physical space. Because the random-number generator is used for the phases of the velocity fluctuations in the associated Fourier space, each computation will be started with a different initial velocity field regardless the constants of u_{turb} and ε_d . Note that during the initialization, the mean velocity components in the computational domain are zero.

3.2.2 Initialization of the Scalar Field

The initial scalar field is generated by initializing the mixture fraction field in the associated Fourier space with von Karman-Pao spectrum. In the following discussion, the mixture fraction is denoted as Z . The initial spatial distribution of the mixture fraction varies from pure fuel to pure oxidizer over a characteristic length scale, L_c , which is defined as

$$L_c = \frac{\int_0^\infty Q_z(r) dr}{Q_z(0)}, \quad (3-15)$$

where $Q_z(r)$ is given as

$$Q_z(r) = \langle Z''(x)Z''(x+r) \rangle. \quad (3-16)$$

In Eq. (3-16), $Q_z(r)$ is the two-point correlation function for the local mixture fraction fluctuation at a distance r . The length scale, L_c , measures the characteristic scale over which the mixture evolves from the fuel to the oxidizer, and vice versa. The resulting initial scalar field is characterized by fuel-centered and oxidizer-centered ‘blobs’ of fluid between which the mixture fraction changes.

A mean value of the mixture fraction is imposed to the fluctuating mixture field to yield an average value of 0.5, which is the stoichiometric mixture fraction. Moreover, the values of the mixture fraction are adjusted with a coefficient and a \tanh profile is used to maintain the mixture field to be from 0 to 1. Figure 3-1 shows the initial mixture fraction field. In the present study, the mixture fraction range is from 0.15 to 0.85.

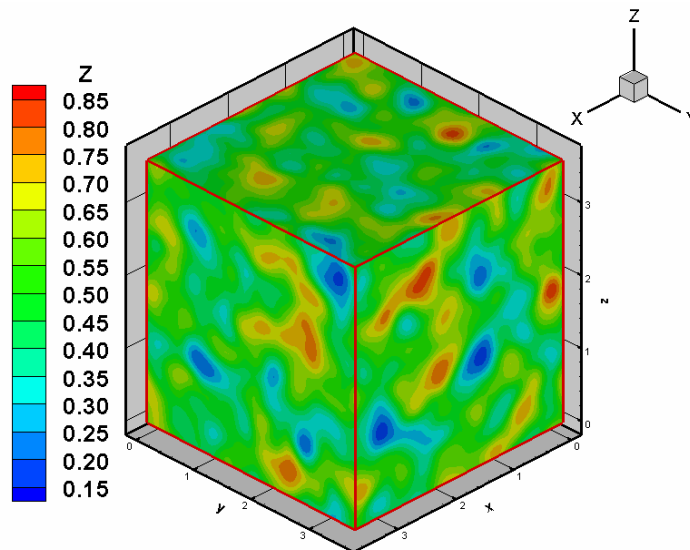


Figure 3-1 Initial mixture fraction field

Based on the initial random field for the mixture fraction, Z , which can be expressed as

$$Z = \frac{Y_F - Y_{F,O}}{Y_{F,F} - Y_{F,O}} = \frac{Y_O - Y_{O,O}}{Y_{O,F} - Y_{O,O}}, \quad (3-17)$$

where Y_F is the fuel mass fraction, Y_O is the oxidizer mass fraction, $Y_{F,F}$ is the fuel mass fraction in the fuel stream, $Y_{F,O}$ is the fuel mass fraction in the oxidizer stream, $Y_{O,F}$ is the oxidizer mass fraction in the fuel stream, and $Y_{O,O}$ is the oxidizer mass fraction in the oxidizer stream. The initial fields for the fuel and the oxidizer mass fraction can be obtained from Eq. (3-17) as follows

$$Y_F = Y_{F,O} + Z(Y_{F,F} - Y_{F,O}), \quad (3-18)$$

$$Y_O = Y_{O,O} + Z(Y_{O,F} - Y_{O,O}). \quad (3-19)$$

Assuming that the fuel stream contains only the pure fuel, i.e. $Y_{F,F} = 1$, $Y_{O,F} = 0$, and that the oxidizer stream contains only the oxidizer, i.e. $Y_{O,O} = 1$, $Y_{F,O} = 0$, the initial fuel and oxidizer mass fractions can be expressed in terms of the mixture fraction field as follows

$$Y_F = Z, \quad (3-20)$$

$$Y_O = 1 - Z. \quad (3-21)$$

To initialize the temperature field, we first write the energy balance equation

$$Y_F h_F + Y_O h_O = Y_F h_{mix} + Y_O h_{mix}, \quad (3-22)$$

where h_F is enthalpy of the fuel stream, h_O is the enthalpy of the oxidizer steam, and h_{mix} is the enthalpy of the mixture. Assuming constant specific heats for both the fuel and the oxidizer, we have

$$Y_F T_F + Y_O T_O = (Y_F + Y_O) T_{mix}, \quad (3-23)$$

where T_F is the temperature of the fuel stream, T_O is the temperature of the oxidizer stream, and T_{mix} is the temperature of the mixture. Substituting Eqs. (3-20) and (3-21) into Eq. (3-23), the initial temperature of the mixture is

$$T = T_F + (1 - Z)(T_0 - T_F). \quad (3-24)$$

Write Eq. (3-24) at the stoichiometric condition

$$T_{st} = T_F + (1 - Z_{st})(T_0 - T_F), \quad (3-25)$$

where T_{st} is the stoichiometric mixture fraction, which is equal to 0.5, and Z_{st} is the corresponding temperature at the stoichiometric mixture fraction prior to the onset of combustion. Because the oxidizer is preheated relative to the fuel to provide a mechanism for the autoignition of the mixture, the stoichiometric temperature is set to zero. Therefore, Eq. (3-25) is reduced to

$$T_F = -T_O. \quad (3-26)$$

3.3 Boundary Conditions

In the present study, periodic boundary conditions are imposed in all three directions during the simulation. Simulations with more complex boundary conditions and analysis of the boundary condition effects on simulation results are recommended for future work.

3.4 Simulation Parameters

Direct numerical simulations of non-homogeneous autoignition in isotropic turbulence are conducted for both low and high initial turbulence conditions. The turbulence conditions play a significant role in the interactions of mixing and chemistry. Thus, studying the turbulence induced effects is very important in autoignition. For the low initial turbulence case, unity Lewis number is used. For the high initial turbulence case, three simulations are performed for Lewis numbers equal to 0.5, 1.0, and 2.0. The purpose of carrying out simulations for different Lewis numbers is to address the importance of mass transport in the autoignition process. Table 3-1 presents a summary of the common parameters used in all the cases. The flow and chemistry parameters have been defined in Eqs. (2-35)–(2-41). The reaction rate and the heat release rate parameters, Da , α and β , are 200, 0.75 and 2.0, respectively. The time step, which is set by the numerical accuracy and the stability requirements, is 0.001. The parameters for initialization are discussed in section 3.2.

Table 3-2 presents a summary of the specific parameters used in each case. The grid resolution with $129 \times 129 \times 129$ grid points over the prescribed non-dimensional domain size of $3.6 \times 3.6 \times 3.6$ is chosen to sufficiently resolve the flame structure and the range of flow and

scalar scales considered. This non-dimensionalization is prescribed by a characteristic Reynolds number, Re , which is defined in Eq. (2-36). The rates of chemistry are sufficiently high such that ignition time scales are shorter than mixing time scales. The initial turbulence intensity is defined as

$$u_{turb} = \left(\overline{u''u''} \right)^{1/2} = \left(\overline{v''v''} \right)^{1/2} = \left(\overline{w''w''} \right)^{1/2}. \quad (3-27)$$

The Taylor time scale is defined as

$$Re_\lambda = \left(\frac{20}{3} Re_L \right)^{1/2}, \quad (3-28)$$

where Re_L is the turbulence Reynolds number and it is defined as

$$Re_L = \frac{u_{turb} L_{turb}}{\nu}. \quad (3-29)$$

In Eq. (3-29), L_{turb} is the integral length scale and ν is the kinetic viscosity and they are defined as

$$L_{turb} = \frac{k^{3/2}}{\varepsilon}, \quad (3-30)$$

where

$$\varepsilon = 2\gamma \overline{S_{ij}S_{ij}}, \quad (3-31)$$

and

$$k = \frac{3}{2} \overline{u_{turb}u_{turb}}. \quad (3-32)$$

The turbulence time scale is defined as

$$\tau_{turb} = \frac{L_{turb}}{u_{turb}}. \quad (3-33)$$

The mixing time scale is expressed by

$$\tau_{mix} = (\overline{Z''Z''}) / \bar{\chi}. \quad (3-34)$$

The over-bar in Eqs. (3-31), (3-32), and (3-34) represents a volume average over the entire computational domain. For the present calculation, $L_C/L = 0.1$, where L is the domain size.

The non-homogeneous field, with the prescribed value of L_C , results in an average of 6 to 7 of these structures in a given direction.

Table 3-1 Common parameters for DNS simulation of non-homogeneous autoignition in isotropic turbulence

Common Parameters		Description	Case/Value
General Characteristics		dimension	3D
		chemistry	reacting
Flow Characteristics	Re	Reynolds number	200
	τ_{turb}	turbulent time scale	13
	τ_{mix}	scalar mixing time scale	0.15
	P_o	zeroth-order pressure	1.0
Chemistry Characteristics	Pr	Prandtl number	0.7
	Da	Damköhler number	200
	α	non-dimensional heat release	0.75
	β	Zel'dovich number	2.0
Numerical Parameters	$N_x \times N_y \times N_z$	grid size	129×129×129
	dx, dy, dz	grid spacing	2.8125×10^{-2}
	Δt	time step	0.001
	ϵ_{SOR}	Successive Over-Relaxation tolerance	2.5×10^{-9}
Initialization Parameters	Z_{mean}	mean value of mixture fraction	0.5
	T_o	initial oxidizer temperature	0.4
Statistics	N_{bin}	number of mixture fraction bins	31

Table 3-2 Specific parameters for DNS simulation of non-homogeneous autoignition in isotropic turbulence

Specific Parameters	Description	Value			
		u_{turb}	turbulence intensity	3.0	
Re_λ	Taylor time scale	405			100
Le	Lewis number	0.5	1.0	2.0	1.0
$N_x = N_y = N_z$	grid size in each direction	129	129	129	129

3.5 Data Post-Processing Using Conditional Moment Closure Approach

In the earliest formulation of CMC, the modeling strategy relied on the assumption that fluctuations in the scalar quantities are primarily correlated with the fluctuation of only one key variable, the mixture fraction. Klimenko (1990) proposed that turbulent diffusion in mixture fraction can be modeled more rigorously than in physical space. Bilger (1993) observed that most of the fluctuations of the reactive scalars can be associated with fluctuations of the mixture fraction and derived the balance equations based on this observation. In the CMC governing equations, the first moments are means or averages; the second moments are variances and covariances of the fluctuations about the averages; the third moments are triple correlations between the fluctuations (Klimenko and Bilger, 1999). The reactive scalars are expressed in terms of averages or variances of these scalars conditioned on the value of the mixture fraction.

In the present study, the singly-conditioned first and second moments of scalars are obtained using CMC. The conditioning is based on the mixture fraction, which is the primary variable adopted in the modeling of autoignition problems. These statistics are of relevance

to the first and second order CMC approach; however, observations may be extended to broader implications to turbulent combustion models of non-homogeneous autoignition.

The first conditional moments include the conditional means for the temperature $\langle T | Z \rangle$, the fuel and the oxidizer mass fractions, $\langle Y_F | Z \rangle$ and $\langle Y_O | Z \rangle$, and the reaction rate, $\langle \omega | Z \rangle$. Here, the mixture fraction, Z , is the conditioning variable; the conditioning operation is expressed in terms of the operator “ $\langle \cdot | Z \rangle$ ” for the scalars.

The second conditional moments include co-variances and the variances of the species mass fractions and the temperature with the dissipation rate. For convenience, we present the co-variances in terms of the root mean square values, $\langle Y_F'' Y_F'' | Z \rangle^{1/2}$, $\langle Y_O'' Y_O'' | Z \rangle^{1/2}$, and $\langle T'' T'' | Z \rangle^{1/2}$. The variances are expressed in terms of correlation functions, which are expressed as

$$R_{\theta\chi} = \frac{\langle \theta'' \chi'' | Z \rangle}{\langle \theta'' \theta'' | Z \rangle^{1/2} \langle \chi'' \chi'' | Z \rangle^{1/2}}, \quad (3-35)$$

where θ represents any one of the reactive scalars, T , Y_F , and Y_O and χ is the scalar dissipation rate, which is given as

$$\chi \equiv 2D(\nabla Z \cdot \nabla Z), \quad (3-36)$$

where D is the mass diffusivity associated with the mixture fraction, which in this problem is identical to the kinematic viscosity of the fluid divided by the Lewis number. The variances and co-variances are prominent closure terms in the first and the second-order CMC

equations (Mastorakos and Bilger, 1998; Swaminathan and Bilger, 1999; Li and Bilger 1993).

From the direct numerical simulation, results for scalars at each computational node are obtained. At any given time, the data of those scalars is used to compute the conditional averages, co-variances, and variances. The calculation of conditional moments involves three steps. First, the mixture fraction values are divided into 31 bins ranging from zero to one. Second, scalars at each computational node are distributed among those bins according to the mixture value at each node. Third, the conditional moments in each bin are calculated. The statistics are evaluated at different snapshots in time. Thus, the autoignition process from the formation of autoignition kernels to the completion of the combustion process is captured by snapshots in sequence. The statistical results are presented in the next section.

3.6 Past Research on DNS of Autoignition

First-order singly-conditioned CMC has been validated for a number of practical combustion flows studied by Bourlioux *et al.* (2000), Fairweather *et al.* (2003), Kim *et al.* (2000), Kronenburg *et al.* (1998, 2001), Smith *et al.* (1995), and Vervisch *et al.* (1998). The work by Mastorakos *et al.* (1997a), Mastorakos and Bilger (1998), and Sreedhara and Lakshmisha (2000) provides validations of the second-order CMC approach in ‘non-premixed’ autoignition. However, there are two problems in those studies. First, fully segregated fuel and oxidizer streams are represented by ‘slabs’ of the fuel and the oxidizer in these studies using DNS. Therefore, the statistics obtained by the above DNS studies

reflect conditions of autoignition that, even though initiated off-stoichiometric conditions, will evolve into combustion in a non-premixed combustion mode (near-stoichiometric). However, it is not evident that a similar modeling strategy can be applied for non-homogeneous autoignition such as the configuration studied by Echehki and Chen (2002) or the more general condition of autoignition in stratified mixtures.

Multiple conditioning within the context of CMC has been proposed as an alternative to higher order conditioning in CMC. Cha *et al.* (2001) proposed the modeling of the dissipation rate as an additional conditioning variable for the prediction of extinction and re-ignition. Bilger (1992) and later Kronenburg (2004) proposed the sensible enthalpy as an additional conditioning variable for problems involving both extinction and re-ignition. Therefore, the principal implementations of double-conditioning are limited to the prediction of extinction and re-ignition. In this application, the use of an additional conditioning variable explicitly accounted for the different processes of mixing and reaction; while, in the traditional single-conditioning approach, a single parameter measuring the progress of mixing was also used to address the progress of reaction.

3.7 Simulation Results of the Present Study

In this section, we present results of the evolution of conditional statistics for the passive and reactive scalars. The statistics are all obtained by post-processing the DNS data. The process of autoignition in non-homogeneous mixtures involves the formation of autoignition in discrete kernels; and the combustion process evolves eventually due to the

propagation of these kernels through the stratified mixture. The temporal evolution of the process is represented in terms of the non-dimensional time. The statistical results show that complete combustion is achieved earlier in the high turbulence cases than in the low turbulence case. For high turbulence cases with different Lewis numbers, the scatter plots show that the second conditioning variable is not enough for cases with non-unity Lewis numbers. In the following discussions, the results for conditional means are presented first. Then the results for conditional variances and co-variances are discussed. Finally, the scatter plots for the second conditioning variable are presented.

3.7.1 Conditional Means of Scalars

Conditional Means of the Scalar Dissipation Rate

Figure 3-2 shows the temporal evolution of the conditional means of the scalar dissipation rate profiles in the mixture fraction space for the different cases considered. The relatively high conditions of dissipation rates at lean and rich conditions are consistent with the presence of local peaks in the mixture fraction.

Turbulence affects the conditional means of χ . At low turbulence conditions, the conditional means of χ gradually decrease with respect to time (Figure 3-2 (a)); on the other hand, at high turbulence conditions, the conditional means of χ increase at earlier times and gradually decrease (Figure 3-2 (b), (c), and (d)) at later times. This is because the scalar gradients are relatively very high at high turbulence conditions, which causes a rapid increase of the conditional means of χ at earlier times. However, at later times, all the mixtures

approach a high extent of mixing and the conditional means of χ decrease in time regardless of the turbulence conditions. Furthermore, turbulence affects the mixture fraction range, which shrinks at a faster speed in the high turbulence cases than in the low turbulence case.

The Lewis number also affects the mixture fraction range and the magnitude of the conditional means of χ . First, a wider mixture fraction range is observed in the high turbulence case with a large Lewis number. A larger Lewis number results in a lower mass diffusivity compared to the energy transport. Therefore, the scalar molecular mixing rate will be lower, which results in a wider mixture fraction range. Second, the magnitude of the conditional means of χ is lower in the high Lewis number case at earlier times. This can be seen by comparing Figure 3-2 (c) with Figure 3-2 (d) for the conditional means of χ at time equal to 0.12. However, although the Lewis number in Figure 3-2 (d) is twice of that in Figure 3-2 (c), a factor of two in the magnitude of the conditional means of χ is not observed between these two cases. This is due to the competing roles of mass diffusion (or Lewis number) and the evolution of scalar gradients. Given two identical mixture fields, a lower mass diffusivity (i.e. higher Lewis number) associated with the mixture fraction results in steeper mixture fraction gradients, and vice-versa. The scalar gradients in the case shown in Figure 3-2 (d) is slightly higher than in the case shown in Figure 3-2 (c) as a consequence of its lower mass diffusivity. Therefore, the total effect of the mass diffusivity and the scalar gradients makes the conditional means of χ only slightly lower in the high Lewis number case than in the low Lewis number case. At later times, Lewis number effects are not significant; indeed, the magnitude of the conditional means of χ is higher in the high Lewis

number case than in the low Lewis number case. Therefore, higher molecular diffusion can precipitate the decay in scalar gradients, and accordingly, the rate of scalar dissipation at later times of the simulation.

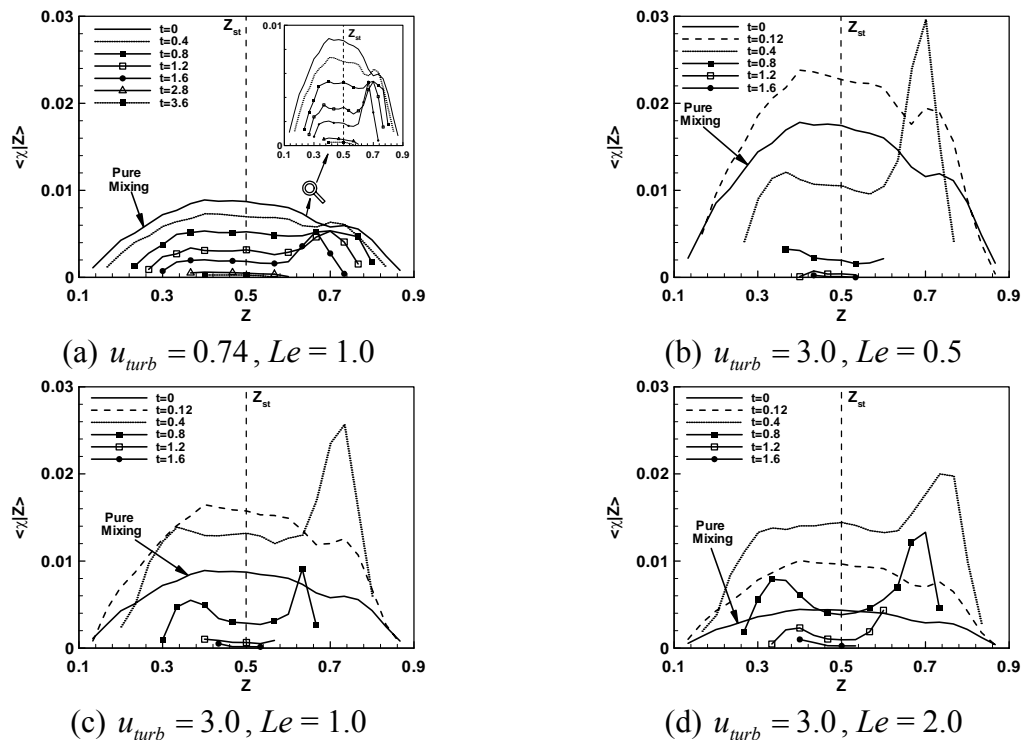


Figure 3-2 DNS conditional means of the scalar dissipation rate for different cases

Conditional Means of the Temperature and the Mass Fractions

Figure 3-3, Figure 3-4, and Figure 3-5 show the temporal evolution of the conditional means of the temperature, the fuel mass fraction, and the oxidizer mass fraction profiles, respectively, in the mixture fraction space for the different cases considered. Note that at time equal to zero, the profile corresponds to pure mixing conditions, which also corresponds to the initial state of the mixture. In the present problem, the pure mixing profile for the

conditional means of the temperature corresponds to a negative-slope linear curve. The linear correlations of the initial temperature with the mixture fraction are consistent with the initialization prescribed in Eq. (3-24), which prescribes the preheated oxidizer at lower values of the mixture fraction and cooler mixtures as the mixture fraction approaches unity.

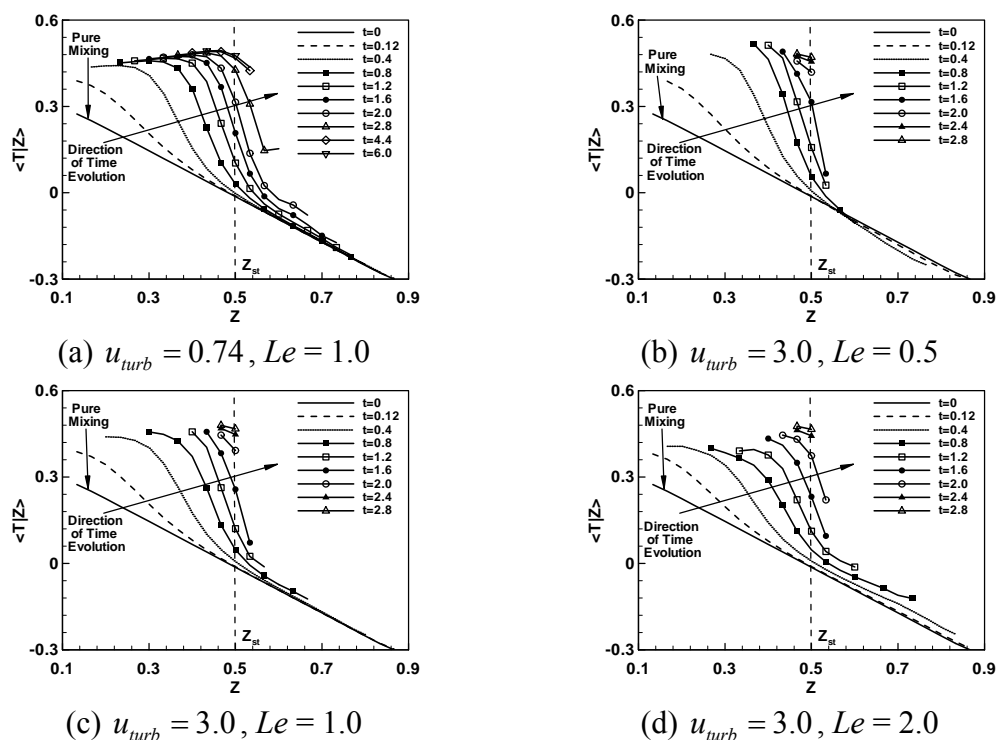


Figure 3-3 DNS conditional means of the temperature for different cases

A similar trend has been observed in the conditional means of the fuel and the oxidizer mass fractions for the different cases considered here. The onset of combustion is characterized by the departure of temperature from the linear profile in the mixture fraction space. Because the oxidizer is preheated, the first departure from the pure mixing profiles occurs at fuel lean conditions, i.e. lower values of the mixture fraction. While leaner mixtures reach their corresponding adiabatic temperature conditions, the next layers of richer mixtures

are ignited, showing an increasing trend for the temperature in time. The corresponding values of the fuel and the oxidizer mixture fraction indicate a depletion of the fuel for mixture fractions below the stoichiometric value of 0.5 and a depletion of the oxidizer at mixture fractions higher than the stoichiometric value. In both conditions, the deficient reactant is depleted; while the excess reactants occupy a new linear curve in the mixture fraction space corresponding to equilibrium conditions with the products. The trend in time clearly indicates a transition from predominantly lean burning at earlier times to rich burning at later times. The highest temperature is achieved at stoichiometric conditions.

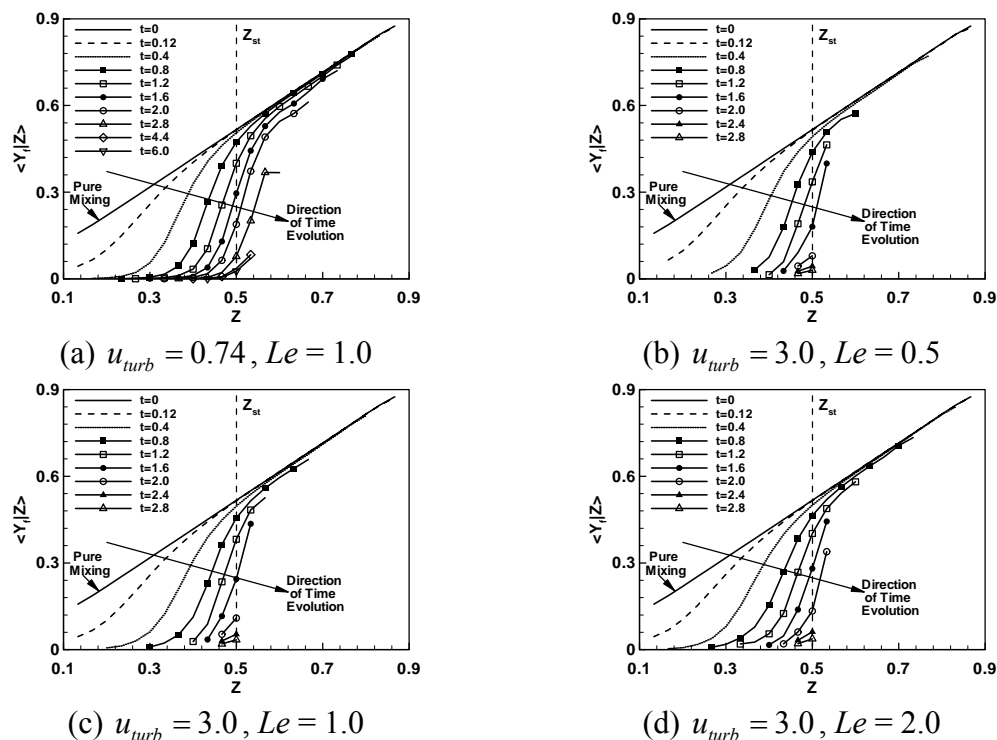


Figure 3-4 DNS conditional means of the fuel mass fraction for different cases

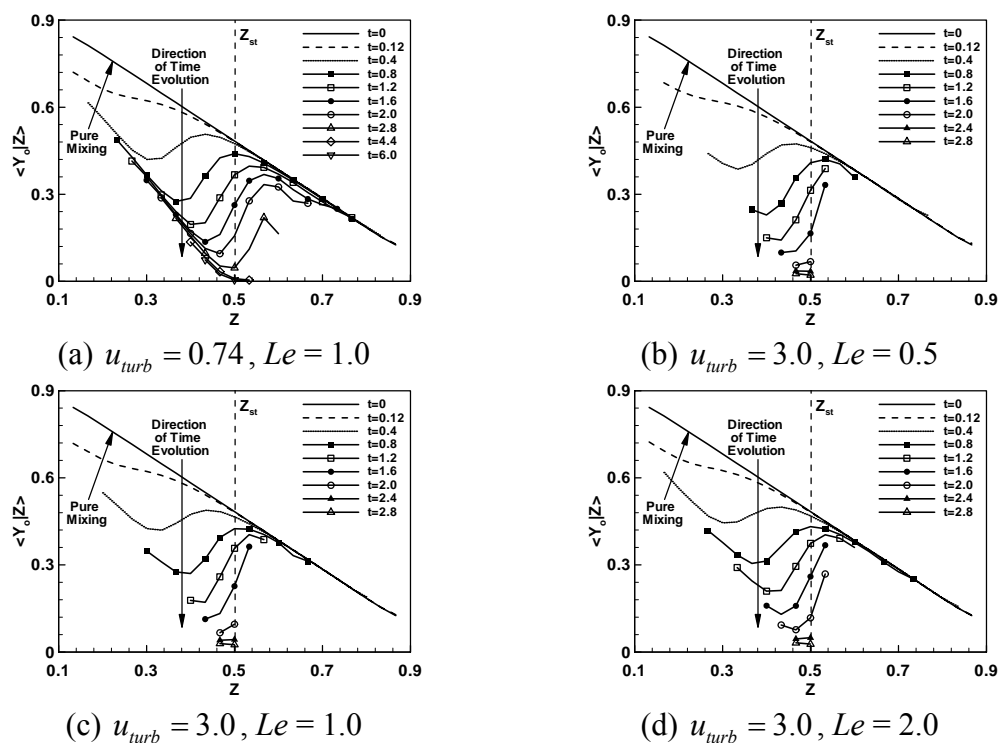


Figure 3-5 DNS conditional means of the oxidizer mass fraction for different cases

Beside the similarities that have been observed in the conditional mean profiles of the temperature and the mass fractions, differences do exist between the low turbulence case and the high turbulence cases, and among cases with different Lewis numbers. Note that we refer to the same time in different cases when we address the effects of turbulence conditions and Lewis numbers. The major effect imposed by the turbulence conditions is that the mixture fraction range corresponding to the conditional means of the temperature and the mass fractions shrinks faster in time (Figure 3-3 (b)–(d), Figure 3-4 (b)–(d), and Figure 3-5 (b)–(d)) at higher turbulence conditions. This is the expected role of turbulent mixing, which results in turbulent scalar transport. The Lewis number effects contribute to the conditional statistics of reactive scalars in two major aspects. Higher Lewis numbers correspond to lower

mass diffusivities compared to the energy transport. This has two consequences. First, the scalar molecular mixing rate is lower, which results in a wider mixture fraction range. Second, because the scalar gradients are higher, the size of the kernels will be smaller. Thus, the heat loss of the kernels is higher, which results in a lower magnitude of the conditional means of the temperature. Consequently the fuel and the oxidizer are consumed less.

Conditional Means of the Reaction Rate

Figure 3-6 shows the temporal evolution of the conditional means of the reaction rate profiles in the mixture fraction space for the different cases considered. The transition in combustion from lean to rich conditions is clearly illustrated in the conditional mean profiles of the reaction rate for the low turbulence case shown in Figure 3-6 (a1) and (a2). An initially single peak of the reaction rate ‘propagates’ from lean mixture fractions at early times to richer conditions at later times and the transitions occur at $Z = 0.5$. For cases with high turbulence conditions, the flame kernels exist at only lean conditions and subside near the stoichiometric conditions before they reach the rich conditions. This is due to the fact that scalars mix faster at high turbulence conditions and complete combustion is achieved earlier. Furthermore, the case with Lewis number equal to 2.0 shows a subtle autoignition delay in time compared to other Lewis number cases. This trend may be attributed to the competing rates of chemistry and turbulent mixing. During early times of autoignition, turbulent mixing can result in high local gradients of the mixture fraction, and accordingly high local rates of dissipation, which tend to delay the autoignition process at a number of autoignition kernels. But, as the other autoignition kernels begin to expand, the same process of turbulent mixing

increases the interface between products and reactants, and enhances the volumetric rate of chemistry. Moreover, the conditional means of reaction rate profiles are broader and span a wider mixture fraction range in the high Lewis number case (i.e. $Le = 2.0$), because the mass diffusivity is smaller in this case.

The magnitude of the peak value of the conditional means of the reaction rate decreases with respect to time in each case. This trend reflects the role played by the preheating of the oxidizer. In actual fuels, both preheating and stoichiometry may play an important role in the rate of reaction and heat release. Furthermore, Lewis number affects the magnitude of the reaction rate. In the high turbulence case with a high Lewis number, the scalar gradients are higher due to a smaller mass diffusivity. As a result, the kernel sizes are smaller and heat loss is higher. As a consequence, the temperature is lower in this case, but the fuel and the oxidizer mass fractions are higher. However, the magnitude of the reaction rate has an exponential dependence on the temperature and only a linear dependence on reactants' mass fractions. Therefore, the magnitude of the conditional means of the reaction rate is lower in this case.

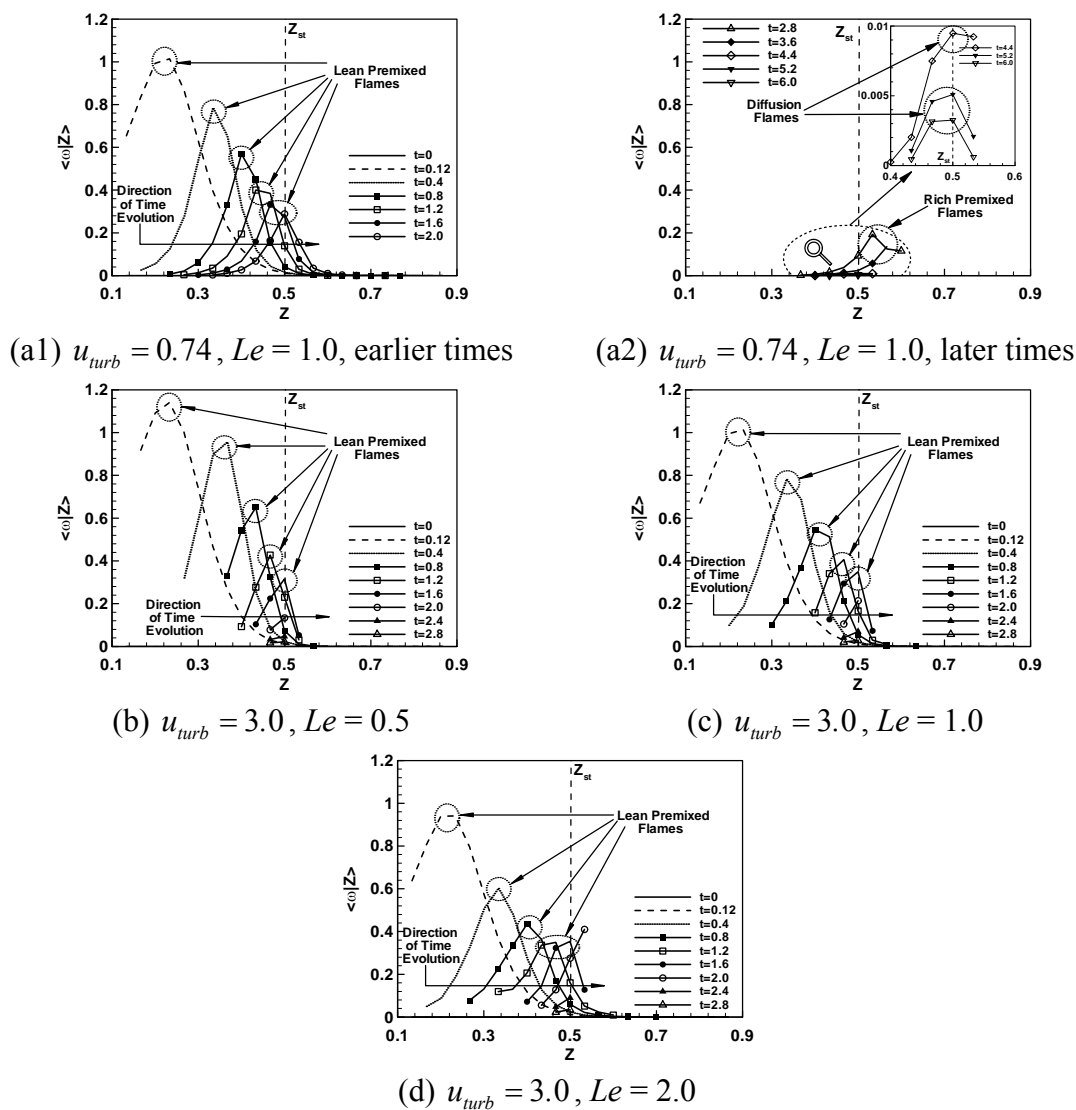


Figure 3-6 DNS conditional means of the reaction rate for different cases

In addition to flame propagation, three different burning modes are observed for the low turbulence case, and they are clearly shown in Figure 3-6 (a1) and (a2). Those burning modes are lean premixed, rich premixed, and non-premixed combustion. The premixed flames are indicated by the shifting peaks in the conditional means of the reaction rate. On the other hand, the non-premixed flame is characterized by a single fixed peak of the reaction

rate around the stoichiometric conditions. This peak is visible at later times as shown in Figure 3-6 (a2). The diffusion and rich premixed flames are an order of magnitude lower than the lean premixed flames. The reduced rates of reaction also results in the relatively long periods of time associated with fuel-rich combustion in contrast with fuel-lean combustion. Furthermore, only one burning mode exists in the high turbulence cases shown in Figure 3-6 (b), (c), and (d). The rich premixed burning mode and the diffusion flame are absent because chemical reaction occurs so fast that fuel and the oxidizer are depleted even before the kernels reach the rich conditions.

3.7.2 Conditional Co-Variance

Conditional RMS of the Scalar Dissipation Rate

Figure 3-7 shows the temporal evolution of the conditional RMS of the scalar dissipation rate profiles in the mixture fraction space for the different cases considered. By comparing Figure 3-7 with Figure 3-2, the turbulence effects and the Lewis number effects that we have observed from the conditional means of χ are also present in the conditional RMS of χ . Moreover, the magnitude of the conditional RMS of χ is nearly two times the magnitude of the conditional means of χ , reflecting the strong spatial variations in the mixture fraction field.

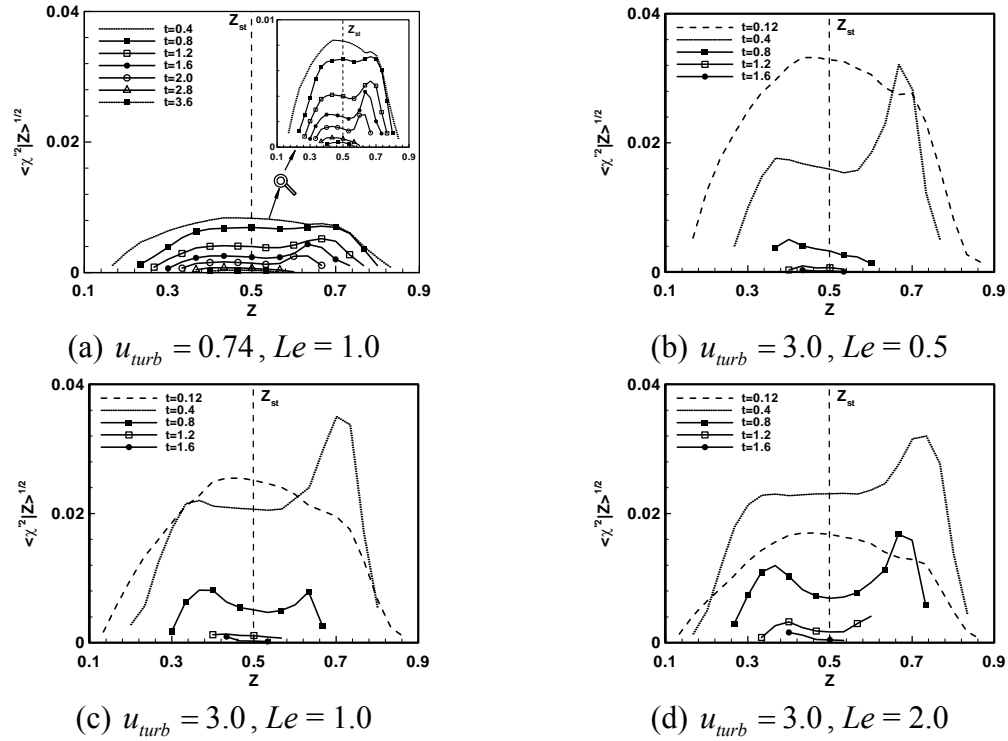


Figure 3-7 DNS conditional RMS of the scalar dissipation rate for different cases

Conditional RMS of the Temperature and the Mass Fractions

Figure 3-8, Figure 3-9, and Figure 3-10 show the temporal evolution of the conditional RMS of the temperature, the fuel mass fraction, and the oxidizer mass fraction profiles, respectively, in the mixture fraction space for the different cases considered. Because the conditional RMS of mass fractions follows the same trend as that of the temperature, the following discussion will address primarily the conditional RMS of the temperature; similar conclusions can be drawn for the mass fractions.

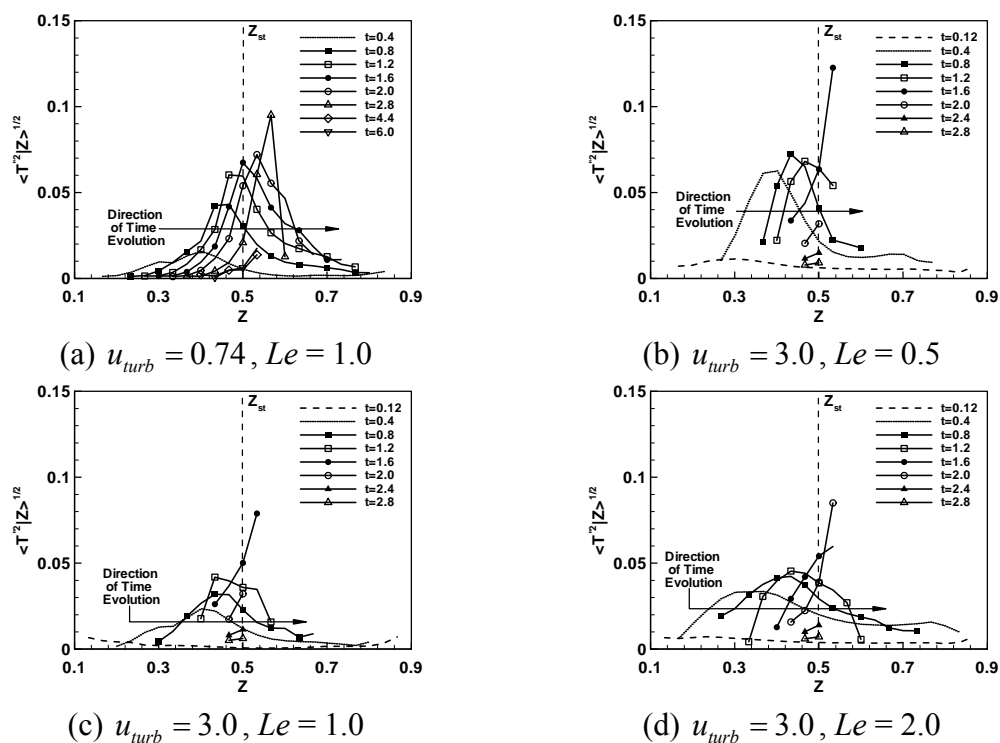


Figure 3-8 DNS conditional RMS of the temperature for different cases

For the low turbulence case shown in Figure 3-8 (a), the peaks of the conditional RMS of the temperature shift from locations corresponding to low mixture fraction values to locations corresponding to high mixture values as flame propagates from fuel-lean to richer mixtures. The fluctuations of the temperature during rich premixed burning are larger compared to lean premixed burning. For the high turbulence cases, the peaks of the conditional RMS of temperature exist at the lean premixed burning side except for time equal to 1.6 for cases with Lewis numbers of 0.5 and 1.0 and for time equal to 2.0 for the case with Lewis number equal to 2.0. At those times, the peaks appear at the rich premixed side and rapidly diminish near the stoichiometric mixture conditions. This is due to the fact that the complete burning is achieved earlier before any transition to burning at fuel-rich conditions

occurs. Furthermore, the mixture fraction range shrinks faster in the high turbulence cases than in the low turbulence case because of the high scalar mixing rate associated with high turbulence intensities.

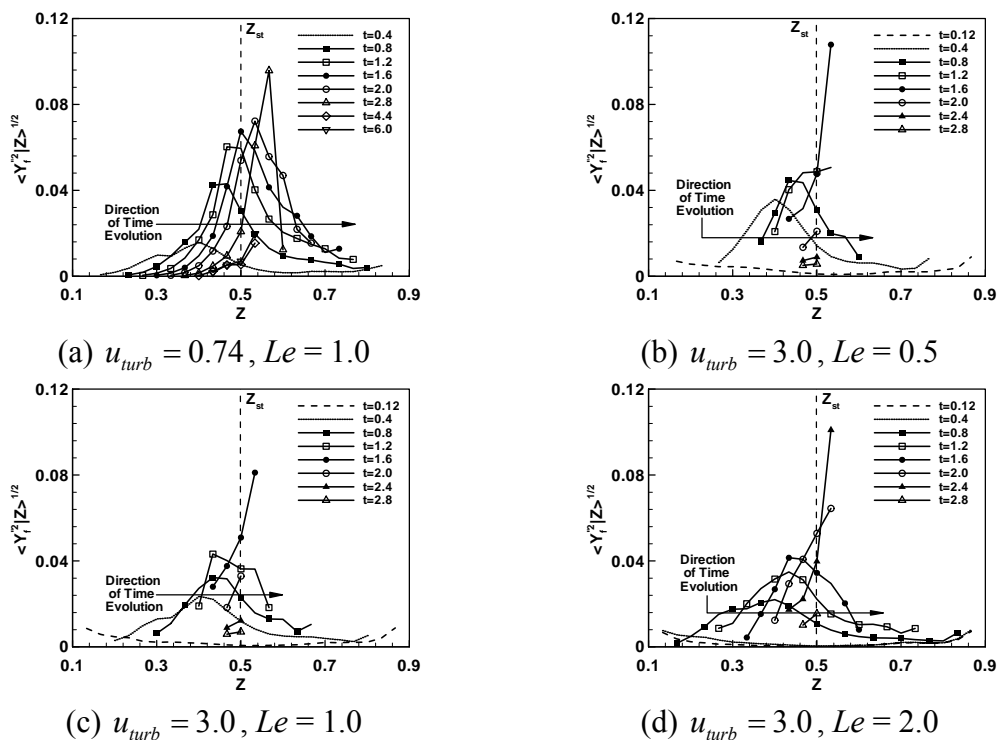


Figure 3-9 DNS conditional RMS of the fuel mass fraction for different cases

Moreover, the overall magnitude of temperature fluctuations shown in the temporal snapshots is a significant fraction of the mean temperature range. Therefore, temperature fluctuations during the autoignition process can not be ignored in any model of autoignition in non-homogeneous mixtures given the strong non-linear dependence of chemical source terms on temperature. In the low turbulence case, the peak at the stoichiometric mixture fraction is formed at the later stage of burning due to the burning of excess fuel and oxidizer from either side of the stoichiometric mixture fraction in the diffusion flame mode.

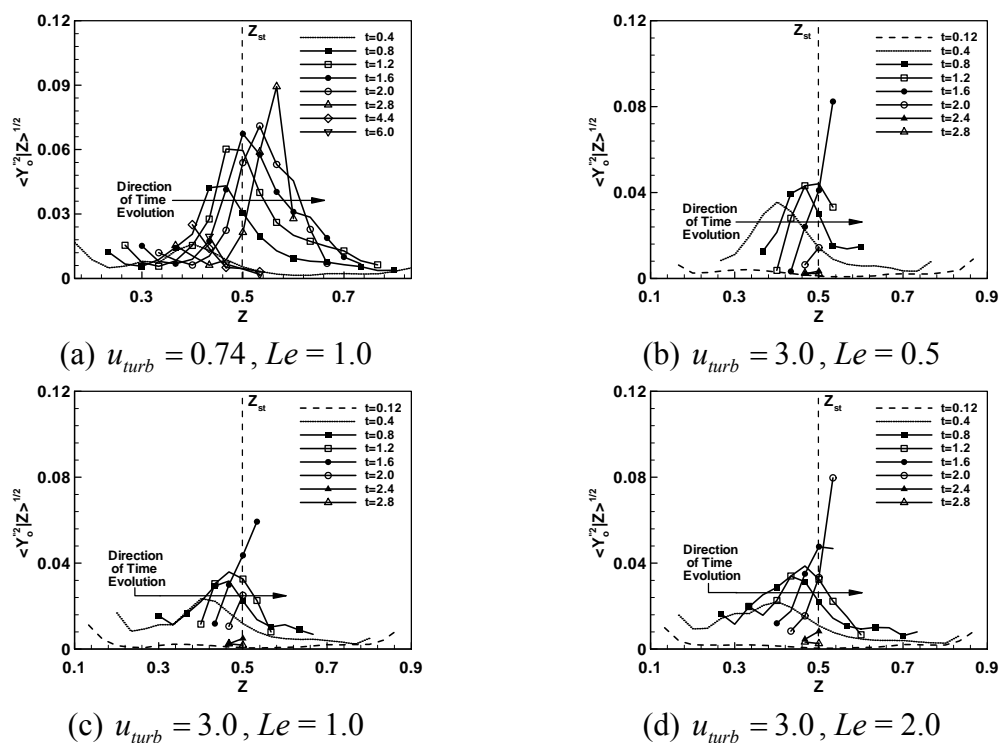


Figure 3-10 DNS conditional RMS of the oxidizer mass fraction for different cases

Lewis number effects are also present in the conditional RMS of the temperature. By comparing high turbulence cases (i.e. Figure 3-8 (b), (c), and (d)), we can see that the mixture fraction range corresponding to the conditional RMS of the temperature is wider for the case with Lewis number equal to 2.0. This is due to a smaller mass diffusivity and a smaller scalar mixing rate associated with the high Lewis number. Moreover, the magnitude of the fluctuations of the temperature is smaller for the case of Lewis number equal to 2.0 because the magnitude of the reaction rate is smaller in this case.

3.7.3 Conditional Variances

In this section, we investigate the evolution of the correlation of reactive scalars with the dissipation rate. To help us to understand this correlation, two reference problems are reviewed first for comparison with our present calculations. In both cases, the mixture fraction fields evolve the same way in the absence of density and transport property changes due to heat release. However, species mass fraction profiles and temperature profiles are expected to evolve differently for the reacting from the non-reacting case.

The first reference problem corresponds to pure mixing without chemistry, in which the initial velocity and mixture fraction fields are identical to the present study, but chemistry is turned off. Figure 3-11 shows the correlation between the conditional means of the temperature and the scalar dissipation rate, R_{T_x} , as a function of the mixture fraction for a low turbulence condition at different times of the scalar field evolution for the non-reacting case. The figure shows that the temperature and the scalar dissipation are fully correlated at mixture fractions near 0 and 1; the correlation is primarily due to the initialization of the mixture fraction field where these conditions represent local peaks, and therefore conditions of zero dissipation rates. Outside these limits, there is no correlation between the temperature and the dissipation rate for the times considered. The same results are found at later times. Therefore, the pure mixing computation shows that in the absence of chemistry, the temperature and the dissipation rate fields are not correlated, except where initial conditions dictate the nature of the correlation.

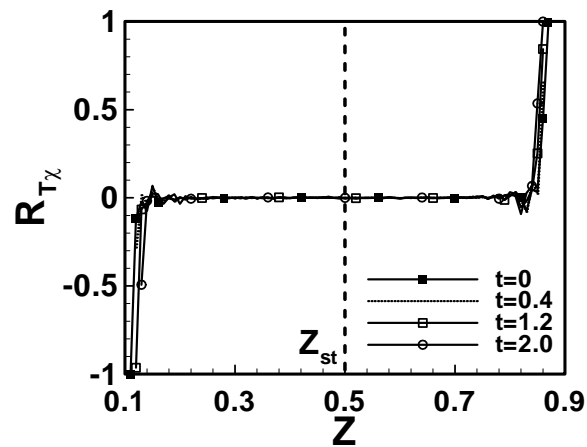


Figure 3-11 Conditional profiles of the variance of the temperature and the dissipation rate for pure mixing

The second reference problem corresponds to the case of autoignition in fully-segregated mixtures, such as the cases obtained using the slab model for the mixture fraction field (Mastorakos and Bilger, 1998). For this problem, a correlation between the temperature and the dissipation rate (Figure 3-12) show a positive correlation with a local peak for rich mixtures and negative correlations with a local minimum for lean mixtures. The overall shape of the correlations remains essentially the same over the course of the evolution of the autoignition process and the peak and minimum values of the correlations do not shift significantly in time. Both correlations for the pure mixing problem and the non-premixed autoignition problem will be compared to the findings based on the present configuration. We will also attempt to explain the mechanisms by which positive and negative correlations between the temperature and the dissipation rate are generated.

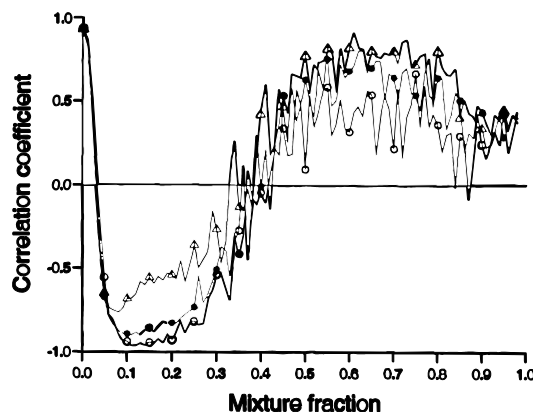


Figure 3-12 The correlation coefficient between the temperature, T , and the scalar dissipation rate, χ , for the homogeneous burning case at different times (Mastorakos *et al.*, 1998)

Correlation between the Temperature and the Scalar Dissipation Rate

In contrast to the reference problems, the conditional correlation between the temperature and the scalar dissipation rate in the present study exhibits different trends. Figure 3-13 shows the results in the present reacting computation for the different cases considered. Although the shapes of the correlation coefficient are similar to that obtained by Mastorakos and Bilger (1998), which shows a leading peak (positively correlated) and a trailing minimum (negatively correlated) around conditions of maximum chemical activity, the optimum values of the correlation functions in our present work shift towards richer conditions, a trend consistent with the shift of chemical activity from lean to rich mixtures. Because the flame takes longer to propagate and the reaction sustains longer in the low turbulence case, Figure 3-13 (a1) only shows the correlation between the temperature and the scalar dissipation rate at earlier stages of burning. The later burning stages are shown in

Figure 3-13 (a2). In all the high turbulence cases, the stages of burning are plotted in the same plot. Figure 3-13 (b), (c), and (d) show the correlation between the temperature and the scalar dissipation rate with Lewis numbers equal to 0.5, 1.0, and 2.0, respectively.

In all the cases, the peaks continue to shift from lean to rich conditions, and eventually diminish when the reaction subsides. Once the combustion process subsides, the pure mixing statistics are recovered with zero correlation functions in the wake of the burning conditions. The pure mixing statistics is reflected by the behavior of these correlations at lean mixture conditions and in the gap separating the stoichiometric conditions and the rich burning conditions at later times in the simulations. In summary, the peaks present in the positive and negative correlations track closely the active combustion regions in the mixture fraction space.

There are some differences in the correlation terms between the high turbulence cases and the low turbulence case. The low turbulence case exhibits a stronger correlation than the high turbulence cases. This can be observed by comparing Figure 3-13 (a) with Figure 3-13 (b), (c), and (d). The magnitude of the correlation term is higher in the low turbulence case than in the high turbulence cases. Furthermore, the transition of the correlation profiles is continuous and the correlation profiles have a clear shape in the low turbulence case. The reason is due to the competing rates of turbulent mixing and chemistry, which are affected significantly by turbulence conditions. In the low turbulence case, the turbulent mixing rate is slow and the correlation between the temperature and the scalar dissipation rate is higher; on the other hand, in the high turbulence cases, the turbulent mixing is very high, thus, the

correlation is much weaker. This is also consistent with what we have observed from the first reference problem. Moreover, the correlation term in the high turbulence case with Lewis number equal to 2.0 spans a wider mixture fraction range due to a smaller mass diffusivity and a smaller scalar mixing rate.

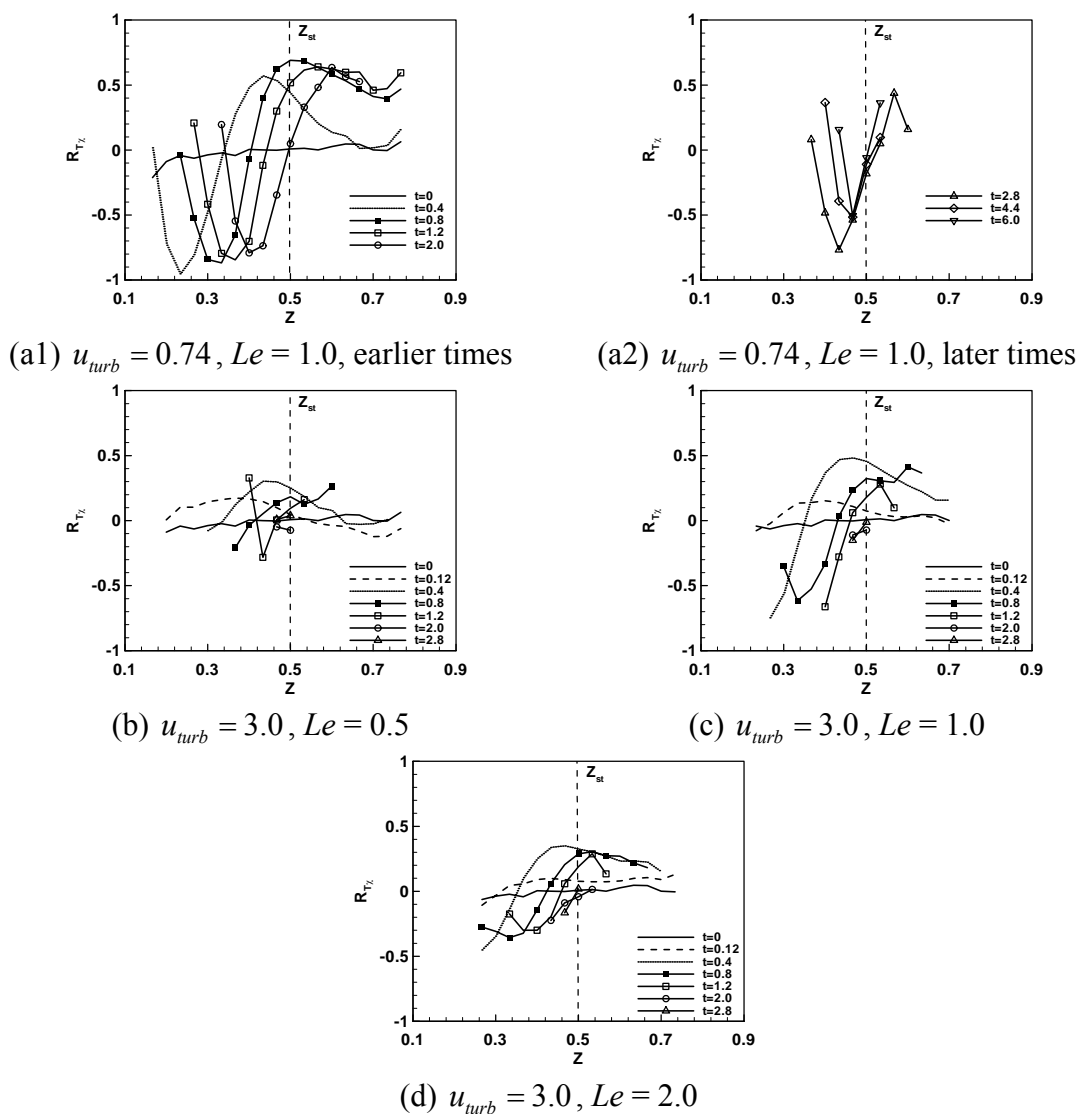
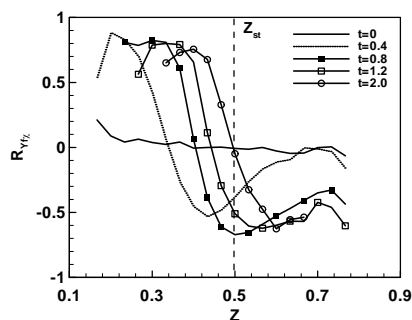
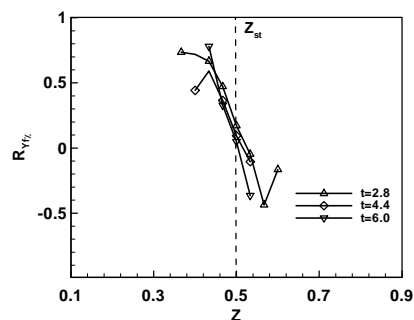


Figure 3-13 DNS conditional profiles of the variance of the temperature and the dissipation rate

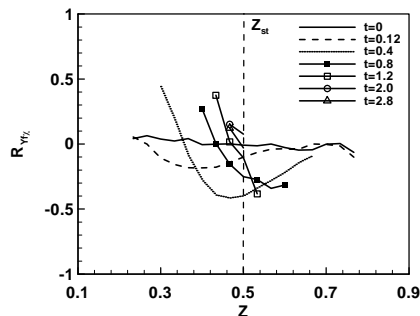
Correlation between the Mass Fractions and the Scalar Dissipation Rate



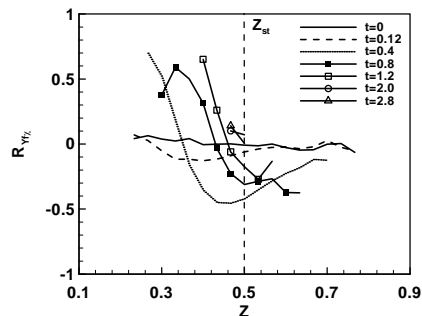
(a1) $u_{turb} = 0.74$, $Le = 1.0$, earlier times



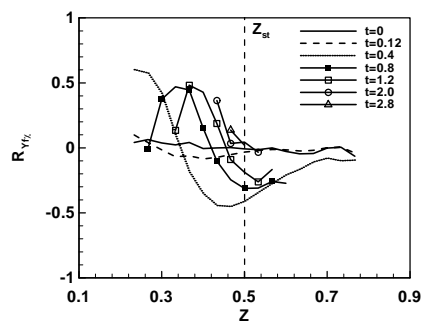
(a2) $u_{turb} = 0.74$, $Le = 1.0$, later times



(b) $u_{turb} = 3.0$, $Le = 0.5$



(c) $u_{turb} = 3.0$, $Le = 1.0$



(d) $u_{turb} = 3.0$, $Le = 2.0$

Figure 3-14 DNS conditional profiles of the variance of the fuel mass fraction and the dissipation rate

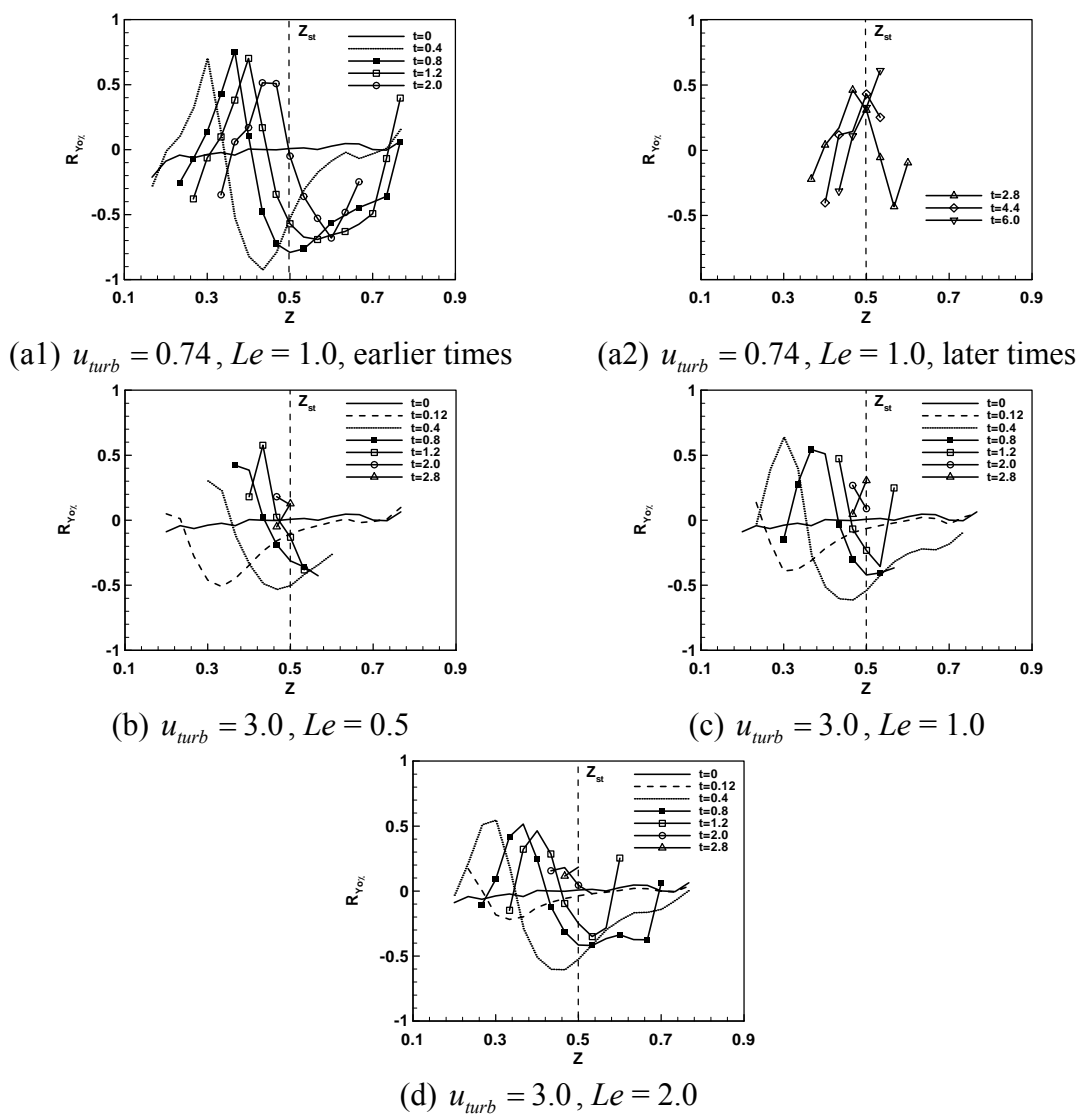


Figure 3-15 DNS conditional profiles of the variance of the oxidizer mass fraction and the dissipation rate

Figure 3-14 and Figure 3-15 show the correlation coefficients of the fuel and the oxidizer mass fraction with the scalar dissipation rate, respectively, for the different cases considered. These correlations are opposite in sign to that of the temperature-scalar dissipation correlation; the fuel and the oxidizer are depleted while the temperature is

increased. Moreover, they also feature a shift of the peaks from lean to rich conditions. Similar to the correlation between the temperature and the scalar dissipation rate, the correlation term for the low turbulence case is also stronger. At high turbulence conditions, the mixture fraction range is also wider in the case with Lewis number equal to 2.0 due to a smaller scalar mixing rate.

3.7.4 The Progress Variable as a Second Conditioning Variable

The transient evolution of singly-conditioned moments underscores the importance of adequately predicting the transitions in burning modes from lean premixed flames to rich premixed flames and the combustion in non-premixed mode. The transient evolution is also characterized by propagation in both physical and phase spaces, and is found in both the first and the second order conditional statistics of passive and reactive scalars. Therefore, a critical modeling element of tracking the transition in combustion modes is still needed with a higher order conditioning. As stated earlier, an alternative strategy to the higher order conditioning is multiple conditioning. Would the choice of a second conditioning variable, which measures the progress of transition in combustion modes, address the principal deficiency, which cannot be addressed with the higher order modeling? The results presented so far suggest the following facts.

In the premixed modes, the mixture exhibits three potential states: an unburned, a burned, and a transition mixture state. Both burned and unburned states are consistent with pure mixing statistics at conditions of the burned and unburned mixture, respectively; while

the transition state corresponds to active burning, and covers a range of mixture fractions. The extent of this range is primarily governed by the extent of stratification of the mixture and the dissipation rate field, which may allow conditions of burning to occur at different mixture conditions at the same time. A secondary diffusion branch is present once the transition to rich premixed burning occurs. Burning in the diffusion flame is relatively slow and insignificant relative to the burning in premixed modes.

A reaction progress variable can provide a measure for the evolution of the transition zone, and therefore a mechanism for tracking the ‘propagation’ of burning in the mixture fraction space. Sensible enthalpy or reduced temperature has been applied by Bilger (1992) and Kronenburg (2004). A reaction progress variable can potentially distinguish the unburned and burned mixture states as well as the transition states. In this section, we provide a preliminary assessment of the addition of a second conditioning variable, which in the present problem is the progress variable, c . The progress variable is expressed as

$$c = \frac{T - T_u(Z)}{T_b(Z) - T_u(Z)} \quad (3-37)$$

In this expression, c , represents a temperature normalized using the unburnt and burned (equilibrium) temperatures, T_u and T_b , which are prescribed for the same mixture fraction. Therefore, the two temperatures are prescribed a priori and correspond to the asymptotic values at a given mixture fraction between pure mixing (initial conditions) and final burned mixtures (the maximum temperatures achieved for a given Z). The value of c varies between 0 and 1 for any given mixture fraction during the autoignition process.

Figure 3-16 and Figure 3-17 show scatter plots of the fuel mass fraction and the reaction rate as a function of the reaction progress variable, c , at different times of the autoignition process and for a narrow range of the mixture fractions between 0.495 and 0.505. Please note that the fuel mass fraction and the reaction rate shown in Figure 3-16 and Figure 3-17 are already singly-conditioned upon values of the mixture fraction. The extent of the scatter of the reactive scalars as a function of the progress variable provides an indication of the value of second conditioning using the progress variable, c .

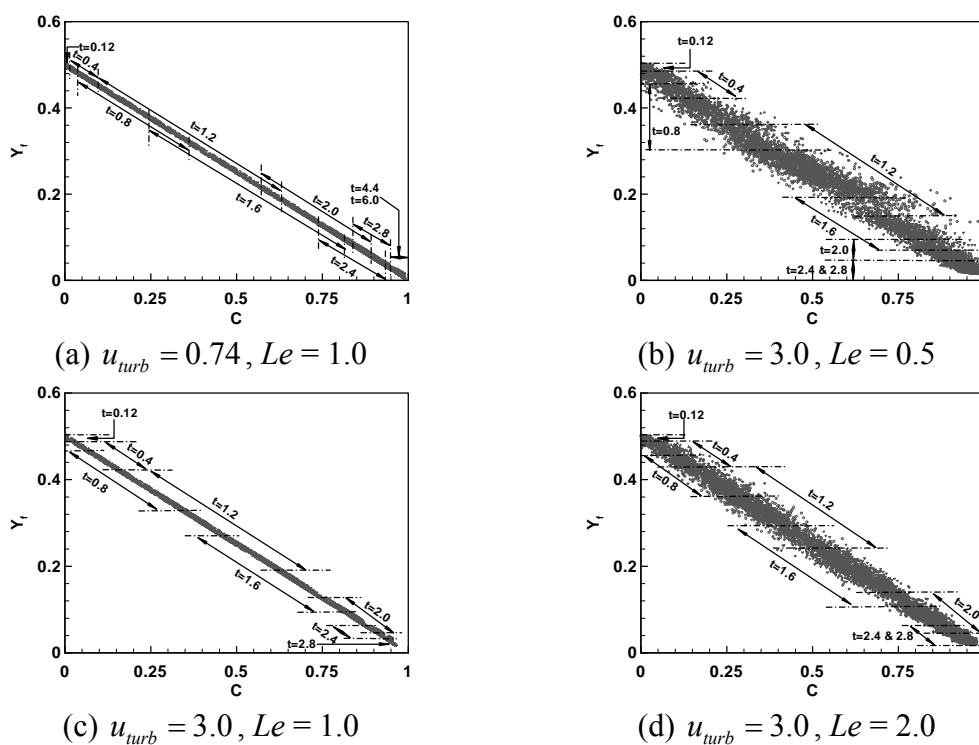


Figure 3-16 Scatter plot of the fuel mass fraction at different times vs. the reaction progress variable, c , for a range of mixture fractions between 0.495 and 0.505

We can see from the Figure 3-16 and Figure 3-17 that a considerable overlap of the scatter points corresponding to different times of the autoignition process is only present in

unity Lewis number cases at both low and high turbulence conditions. In the unity Lewis number cases, the degree of scatter is relatively narrow compared to the conditional mean value. Despite the presence of this scatter, the results clearly show that a coherent correlation for the reactive scalars at different times as a function of the progress variable, c . Both profiles of the fuel mass fraction and the reaction rate for unity Lewis number cases closely follow the autoignition profiles of a homogeneous mixture in the progress variable space. Because of similarities of the governing equations between the reactants' mass fractions and the temperature, the profiles of the reactants' mass fraction as a function of the progress variable are linear. The magnitude of the reaction rate and its shape are governed by the relative composition of the fuel and the oxidizer and the preheating effect. The shape of the reaction rate is determined by the pre-exponential term represented by the reactants' mass fractions and the exponential term, which contains the explicit contribution of the temperature. The rates of reaction at earlier ($c = 0$) and later times ($c = 1$) approach zero because either the temperature is low or the reactants are depleted, respectively.

However, in non-unity Lewis number cases, the overlap of the scatter points corresponding to different times of the autoignition process is not clear and the degree of scattering is more pronounced. Therefore, the results from non-unity Lewis number cases suggest that the correlation between the reactive scalars at different times as a function of the process variable is not valid. In order to arrive at a conclusion, let us examine another set of results.

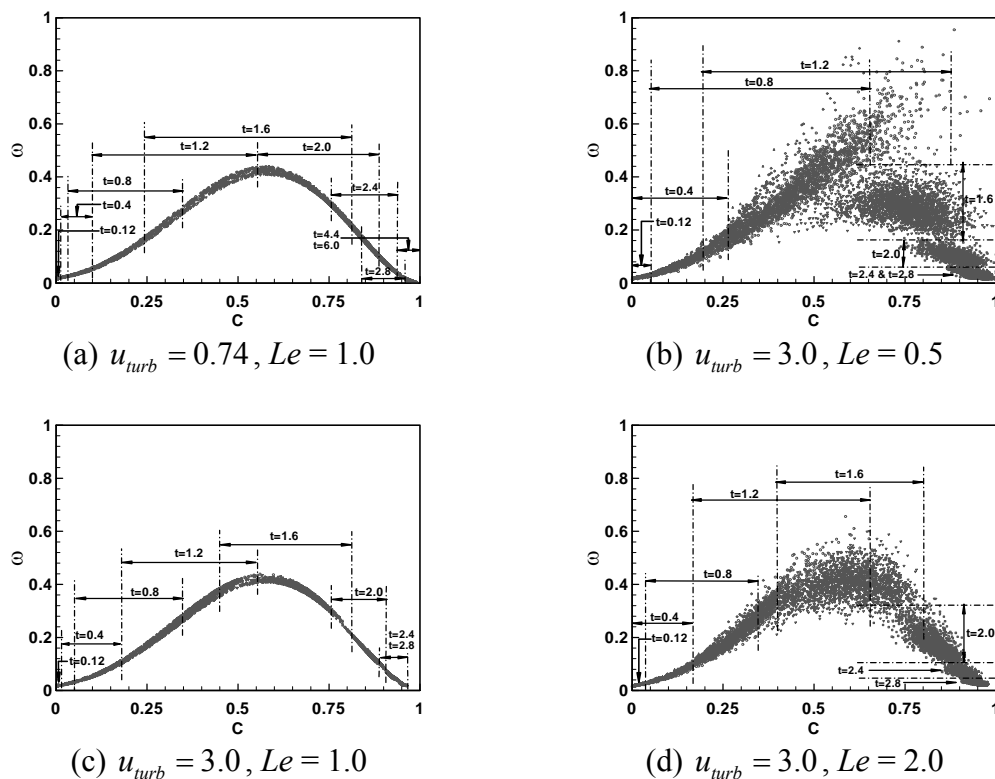


Figure 3-17 Scatter plot of the reaction rate at different times vs. the reaction progress variable, c , for a range of mixture fractions between 0.495 and 0.505

Figure 3-18 and Figure 3-19 show the scatter plots of the same variables for a range of the mixture fractions between 0.595 and 0.605. In Figure 3-18 and Figure 3-19, the scatter points are not present at high progress variable values, because these values correspond to a completion of the combustion process. We can see from those figures that the correlation between the reactive scalars and the progress variable is only valid for cases with unity Lewis numbers. Therefore, within the context of the present chemical model with the simplified mixture and flow configuration, in unity Lewis number cases, a second conditioning variable based on the progress variable offers a reasonable prediction of scalar statistics over the

entire period of the autoignition process. However, in non-unity Lewis number cases, a second conditioning variable is not sufficient.

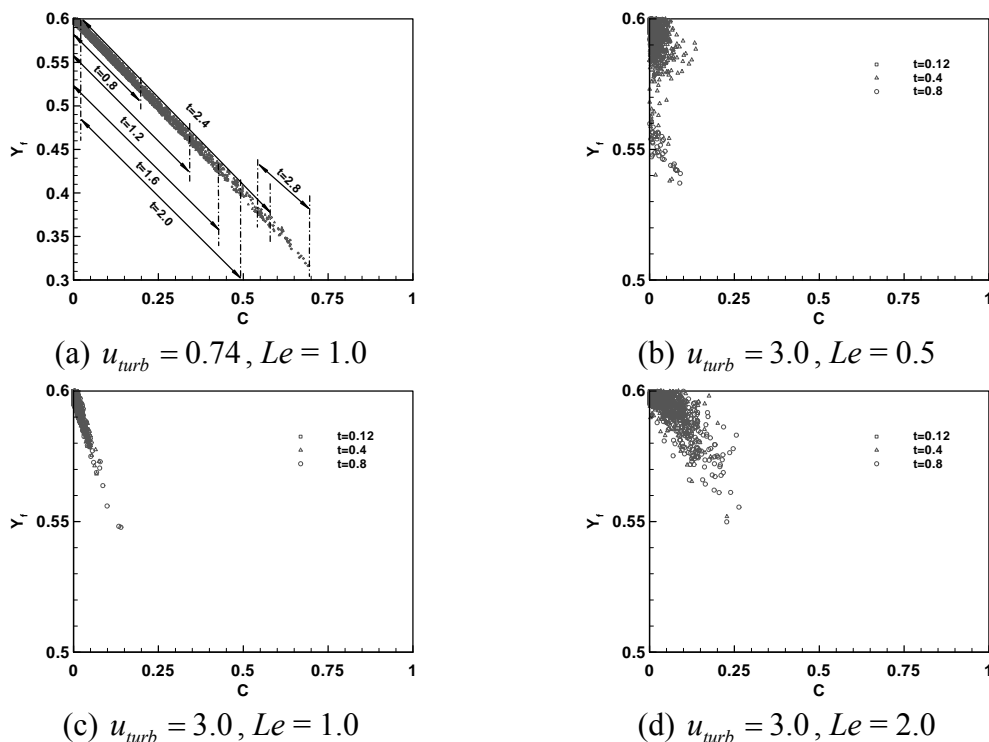


Figure 3-18 Scatter plot of the fuel mass fraction at different times vs. the reaction progress variable, c , for a range of mixture fractions between 0.595 and 0.605

A model that includes the progress variable in addition to the mixture fraction as measures of the progress of chemistry during the autoignition process has been proposed recently by Tap *et al.* (2004). The model is presented in the context of the flamelet approach. It represents the mean heat release rate in terms of the product of a generalized flame surface density and a generalized surface average of the reaction rate. A principal assumption of the model is that the surface average of the reaction rate can be uniquely expressed in terms of a generalized progress variable, which can be evaluated using the laminar autoignition data.

Therefore, the model by Tap *et al.* (2004) does not contain any conditioning with respect to local mixture fractions or progress variables as presented here. Therefore, it also does not explicitly or implicitly account for the potentially non-linear effects of fluctuations of these local quantities on the chemical source terms. Moreover, the non-unity Lewis number cases were not addressed by the author and the validation of the model is not performed for non-unity Lewis number cases. From the results obtained from the present study on the different turbulence cases with different Lewis numbers, we can see that a second conditioning variable is not sufficient for the non-unity Lewis number cases.

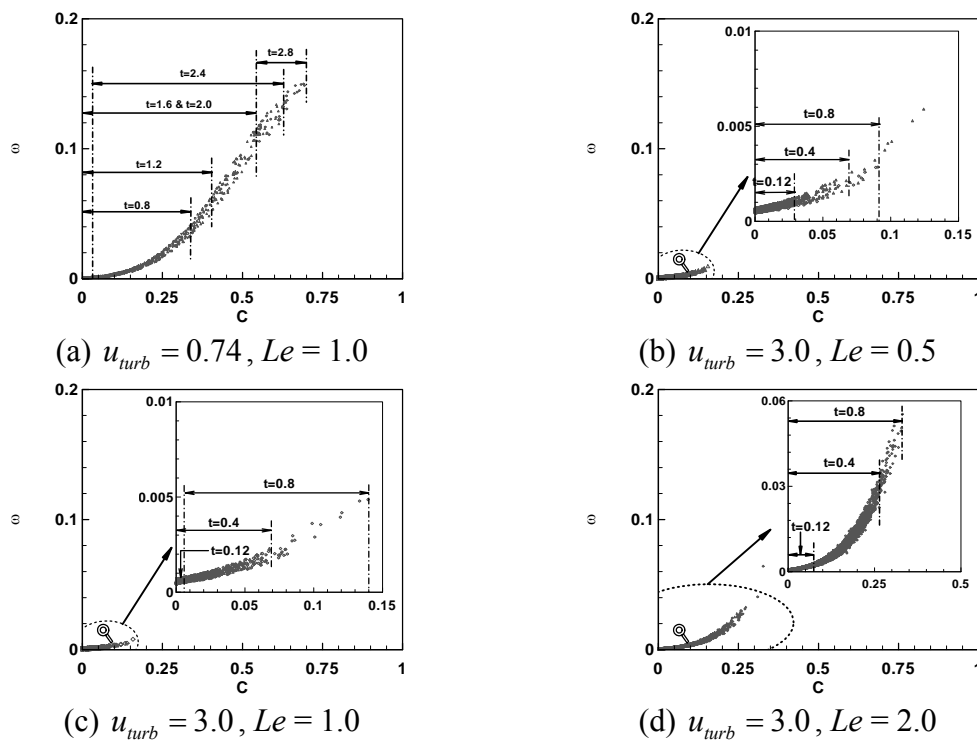


Figure 3-19 Scatter plot of the reaction rate at different times vs. the reaction progress variable, c , for a range of mixture fractions between 0.595 and 0.605

3.8 Conclusions

We have studied the autoignition process in non-homogeneous mixtures in isotropic turbulence using DNS and simple chemistry. The turbulence intensity plays an important role in the evolution of autoignition in non-homogeneous mixtures, since it affects the competition between mixing and chemistry. Three burning modes exist in the low turbulence case, but only one burning mode exists in the high turbulence cases. Furthermore, Lewis number effects are studied. These effects contribute to the conditional statistics of reactive scalars in two major aspects. Higher Lewis numbers correspond to lower mass diffusivity compared to the energy transport. This has two consequences. First, the scalar molecular mixing rate is lower, which results in a wider mixture fraction range. Second, because the scalar gradients are higher, the size of the kernels will be smaller. Thus, the heat loss of the kernels is higher, which results in a lower magnitude of the conditional means of temperature and reaction rate, and a lower magnitude of conditional RMS of thermo-chemical scalars. Consequently the fuel and the oxidizer are consumed less.

The study attempted to explore the modeling consequences of non-homogenous autoignition using conditional statistics with respect to one conditioning variable, the mixture fraction. The addition of a second conditioning variable, a reduced temperature, is assessed. The results show that there are two distinct burning modes present at various stages of the autoignition process: premixed (lean and rich) and diffusion burning. Both scalar profiles in physical space and conditional statistics in the mixture fraction space indicate clear transitions and ‘propagation’ from predominately lean burning to rich burning due to the

onset of autoignition at the preheated lean mixtures. The presence of these transitions and propagation underscore the transient nature of autoignition in non-homogeneous mixtures, which is also reflected in the conditional statistics. These statistics depart fundamentally from those obtained by using fully segregated mixtures of the fuel and the oxidizer (Mastorakos, 1998 and Sreedhara, 2000). The conditional moments show that the temporally-varying statistics are present in higher conditional statistics; therefore, higher order CMC approach may not adequately address the complexity exhibited by propagation of burning in both the mixture fraction and physical spaces.

In the present problem, we also found that the using of a second conditioning variable, a reduced temperature, yields consistent profiles for unity Lewis number cases during the entire period of the autoignition process. For autoignition processes with non-unity Lewis numbers, more conditioning variables may be needed to represent the flame propagation. More importantly, the addition of a conditioning variable in coarse-grained simulations generally requires the solution of an additional transport equation for that variable.

Finally, we propose the problem of non-homogeneous autoignition as a critical test problem for turbulent combustion models. The autoignition process is inherently transient and may involve important transitions during the evolution of the process in dominant chemistries and burning modes. Moreover, the coupling between chemistry, molecular transport, and turbulent transport is critical to the fate of ignition kernels and the rate of their evolution in physical and phase spaces. The direct numerical simulation data provides us

basis for validation of the model of the hybrid scheme that will be introduced in the rest of the thesis.

Chapter 4 LES-ODT Formulation and Numerical Implementation

4.1 Objectives

The goal of this chapter is to present the formulation and the numerical implementation of the proposed LES-ODT model. The governing equations for both LES and ODT are derived and discussed. A LES-ODT simulation is in fact a hybrid simulation procedure of both a LES code and a set of ODT domains embedded within the LES-computational domain. The simulations are carried out simultaneously, albeit at different time steps associated with the integration of the LES governing equations and the different processes making up the ODT formulation. Because the ODT 1D governing equations are inspired by Navier-Stokes equations, the hybrid scheme can be implemented in different ways and may be carried out with redundancies in the quantities that are transported. The discussion below only refers to one such implementation; while whenever useful, we will discuss alternative coupling strategies between LES and ODT solutions.

ODT contains three key features to simulate turbulent combustion: (1) a representation of 3D turbulent stirring with a stochastic process involving instantaneous mappings along each ODT 1D domain, (2) a representation of the molecular diffusion and reaction processes with deterministic solutions of unsteady reaction-diffusion transport equations along each ODT 1D domain, and (3) a representation of the convection events

along each ODT 1D domain. In the present model, a novel convection scheme denoted as ‘node convection’ and ‘intra-node relaxation’ or ‘co-linear convection’ is proposed and implemented. This convection scheme enables the coupling of the different ODT domains, albeit at their intersections, and the LES solution for momentum. The procedures for coupling LES with ODT in the current work are addressed. The numerical implementation of LES-ODT methodology is examined. The convection scheme is numerically implemented using the total vanishing diminishing (TVD) scheme to enforce scalar boundedness.

4.2 Model Strategy

Figure 4-1 shows a schematic layout of the ODT elements in the x - y plane. ODT elements can be laid on a 3D lattice on LES grids or in between. Fine DNS-like uniform grids are embedded on each ODT element. Solutions for dependent variables u , v , w , T , Y_F , and Y_O at ODT grids are obtained. The ODT nodes are defined as the intersection points of ODT elements in all three directions. In general, ODT nodes can either be at the same location as LES grids or in between. Each node is associated with a continuity cell for which the node convection based on LES interpolated velocity is carried out. In the present study, simulations are carried out in three dimensions.

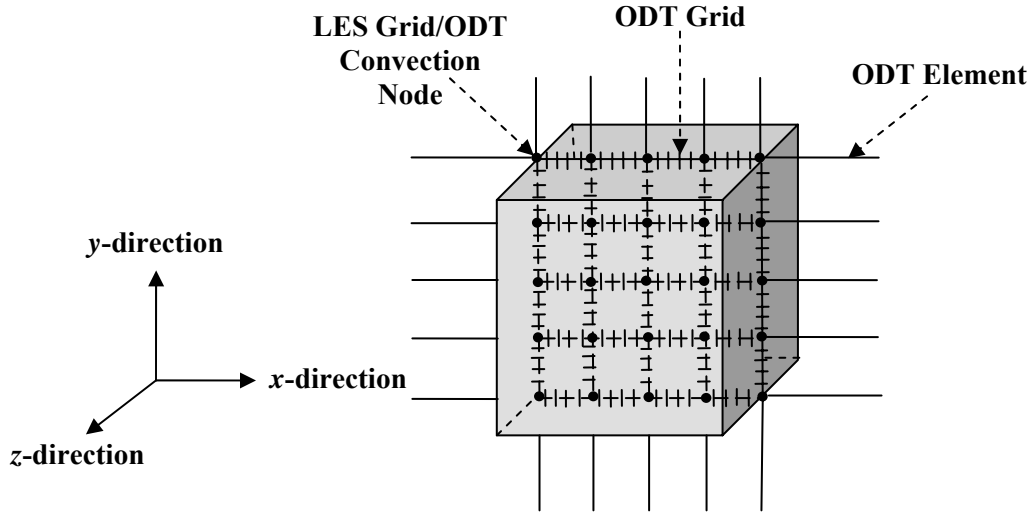


Figure 4-1 Schematic layout of the ODT elements in x-y plane

4.3 The Governing Equations

4.3.1 LES Governing Equations

The LES governing equations are obtained by performing the filtering operation on the transport equations for scalars and momentum. These equations serve as the basis of LES-ODT model formulation and can be used for variable density as well as constant density flows. The equations are given as

Continuity:

$$\frac{\partial \bar{\rho}}{\partial t} + \frac{\partial \bar{\rho} \tilde{u}_i}{\partial x_i} = 0 \quad (4-1)$$

Conservation of Momentum:

$$\bar{\rho} \frac{\partial \tilde{u}_i}{\partial t} = \frac{\partial \bar{\tau}_{i\eta}}{\partial \eta} + \frac{\partial}{\partial x_j} \left[\bar{\rho} (\tilde{u}_i \tilde{u}_j - \tilde{u}_i \tilde{u}_j) \right] + \left\{ -\frac{\partial \bar{P}}{\partial x_i} - \bar{\rho} \tilde{u}_j \frac{\partial \tilde{u}_i}{\partial x_j} + \frac{\partial \bar{\tau}_{i1}}{\partial x_1} + \frac{\partial \bar{\tau}_{i2}}{\partial x_2} \right\} \quad (4-2)$$

Conservation of Energy:

$$\begin{aligned} \bar{\rho} \frac{\partial \tilde{T}}{\partial t} = & \frac{1}{c_p} \frac{\partial \bar{P}}{\partial t} + \frac{1}{c_p} \frac{\partial \bar{q}_\eta''}{\partial \eta} - \frac{1}{c_p} \overline{\sum_{k=1}^N h_k \dot{\omega}_k} \\ & + \frac{\partial}{\partial x_i} \left[\bar{\rho} (\tilde{u}_i \tilde{T} - \tilde{u}_i \tilde{T}) \right] + \frac{1}{c_p} \left\{ -\bar{\rho} \tilde{u}_i \frac{\partial \tilde{T}}{\partial x_i} + \frac{\partial \bar{q}_1''}{\partial x_1} + \frac{\partial \bar{q}_2''}{\partial x_2} \right\} \end{aligned} \quad (4-3)$$

Conservation of Mass Fractions

$$\bar{\rho} \frac{\partial \tilde{Y}_k}{\partial t} = \frac{\partial \bar{J}_{k,\eta}}{\partial \eta} + \bar{\omega}_k + \frac{\partial}{\partial x_i} \left[\bar{\rho} (\tilde{u}_i \tilde{Y}_k - \tilde{u}_i \tilde{Y}_k) \right] + \left\{ -\bar{\rho} \tilde{u}_i \frac{\partial \tilde{Y}_k}{\partial x_i} + \frac{\partial \bar{J}_{k,1}}{\partial x_1} + \frac{\partial \bar{J}_{k,2}}{\partial x_2} \right\} \quad (4-4)$$

In Eq. (4-2), τ_{ij} is as follows

$$\tau_{ij} = \mu \left[\left(\frac{\partial u_i}{\partial x_j} + \frac{\partial u_j}{\partial x_i} \right) - \frac{2}{3} \frac{\partial u_k}{\partial x_k} \right]. \quad (4-5)$$

In Eq. (4-4), $\bar{J}_{k,i}$ is defined as

$$\bar{J}_{k,i} = \left[\bar{\rho} \left(D_k \frac{\partial \tilde{Y}_k}{\partial x_i} \right) \right]. \quad (4-6)$$

The ‘ \sim ’ in Eqs. (4-1)–(4-4) corresponds to a density weighted (Favre-averaged) filtering of a given quantity, $\phi = \tilde{\phi} + \phi''$, which is expressed by $\tilde{\phi} = \frac{\bar{\rho} \phi}{\bar{\rho}}$. Term $(\tilde{u}_i \tilde{u}_j - \tilde{u}_i \tilde{u}_j)$ in Eq. (4-2)

is the subgrid stresses. Terms $(\tilde{u}_i \tilde{T} - \tilde{u}_i \tilde{T})$ in Eq. (4-3) and $(\tilde{u}_i \tilde{Y}_k - \tilde{u}_i \tilde{Y}_k)$ in Eq. (4-4) are

subgrid fluxes. Those subgrid stresses and fluxes need to be modeled using a subgrid closure model.

4.3.2 ODT Governing Equations

The ODT governing equations provide us necessary guidance to obtain information on physics of turbulence. Formulation of the momentum and scalar equations for each ODT domain is critical to the development of the model. In this section, the transport equations that govern the temporal and spatial evolution of the momentum and the energy on ODT 1D elements are presented. The governing equations are obtained by writing the instantaneous transport equations for scalars and momentum along ODT 1D elements with contributions from LES resolved terms in Eqs. (4-2)–(4-4). Those equations can be used for both variable density and constant density flows.

Conservation of Momentum

$$\rho \frac{\partial u_i}{\partial t} = \left[\frac{\partial}{\partial \eta} \left(\mu \frac{\partial u_i}{\partial \eta} \right) + \Omega_{u_i} \right] + \left\{ -\frac{\partial \hat{P}}{\partial x_i} - \rho \hat{u}_j \frac{\partial u_i}{\partial x_j} + \frac{\partial \hat{\tau}_{i1}}{\partial x_1} + \frac{\partial \hat{\tau}_{i2}}{\partial x_2} \right\} \quad (4-7)$$

Conservation of Energy

$$\rho \frac{\partial T}{\partial t} = \left[\frac{1}{c_p} \frac{\partial P}{\partial t} + \frac{1}{c_p} \frac{\partial \hat{q}_\eta''}{\partial \eta} - \frac{1}{c_p} \sum_{k=1}^N h_k \dot{\omega}_k + \Omega_T \right] + \frac{1}{c_p} \left\{ -\rho \hat{u}_i \frac{\partial T}{\partial x_i} + \frac{\partial \hat{q}_1''}{\partial x_1} + \frac{\partial \hat{q}_2''}{\partial x_2} \right\} \quad (4-8)$$

Conservation of Mass Fractions

$$\rho \frac{\partial Y_k}{\partial t} = \left[\frac{\partial J_{k,\eta}}{\partial \eta} + \dot{\omega}_k + \Omega_{Y_k} \right] + \left\{ -\rho \hat{u}_i \frac{\partial Y_k}{\partial x_i} + \frac{\partial \hat{J}_{k,1}}{\partial x_1} + \frac{\partial \hat{J}_{k,2}}{\partial x_2} \right\} \quad (4-9)$$

In Eqs. (4-7)–(4-9), “ η ” denotes the direction along each ODT element and “ \wedge ” denotes the inverse filtering of LES solutions. In Eqs. (4-7) – (4-9), “ Ω_i ” denotes the stochastic contributions. The terms inside the brackets ‘[.]’ represent contributions from the resolved diffusion terms, the source terms, and the stochastic process along ODT 1D elements. The stochastic contributions represent 3D transport events, including stirring, pressure scrambling, and contributions from fluctuating terms in the different variables. The stochastic contributions are implemented as instantaneous stirring events through triplet maps, which are described in detail in section 4.4. The molecular diffusion and reaction terms are obtained by solving the reaction-diffusion transport equations and will be addressed in detail in section 4.5.

The terms inside the brackets ‘{.}’ represent contributions from unresolved terms along ODT 1D elements and they are obtained from LES simulations. These terms are crucial for momentum and scalar transport between ODT elements. The convection terms are currently implemented as ‘node convection’ at each ODT node and as ‘intra-node relaxation’ or ‘co-linear’ convection along each ODT element. The convection scheme will be examined in section 4.6.

4.4 The Representation of Turbulent Transport in ODT

One of the inherent attributes of turbulence is its 3D nature. In order to capture the 3D turbulent flow structures with 1D line of sight in ODT, each individual eddy turnover, an ‘eddy event’, is emulated through a stochastic process by applying a random, instantaneous

mapping to an interval of the domain corresponding to the range of the stirring motion being represented. The mapping method employed here is known as the ‘triplet maps’ (Kerstein *et al.*, 2001). During each eddy event, a triplet map is followed by kernel transformations to physically represent pressure-induced redistribution of energy among velocity components (Kerstein *et al.*, 2001). Both velocity and scalar fields are modified during an eddy event, which is governed by a distribution function obtained instantaneously from the kinetic energy. In the following discussion, the triplet map, the kernel transformation function, and the eddy rate distribution function are presented.

It is important to note here, that the procedure adopted here to model turbulent transport is essentially the same procedure adopted by Kerstein and co-workers (Kerstein *et al.*, 2001). It is based on the model affectionately called “Neapolitan” ODT by Kerstein and co-workers or “vector ODT”, which involves the transport of the three components of the velocity vector.

4.4.1 The Triplet Map

The triplet map is the simplest of a class of mappings that satisfy the physical requirements of mass, momentum, and energy conservation laws. This means that the all integral properties remain the same before and after employing the triplet mapping. The triplet map (Kerstein *et al.*, 2001) is defined as

$$f(y) \equiv y_0 + \begin{cases} 3(y - y_0) & \text{if } y_0 \leq y \leq y_0 + \frac{1}{3}l \\ 2l - 3(y - y_0) & \text{if } y_0 + \frac{1}{3}l \leq y \leq y_0 + \frac{2}{3}l, \\ 3(y - y_0) - 2l & \text{if } y_0 + \frac{2}{3}l \leq y \leq y_0 + l \\ y - y_0 & \text{otherwise} \end{cases} \quad (4-10)$$

where $f(y)$ is the mapping function, y_0 is the starting location of the eddy, and l is the length scale of the eddy. First, the mapping takes a line segment $[y_0, y_0 + l]$ and compresses it to a third of its original length. Then, the original domain is replaced with three copies of the compressed segments. Thus, the local gradients are increased geometrically and the turbulence cascade is enhanced. At last, the middle copy of the map is reversed and the meanings are twofold. The first meaning is to mimic the rotational folding effect inherent to turbulent flows. The second meaning is to maintain the continuity of the function. The vector and scalar fields outside the selected segment are unaffected. Because the mapping function is continuous, the fluid elements that were close to each other before the mapping are close to each other after the mapping, therefore avoids introducing discontinuity to the vector and the scalar fields. Figure 4-2 is a schematic show of the triplet mapping procedure of compression, copy, and inversion.

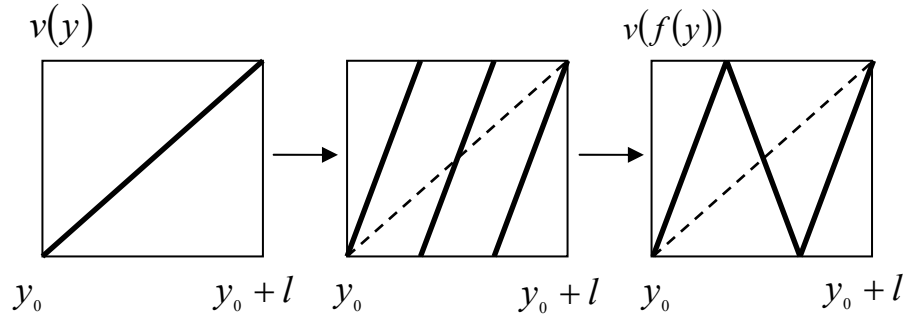


Figure 4-2 The triplet mapping procedure

For the numerical implementation of the triplet map, the number of discrete points spanning the eddy should be a multiple of 3. The discrete mapping formula (McDermott, 2005) is defined as

$$f(j) \equiv j_0 + \begin{cases} 3(j - j_0) & \text{if } j_0 \leq j \leq j_0 + \frac{1}{3}ke \\ 2ke - 3(j - j_0) & \text{if } j_0 + \frac{1}{3}ke + 1 \leq j \leq j_0 + \frac{2}{3}ke \\ 3(j - j_0) - 2ke & \text{if } j_0 + \frac{2}{3}ke + 1 \leq j \leq j_0 + ke + 1 \\ j - j_0 & \text{otherwise} \end{cases}, \quad (4-11)$$

where $f(j)$ is the discrete mapping function, j_0 is the discrete starting location of an eddy, and ke is the discrete eddy size. The eddy length scale is defined as $l = ke \cdot h$. Figure 4-3 shows a schematic of a triplet map event of a vector, $v(y)$, over a segment that is discretized with 9 discrete points. The points before mapping are denoted as diamonds and circles after mapping. The end points of the eddy stay at the same location during triplet mapping, in other words, $f(j_0) = j_0$ and $f(ke) = ke$. Because triplet mapping with eddy size equal to 3 does not change the field, the next available eddy size that is a multiple of 3 is ke equal to 6.

In practice, the smallest turbulence scales should span a range that is larger than this minimum set of grid points (i.e. larger than 6 grid points).

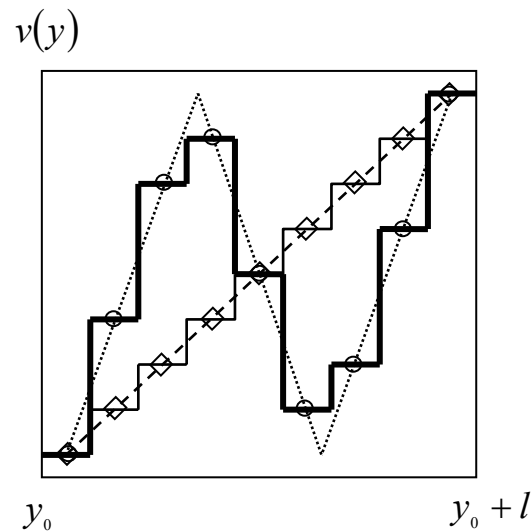


Figure 4-3 The discrete triplet map with $ke = 9$. Dashed line: original line segment; Dotted line: line after triplet mapping. (McDermott, 2005)

4.4.2 The Pressure-Scrambling Model

In the study of buoyant stratified flows, Wunsch and Kerstein (2001) encountered a circumstance under which triplet mapping of the density field alters the total potential energy while leaving the total kinetic energy unchanged. In order to enforce energy conservation, they added a kernel transformation function to the velocity field to allow the transferring of energy on the same length scale as the eddy size. The added kernel transformation term introduces kinetic energy change that balances the total potential energy change and emulates the pressure-velocity interactions.

Kerstein (2001) addressed effects of pressure-induced energy redistribution among velocity components using free shear flows. The study shows that the scheme, which maximizes the inter-component energy transfer during an eddy event, can capture the shear flow structure and fluctuation properties and it generates more accurate results than a model based on equi-partition of turbulent kinetic energy on an eddy-by-eddy basis.

In the present study, the velocity in ODT is treated as a three-component vector as in “Vector ODT” (Kerstein *et al.*, 2001) to include the pressure scrambling effects. An eddy event maps the velocity and scalar fields in the i th direction as

$$u_i(y) \rightarrow u_i[f(y)] + c_i K(y), \quad (4-12)$$

$$\phi_i(y) \rightarrow \phi_i[f(y)], \quad (4-13)$$

where c_i is the amplitude and $K(y)$ is the kernel transformation function, which is defined as

$$K(y) \equiv y - f(y). \quad (4-14)$$

Notice that the kernel transformation function only affects the velocity field because it represents pressure-induced energy redistribution among velocity components. $K(y)$ is only effective inside an eddy interval and it integrates to zero so that the energy redistribution leaves the total momentum of velocity components unchanged.

The amplitudes c_i are determined based on the kinetic energy change for each individual eddy. The kinetic energy of an individual velocity component is defined as

$$E_i = \frac{1}{2} \rho_0 \int u_i^2(y) dy. \quad (4-15)$$

The change of kinetic energy for a given velocity component due to mapping and kernel transformation is

$$\begin{aligned}
\Delta E_i &= \frac{1}{2} \rho_0 \int_{y_0}^{y_0+l} [(u_i(f(y)) + c_i K(y))^2 - u_i(y)^2] dy \\
&= \frac{1}{2} \rho_0 \int_{y_0}^{y_0+l} [u_i(f(y))^2 + 2c_i u_i(f(y))K(y) + c_i^2 K^2(y) - u_i(y)^2] dy \quad (4-16) \\
&= c_i \rho_0 \int_{y_0}^{y_0+l} [u_i(f(y))K(y)] dy + \frac{1}{2} c_i^2 \rho_0 \int_{y_0}^{y_0+l} K(y)^2 dy \\
&= c_i \rho_0 l^2 u_{i,K} + c_i^2 \frac{2}{27} \rho_0 l^3
\end{aligned}$$

In the above derivation, the energy conservation of triplet maps has been applied, that is

$$\int_{y_0}^{y_0+l} [u_i(f(y))^2 - u_i(y)^2] dy = 0. \quad (4-17)$$

The first term in the final step of Eq. (4-16), $u_{i,K}$ is defined as

$$u_{i,K} \equiv \frac{1}{l^2} \int_{y_0}^{y_0+l} u_i(f(y))K(y) dy. \quad (4-18)$$

Substituting the expression of $f(y)$ in Eq. (4-10) and $K(y)$ in Eq. (4-14) into Eq. (4-18)

yields

$$u_{i,K} = \frac{4}{9l^2} \int_{y_0}^{y_0+l} u_i(y)[l - 2(y - y_0)] dy. \quad (4-19)$$

Moreover, the second term in the last step of Eq. (4-16) is obtained through the following integration

$$\begin{aligned}
\int K(y)^2 dy &= \int [y - f(y)]^2 dy \\
&= \frac{4}{27} l^3.
\end{aligned} \quad (4-20)$$

With the quadratic Eq. (4-16) of the kernel amplitudes, we can solve for c_i and get

$$\begin{aligned}
c_i &= \frac{-(\rho_0 l^2 u_{i,K}) \pm \sqrt{(\rho_0 l^2 u_{i,K})^2 - 4 \left(\frac{2}{27} \rho_0 l^3 \right) (-\Delta E)}}{2 \left(\frac{2}{27} \rho_0 l^3 \right)} \\
&= \frac{27}{4l} \left(-u_{i,K} \pm \sqrt{u_{i,K}^2 + \frac{8}{27} \frac{\Delta E_i}{\rho_0 l}} \right)
\end{aligned} \tag{4-21}$$

Under conditions that neglect the potential energy, the kinetic energy change between velocity components must sum to zero, $\sum_i \Delta E_i = 0$. In cases that no pressure scrambling is allowed, c_i can be set to zero and kernel transformation is removed to recover the original formulation of ODT (Kerstein *et al.*, 2001).

In order to implement the pressure scrambling model, we need to find a more explicit form for ΔE_i in Eq. (4-21). Motivated by the interpretation of the pressure scrambling as a tendency to restore isotropy, Kerstein *et al.* (2001) delved more into the model and found out that the form of ΔE_i must satisfy

$$\Delta E_i = \alpha_0 \sum_j T_{ij} Q_j, \tag{4-22}$$

where Q_j ($j = 1, 2$, or 3) is a quantity with units of energy that depends on $u_j(y)$ and scalars, α_0 is a free parameter, and the transfer matrix T is defined as

$$T \equiv \frac{1}{2} \begin{pmatrix} -2 & 1 & 1 \\ 1 & -2 & 1 \\ 1 & 1 & -2 \end{pmatrix}, \tag{4-23}$$

where matrix T is symmetric and is formulated so that $\sum_i \Delta E_i = 0$ is invariant under exchange of indices. α_0 represents the fraction of maximum allowable energy that is to be

exchanged and its physical realizable range is $[0, 1]$. When $\alpha_0 = 0$, there is no exchange of energy between velocity components; while $\alpha_0 = 2/3$ results in equi-partition of energy in the pressure scrambling model.

The task of finding ΔE_i is now reduced to specifying Q_i in Eq. (4-22). Based on the observation that the amount of energy that can be removed from a velocity component is bounded and the bound is determined by maximizing $-\Delta E_i$ with respect to c_i in Eq. (4-16), we can differentiate Eq. (4-16) with respect to c_i

$$\frac{\partial(-\Delta E_i)}{\partial c_i} = -\rho_0 l^2 u_{i,K} - \frac{4}{27} \rho_0 l^3 c_i = 0, \quad (4-24)$$

and find the value for c_i that makes the derivative zero

$$c_i = -\frac{27}{4} \frac{u_{i,K}}{l}. \quad (4-25)$$

Kerstein *et al.* (2001) proposed to set Q_i to be equal to the bound of the maximum removable energy from a velocity component because α_0 can be conveniently interpreted as the energy extracted from each velocity component, expressed as the fraction of the maximum possible energy that can be extracted, for redistribution to the other components. Therefore, Q_i can be obtained by substituting Eq. (4-25) into Eq. (4-16)

$$Q_i = -\Delta E_i \Big|_{\max} = \frac{27}{8} \rho_0 l u_{i,K}^2. \quad (4-26)$$

Inserting Eq. (4-26) into Eq. (4-22) and then into Eq. (4-21) gives the result for the kernel amplitude in vector ODT

$$c_i = \frac{27}{4l} \left(-u_{i,K} + \text{sign}(u_{i,K}) \sqrt{u_{i,K}^2 + \alpha_0 \sum_j T_{i,j} u_{j,K}^2} \right). \quad (4-27)$$

4.4.3 The Eddy Rate Distribution

Eddy events should occur with frequencies comparable to the turbulent eddy turnover frequencies. The eddy rate is parameterized by the position, y_0 , and the eddy size, l . In ODT, eddy events are governed by the eddy rate distribution, which is defined by associating it with a time scale $\tau(t; y_0, l)$ with every eddy event (Kerstein *et al.*, 2001). The time scale is obtained based on the instantaneous velocity field. The eddy event rate is defined as

$$\lambda(t; y_0, l) \equiv \frac{C}{l^2 \tau(t; y_0, l)}, \quad (4-28)$$

where C is an arbitrary constant. For a quantitative definition of τ , Kerstein *et al.* (2001) employed a measure of the turbulent kinetic energy that is associated with each mapping interval. Based on the dimensional analysis

$$\frac{\rho_0 l^3}{\tau^2} \sim \sum_j B_j Q_j, \quad (4-29)$$

where B_j are arbitrary dimensionless constants and Q_j are chosen as the available kinetic energy of component j . The determination of time scales is based on the available kinetic energy of the velocity component that is parallel to the ODT domain. This is because the eddy events represent motions in this direction. In the present study, we have ODT domains line in three directions, x , y , and z . For explanation purposes, we arbitrarily choose y

direction, denoted as '2', as the direction of the ODT domain. Note that this direction preference is only for determining the sequence of events, thus breaking the symmetry under index change due to this choice will not affect the implementation of each individual eddy event. Assembling Eqs. (4-22), (4-23), and (4-26), we can formulate

$$\left(\frac{l}{\tau}\right)^2 \sim u_{2,K}^2 + \alpha_0 \sum_j T_{2j} u_{j,K}^2, \quad (4-30)$$

where the first term on the right hand side is the kinetic energy added to the velocity component in y direction during triplet mapping and the second term represents the amount of kinetic energy that can be extracted. Thus, the right hand side of Eq. (4-30) represents the available kinetic energy of the velocity component, u_2 .

A final consideration in determining the eddy time scale is viscous damping (Kerstein *et al.*, 2001). Under conditions when the viscous time scale is smaller than the eddy time scale, the eddy event is prohibited. Therefore, the viscous penalty is added to the right hand side of Eq. (4-30) and the following expression is obtained

$$\left(\frac{l}{\tau}\right)^2 \sim u_{2,K}^2 + \alpha_0 \sum_j T_{2j} u_{j,K}^2 - Z \left(\frac{\nu}{l}\right)^2, \quad (4-31)$$

where the last term accounts for the viscous damping effects because the viscous time scale is

$$\tau_v \sim \frac{l^2}{\nu}. \quad (4-32)$$

Substituting Eq. (4-32) into Eq. (4-28), we can get

$$\lambda(t; y_0, l) \equiv \frac{C}{l^2 \tau(t; y_0, l)} = \frac{C\nu}{l^4} \sqrt{\left(\frac{u_{2,K}l}{\nu}\right)^2 + \alpha_0 \sum_j T_{2,j} \left(\frac{u_{j,K}l}{\nu}\right)^2} - Z. \quad (4-33)$$

If the right-hand side of Eq. (4-33) is negative, the eddy event is suppressed and λ is set to zero. The terms proceeding Z in the square root of Eq. (4-33) have the form of a Reynolds number and Z can be viewed as a parameter that controls the critical Reynolds number for eddy events.

The eddy rate distribution function determined in Eq. (4-33) involves three free parameters, namely, C , α_0 , and Z . C is a coefficient that represents the turbulence intensity; α_0 denotes the degree of kinetic energy exchange among velocity components; Z is a viscous cut-off parameter and determines the smallest eddy size for given local flow conditions (Kerstein *et al.*, 2001).

The sequence of the eddy events is governed by the eddy rate distribution, λ . Given a time t , the probability that an eddy event will occur at location, y_0 , and within range $[y_0, y_0 + l]$ is $\lambda(t; y_0, l)$. Each eddy event changes the velocity field and consequently modifies the eddy rate distribution function, λ . In LEM, a mixing model, the eddy rate distribution, λ , is prescribed *a priori*.

4.4.4 Sampling the Distribution

Although a sampling of the eddy rate distribution can be used to determine the eddy event sequence, the explicit reconstruction of the rate distribution is numerically

unaffordable. To overcome this problem, an alternative implementation is used. This implementation is based on the ‘rejection method’ described by Ross (1990). In this method, the trial values from the sample space are proposed first and then accepted with a probability proportional to the probability evaluated with the trial value. The acceptance probability is the ratio of the desired probability to the presumed probability, which is properly normalized. Again, this is the same strategy that has been adopted by Kerstein and co-workers (Kerstein, 1999; Echehki *et al.*, 2001) to efficiently compute the velocity and scalar fields within ODT.

The ODT Acceptance Probability

The ODT acceptance probability is evaluated based on the eddy rate distribution normalized by the guessed probability density functions of l and y_0 following Kerstein (1999) and Echehki *et al.* (2001)

$$P_a = \frac{\lambda(t; y_0, l) \Delta t_s}{f(l)g(y_0)}, \quad (4-34)$$

where Δt_s is the time step between successive eddy events, $f(l)$ and $g(y_0)$ are the presumed shapes of the probability density functions for an eddy length scale, l , and an eddy location, y_0 , respectively. Choosing a correct Δt_s is very critical. If Δt_s is too small, then we are over sampling the eddy events resulting in added simulation cost; if Δt_s is too large, we are under sampling the events and the results will be less accurate. The forms for $f(l)$ and $g(y_0)$ are not unique and they are discussed below.

The ODT Length-Scale Distribution

Following Kerstein (1999) and Echehki *et al.* (2001), the trial length-scale distribution is as follows

$$f(l) = \frac{A}{l^2}, \quad (4-35)$$

where A is a constant and l is the eddy length scale. Let the smallest eddy size be denoted as “ a ” and the largest eddy size be denoted as “ b ”. The total distribution spanning from the smallest eddy length to the largest eddy length is

$$\int_a^b f(l) dl = 1. \quad (4-36)$$

Substituting Eq. (4-35) into Eq. (4-36) yields

$$A = \frac{a \cdot b}{b - a}. \quad (4-37)$$

Thus, the trial length distribution function can be written as

$$f(l) = \frac{a \cdot b}{b - a} \frac{1}{l^2}. \quad (4-38)$$

The Eddy Location Selection

The eddy location is sampled from a uniform distribution function on the ODT domain. Thus, the distribution function for the eddy location is expressed as

$$g(y_0) = \frac{1}{L}. \quad (4-39)$$

where L is the length of each ODT element.

4.5 The Molecular Diffusion and Reaction Processes in ODT

The molecular diffusion and the reaction terms in the energy and species equations are represented by deterministic solutions of the 1D reaction-diffusion transport equations for the scalars. The diffusion terms in the momentum equation are represented by deterministic solutions of the 1D momentum transport equation. The equations along ODT 1D element can be obtained through decomposing Eqs. (4-7)–(4-9). In practical implementations, the diffusion terms in Eqs. (4-40)–(4-42) can be multiplied by a factor of 3 to account for the diffusion in the two directions that are normal to the ODT 1D element.

Diffusion for the Velocity Components

$$\rho \frac{\partial u_i}{\partial t} = \frac{\partial}{\partial \eta} \left(\mu \frac{\partial u_i}{\partial \eta} \right) \quad (4-40)$$

Reaction-Diffusion for the Temperature

$$\rho \frac{\partial T}{\partial t} = \frac{1}{c_p} \frac{\partial \dot{q}''}{\partial \eta} - \frac{1}{c_p} \sum_{k=1}^N h_k \dot{\omega}_k \quad (4-41)$$

Reaction-Diffusion for the Mass Fractions

$$\rho \frac{\partial Y_k}{\partial t} = \frac{\partial J_{k,\eta}}{\partial \eta} + \dot{\omega}_k \quad (4-42)$$

For the energy and species equations, the reaction rate terms are computed based on the instantaneous and local thermodynamic state of the mixture (i.e. pressure, temperature, and composition).

4.6 The Convection Process in ODT

The representation of 3D contributions on the ODT 1D element is the most challenging task of developing a hybrid LES-ODT approach. On the ODT 1D element, only contributions defined along the 1D domain (e.g. diffusion or convection along ODT) or at a ODT cell (e.g. reaction) can be adequately integrated with ODT temporal and spatial resolutions. Contributions from the remaining directions are implemented with terms that are resolved on a coarser LES grid and time step. In the present formulation, we represent the contribution from convective terms (the principal terms to be modeled with 3D contributions) using a two-step process: ‘node convection’ at each ODT node combined with ‘intra-node relaxation’ or ‘co-linear convection’ along each ODT element. The nodes of ODT are illustrated in Figure 4-1, and correspond to the common intersection of ODT domains (3 in a Cartesian 3D lattice). Again, we adopt a split operator scheme for the governing equations for ODT elements that integrate each process with its own time step. The transport equations for convection can be obtained by decomposing Eqs. (4-7) – (4-9).

Convection for the Velocity Components

$$\frac{\partial u_i}{\partial t} = -\hat{u}_j \frac{\partial u_i}{\partial x_j} \quad (4-43)$$

Convection for the Temperature

$$\frac{\partial T}{\partial t} = -\hat{u}_j \frac{\partial T}{\partial x_j} \quad (4-44)$$

Convection for the Mass Fractions

$$\frac{\partial Y_k}{\partial t} = -\hat{u}_j \frac{\partial Y_k}{\partial x_j} \quad (4-45)$$

In Eqs. (4-43) – (4-45), \hat{u}_j represents the term solved by LES governing equations.

4.7 Operations for LES-ODT Coupling

Two operations, interpolation and filtering, are adopted in the present study to couple the LES and ODT solutions. Interpolation represents in fact an operation of inverse filtering. The interpolation is employed to interpolate the LES resolved velocity field to ODT grids during simulations. The filtering operation is used to filter the initial ODT flow field to LES grids for initializing the LES field.

4.7.1 Interpolation

Interpolation is designed to represent an inverse LES filter. The interpolation is conducted in three dimensions using a tri-linear interpolation. The tri-linear interpolation is similar to the bilinear interpolation (Press *et al.*, 1996). Here, we will present the tri-linear interpolation in a discretized way. We want to find an estimate of $g(x,y,z)$ from a three-dimensional grid of tabulated values g and 3 one-dimensional vectors giving the tabulated values of each of the independent variables x , y , z . To implement it numerically, let's consider a given matrix of functional values $f_{i,j,k}$, where i varies from 1 to m , j varies from 1

to n , k varies from 1 to p . We are also given three arrays x_i of length m , y_j of length n , and z_k of length p . The relation of these arrays to the function $g(x,y,z)$ is

$$f_{i,j,k} = g(x_i, y_j, z_k), \quad (4-46)$$

and we want to estimate the function, g , at point (x,y,z) by interpolation.

Figure 4-4 illustrates the surrounding points and the interior point in 3D for tri-linear interpolation. The eight tabulated points surrounding the desired interior point (x,y,z) are $f_{i,j,k}$, $f_{i+1,j,k}$, $f_{i,j,k+1}$, $f_{i+1,j,k+1}$, $f_{i,j,k+1}$, $f_{i+1,j,k+1}$, $f_{i+1,j+1,k}$, $f_{i+1,j+1,k+1}$. The location of the interior point satisfies

$$\begin{aligned} x_i &\leq x \leq x_{i+1} \\ y_j &\leq y \leq y_{j+1} \\ z_k &\leq z \leq z_{k+1} \end{aligned} \quad (4-47)$$

The formula for tri-linear interpolation on the surrounding points is

$$\begin{aligned} g(x,y,z) &= (1 - \Delta x) (1 - \Delta y) (1 - \Delta z) f_{i,j,k} \\ &+ (1 - \Delta x) (1 - \Delta y) (\Delta z) f_{i,j,k+1} \\ &+ (1 - \Delta x) (\Delta y) (1 - \Delta z) f_{i+1,j,k} \\ &+ (1 - \Delta x) (\Delta y) (\Delta z) f_{i+1,j,k+1} \\ &+ (\Delta x) (1 - \Delta y) (1 - \Delta z) f_{i,j+1,k} \\ &+ (\Delta x) (1 - \Delta y) (\Delta z) f_{i,j+1,k+1} \\ &+ (\Delta x) (\Delta y) (1 - \Delta z) f_{i+1,j+1,k} \\ &+ (\Delta x) (\Delta y) (\Delta z) f_{i+1,j+1,k+1} \end{aligned} \quad (4-48)$$

where

$$\Delta x = \frac{x - x_i}{x_{i+1} - x_i}$$

$$\Delta y = \frac{y - y_j}{y_{j+1} - y_j}$$

$$\Delta z = \frac{z - z_k}{z_{k+1} - z_k}$$
(4-49)

The interpolated velocity field is employed in ‘node convection’ and ‘intra-node relaxation’ or ‘co-linear convection’ on ODT elements. The benefit of ‘node convection’ and ‘co-linear convection’ is to enable the 3D effects of large turbulent eddy motion, and to couple the different ODT domains, thus allowing the filtered motion to cascade to small scales within ODT.

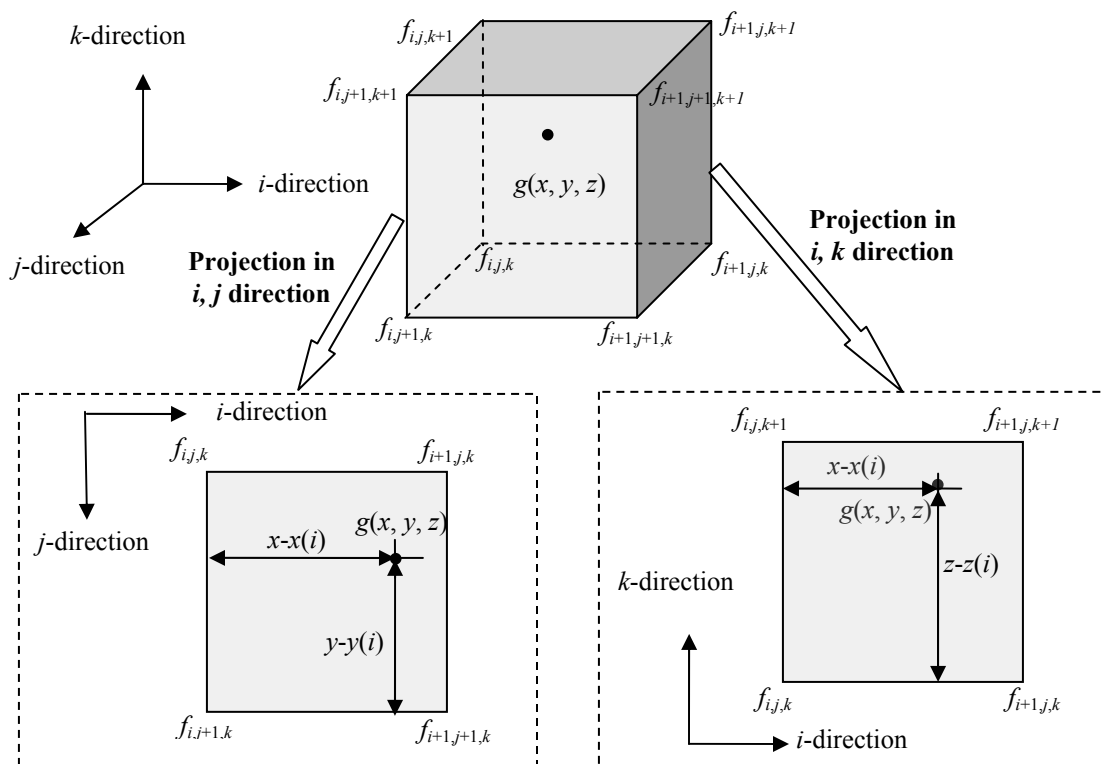


Figure 4-4 Tri-linear interpolation

4.7.2 Filtering

The filtering operation is carried out in the physical space where weighted averages of a variable are computed over a given volume. The filtering operation in the physical space is defined as

$$\bar{f}(x) = \int f(x') G(x - x') dx', \quad (4-50)$$

where the integration is over the entire flow domain, \bar{f} is the filtered vector or scalar, f is the original vector or scalar, and G is the filter function that must satisfy the normalization condition

$$\int G(x') dx' = 1. \quad (4-51)$$

There are many types of filter functions G . The most commonly used filters are the box filter, the Gaussian filter, and the spectral cut-off filter. In the present study, we used the box filter. With the box filter, the filtered quantity $\bar{f}(x)$ is the average of the original quantity $f(x')$ in the interval $x - \frac{1}{2}\Delta < x' < x + \frac{1}{2}\Delta$. The box filter function is given below:

$$G(x') = \begin{cases} 0, & |x - x'| > \Delta/2 \\ 1/\Delta, & |x - x'| \leq \Delta/2 \end{cases}. \quad (4-52)$$

4.8 Numerical Implementation of Large-Eddy Simulation

In order to solve the LES governing equations, the closure terms in Eqs. (4-2)–(4-4) have to be modeled. Those subgrid closure terms can be modeled using the Smagorinsky model (1963), the Germano dynamic model (1991), or the scalar similarity model (Poinso

and Veynante, 2001). However, those gradient-diffusion based models have limitations in representing the subgrid fluxes as we have addressed in Chapter 1. Furthermore, our major focus is to develop a coupled LES-ODT strategy to model turbulent combustion, not to address the details of subgrid flux closure modeling. Therefore, in the present study, we only solve the velocity field based on the LES momentum equation. The Smagorinsky model is chosen due to its simplicity to model the subgrid stresses by defining the model constant using a *priori* test. A more advanced model may be used in the future work. The numerical implementation of the LES momentum equation follows the same procedure discussed in section 2.5.4 in Chapter 2. However, both the spatial and the temporal resolution are much coarser in LES than in DNS in a real run.

The Smagorinsky Model

Smagorinsky (1963) proposed the most common subgrid stress model. The model is based on the assumption that the subgrid stress or flux tensor is a scalar multiple of the resolved rate of the strain tensor or of the scalar gradient. It has gained more and more popularity since it was proposed because of its simple formulation. In the Smagorinsky model, the subgrid stresses are expressed as

$$\tau_{ij} \approx -2\nu_t \bar{S}_{ij}, \quad (4-53)$$

where \bar{S}_{ij} is the resolved strain

$$\bar{S}_{ij} = \frac{1}{2} \left(\frac{\partial \bar{u}_i}{\partial x_j} + \frac{\partial \bar{u}_j}{\partial x_i} \right), \quad (4-54)$$

and ν_t is the subgrid scale eddy viscosity that can be modeled from dimensional arguments as

$$\nu_t = C_s^2 \Delta^{4/3} l_t^{2/3} |\bar{S}|, \quad (4-55)$$

where l_t is the turbulence integral length scale, C_s is a model constant, and $|\bar{S}|$ is defined as

$$|\bar{S}| \equiv (2\bar{S}_y \bar{S}_y)^{1/2}. \quad (4-56)$$

Eq. (4-55) can be simplified by assuming that the integral length scale l_t is of the order of the grid size $l_t \approx \Delta$, thus

$$\nu_t = (C_s \Delta)^2 |\bar{S}|. \quad (4-57)$$

It should be noted that C_s depends on the filter type, the numerical method, and the flow configuration. For different flows, the constant C_s is different. For the homogeneous isotropic turbulence case, C_s is approximately 0.2. The model requires a *priori* knowledge of the flow in order to define the coefficient, C_s .

4.9 Numerical Implementation on ODT Elements

ODT simulations at each ODT element are implemented as three parallel processes: molecular, stirring, and convection. Here, operators in the governing equations for these processes are split to integrate the different processes individually. Each process has its own time step and timer. One LES time step is divided into several ODT time steps. Each ODT time step is equal to the DNS time step. The purpose of letting the ODT time step equal to

the DNS time step is to generate ODT statistics that are comparable to DNS statistics at each LES time step.

Figure 4-5 shows a rendering of the parallel processes for the ODT simulation. The process with the smallest time step is executed first. The time for this process is advanced with the process' time step at the end of the execution. The next process, which is in line for execution because it has the lowest time, is selected and implemented. Once it is implemented, its time is advanced by its prescribed increment, and the selection of the next process is repeated. This is continued until the integral time of ODT is achieved. Processes concerned with the ODT implementation include: turbulent stirring, reaction-diffusion integration, and convection integration.

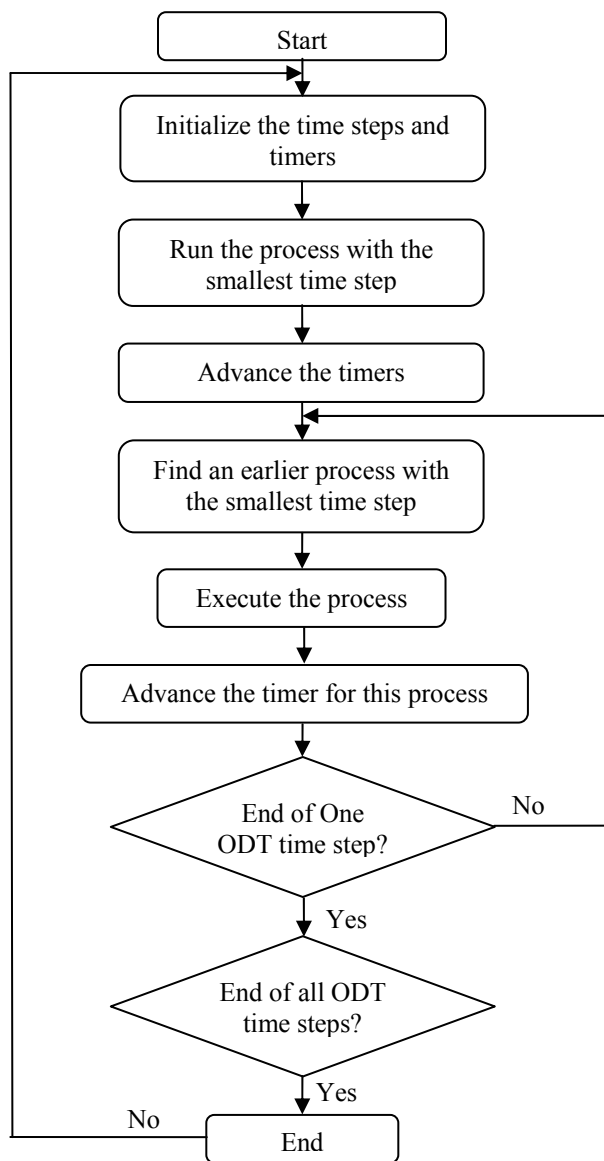


Figure 4-5 Implementation of ODT simulations in parallel processes

In the following discussions, the numerical implementation of the turbulent stirring process, the molecular diffusion and reaction processes, and the convection process is addressed.

4.9.1 Implementation of the Turbulent Transport

Steps for the Stirring Process

The turbulent stirring process, denoted as Ω in Eqs. (4-7) – (4-9), is carried out in five steps: the eddy size selection, the eddy location selection, the eddy rate distribution function and the probability computation, the probability acceptance determination, and the triplet mapping. The turbulent eddy size is selected according to the length distribution function in Eq. (4-38). The discrete eddy size is randomly selected within the range of 6 to the smallest eddy size that can be solved by LES, which equals to the ratio of ODT grids along one ODT element to LES grids in one direction. Eddy location is randomly selected along an ODT element. The probability is then computed based on the rate distribution function and Eq. (4-34). The last step is to compare the probability with a random seed to determine the acceptance of the eddy. If the probability is smaller than the random seed of $[0,1]$, then the eddy stirring events are prohibited; otherwise, if the probability is larger than the random seed and smaller than 1, the eddy stirring events are allowed. Then the kernel transformation amplitude and function are computed and the triplet mapping of both the vector and the scalar fields are carried out. Figure 4-6 is a flow chart that shows the steps of the turbulent stirring process.

Stirring Time Step Adjustment

The stirring time step is adjusted based on the sampling data and the target probability, which is set to 1.0 currently. The time step is adjusted as follows

$$\Delta t_S^n = \Delta t_S^o \cdot \frac{P_t}{P_{max}}, \quad (4-58)$$

where P_t is the target probability, P_{max} is the maximum probability during sampling, Δt_S^n is the new adjusted stirring time step, and Δt_S^o is the old stirring time step. In the present study, P_t is set to 0.1 following the recommendations by McDermott (2005).

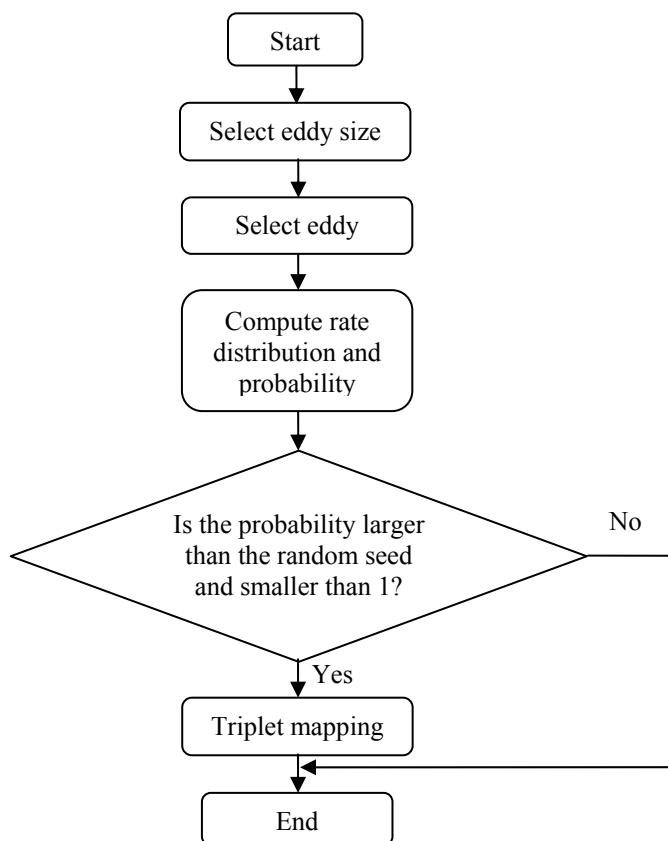


Figure 4-6 The turbulent stirring process

4.9.2 Implementation of Molecular Diffusion and Reaction

Eqs. (4-40) – (4-42) are solved explicitly using a second-order central finite difference method. In Eqs. (4-41) – (4-42), the reaction rate terms are computed instantaneously based on the scalar field and integrated with the diffusion terms with respect to time. A check for scalar boundedness is implemented during the time integration. Scalar boundedness is equally enforced during the integration of the filtered convection operator.

4.9.3 Implementation of Convection

In ODT, the representation of convection is implemented by two distinct processes. The first process corresponds to the turbulent stirring events, in which the largest scales are comparable to the LES filter size (the smallest scales resolved in LES). The second process represents a mean or filtered advection. This advection process is problematic for a number of reasons. First, advection occurs in three directions, thus at least two directions can not be solved at the ODT time scale or on the ODT 1D element. Second, non-linear contributions from convection processes pose important constraints on scalar boundedness.

In the present study, we implemented a novel method to address the 3D convection using ‘node convection’ combined with ‘intra-node relaxation’ or ‘co-linear convection’. We will also address the scalar boundedness using the total variation diminishing method (TVD) with a flux limiter.

The Total Variation Diminishing Method

The total variation diminishing (TVD) scheme (Tannehill, 1997) is implemented to limit the flux and to avoid oscillations that can result in mass fractions going beyond limit.

Considering Eq. (4-43), the total variation (TV) for the discrete case is given by

$$\text{TV} = \sum_i |u_{i+1} - u_i|. \quad (4-59)$$

A numerical method is total variation diminishing, or TVD, if

$$\text{TV}(u^{n+1}) \leq \text{TV}(u^n). \quad (4-60)$$

The second-order upwind scheme proposed by Warming and Beam (1975) is used to compute the fluxes for convection. The scheme includes the predictor and the corrector steps and uses backward (upwind) differences in both steps.

Case 1: $\hat{u}_j > 0$

The predictor is

$$u_i^{\bar{n+1}} = u_i^n - \frac{\hat{u}_j \Delta t_c}{\Delta x} (u_i^n - u_{i-1}^n), \quad (4-61)$$

where Δt_c is the convection time step, and the corrector is

$$u_i^{n+1} = \frac{1}{2} \left[u_i^n + u_i^{\bar{n+1}} - \frac{\hat{u}_j \Delta t_c}{\Delta x} (u_i^{\bar{n+1}} - u_{i-1}^{\bar{n+1}}) - \frac{\hat{u}_j \Delta t_c}{\Delta x} (u_i^n - 2u_{i-1}^n + u_{i-2}^n) \right]. \quad (4-62)$$

Substituting Eq. (4-61) into Eq. (4-62), the following one-step algorithm is obtained

$$u_i^{n+1} = u_i^n - \frac{\hat{u}_j \Delta t_c}{\Delta x} (u_i^n - u_{i-1}^n) + \frac{1}{2} \frac{\hat{u}_j \Delta t_c}{\Delta x} \left(\frac{\hat{u}_j \Delta t_c}{\Delta x} - 1 \right) (u_i^n - 2u_{i-1}^n + u_{i-2}^n). \quad (4-63)$$

The third term on the right-hand side of Eq. (4-63) represents contributions from the second-order corrections to the first order difference. We want to restrict the corrections in regions of rapid change to avoid undesirable behavior by limiting the magnitude of the difference in u or, more generally, the flux or variable gradients. The scheme can be written as

$$u_i^{n+1} = u_i^n - \frac{\hat{u}_j \Delta t_c}{\Delta x} (u_i^n - u_{i-1}^n) + \frac{1}{2} \frac{\hat{u}_j \Delta t_c}{\Delta x} \left(\frac{\hat{u}_j \Delta t_c}{\Delta x} - 1 \right) \left[\psi_{i-1/2}^+ (u_i^n - u_{i-1}^n) - \psi_{i-3/2}^+ (u_{i-1}^n - u_{i-2}^n) \right] \quad (4-64)$$

where ψ is a limiter function, and is defined as a function of the ratios of consecutive variations. For simplicity, the limiters can be written based on only the single ratio of the local point

$$\begin{aligned} \psi_{i-1/2}^+ &= \psi(r_{i-1/2}^+) \\ \psi_{i-3/2}^+ &= \psi(r_{i-3/2}^+) \end{aligned} \quad (4-65)$$

where the ratios are given as

$$r_{i-1/2}^+ = \frac{u_{i+1} - u_i}{u_i - u_{i-1}}, \quad (4-66)$$

and

$$r_{i-3/2}^+ = \frac{u_i - u_{i-1}}{u_{i-1} - u_{i-2}}. \quad (4-67)$$

Case 2: $\hat{u}_j < 0$

The predictor is

$$u_i^{\bar{n}+1} = u_i^n - \frac{\hat{u}_j \Delta t}{\Delta x} (u_{i+1}^n - u_i^n), \quad (4-68)$$

and the corrector is

$$u_i^{n+1} = \frac{1}{2} \left[u_i^n + u_i^{\bar{n}+1} - \frac{\hat{u}_j \Delta t_c}{\Delta x} (u_{i+1}^{\bar{n}+1} - u_i^{\bar{n}+1}) - \frac{\hat{u}_j \Delta t_c}{\Delta x} (u_{i+2}^n - 2u_{i+1}^n + u_i^n) \right], \quad (4-69)$$

Substituting Eq. (4-68) into Eq. (4-69), the following one-step algorithm is obtained

$$u_i^{n+1} = u_i^n - \frac{\hat{u}_j \Delta t_c}{\Delta x} (u_{i+1}^n - u_i^n) + \frac{1}{2} \frac{\hat{u}_j \Delta t_c}{\Delta x} \left(\frac{\hat{u}_j \Delta t_c}{\Delta x} - 1 \right) (u_{i+2}^n - 2u_{i+1}^n + u_i^n). \quad (4-70)$$

Applying the flux limiter yields

$$u_i^{n+1} = u_i^n - \frac{\hat{u}_j \Delta t}{\Delta x} (u_{i+1}^n - u_i^n) + \frac{1}{2} \frac{\hat{u}_j \Delta t}{\Delta x} \left(\frac{\hat{u}_j \Delta t}{\Delta x} - 1 \right) \left[\psi_{i+3/2}^- (u_{i+2}^n - u_{i+1}^n) - \psi_{i+1/2}^- (u_{i+1}^n - u_i^n) \right], \quad (4-71)$$

where the flux limiters are given as

$$\begin{aligned} \psi_{i+1/2}^- &= \psi(r_{i+1/2}^-) \\ \psi_{i+3/2}^- &= \psi(r_{i+3/2}^-) \end{aligned} \quad (4-72)$$

where the ratios are given as

$$r_{i+1/2}^- = \frac{u_i - u_{i-1}}{u_{i+1} - u_i}, \quad (4-73)$$

and

$$r_{i+3/2}^- = \frac{u_{i+1} - u_i}{u_{i+2} - u_{i+1}}. \quad (4-74)$$

There are various versions of flux limiter functions that satisfy the TVD condition (4-59). In the present study, we implemented the ‘‘Superbee’’ limiter of Roe (Tannehill, 1997), which is

$$\psi(r) = \max[0, \min(2r, 1), \min(r, 2)]. \quad (4-75)$$

The TVD scheme can be applied in a similar manner for the scalar Eqs. (4-44) and (4-45).

The Convection Process

The convection Eq. (4-43) can be rewritten using Eqs. (4-64) and (4-71)

$$\rho \frac{du_i}{dt} = -\bar{\rho} \frac{\hat{u}_j}{\Delta x} (u_i^n - u_{i-1}^n) + \frac{1}{2} \bar{\rho} \frac{\hat{u}_j}{\Delta x} \left(\frac{\hat{u}_j \Delta t_c}{\Delta x} - 1 \right) \left[\psi_{i-1/2}^+ (u_i^n - u_{i-1}^n) - \psi_{i-3/2}^+ (u_{i-1}^n - u_{i-2}^n) \right] \quad (4-76)$$

for $\hat{u}_j > 0$

and

$$\rho \frac{du_i}{dt} = -\bar{\rho} \frac{\hat{u}_j}{\Delta x} (u_{i+1}^n - u_i^n) + \frac{1}{2} \bar{\rho} \frac{\hat{u}_j}{\Delta x} \left(\frac{\hat{u}_j \Delta t_c}{\Delta x} - 1 \right) \left[\psi_{i+3/2}^- (u_{i+2}^n - u_{i+1}^n) - \psi_{i+1/2}^- (u_{i+1}^n - u_i^n) \right] \quad (4-77)$$

for $\hat{u}_j < 0$.

Figure 4-7 illustrates the ‘node convection’ in three directions. The ‘node convection’ for velocity vectors is implemented at each ODT node in the following steps. First, the convection terms on the right hand side of Eq. (4-76) or Eq. (4-77) are computed in x , y , and z directions depending on the sign of the LES interpolated velocity \hat{u}_j in each direction and are accumulated. Second, Eq. (4-43) is integrated with respect to time and velocities at each node are updated in all three directions. Third, the updated velocities are averaged over

three directions and the averaged velocity is used as the new velocity at each node. The ‘node convection’ for scalars is implemented similarly following the same procedures.

‘Intra-node convection’ or ‘co-linear convection’ for the velocity vectors and the scalars is carried out similarly as ‘node convection’ except that it is performed along ODT 1D elements. This process enables the transfer of statistical contributions from the nodes to grid points between the nodes. This is treated as an ‘intra-node relaxation’ or ‘co-linear convection’ procedure because the “flow” of statistics is largely governed by the rate of transport, which also determines the relative contribution from the nodes.

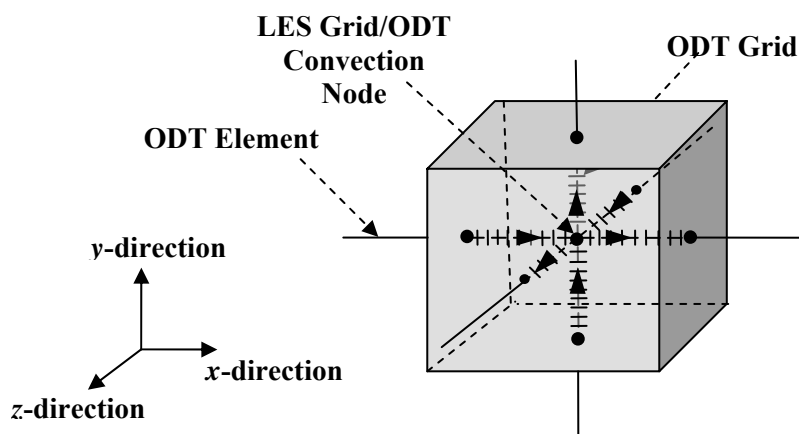


Figure 4-7 Schematic show of the node convection

4.10 Numerical Coupling of LES and ODT

4.10.1 Solution Algorithm

In the present study, the solution algorithm of LES-ODT includes initializing the LES field and ODT elements, solving the LES governing equations, interpolating the LES

velocity field to ODT elements, adjusting the ODT solution, and carrying out the parallel processes in ODT. Figure 4-8 shows the solution algorithm using a flow chart.

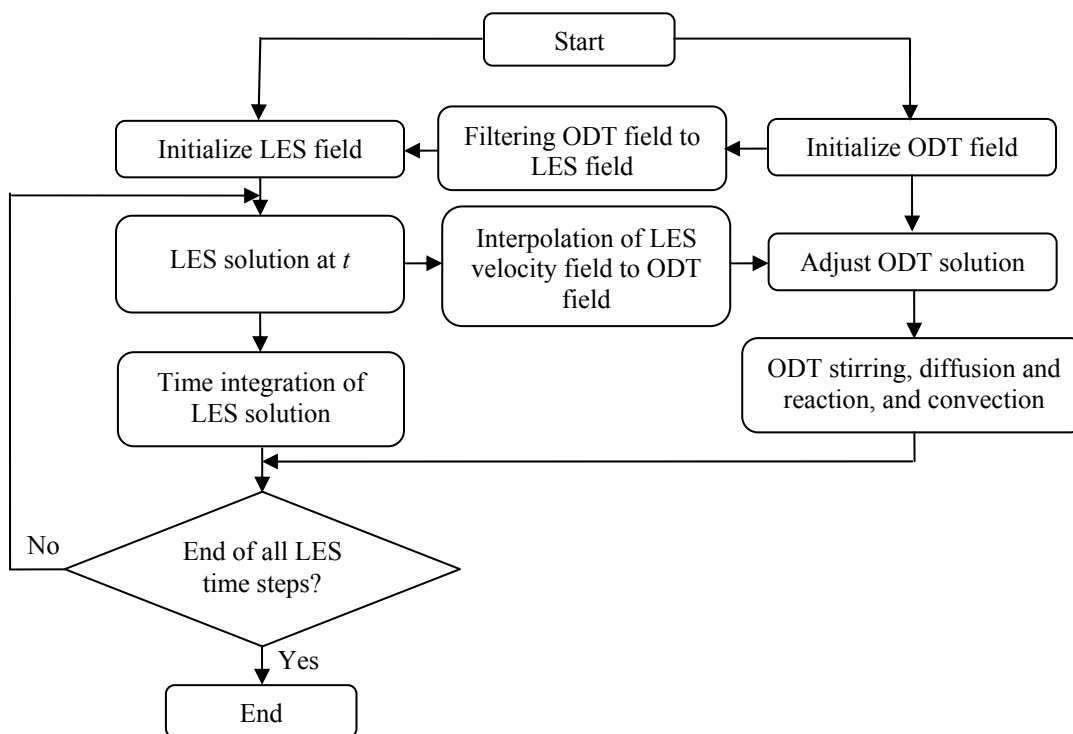


Figure 4-8 Solution algorithm of LES and ODT

4.10.2 Coupling Procedure

The coupling of LES and ODT solutions needs to be carried out both temporally and spatially. The procedure is presented in the following discussions.

Time Integration Coupling

The LES and ODT solutions are coupled at each LES time step. Figure 4-9 shows the coupling procedure schematically. The time integration of LES solutions and ODT processes

is carried out in four steps. First, the ODT stirring, diffusion and reaction, and convection processes are integrated in time for half of a LES time step. Second, the LES field is integrated with a LES time step. Third, the ODT velocity field is adjusted based on the LES velocity field after integration. Fourth, the ODT field is integrated with a full LES time step. Those four steps are repeated until the program reaches the end of all the LES time steps. The above time integration procedures are carried out so that the ODT statistics built up over the time integration represent the statistics averaged over a LES time step.

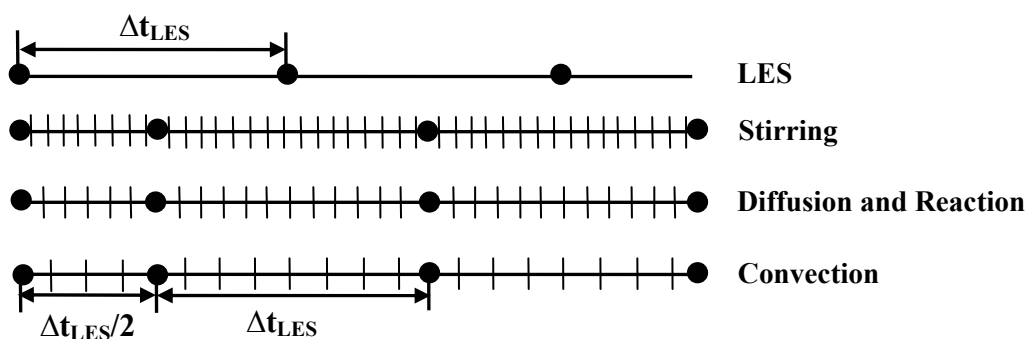


Figure 4-9 Coupling of LES and ODT

Spatial Coupling

The coupling of LES and ODT in space involves: (1) interpolating the velocity from LES grids to ODT grids along each element for ‘node convection’ and ‘co-linear convection’ in ODT and (2) adjusting the ODT velocity field with a corrector. It is important to note that the correction is carried out on the velocity field and not on the scalar field. The interpolation is carried out based on Eq. (4-48). The ODT velocity adjustment is discussed below.

The ODT velocity adjustment is accomplished by adding a corrector to the ODT velocity. The corrector is computed as

$$\begin{aligned}
C_{ODT}(x, y, z) = & (1 - \Delta x)(1 - \Delta y)(1 - \Delta z) \left(V_{i,j,k}^{LES} - V_{i,j,k}^{fODT} \right) \\
& + (1 - \Delta x) \left(\Delta y \right) (1 - \Delta z) \left(V_{i,j+1,k}^{LES} - V_{i,j+1,k}^{fODT} \right) \\
& + (1 - \Delta x)(1 - \Delta y) \left(\Delta z \right) \left(V_{i,j,k+1}^{LES} - V_{i,j,k+1}^{fODT} \right) \\
& + (1 - \Delta x) \left(\Delta y \right) \left(\Delta z \right) \left(V_{i,j+1,k+1}^{LES} - V_{i,j+1,k+1}^{fODT} \right) \\
& + \left(\Delta x \right) (1 - \Delta y)(1 - \Delta z) \left(V_{i+1,j,k}^{LES} - V_{i+1,j,k}^{fODT} \right) \\
& + \left(\Delta x \right) (1 - \Delta y) \left(\Delta z \right) \left(V_{i+1,j,k+1}^{LES} - V_{i+1,j,k+1}^{fODT} \right) \\
& + \left(\Delta x \right) \left(\Delta y \right) (1 - \Delta z) \left(V_{i+1,j+1,k}^{LES} - V_{i+1,j+1,k}^{fODT} \right) \\
& + \left(\Delta x \right) \left(\Delta y \right) \left(\Delta z \right) \left(V_{i+1,j+1,k+1}^{LES} - V_{i+1,j+1,k+1}^{fODT} \right)
\end{aligned} \tag{4-78}$$

where C_{ODT} denotes the velocity corrector to ODT field, $V_{i,j,k}^{LES}$ denotes the LES velocity field, and $V_{i,j,k}^{fODT}$ denotes the ODT velocity filtered to the LES field. The box filter (4-52) is used in the present study due to its simplicity.

The adjustment of ODT velocity field enforces the consistency of the velocity fields between LES and ODT. Thus, the turbulence decay between LES and ODT are consistent. This is very important when turbulence intensity is very high, which generates vigorous velocity fluctuations that enhance the turbulent mixing at subgrid scales resolved by ODT.

4.11 Conclusions

In this chapter, we have addressed LES and ODT model formulation and the numerical implementation in detail. The LES and ODT governing equations for the conservation of momentum, energy, and mass fractions are presented. The LES-ODT formulation proposed in the present study enables a structure-based strategy to predict

subgrid scale processes directly. Moreover, the LES and ODT governing equations are formulated to be consistent, and, therefore, different degrees of redundancies between the LES and ODT solutions can be established. This consistency also establishes a choice in the type of closure used to solve the LES equations. Here, we have adopted a less than full coupling between LES and ODT that may use ODT data to build closure models for SGS fluxes and stresses, and filtered source terms. The strategy solves the LES momentum equations using a “standard” LES closure for SGS stresses. The LES velocity field components are used to force consistency between the LES and ODT solutions. Scalar transport equations along with momentum equations are solved in the ODT solutions.

The proposed LES-ODT formulation addresses the limitations faced by traditional modeling approaches such as the inadequacy of predicting local extinction and reignition and the enormous demand of computational power. ODT is a more advanced model than LEM in that the vector field is resolved instantaneously, which allows the eddy rate distribution function to be determined based on the available kinetic energy.

The novel formulation of ODT convection scheme proposed in the present study offers a great improvement in addressing the limitations faced by the one-dimensional convection along the ODT element. The 3D convection strategy, denoted as ‘node convection’, combined with the 1D convection mechanism, denoted as ‘intra-node relaxation’ or ‘co-linear convection’, allows three-dimensional convection effect to be accounted in the ODT formulation. This feature is critical in predicting the turbulence mixing-reaction coupling at subgrid scales.

Most importantly, the computational cost for LES-ODT is dramatically reduced compared to DNS. Let N_x , N_y , and N_z represent the number of LES grid points in x , y , and z direction, respectively. Let λ denote the ratio of ODT grid points to LES grid points, which also represent the ratio of the DNS grid points in one direction to LES grid points in the same direction. Thus, the ODT grid points required during the simulation is $3\lambda (N_x \times N_y \times N_z)$. Given the condition that DNS grid points in each direction is equal the ODT grid points along one ODT element, the number of DNS grid points required during the simulation is $\lambda^3 (N_x \times N_y \times N_z)$. Therefore, the computational cost for ODT is much cheaper than DNS, yet it provides robust predictions of turbulent combustion. Typical values for λ are of the order of 10 and ideally even higher than that, while requirements for LES resolution in practical systems place the values of N_x , N_y , or N_z in the range of hundreds, thousands or even higher. Therefore, it is easy to see that computational saving in terms of grid points compared to DNS can be of the order of 100 or higher.

Chapter 5 LES-ODT Simulation Conditions: Autoignition in Non-Homogeneous Mixtures

5.1 Objectives

In this chapter, the simulation conditions are presented for LES-ODT modeling of non-homogeneous autoignition in isotropic turbulence. The autoignition problem has been chosen due to the fact that the autoignition in non-homogeneous mixtures offers a number of critical challenges to traditional turbulent combustion modeling. The details have been addressed in Chapter 3. This chapter is organized as follows. First, the initialization and boundary conditions are presented. In order to make LES-ODT results comparable to DNS, the initial LES-ODT field is obtained by interpolating the DNS initial flow field. Second, the simulation conditions and parameters are discussed. In the present study, both low and high turbulence conditions are addressed, with three different Lewis number cases included for the high turbulence conditions. For each case, two simulations with different LES spatial resolutions are carried out. Finally, the mechanisms for post processing LES-ODT results are addressed.

5.2 The Governing Equations for Autoignition

5.2.1 LES Equations

Using the same assumptions presented in section 2.4 in Chapter 2, LES governing equations in section 4.3.1 for constant density flow are presented below. The equations are non-dimensionalized similarly as Eqs. (2-27)–(2-31).

Continuity:

$$\frac{\partial \bar{\rho}}{\partial t} + \frac{\partial \bar{\rho} \bar{u}_i}{\partial x_i} = 0 \quad (5-1)$$

Conservation of Momentum:

$$\frac{\partial \bar{u}_i}{\partial t} + \bar{u}_j \frac{\partial \bar{u}_i}{\partial x_j} = -\frac{1}{\bar{\rho}} \frac{\partial \bar{p}}{\partial x_i} + \frac{1}{\bar{\rho} Re} \frac{\partial^2 \bar{u}_i}{\partial x_j \partial x_j} + \frac{1}{3\bar{\rho} Re} \frac{\partial}{\partial x_i} \left(\frac{\partial \bar{u}_j}{\partial x_j} \right) + \frac{\partial}{\partial x_j} (\bar{u}_i \bar{u}_j - \overline{u_i u_j}) \quad (5-2)$$

Conservation of Energy:

$$\frac{\partial \bar{T}}{\partial t} + \bar{u}_i \frac{\partial \bar{T}}{\partial x_i} = \frac{1}{\bar{\rho} Pr Re} \frac{\partial^2 \bar{T}}{\partial x_i \partial x_i} + \bar{\omega} + \frac{\partial}{\partial x_i} (\bar{u}_i \bar{T} - \overline{u_i T}) \quad (5-3)$$

Conservation of the Fuel:

$$\frac{\partial \bar{Y}_F}{\partial t} + \bar{u}_i \frac{\partial \bar{Y}_F}{\partial x_i} = \frac{1}{\bar{\rho} Le Pr Re} \frac{\partial^2 \bar{Y}_F}{\partial x_i \partial x_i} - \bar{\omega} + \frac{\partial}{\partial x_i} (\bar{u}_i \bar{Y}_F - \overline{u_i Y_F}) \quad (5-4)$$

Conservation of the Oxidizer:

$$\frac{\partial \bar{Y}_o}{\partial t} + \bar{u}_i \frac{\partial \bar{Y}_o}{\partial x_i} = \frac{1}{\bar{\rho} Le Pr Re} \frac{\partial^2 \bar{Y}_o}{\partial x_i \partial x_i} - \bar{\omega} + \frac{\partial}{\partial x_j} (\bar{u}_i \bar{Y}_o - \overline{u_i Y_o}) \quad (5-5)$$

The over bars in Eqs. (5-1)–(5-5) represent LES-filtered quantities. The term $(\overline{u_i u_j} - \overline{u_i} \overline{u_j})$ in Eq. (5-2) is the subgrid stress. Terms $(\overline{u_i T} - \overline{u_i} \overline{T})$ in Eq. (5-3), $(\overline{u_i Y_F} - \overline{u_i} \overline{Y_F})$ in Eq. (5-4), and $(\overline{u_i Y_O} - \overline{u_i} \overline{Y_O})$ in Eq. (5-5) are subgrid fluxes. Those subgrid stress and fluxes terms need to be modeled using a subgrid closure model.

5.2.2 ODT Equations

The ODT equations are obtained from (4-7)–(4-9) based on the assumptions in section 2.4 in Chapter 2 and are simplified for constant density flow. The equations are also non-dimensionalized similarly as Eqs. (2-27)–(2-31). The factor of 3 in front of the resolved diffusion terms in Eqs. (5-6) – (5-9) is to account for the terms contributing to the dissipation rate from the two directions that are normal to the ODT 1D element.

Conservation of Momentum

$$\rho \frac{\partial u_i}{\partial t} = \left[\frac{3}{Re} \frac{\partial^2 u_i}{\partial \eta \partial \eta} + \Omega_i \right] + \left\{ -\frac{\partial \hat{P}}{\partial x_i} - \rho \hat{u}_j \frac{\partial u_i}{\partial x_j} + \frac{1}{3 Re} \frac{\partial}{\partial x_i} \left(\frac{\partial \hat{u}_j}{\partial x_j} \right) \right\} \quad (5-6)$$

Conservation of Energy

$$\rho \frac{\partial T}{\partial t} = \left[\frac{3}{Pr Re} \frac{\partial^2 T}{\partial \eta \partial \eta} + \omega + \Omega_T \right] + \left\{ -\rho \hat{u}_j \frac{\partial T}{\partial x_j} \right\} \quad (5-7)$$

Conservation of the Fuel

$$\rho \frac{\partial Y_F}{\partial t} = \left[\frac{3}{Le Pr Re} \frac{\partial^2 Y_F}{\partial \eta \partial \eta} - \omega + \Omega_{Y_F} \right] + \left\{ -\rho \hat{u}_j \frac{\partial Y_F}{\partial x_j} \right\} \quad (5-8)$$

Conservation of the Oxidizer

$$\rho \frac{\partial Y_o}{\partial t} = \left[\frac{3}{Le Pr Re} \frac{\partial^2 Y_o}{\partial \eta \partial \eta} - \omega + \Omega_{Y_o} \right] + \left\{ -\rho \hat{u}_j \frac{\partial Y_o}{\partial x_j} \right\} \quad (5-9)$$

5.3 Initialization of the LES-ODT Flow Field

The initialization of the flow field including initializing the velocity vectors, the temperature, and the fuel and the oxidizer mass fractions in all three directions, x , y , and z . In order to generate LES-ODT statistics that are comparable to DNS, the initial vector and scalar fields of LES and ODT are obtained from the DNS field. First, the initial flow field is generated using DNS employing the steps presented in section 3.2 of Chapter 3. Second, the flow field from DNS is interpolated to the ODT field via tri-linear interpolation presented in section 4.7.1 of Chapter 4. Finally, the initial LES flow field is obtained from filtering the ODT flow field using the box filter in Eq. (4-52).

5.4 Boundary Conditions

Periodic boundary conditions are imposed in all three directions for LES-ODT simulations. Specifying the periodic boundary conditions during triplet mapping is tricky and special care is recommended. The starting location of an eddy that is selected randomly can be near the right boundary of the ODT element. If the lengths for these eddies happen to be

long enough such that those eddies extend beyond the boundary, correct boundary conditions have to be specified with care to ensure the precision of mapping.

5.5 Simulation Conditions

The concept of the turbulence energy spectrum is employed to specify the simulation conditions. The energy spectrum is the most important single quantity that characterizes the part of the turbulence that is associated with a given length scale (Batchelor, 1982). Theories on deriving the turbulence spectrum formula can be found in Pope (2000) and Batchelor (1982). Here we only included the expression for the spectrum

$$E(\mathbf{k}) = \oint_{\frac{1}{2}} \Phi_{ii}(\mathbf{k}) dS(k), \quad (5-10)$$

where $\Phi_{ii}(\mathbf{k})$ is the velocity spectrum tensor and $S(k)$ is a sphere in the wave space centered at the origin with a radius of k .

The turbulent energy spectrum is plotted against the wave number in Figure 5-1. As we examine the numerical simulation approaches for turbulent combustion from the energy-spectrum point of view, it is important to re-iterate the distinction between two simulation approaches considered here. The first approach is the Direct Numerical Simulation (DNS) approach, in which details of the flow at all energy scales are solved completely. The second approach is the so-called Very Large-Eddy Simulation (VLES) approach. VLES is a coarse-grid LES in which the filter size is significantly larger than the DNS spatial resolution. All other immediate LES approaches fall inside the range between VLES and DNS. While DNS provides detailed, extensive information about the flow, it is computationally too expensive

and may not be achievable in complex or industrial flows. VLES is computationally cheap, but the detailed information of the flow is missing and modeling this information may not be adequately represented by the standard approaches of LES based on extrapolation of resolved fields to represent subgrid scales. In the present study, we used two LES spatial resolutions that fall between DNS and VLES. Part of the motivation for this choice is to show that the proposed LES-ODT approach may be used to represent a broad range of cut-off scales, which can span from near DNS to near VLES.

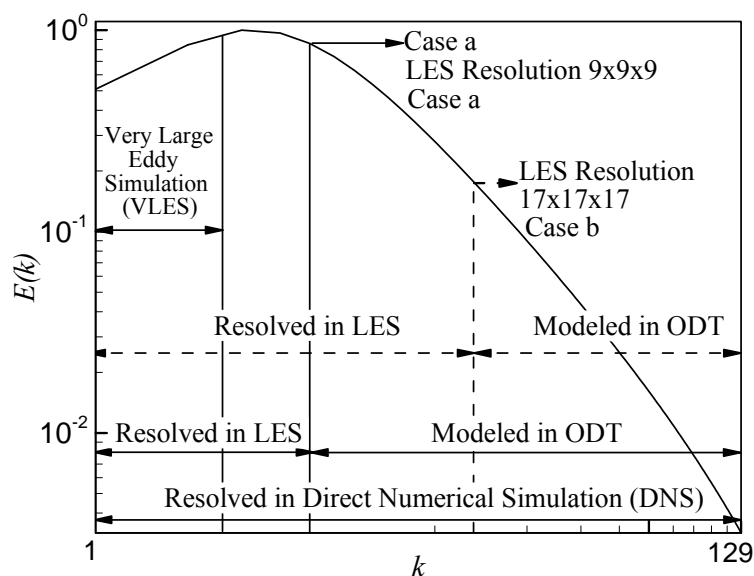


Figure 5-1 Turbulence energy spectrum plotted as a function of wave numbers

LES-ODT simulations of non-homogeneous autoignition in isotropic turbulence are performed for both low and high initial turbulence conditions. The turbulence condition imposes a stringent test of the model in predicting the interactions of turbulence and chemistry. Therefore, validation of the model for autoignition at both low and high

turbulence conditions is essential. Unity Lewis number is used for the low initial turbulence case. Three cases with Lewis number equal to 0.5, 1.0, and 2.0 are studied at high turbulence conditions. The purpose of carrying out LES-ODT simulations for different Lewis numbers is to validate the model against DNS for cases when mass transport plays an important role in the autoignition process. For each specific case, different LES resolutions are chosen according to the turbulence spectrum perspective. The simulation parameters for all the cases are presented in the next section.

5.6 Simulation Parameters

The common parameters for all the LES-ODT simulations are listed in Table 5-1. The flow and chemistry parameters have been discussed in chapters 2 and 3. The ODT model constants α_0 , C , and C_z have been presented in Chapter 4. The ODT model constant S_{min} denotes the minimum eddy size and should be equal to or larger than 6 and also be a multiple of 3. The model constant L_{max}/Δ denotes the maximum ODT eddy size divided by the minimum LES eddy size and should be unity. The model constant for the filter size is chosen to be 2 for the box filter during filtering operations applied to the ODT field. The numerical parameter of the LES time step is chosen to be 40 times of the DNS time step according to the resolution requirement. The ODT time step equals to the DNS time step. The stirring time step for ODT is chosen small enough to allow sufficient stirring events to happen without over or under sampling the events. The diffusion and reaction time step and the convection

time step are all chosen to be at the same magnitude as the stirring time step but are different from each other.

Table 5-1 Common parameters for LES-ODT simulation of non-homogeneous autoignition in isotropic turbulence

Common Parameter		Description	Case/ Value
General Characteristics		dimension	3D
		chemistry	reacting
Flow Characteristics	Re	Reynolds number	200
	τ_{turb}	turbulent time scale	13
	τ_{mix}	scalar mixing time scale	0.15
	P_o	zeroth-order pressure	1.0
Chemistry Characteristics	Pr	Prandtl number	0.7
	Da	Damköhler number	200
	α	non-dimensional heat release	0.75
	β	Zel'dovich number	2.0
Model Constants	α_0	degree of energy exchange among velocities in ODT	0.33
	C	stirring event frequency control parameter	3.78
	C_Z	viscosity penalty	0.002
	S_{min}	minimum eddy size	6
	L_{max}/Δ	ratio of maximum ODT eddy size to minimum LES eddy size	1.0
	f_c	filter size	2.0
Numerical Parameters	Lld	number of ODT elements in each direction	17
	N_{ODT}	ODT grid size along each ODT element	129
	L	domain size in each direction	3.6
	Δt_{LES}	LES time step	0.04
	Δt_{ODT}	ODT time step	0.001
	Δt_S	ODT stirring time step	1.0×10^{-5}
	Δt_D	ODT diffusion and reaction time step	1.2×10^{-5}
	Δt_C	ODT convection time step	9.0×10^{-6}
	ε_{SOR}	Successive Over-Relaxation tolerance	2.5×10^{-9}
Statistics	N_{bin}	number of mixture fraction bins	31

The simulation parameters that are specific to each case are listed in Table 5-2. The turbulence intensity is defined in Eq. (3-27) and Lewis number is defined in Eq. (2-38). The

Taylor microscale is defined in (3-28) and the turbulent time scale and the scalar mixing scale are defined in (3-33) and (3-34), respectively. The LES grid size is selected based on the spectrum analysis. The number of ODT elements is specified in order to obtain sufficient statistics. The ODT grid size is consistent with the DNS grid size so that the statistics collected are comparable to DNS statistics. The domain size is also consistent with that used in DNS. In Chapter 6 and Chapter 7, case (a) is characterized by the LES grid size equal to 9 and case (b) is characterized by the LES grid size equal to 17.

Table 5-2 Specific parameters for LES-ODT simulation of non-homogeneous autoignition in isotropic turbulence

Specific Parameters	Description	Value							
		u_{turb}	turbulence intensity	3.0					
Re_λ	Taylor time scale	405						100	
Le	Lewis number	0.5		1.0		2.0		1.0	
N_{LES}	LES grid size in each direction	9 ¹	17 ²	9 ¹	17 ²	9 ¹	17 ²	9 ¹	17 ²

5.7 Data Post-Processing

Simulation results of autoignition in non-homogeneous mixtures using the proposed LES-ODT model are post-processed in order to compare with the DNS results. Here, the comparisons are based on both volume-averaged statistics and conditional statistics of thermo-chemical scalars. Volume-averaged statistics provide measures for the global evolution of the mixture and the progress of reaction. Conditional statistics provide further

¹ Represent LES-ODT case (a)

² Represent LES-ODT case (b)

insight into the finite-rate chemistry effects. For an acceptable outcome of the simulations, both sets of statistics must be consistent qualitatively and to a large extent quantitatively to statistics obtained from DNS.

5.7.1 Volume-Averaged Statistics

The first validation experiment is to compare LES-ODT simulation results with DNS using volume-averaged statistics, which provide global information on the model performance. Note here we will present the results for the LES-ODT case (b), which has a LES spatial resolution with 17 grid points in each direction, and compare the results with that from DNS. The means include the volume-averaged means of the progress variable (defined in 3-37), \bar{c} , the reaction rate, $\bar{\omega}$, the temperature, \bar{T} , and the mass fractions, \bar{Y}_F and \bar{Y}_O . The RMS include the volume-averaged RMS of the temperature, $\overline{T^{n^2}}$, and the mass fractions, $\overline{Y_F^{n^2}}$, and $\overline{Y_O^{n^2}}$.

5.7.2 Conditional Statistics

The statistics from ODT are obtained in such a way that the conditional means and RMS of scalars are computed based on averaging the instantaneous scalar field of ODT over time and space with respect to the mixture fraction field within a LES time step. The conditional mean of a scalar is expressed as

$$\bar{\phi} = \left\langle \sum_{i=1}^n \sum_{j=1}^m \phi_{ij} \middle| Z \right\rangle, \quad (5-11)$$

where $\bar{\phi}$ is the conditional mean of a scalar, and ϕ_{ij} is the instantaneous value of the scalar, i is the index varies from 1 to the total number of ODT time steps, j is the index varies from 1 to the total number of ODT points, which equals to ODT grid points multiplied by the number of ODT elements. Therefore, the conditional mean of a scalar is time and volume-averaged with respect to the mixture fraction. The conditional mean square of a scalar is computed in the same way

$$\overline{\phi^2} = \left\langle \sum_{i=1}^n \sum_{j=1}^m \phi_{ij}^2 \middle| Z \right\rangle, \quad (5-12)$$

where the instantaneous square value of the scalar ϕ_{ij} is averaged over time and space with respect to the mixture fraction. Thus, the RMS of the scalar can be expressed as

$$\overline{\phi''\phi''} = \left(\overline{\phi^2} - \bar{\phi}^2 \right)^{1/2}. \quad (5-13)$$

5.8 Conclusions

In this chapter, we have presented the initialization procedure for the LES-ODT field. It is accomplished by interpolating the initial DNS flow field to LES and ODT so that LES-ODT can generate comparable results with DNS. To be consistent with DNS, we used periodic boundary conditions for both LES and ODT simulations. The simulation conditions

are presented in an energy spectrum perspective. In each case, two simulation cases with different LES spatial resolutions are selected based on the energy resolved by LES.

Chapter 6 LES-ODT Model Validation: Autoignition in Non-Homogeneous Mixtures – Volume-Averaged Statistics

6.1 Objectives

The principal objective of this chapter is to validate the coupled LES-ODT scheme by comparing volume-averaged statistics of thermo-chemical scalars during non-homogeneous autoignition in isotropic turbulence with DNS. The unity Lewis number case is studied at both low and high turbulence conditions. The simulation time for the low turbulence case is longer than for the high turbulence case because the reaction sustains longer. Note here we only compare the LES-ODT case (b), which has a LES spatial resolution with 17 grid points in each direction, with DNS; similar results can be obtained by comparing LES-ODT case (a) with DNS.

6.2 Extent of Scalar Mixedness

The extent of scalar mixedness is defined as

$$\zeta = \frac{\overline{Z'^2}}{\overline{Z}(1-\overline{Z})}, \quad (6-1)$$

where \overline{Z} is the volume-averaged mean of the mixture fraction, and $\overline{Z'^2}$ is the volume-averaged RMS of the mixture fraction. The extent of scalar mixedness represents the extent of the fluctuations relative to the means of a scalar. The theoretical range for the extent of

scalar mixedness is between 0, representing total mixedness, and 1, representing fully segregated mixtures. The temporal evolution of this quantity represents the rate of scalar mixing.

Figure 6-1 shows a comparison of the scalar mixedness as a function of time between LES-ODT and DNS for the unity Lewis number case at both low and high turbulence conditions. Overall, the prediction for the extent of global scalar mixedness by LES-ODT is very good. The results from LES-ODT and DNS follow each other very closely. Initially, the mixtures are partially mixed. The mixtures approach a state of complete mixing with a relatively high scalar mixing rate at earlier times and a moderate scalar mixing rate at later times. This is because the scalar gradients are high initially, thus the mixtures tend to mix and diffuse faster. At later stages, the mixtures are approaching homogenization and the scalar mixing rate is much lower. The turbulence intensities play an important role on scalar mixing. The scalar mixing rate is much higher and the time to approach total mixing is much shorter when the turbulence intensity is higher, which is clearly shown in Figure 6-1.

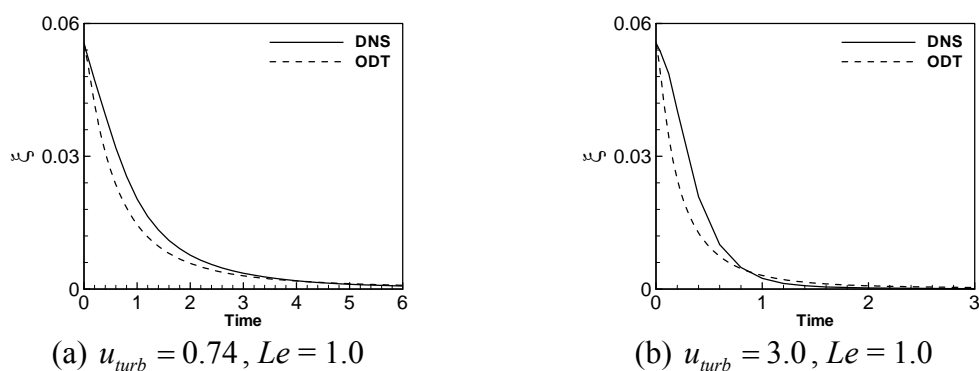


Figure 6-1 Comparison between LES-ODT and DNS for the extent of scalar mixedness as a function of time

6.3 Volume-Averaged Means

Figure 6-2 shows a comparison of the volume-averaged means of the progress variable as a function of time between LES-ODT and DNS for the unity Lewis number case at both low and high turbulence conditions. In both cases, LES-ODT generates excellent predictions of the global progress of chemistry in time. At low turbulence conditions, LES-ODT results are almost exactly the same as DNS. In the high-turbulence case, there appears to be a shift in the ODT results, which is also observed in the results below for the reaction rate. This indicates that a slightly larger number of “failed” ignition kernels are found in the LES-ODT simulations, which explains the overall delay in ignition in the LES-ODT results. However, this is only a statistical delay due to the fact that the number of total ignition kernels is small. Consequently, if a single ignition kernel fails, the global reaction progress will be delayed, and this is verified by the fact that this delay is not present locally in the conditional statistics included in the next chapter. As expected, given enough time, the mixture evolves towards complete combustion as indicated by the asymptotic value of unity approaches at later times. Furthermore, the reaction progresses at a much higher speed at high turbulence conditions because turbulence enhances mixing. However, turbulence not only enhances mixing, but also generates instabilities and flame extinctions especially at early stages of ignitions. This is the reason why a small dip is observed at time equal to 1.0 approximately in the high turbulence case.

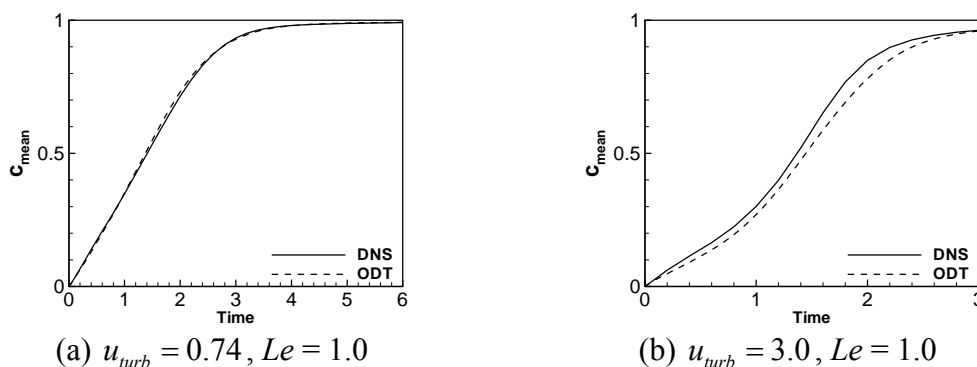


Figure 6-2 Comparison between LES-ODT and DNS for volume-averaged means of the progress variable as a function of time

Figure 6-3 shows a comparison of the volume-averaged means of the reaction rate as a function of time between LES-ODT and DNS for the unity Lewis number case at both low and high turbulence conditions. The figure shows that LES-ODT predicts the global evolution of the reaction rate very accurately. In both cases, the reaction rate exhibits a rapid increase initially with subsequently a more moderate increase to an intermediate peak value; as the mixture evolves towards complete burning, the volume-averaged reaction rate decays rapidly to zero. The rates of rise and decay of the mean reaction rates are captured successfully by LES-ODT simulations, with the lower turbulence conditions exhibiting an approximately factor of 2 decay time in comparison to the high-turbulence conditions (Figure 6-3 (b)). While the times corresponding to the peak values of the reaction rates are essentially the same between LES-ODT and DNS results, the magnitude of the peaks associated with the LES-ODT simulations are lower by as much as 18% in the high-turbulence case (Figure 6-3 (b)) and are slightly higher for the low turbulence case (Figure 6-3 (a)). This difference is

consistent with what we have observed from the volume-averaged means of the progress variable and the reason has been stated clearly.

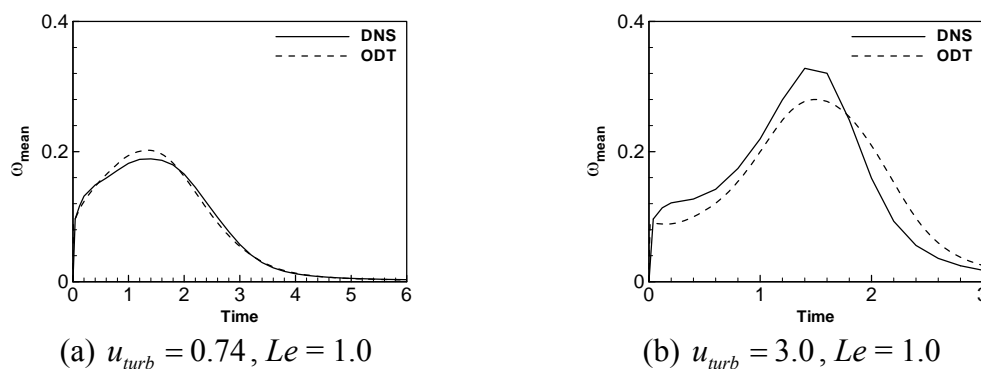


Figure 6-3 Comparison between LES-ODT and DNS for volume-averaged means of the reaction rate as a function of time

Figure 6-4, Figure 6-5, and Figure 6-6 show a comparison of volume-averaged means of the temperature, the fuel mass fraction, and the oxidizer mass fraction, respectively, between LES-ODT and DNS for the unity Lewis number case at both low and high turbulence conditions. The figures show that the agreement between LES-ODT and DNS results is very good. Both of them exhibit the same trends in time including the initial rapid rise of the temperature and the initial rapid decay of the reactants' mass fractions followed by the leveling off of chemical conversion at later stages of the mixture evolution. In all the cases, the volume-averaged means of the temperature and the reactants' mass fractions approach an asymptotic value that indicates complete burning of the mixture. Later comparisons of conditional statistics reveal that the particular modes of burning reach this asymptotic state. Again, the time scales associated with the volume-averaged statistics also occur over similar scales between LES and DNS, and take approximately twice as long for

the lower turbulence case (Figure 6-4, Figure 6-5, and Figure 6-6 (a)). A difference of approximately 2% between LES-ODT and DNS results is observed at high turbulence conditions. Volume-averaged means of LES-ODT temperature is slightly slower than that of DNS temperature due to the slightly lower magnitude of the reaction rate and the subtle delay of the ignition as observed before in the volume-averaged means of the progress variable. As a result, the prediction by LES-ODT exhibits a slower consumption rate of reactants compared to DNS.

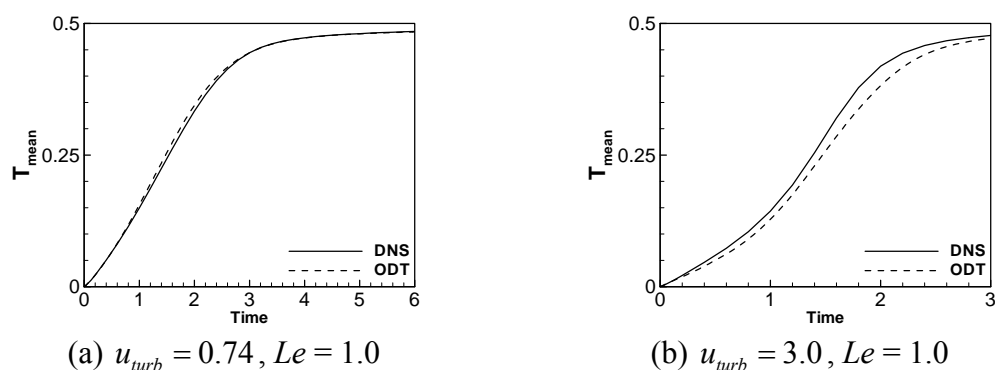


Figure 6-4 Comparison between LES-ODT and DNS for volume-averaged means of the temperature as a function of time

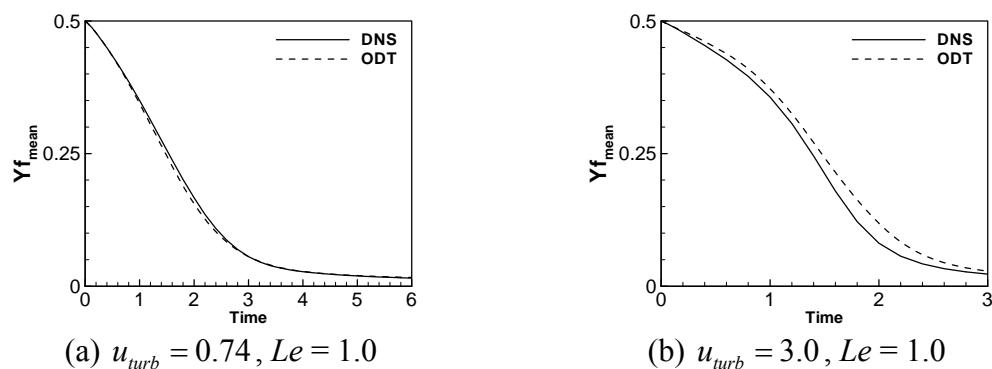


Figure 6-5 Comparison between LES-ODT and DNS for volume-averaged means of the fuel mass fraction as a function of time

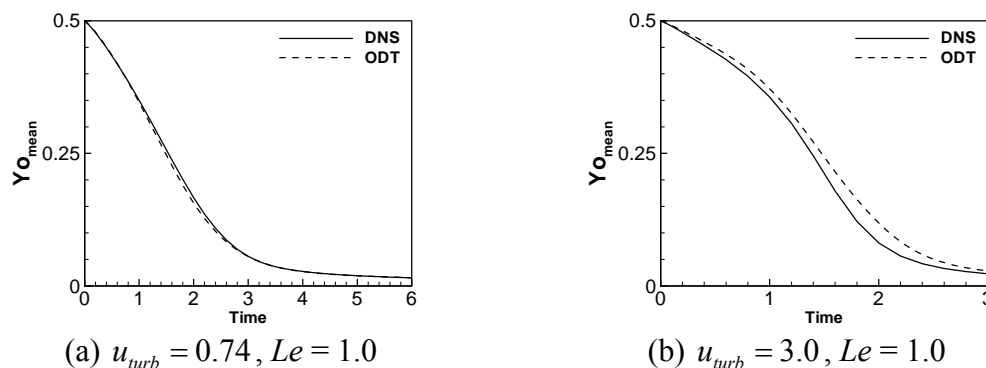


Figure 6-6 Comparison between LES-ODT and DNS for volume-averaged means of the oxidizer mass fraction as a function of time

In summary, the volume-averaged means show that LES-ODT generates excellent predictions of the global scalar mixing rate, the progress of chemistry, the global evolution of the reaction rate and the temperature, and the global consumption rate of the reactants' mass fractions. The subtle delay in ignition shown in the LES-ODT simulation results at high turbulence conditions is only a statistical delay, which is not present in the conditional statistics included in the next chapter. The reason attributes to the fact that the number of total ignition kernels is small and consequently, if a single ignition kernel fails, the global reaction progress will be delayed. Overall, the volume-averaged means provide us a solid validation of the LES-ODT model against DNS. However, it is extremely difficult to capture the higher-order moments of the volume-averaged statistics, especially at high turbulence conditions. The following discussion will be focused on comparing the second moments of volume-averaged statistics between LES-ODT and DNS.

6.4 Volume-Averaged RMS

Higher order statistics present more significant challenges to models of turbulent combustion. They also reflect additional moments of the statistical distribution of thermochemical scalars, such as the shape of the probability-density function (PDF) of these scalars. The discussion below provides additional comparisons of LES-ODT and DNS results based on the second moments of the scalar statistics.

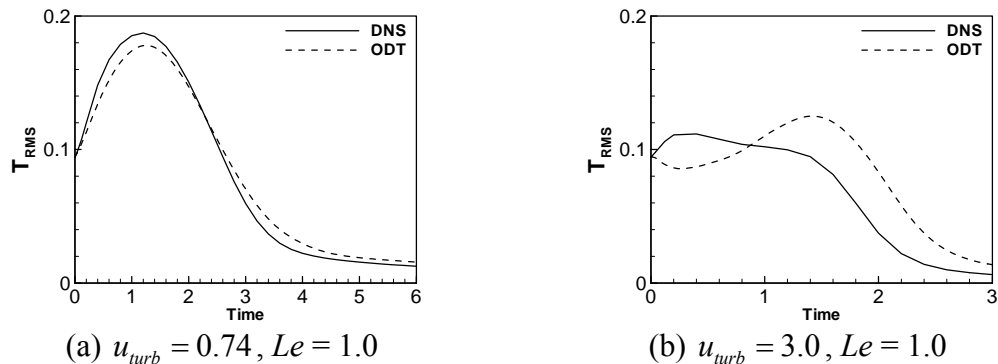


Figure 6-7 Comparison between LES-ODT and DNS for volume-averaged RMS of the temperature as a function of time

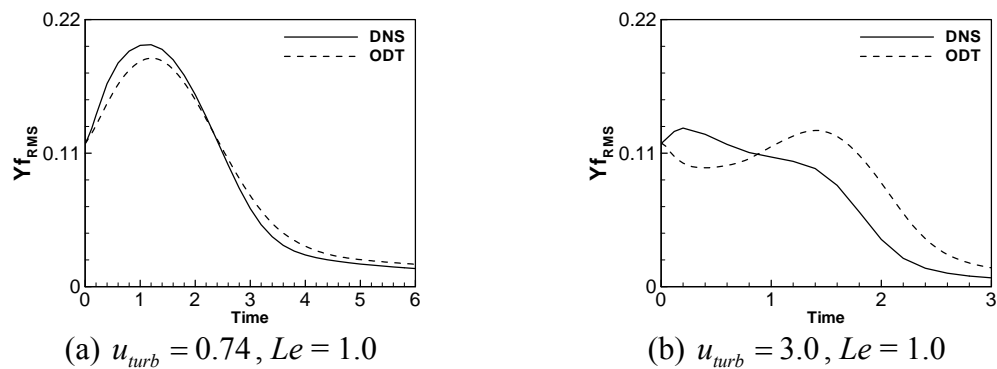


Figure 6-8 Comparison between LES-ODT and DNS for volume-averaged RMS of the fuel mass fraction as a function of time

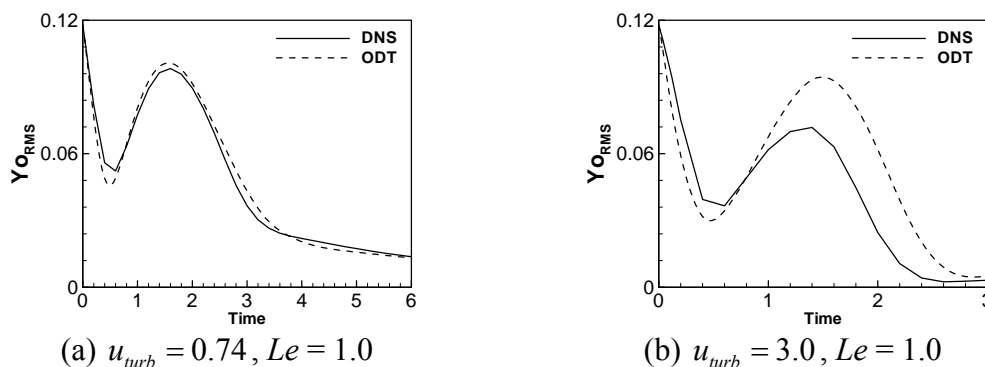


Figure 6-9 Comparison between LES-ODT and DNS for volume-averaged RMS of the oxidizer mass fraction as a function of time

Figure 6-7, Figure 6-8, and Figure 6-9 show a comparison of the volume-averaged RMS of the temperature, the fuel mass fraction, and the oxidizer mass fraction, respectively, between LES-ODT and DNS for the unity Lewis number case at both low and high turbulence conditions. LES-ODT provides an excellent prediction of the global fluctuations of thermo-chemical scalars overall. At both turbulence conditions, the global fluctuations of thermo-chemical scalars are successfully captured by LES-ODT compared to DNS. At high turbulence conditions, the fluctuations of quantities from LES-ODT show a small difference compared to DNS. Given the fact the overall magnitude of the RMS is small, the difference between LES-ODT and DNS is not significant. The reason again attributes to the subtle statistical ignition delay due to the fact that the number of total ignition kernels is small.

6.5 Conclusions

In this chapter, we validate the LES-ODT against DNS based on volume-averaged statistics. Both low and high turbulence conditions are studied. LES-ODT provides very good

predictions of the global scalar mixing rate, the global progress of chemistry, the global evolution of the reaction rate and the temperature, and the global consumption rate of the reactants' mass fractions. Moreover, the predictions of the global fluctuations of the thermochemical scalars by LES-ODT are excellent. The time for the global progress of autoignition process at low turbulence conditions is twice as long as at high turbulence conditions, which is captured by LES-ODT successfully. Furthermore, a subtle statistical ignition delay is observed in LES-ODT simulations for the high turbulence case. The reason attributes to the fact that the number of total ignition kernels is small. Thus, a single failed ignition kernel may have an effect on the total ignition progress. This explanation can be verified by the results included in the next chapter because this delay is not present in the conditional statistics.

Chapter 7 LES-ODT Model Validation: Autoignition in Non-Homogeneous Mixtures – Conditional Statistics

7.1 Objectives

In the previous chapter, we validate LES-ODT model by comparing the volume-averaged statistics between LES-ODT and DNS. While volume-averaged statistics provide us information on the global performance of the model, conditional statistics shed more light onto finite-rate chemistry effects involved in the autoignition process. Therefore, validation of the LES-ODT model formulation by comparing the conditional statistics from LES-ODT with that from DNS is another important indicator of the LES-ODT model performance.

In the following discussion, we will compare the conditional statistical results obtained from LES-ODT with that from DNS. The DNS statistics are generated by averaging over a time period that equals to 40 DNS time steps, with 20 time steps before and 20 time steps after the actual, instantaneous time. This is because LES time step equals to 40 DNS time steps. The remainder sections are organized as follows. First, the unity Lewis number case with low turbulence conditions is presented. Second, the three Lewis number cases with high turbulence conditions are discussed. In each case, the results of conditional means and RMS are compared between two LES-ODT cases and the DNS case.

7.2 Case with the Low Turbulence Intensity

The comparison between LES-ODT and DNS conditional statistics at low turbulence conditions is performed in this section. The non-dimensional time period is from 0 to 6.0, in which the kernels start with ignition at lean mixture conditions, propagate from lean to rich conditions, and then subside near stoichiometric conditions with a diffusion flame burning mode. The conditional means and RMS are compared between two LES-ODT cases (a) and (b) with DNS. In case (a) of LES-ODT, the LES spatial resolution with 9 grid points in each direction is used and in case (b), a higher LES spatial resolution with 17 grid points in each direction is employed. The conditional means are discussed first and the conditional RMS is presented second.

7.2.1 Conditional Means of the Temperature

Figure 7-1 shows a comparison of the conditional means of the temperature between LES-ODT and DNS for the low turbulence case. Overall, LES-ODT results agree very well with DNS results during the whole autoignition process. The ignition is characterized by the departure of the temperature from the pure mixing linear profile, which is a straight line with a negative slope. Then the ignition kernels propagate from lean to rich mixtures and the peak temperature is found near the stoichiometric conditions due to the formation of diffusion flames at later stages of burning. The LES-ODT simulations successfully capture the onset of ignition and the transition of burning modes from lean premixed to rich premixed flames, the location and the magnitude of the peak values, and the shrinking speed of the mixture

fraction range due to mixing. Both LES-ODT cases (a) and (b) agree very well with the DNS results. This indicates that LES-ODT is reasonably independent of the LES spatial resolution.

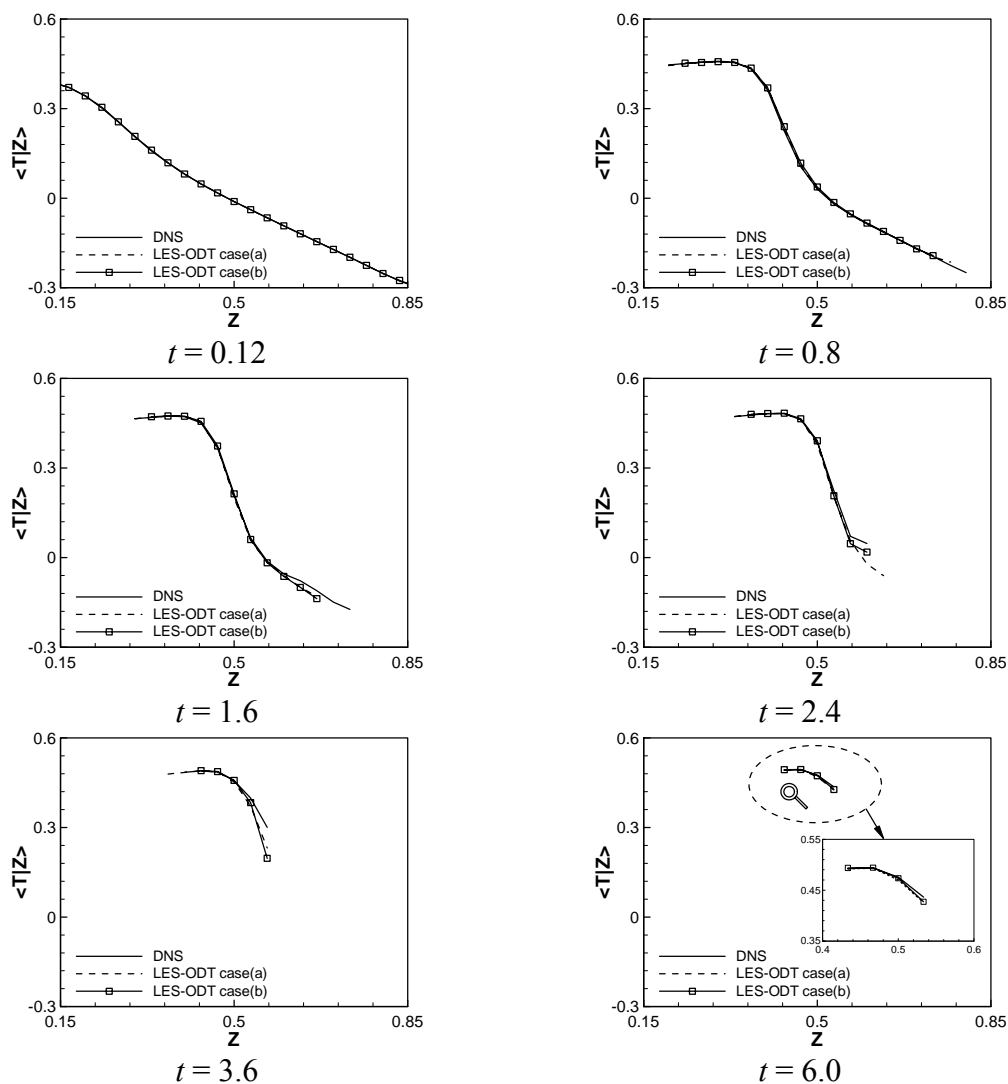


Figure 7-1 Comparison of conditional means of the temperature between LES-ODT and DNS at different times for the low turbulence case with $Le = 1$

7.2.2 Conditional Means of the Mass Fractions

Figure 7-2 and Figure 7-3 show the conditional means of the fuel and the oxidizer mass fractions obtained from LES-ODT and DNS, respectively, at different times for the low turbulence condition. In general, LES-ODT predicts the conditional means of the reactants' mass fractions very well. The onset of ignition is characterized by the departure of the reactants' mass fractions from the pure mixing linear line at lean conditions due to the initially preheated oxidizer. As the ignition kernels propagate from lean to rich mixtures, reactants are consumed and further departure of the mass fractions from the pure mixing profile is observed. During the whole autoignition process, the fuel and the oxidizer diffuse towards each other and the mixture fraction range shrinks due to mixing. At the later stages of burning, diffusion flames are formed near the stoichiometric condition due to burning of excess fuel and oxidizer. LES-ODT is able to capture the ignition in lean mixtures, the propagation of the kernels, the distinct burning modes, and the shrinking of the mixture fraction range. Similar to what we have observed from the conditional means of the temperature, both LES-ODT cases generate accurate results compared to DNS and provide excellent predictions of the physics. Again, the LES-ODT model is reasonably independent of the LES spatial resolution.

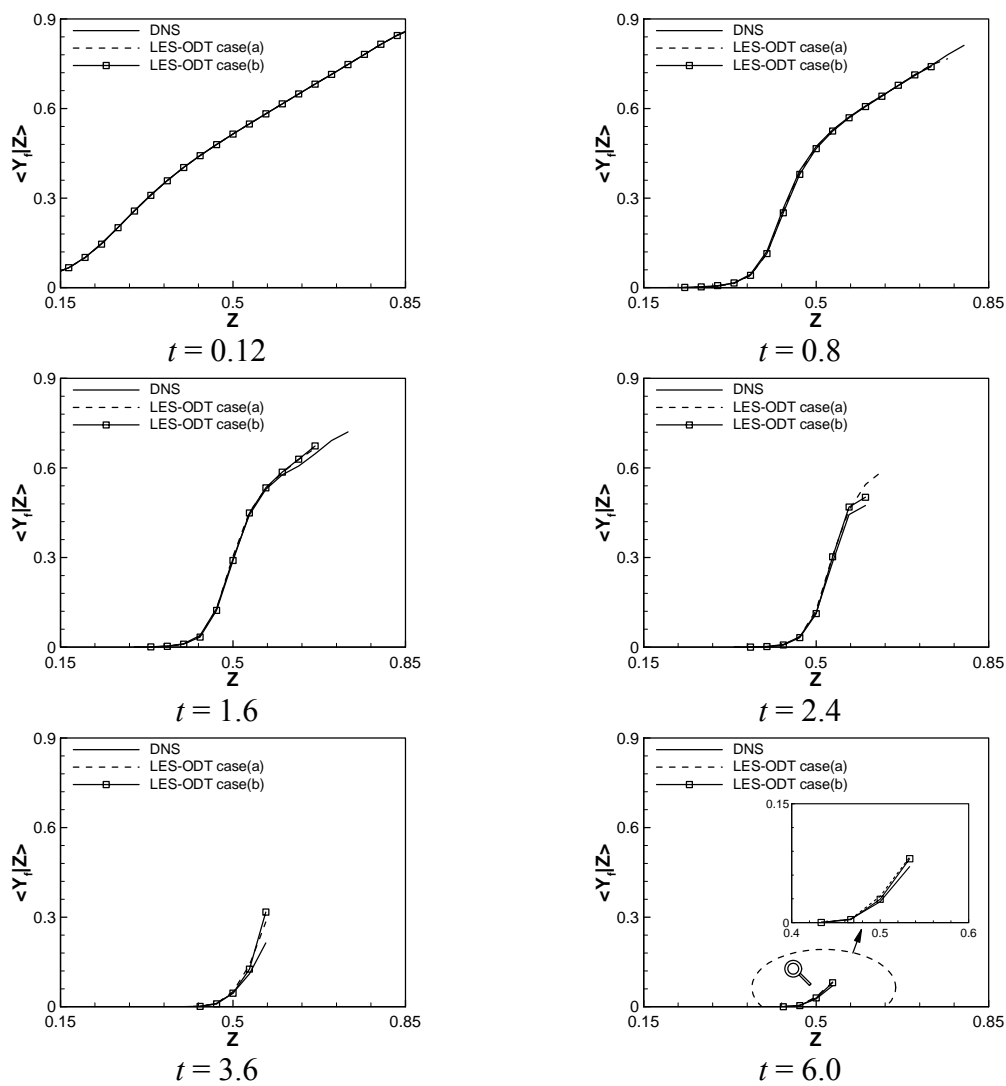


Figure 7-2 Comparison of conditional means of the fuel mass fraction between LES-ODT and DNS at different times for the low turbulence case with $Le = 1$

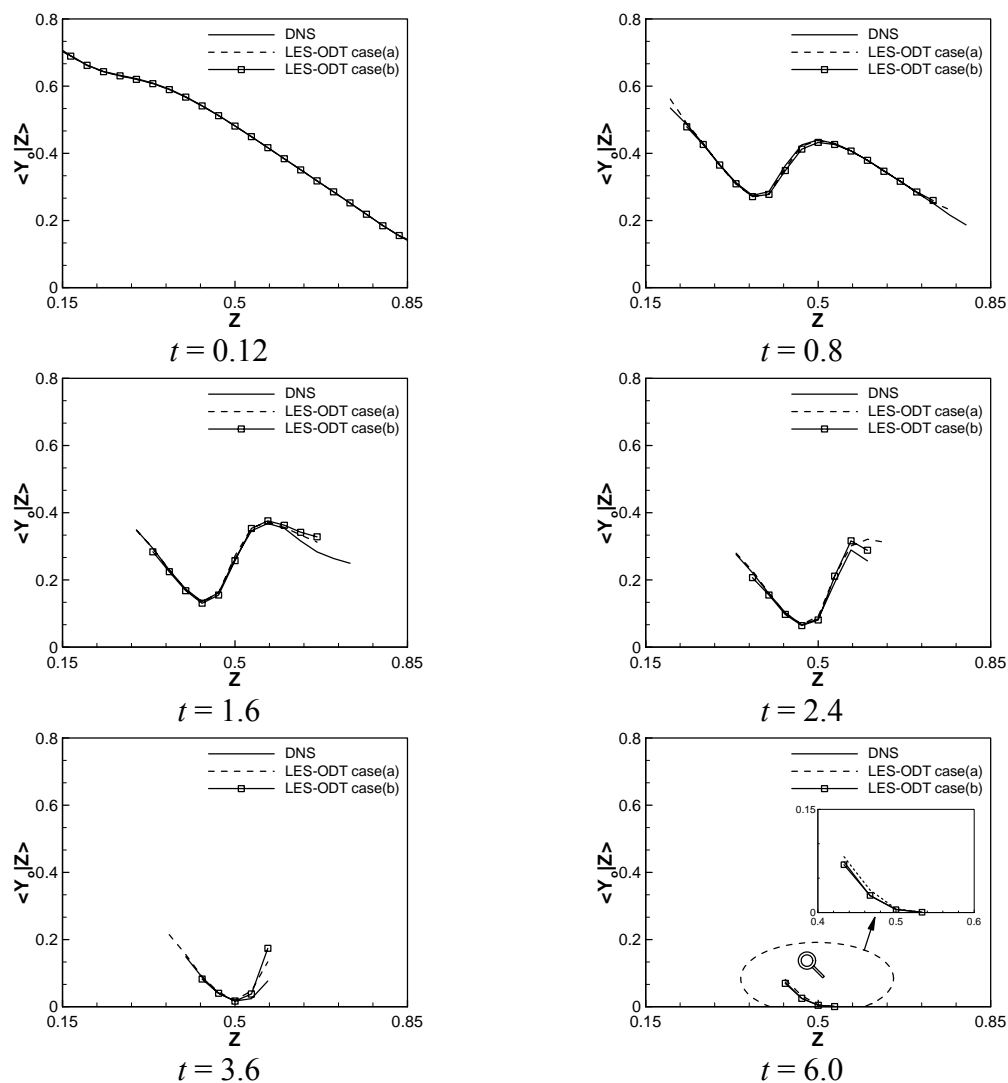


Figure 7-3 Comparison of conditional means of the oxidizer mass fraction between LES-ODT and DNS at different times for the low turbulence case with $Le = 1$

7.2.3 Conditional Means of the Reaction Rate

Figure 7-4 shows a comparison of the conditional means of the reaction rate between LES-ODT and DNS for the low turbulence case at different times. Overall, the results show excellent agreement between LES-ODT and DNS. The ignition takes place in discrete

kernels at lean conditions due to the preheated oxidizer. The transition of burning modes from lean to rich premixed flames occur at stoichiometric conditions as flame kernels propagate from lean to rich conditions. At the end of the burning process (time equal to 6.0), only non-premixed burning is observed in the diffusion flame mode. Those physics are clearly represented by LES-ODT simulation results. Moreover, the shrinking of the mixture fraction range during the autoignition process is captured by LES-ODT accurately. Again both LES-ODT cases (a) and (b) show comparable results to DNS and LES-ODT model is independent of the LES spatial resolution. As we can see from the results, the magnitude of diffusion flames is tremendously lower compared to the lean and rich premixed flames and it is much harder to predict. Nevertheless, LES-ODT is able to capture not only the non-premixed burning mode at the end of the burning process but also the magnitude of the diffusion flames with comparable accuracy to DNS. Thus, LES-ODT is a very promising model for predicting the transient nature of the autoignition process in non-homogeneous mixtures.

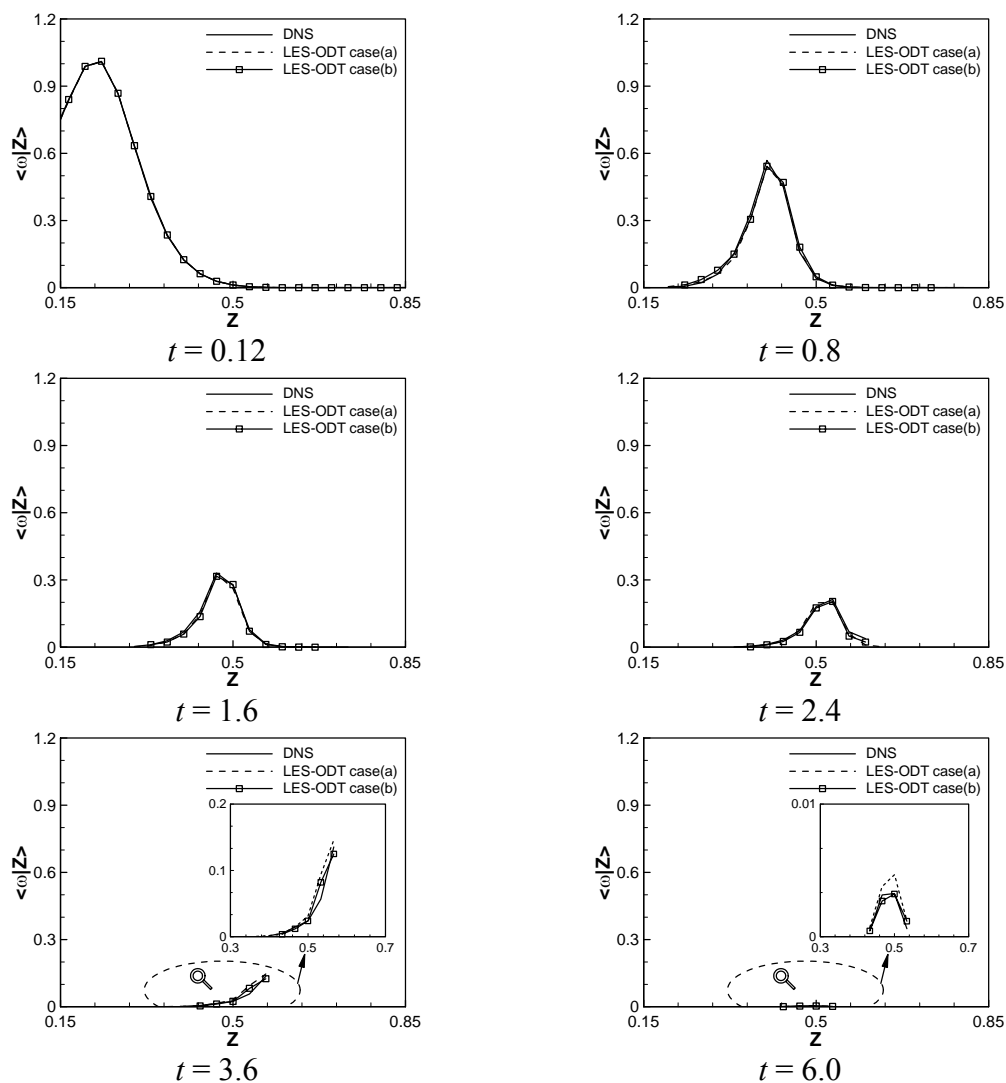


Figure 7-4 Comparison of conditional means of the reaction rate between LES-ODT and DNS at different times for the low turbulence case with $Le = 1$

LES-ODT successfully predicts the physics that are represented by DNS. The physics include the onset of ignition, the distinct burning modes, the transition of these burning modes, and the locations and the magnitude of the peak values in the mixture fraction space. This provides us a fundamental validation of the LES-ODT model. The next task is to validate the LES-ODT model based on the RMS of reactive scalars. The second moments of

the conditional statistics are much harder to model; however, modeling higher order moments is an integral part of the model validation process because the fluctuations of scalars and interactions of mixing and chemistry at subgrid scales must be represented with reasonable accuracy in order to simulate the turbulent combustion process successfully.

7.2.4 Conditional RMS of the Temperature and the Mass Fractions

Figure 7-5, Figure 7-6, and Figure 7-7 show a comparison of conditional RMS of the temperature, the fuel mass fraction, and the oxidizer mass fraction, respectively, between LES-ODT and DNS at different times. The overall prediction of fluctuations of the thermochemical scalars by LES-ODT is very good. The shifting of peaks corresponds to the propagation of ignition kernels from lean to rich conditions. The fluctuations of thermochemical scalars during rich premixed burning are larger than those during lean premixed burning. At later stages of the autoignition process, the fluctuations are only present near the stoichiometric conditions due to non-premixed burning in the diffusion flame mode. LES-ODT is able to represent not only the kernel propagation and distinct burning modes but also the magnitude and the location of the peaks at different mixture fraction values during the whole autoignition process. Moreover, the mixture fraction range corresponds to the conditional RMS of the temperature shrinks during the autoignition process due to mixing. This is also predicted by LES-ODT accurately. Furthermore, both LES-ODT cases (a) and (b) represent the fluctuations with comparable accuracy to DNS and the effects of the LES spatial resolution on the model performance are negligible.

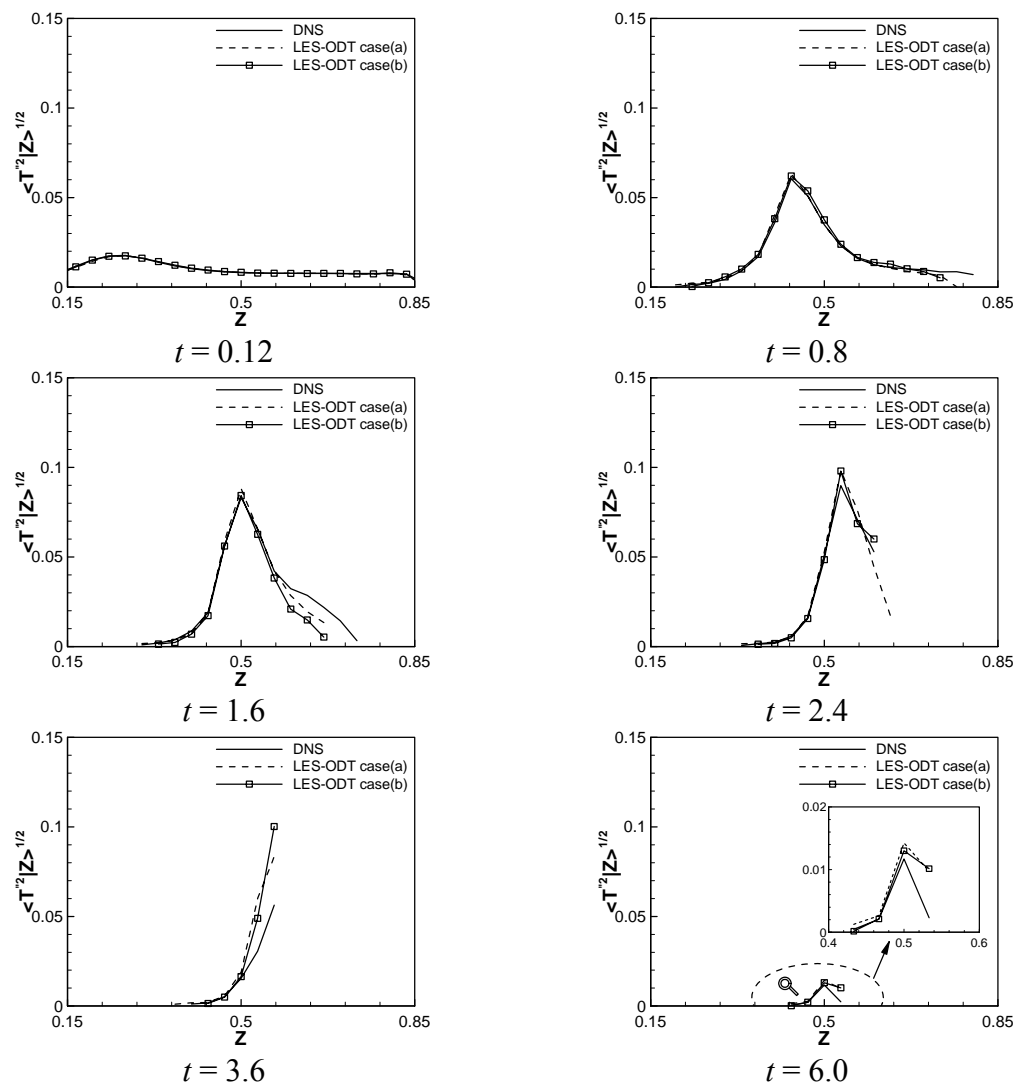


Figure 7-5 Comparison of conditional RMS of the temperature between LES-ODT and DNS at different times for the low turbulence case with $Le = 1$

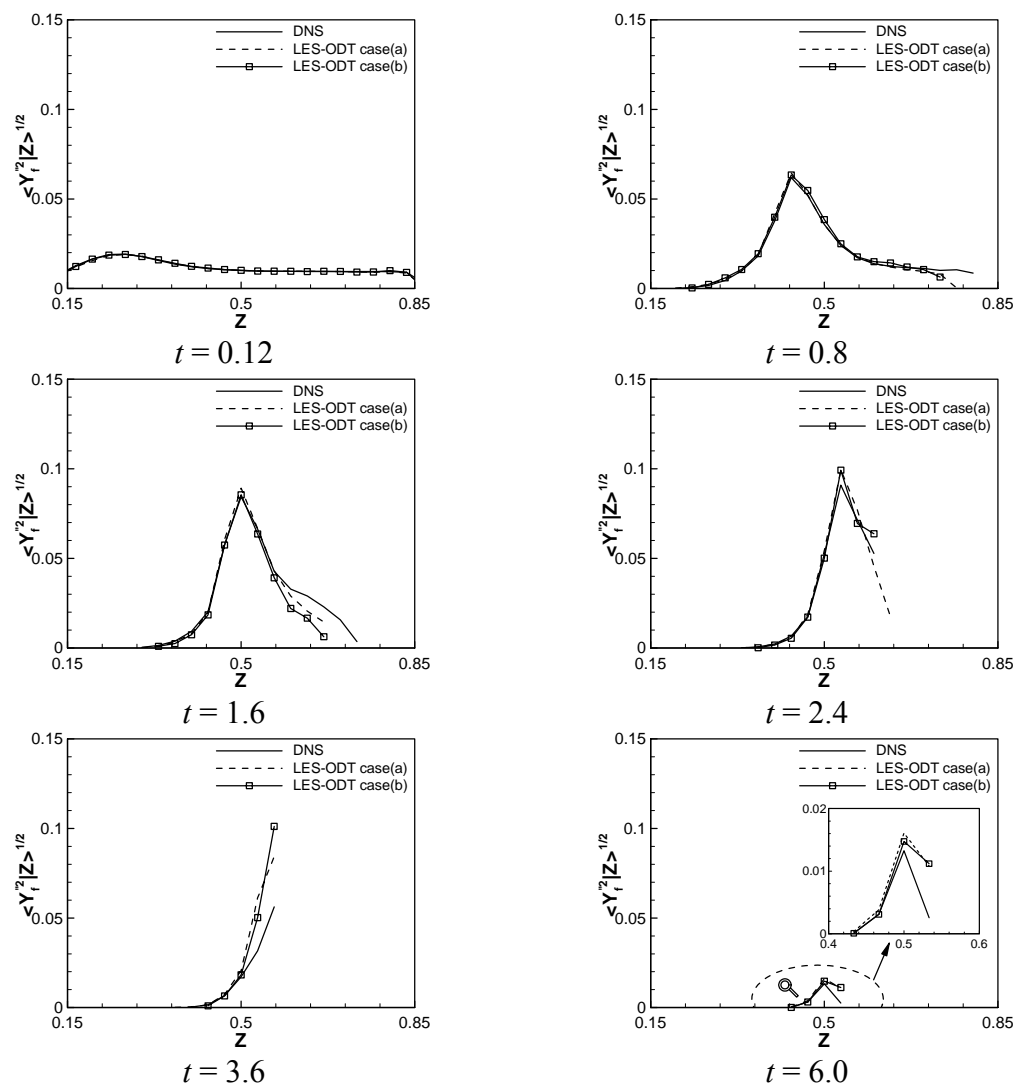


Figure 7-6 Comparison of conditional RMS of the fuel mass fraction between LES-ODT and DNS at different times for the low turbulence case with $Le = 1$

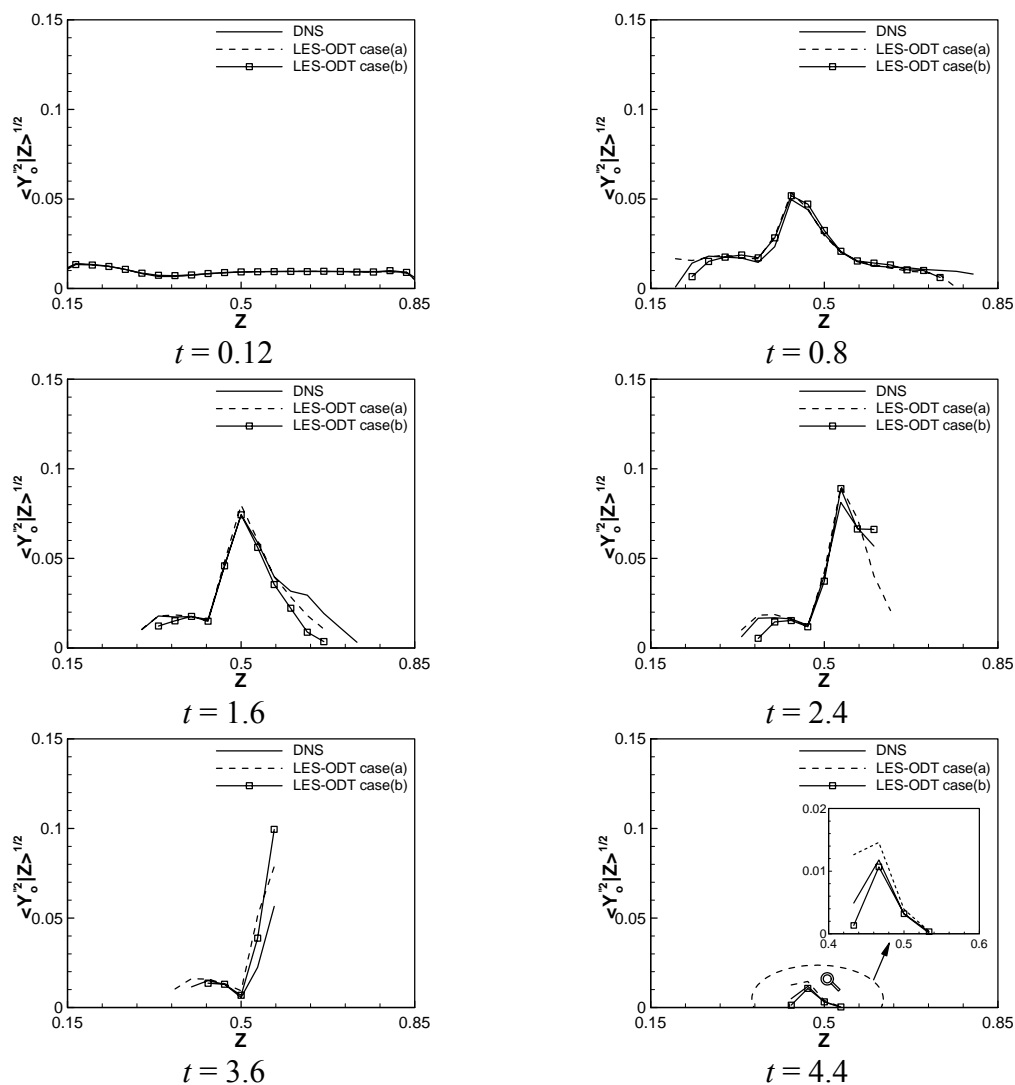


Figure 7-7 Comparison of conditional RMS of the oxidizer mass fraction between LES-ODT and DNS at different times for the low turbulence case with $Le = 1$

As a short conclusion of this section, LES-ODT provides very good predictions of fluctuations of thermo-chemical scalars in the mixture fraction space. LES-ODT is able to capture the onset of ignition, the kernel propagation, and the transition of burning modes during the whole combustion process. Furthermore, the magnitudes and the location of peaks

are represented by LES-ODT accurately. In the next section, the validation of LES-ODT model is carried out further for high turbulence conditions.

7.3 Case with the High Turbulence Intensity

High turbulence conditions can generate effects such as flame instabilities and high fluctuations of vector and scalar fields. Thus, validation of the LES-ODT model against DNS is essentially harder compared to the low turbulence case. In this section, the conditional statistics from LES-ODT and DNS are compared for three different Lewis number cases, in which Lewis number equal to 0.5, 1.0, and 2.0, respectively. In each Lewis number case, the conditional means and RMS are compared between two LES-ODT cases (a) and (b) with DNS. In case (a) of LES-ODT, LES spatial resolution with 9 grid points in each direction is used and in case (b), a higher LES spatial resolution with 17 grid points in each direction is employed. For the high turbulence cases, time period from 0 to 2.8 is sufficient to compare the statistics because complete combustion is achieved earlier compared to the low turbulence case.

7.3.1 Conditional Means of the Temperature

Figure 7-8, Figure 7-9, and Figure 7-10 show a comparison of the conditional means of temperature between LES-ODT and DNS at different times for high turbulence conditions with Lewis numbers equal to 0.5, 1.0, and 2.0, respectively. The overall agreement between LES-ODT and DNS is excellent. Similar to what we have observed from the low turbulence

case, the onset of ignition is again captured by LES-ODT correctly. Different from the low turbulence case, complete combustion is achieved before flames reach the rich mixtures and only lean premixed burning mode is present. This is predicted by LES-ODT accurately. Moreover, the magnitude and the location of the peaks are represented in LES-ODT with reasonable accuracy. The Lewis number effects and turbulence condition effects are represented by LES-ODT precisely. Discussions on the details of those effects are included in section 3.7.1 on page 54. Furthermore, results from both LES-ODT cases (a) and (b) are accurate and the LES grid size has negligible effects on LES-ODT model performance.

The difference in the mixture fraction range between LES-ODT and DNS indicates that the local dissipation of turbulence between LES-ODT and DNS is marginally different and further refinements of the SGS models for SGS stresses can provide additional improvements in the LES-ODT model predictions. Potentially, the Germano dynamic model, in which the model constant is computed instantaneously based on the flow field, or more complex refinements in the modeling of SGS stresses can be used to refine the closure model for LES subgrid stresses. Ultimately, a direct evaluation of these terms can be achieved using the ODT data.

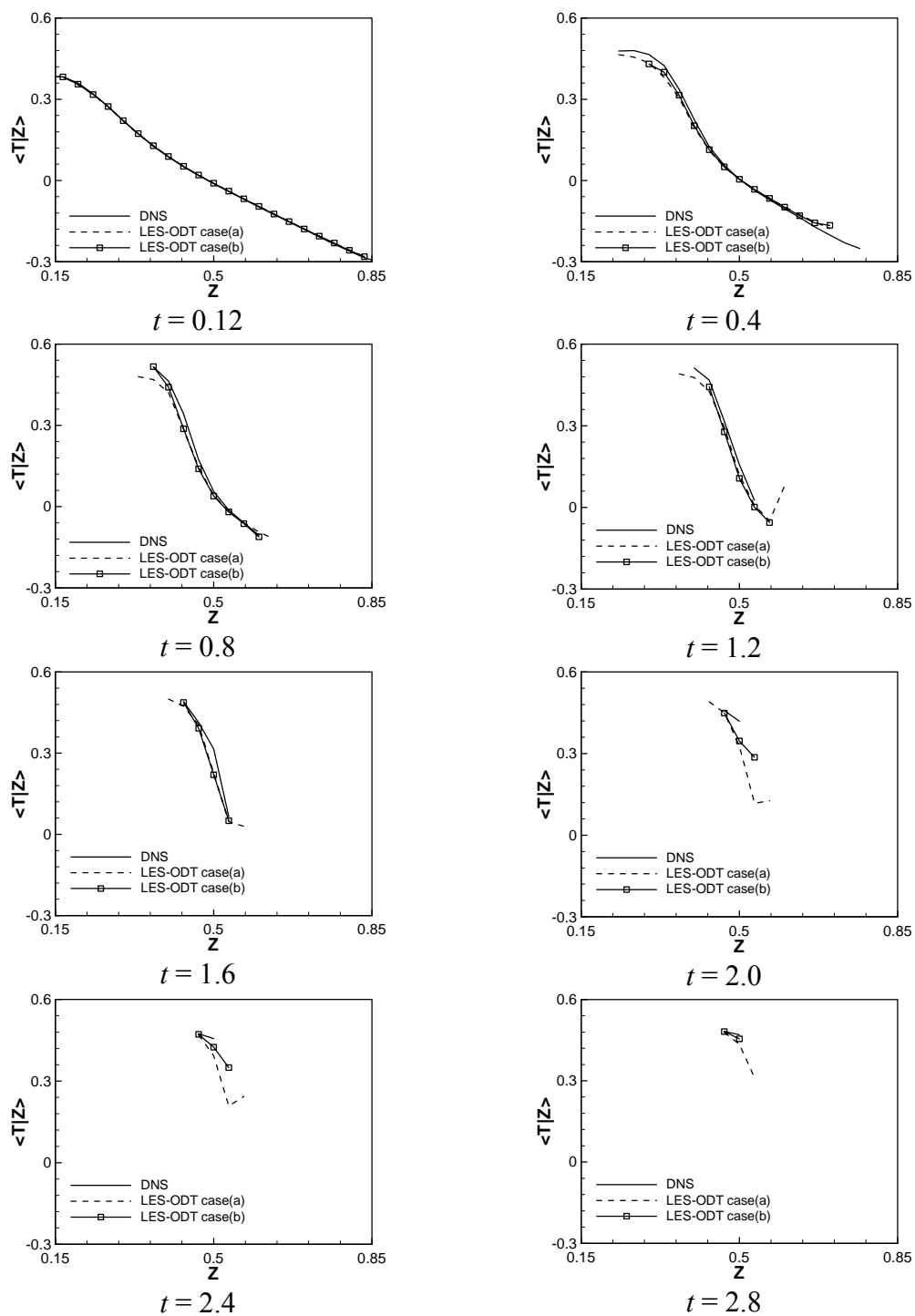


Figure 7-8 Comparison of conditional means of the temperature between LES-ODT and DNS at different times for the high turbulence case with $Le = 0.5$

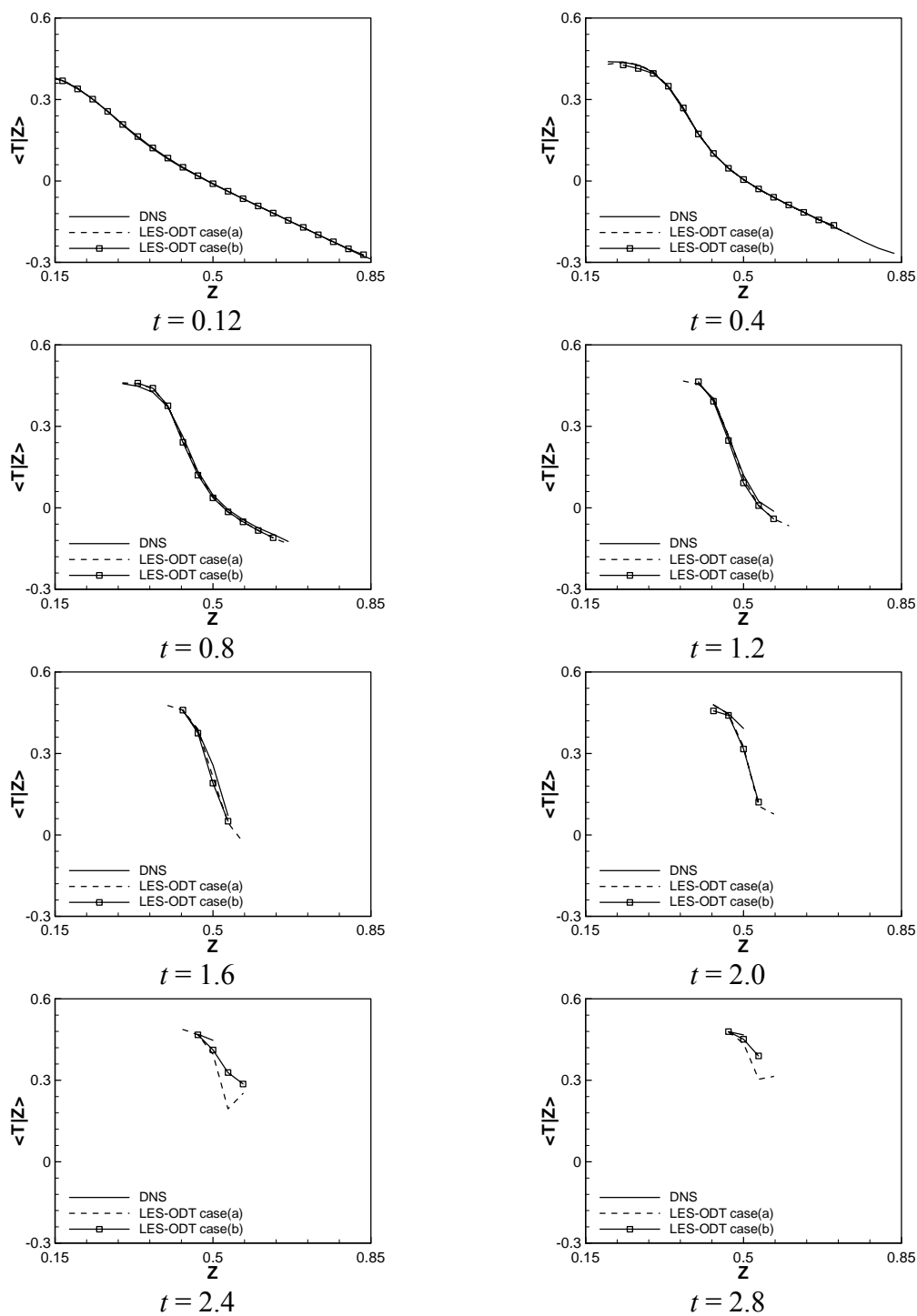


Figure 7-9 Comparison of conditional means of the temperature between LES-ODT and DNS at different times for the high turbulence case with $Le = 1.0$

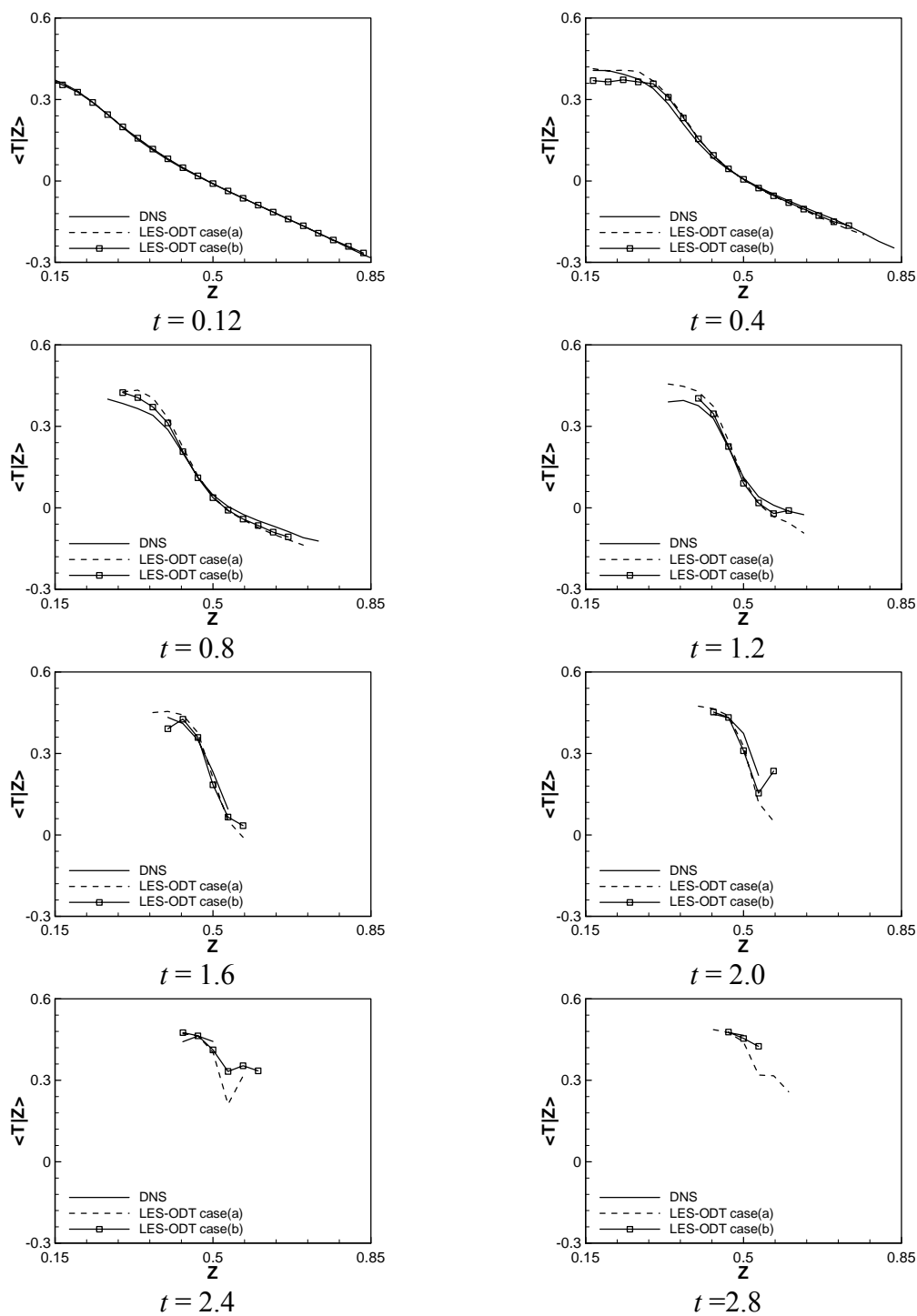


Figure 7-10 Comparison of conditional means of the temperature between LES-ODT and DNS at different times for the high turbulence case with $Le = 2.0$

7.3.2 Conditional Means of the Fuel Mass Fraction

Figure 7-11, Figure 7-12, and Figure 7-13 show a comparison of the conditional means of the fuel mass fractions between LES-ODT and DNS at different times at high turbulence conditions with Lewis numbers equal to 0.5, 1.0, and 2.0, respectively. LES-ODT provides an excellent agreement with DNS in the predictions of the fuel consumption during the autoignition process in the mixture fraction. The onset of the ignition characterized by the departure of the fuel mass fraction from the pure mixing linear profile is clearly represented by LES-ODT. Due to high turbulence conditions, the fuel is depleted in the lean conditions. LES-ODT reproduces the physics represented by DNS results. Furthermore, LES-ODT provides excellent predictions of the Lewis number effects and the turbulence effects documented in section 3.7.1. Results from both LES-ODT cases (a) and (b) are accurate and LES-ODT model performance is reasonably independent of the LES grid size.

Again, the difference in the mixture fraction range between LES-ODT and DNS may be attributed to the marginal difference in the local turbulence dissipation between those two schemes. Some strategies for improvement have been addressed in section 7.3.1.

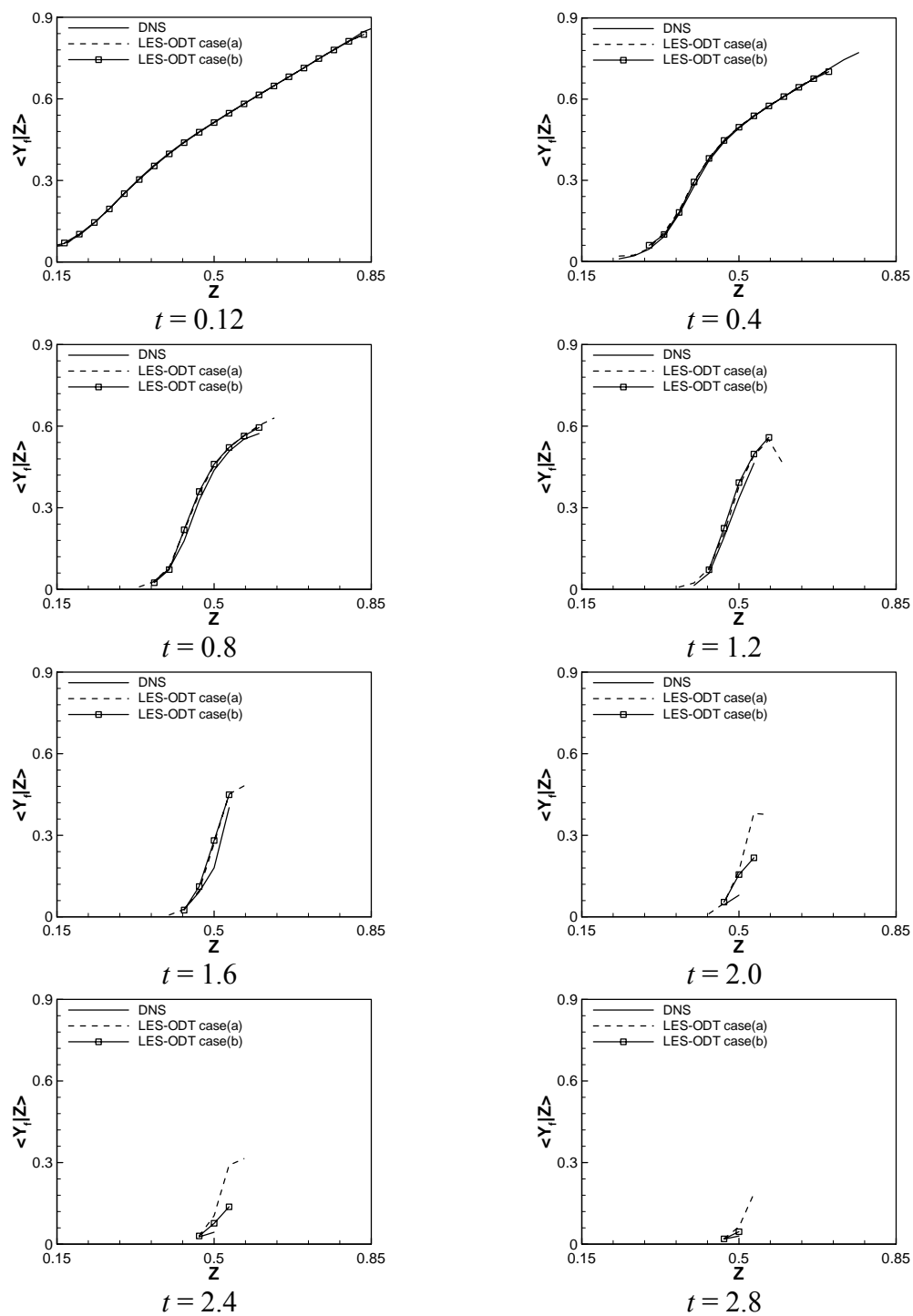


Figure 7-11 Comparison of conditional means of the fuel mass fraction between LES-ODT and DNS at different times for the high turbulence case with $Le = 0.5$

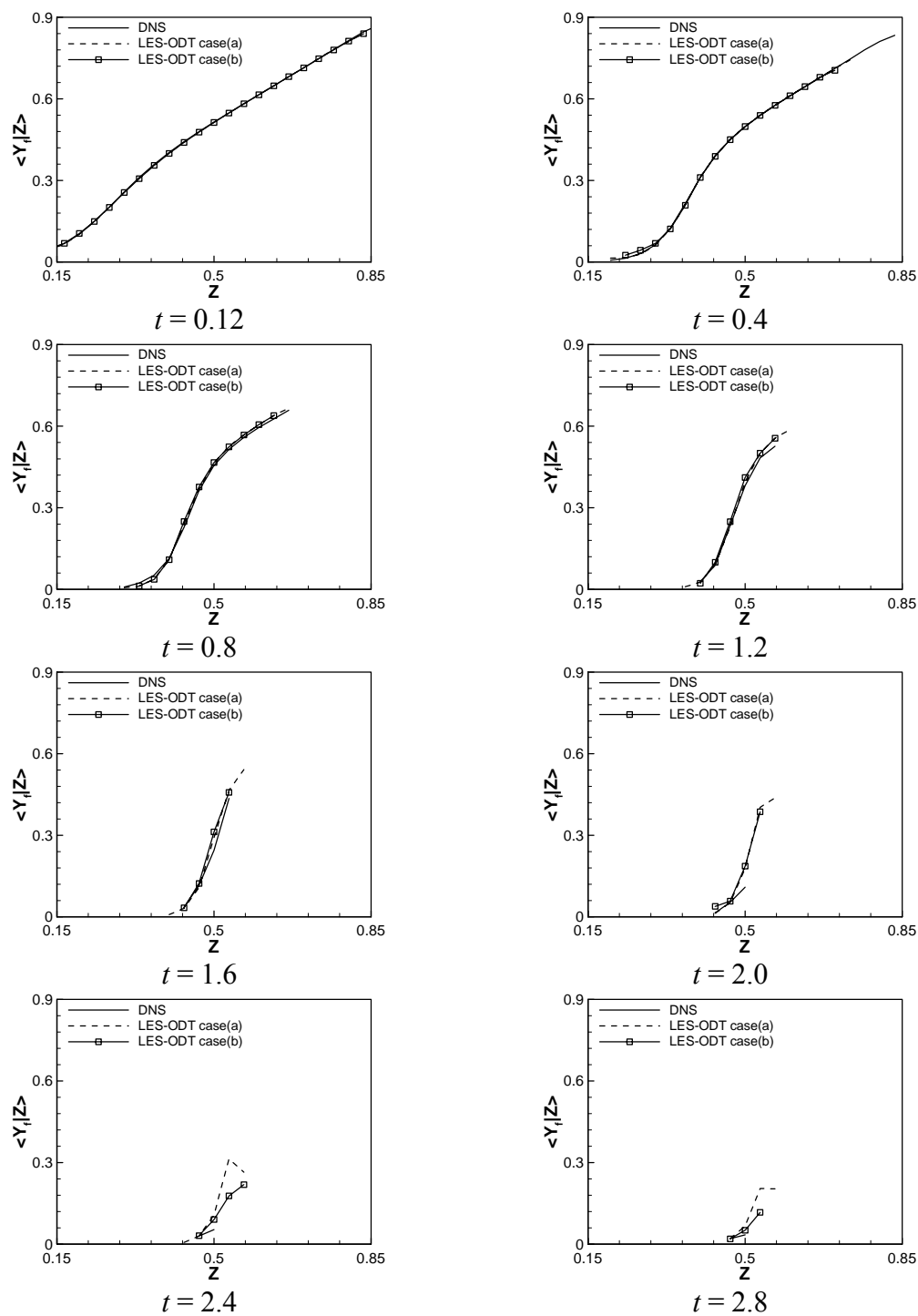


Figure 7-12 Comparison of conditional means of the fuel mass fraction between LES-ODT and DNS at different times for the high turbulence case with $Le = 1.0$

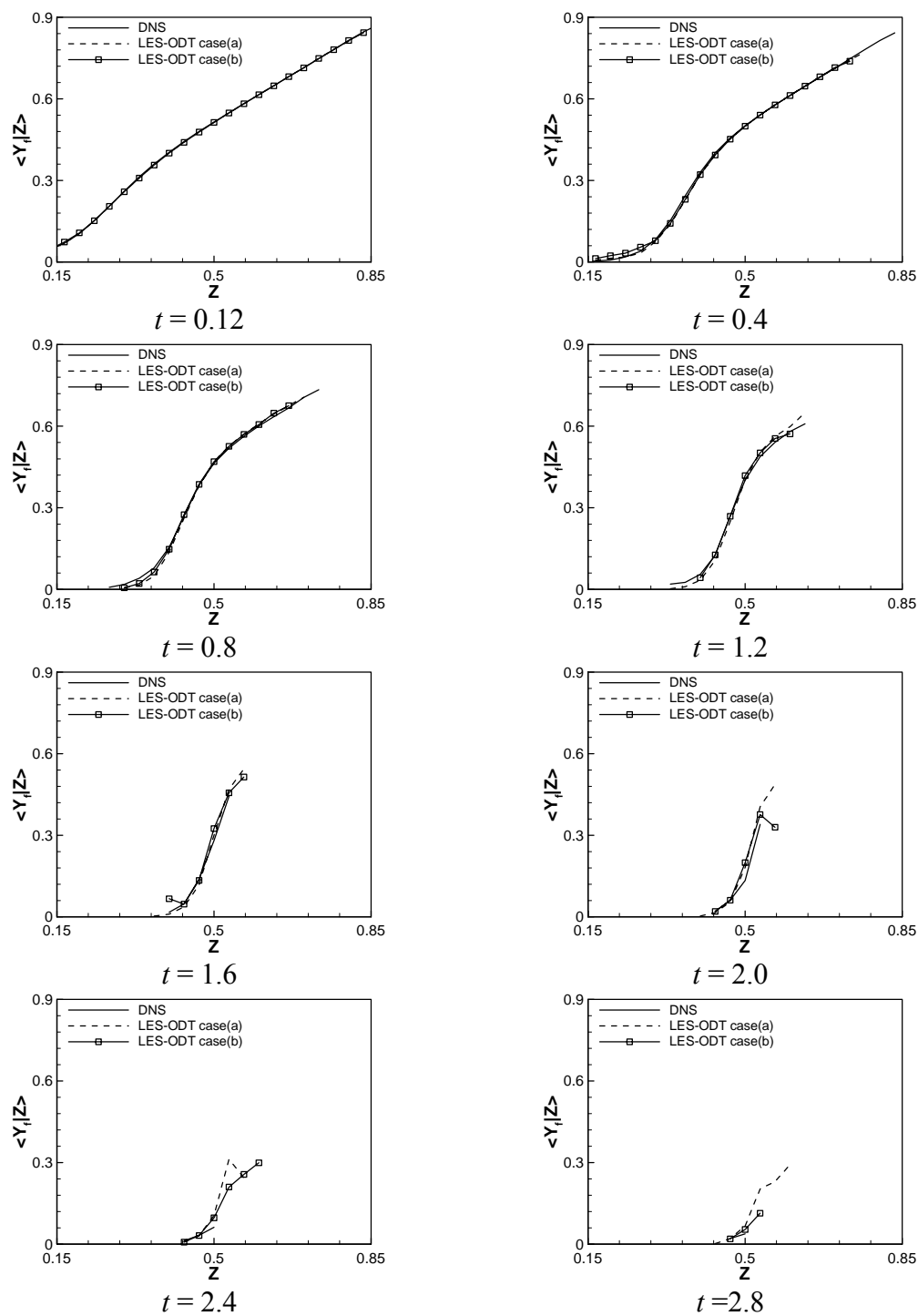


Figure 7-13 Comparison of conditional means of the fuel mass fraction between LES-ODT and DNS at different times for the high turbulence case with $Le = 2.0$

7.3.3 Conditional Means of the Oxidizer Mass Fraction

Figure 7-14, Figure 7-15, and Figure 7-16 show a comparison of the conditional means of the oxidizer mass fractions between LES-ODT and DNS at different times at high turbulence conditions with Lewis numbers equal to 0.5, 1.0, and 2.0, respectively. LES-ODT generates excellent predictions of the oxidizer consumption in the mixture fraction space during the autoignition process. The onset of the ignition is characterized by the departure of the oxidizer mass fraction from the pure mixing linear profile and this is clearly represented by LES-ODT. Due to high turbulence conditions, the oxidizer is depleted before flames reach the rich conditions. LES-ODT reproduces the physics represented by DNS results. Furthermore, LES-ODT accurately captures the Lewis number effects and the turbulence condition effects documented in section 3.7.1. Results from both LES-ODT cases (a) and (b) are consistent and LES-ODT model performance is reasonably independent of the LES grid size.

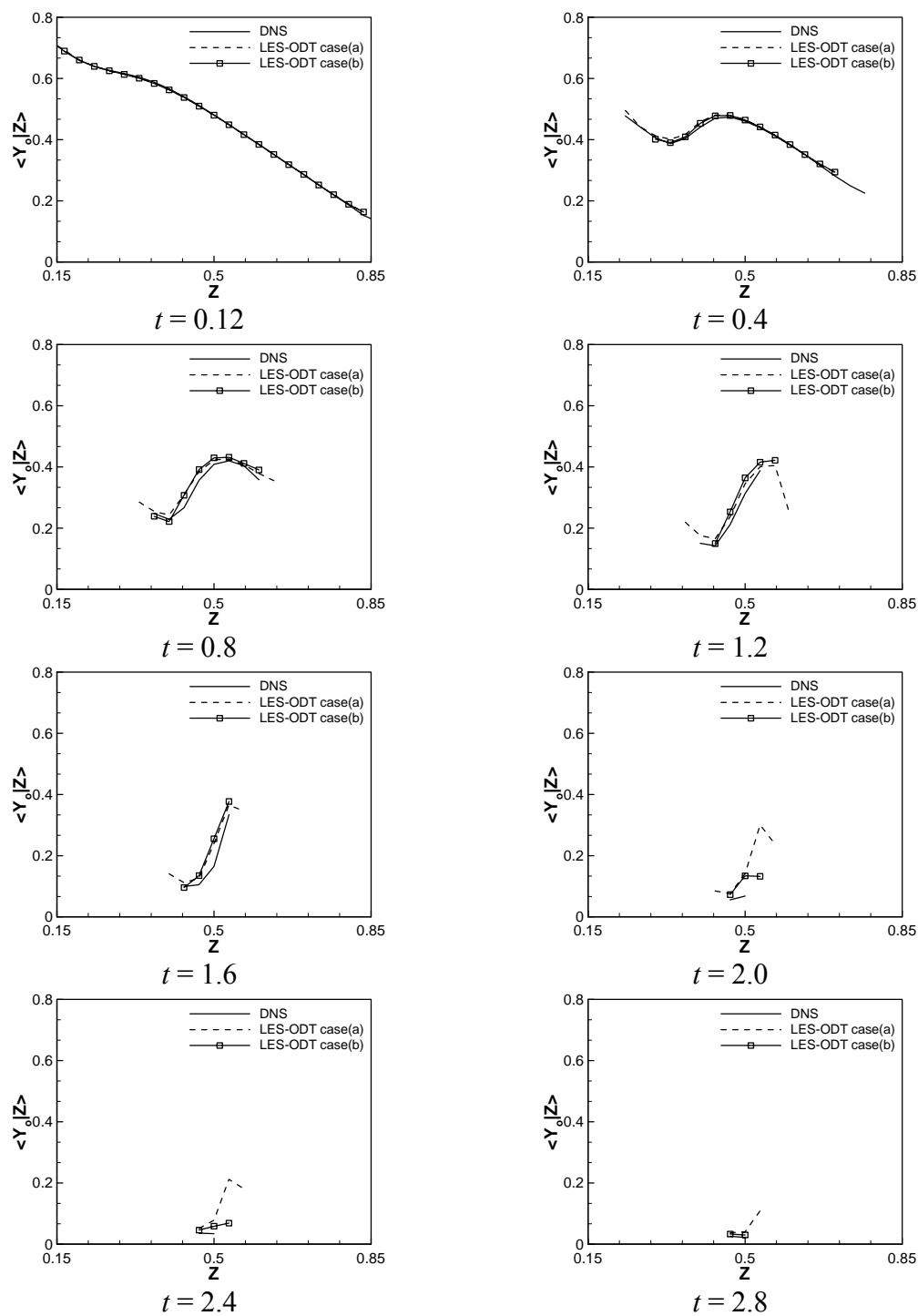


Figure 7-14 Comparison of conditional means of the oxidizer mass fraction between LES-ODT and DNS at different times for the high turbulence case with $Le = 0.5$

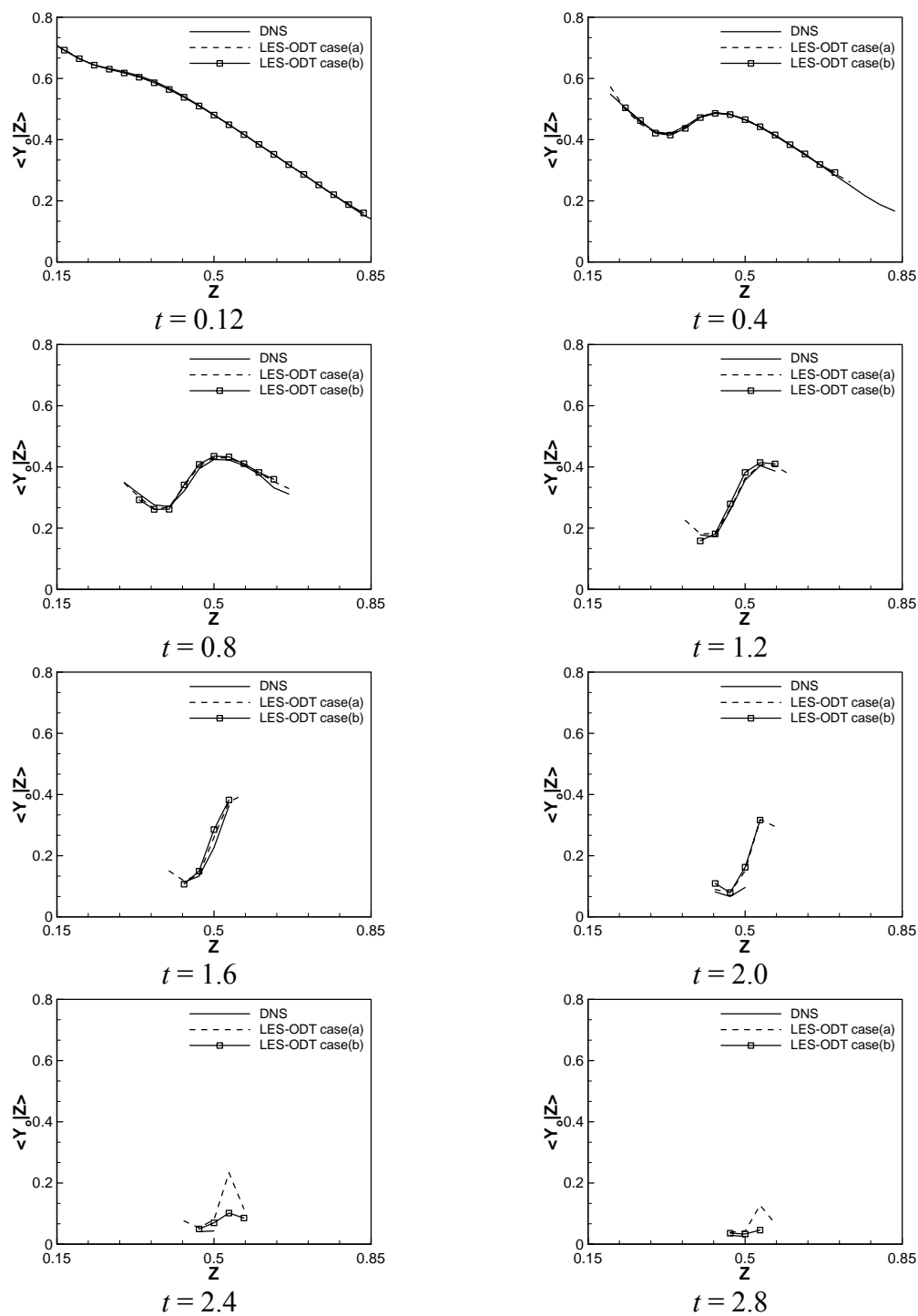


Figure 7-15 Comparison of conditional means of the oxidizer mass fraction between LES-ODT and DNS at different times for the high turbulence case with $Le = 1.0$

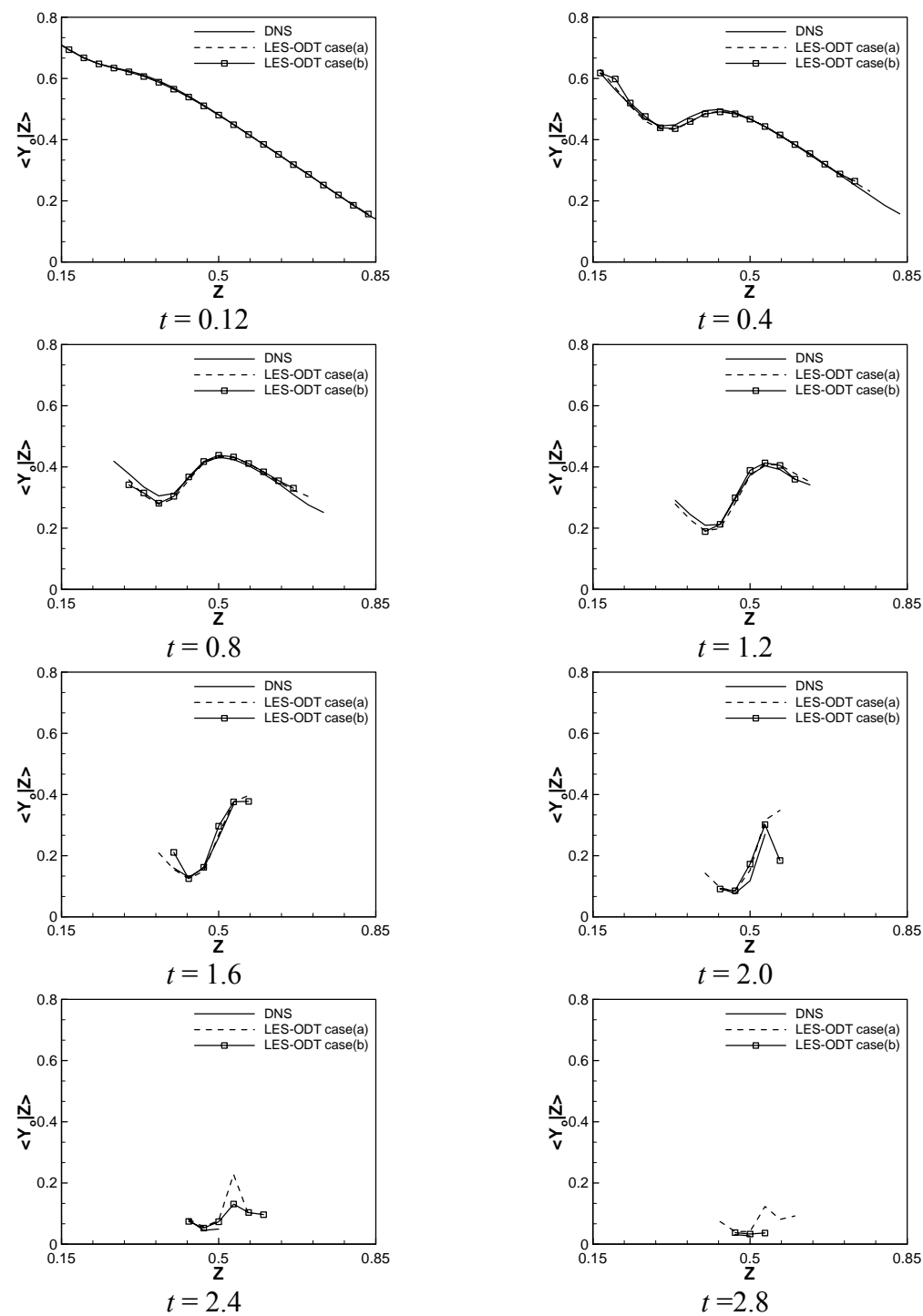


Figure 7-16 Comparison of conditional means of the oxidizer mass fraction between LES-ODT and DNS at different times for the high turbulence case with $Le = 2.0$

7.3.4 Conditional Means of the Reaction Rate

The conditional means of the reaction rate are presented based on LES-ODT and DNS statistics at high turbulence conditions with different Lewis numbers of 0.5, 1.0, and 2.0. The results are shown in Figure 7-17, Figure 7-18, and Figure 7-19, respectively. The overall prediction of the conditional means of the reaction rate by LES-ODT is very good. Ignition occurs in discrete kernels at fuel lean conditions and kernels propagate from low mixture fraction values to high mixture values. However, as observed earlier, there are no indications of fuel rich burning because the higher mixing rates associated with the higher turbulence intensities. Therefore, only the lean premixed burning mode is present in both LES-ODT and DNS results. The rich premixed and diffusion flame burning modes are absent in the high turbulence cases. Furthermore, the locations of the peak values of conditional means of the reaction rate are captured accurately by LES-ODT. The turbulence intensity effects and Lewis number effects documented in section 3.7.1 are also captured by both simulation approaches. Results from both LES-ODT cases (a) and (b) are consistent, and LES-ODT model performance is reasonably independent of the LES grid size.

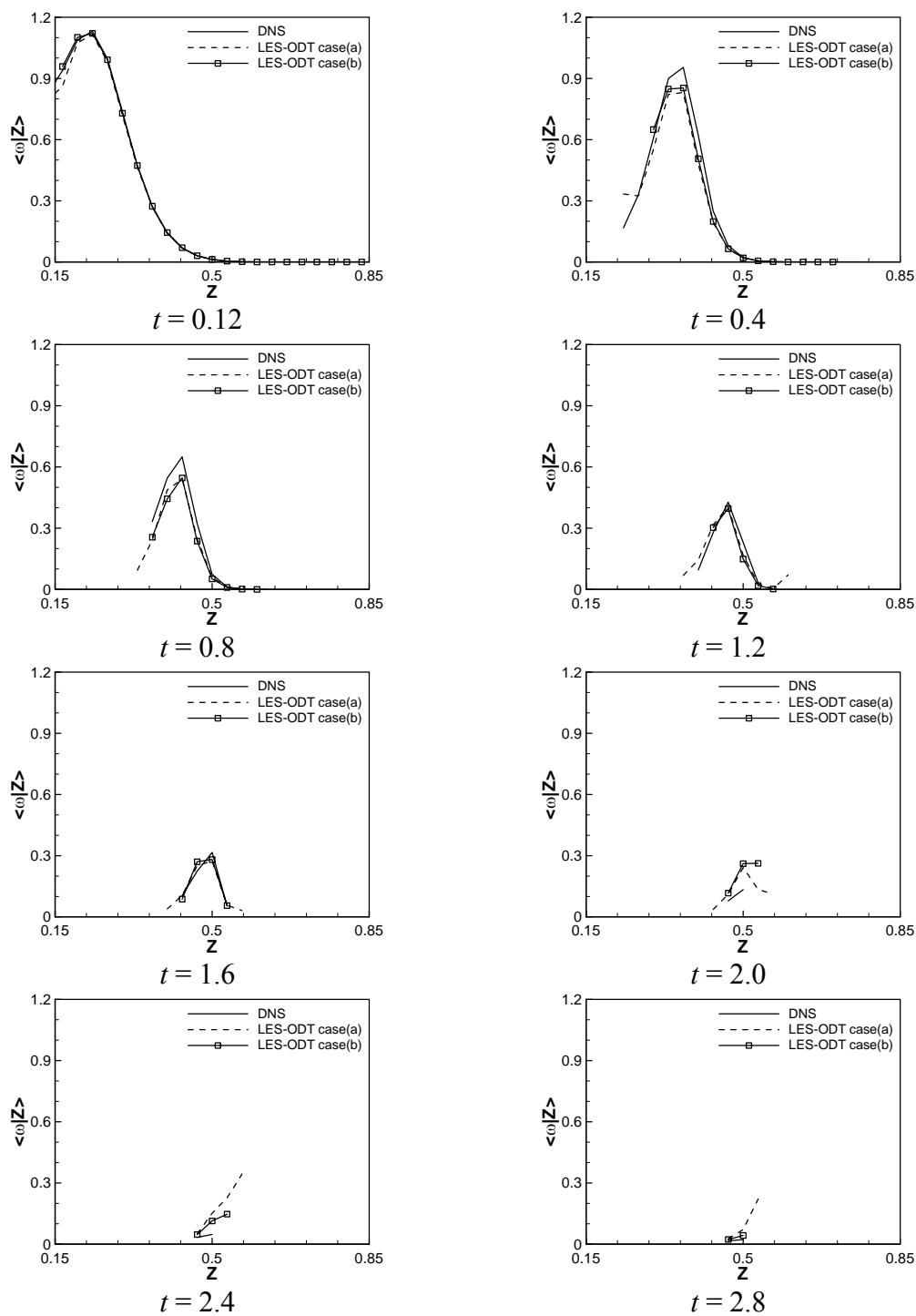


Figure 7-17 Comparison of conditional means of the reaction rate between LES-ODT and DNS at different times for the high turbulence case with $Le = 0.5$

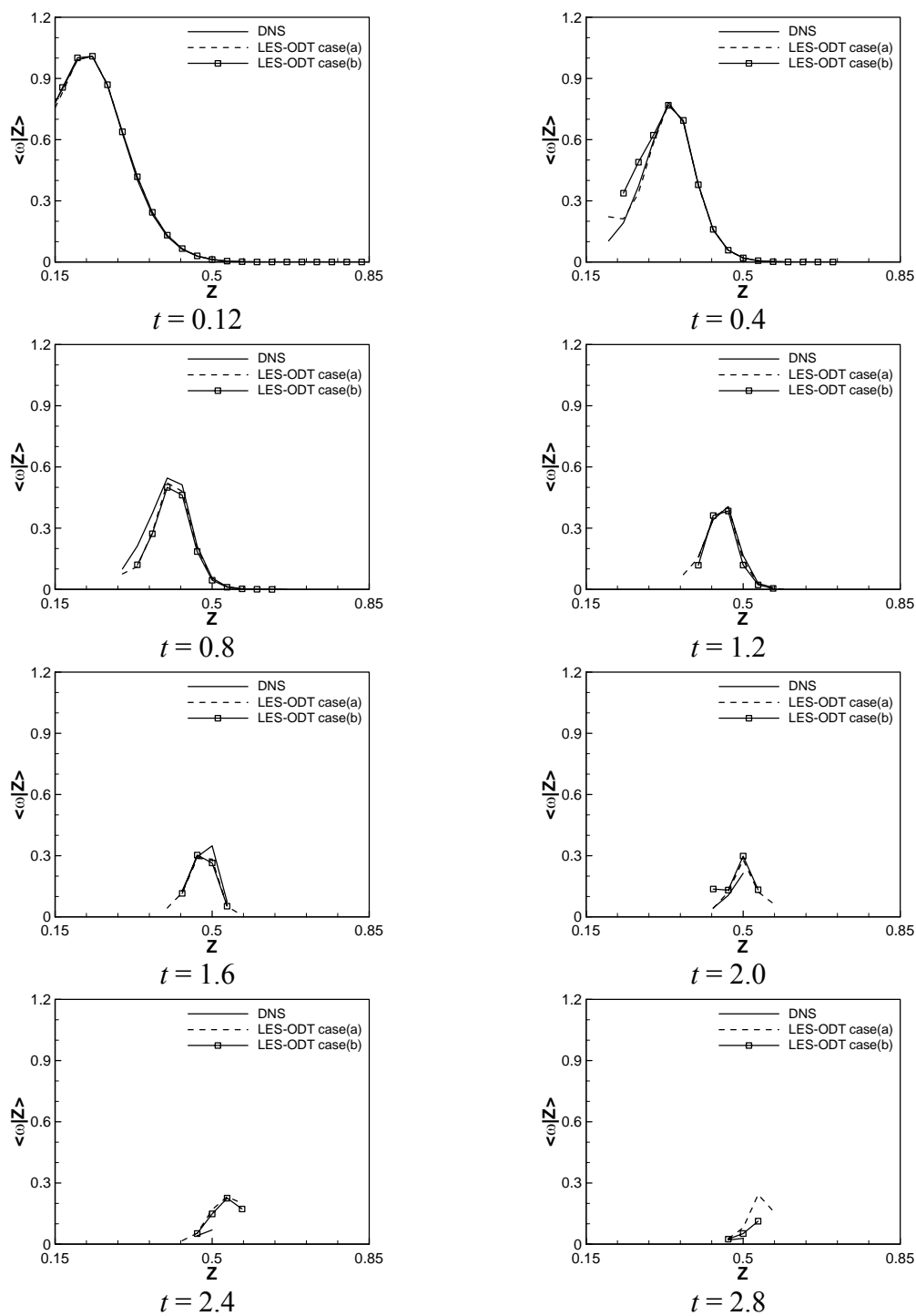


Figure 7-18 Comparison of conditional means of the reaction rate between LES-ODT and DNS at different times for the high turbulence case with $Le = 1.0$

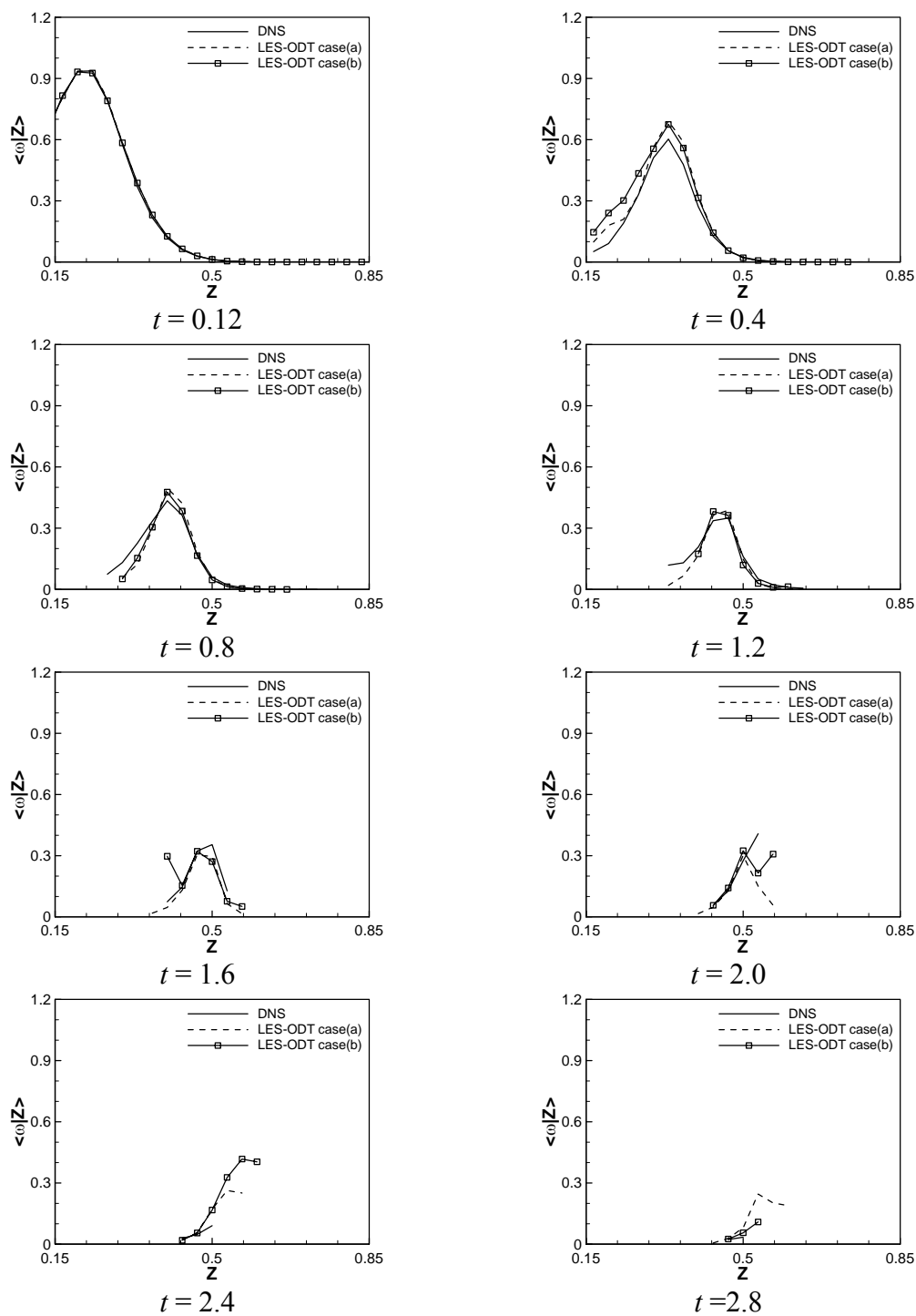


Figure 7-19 Comparison of conditional means of the reaction rate between LES-ODT and DNS at different times for the high turbulence case with $Le = 2.0$

The above discussion has been focused on validating the LES-ODT model against DNS at high turbulence intensity conditions using the conditional mean values. The results obtained from two LES-ODT simulations cases provide very good agreement with DNS results for all the Lewis number cases at high turbulence conditions. Modeling of the fluctuations poses a difficult task and we will address it in the following discussion.

7.3.5 Conditional RMS of the Temperature

Figure 7-20, Figure 7-21, and Figure 7-22 show a comparison of the conditional RMS of the temperature between LES-ODT and DNS at high turbulence conditions with Lewis numbers equal to 0.5, 1.0, and 2.0, respectively. The results show that the fluctuations of temperature in the mixture fraction space are represented accurately by LES-ODT and the overall agreement between LES-ODT and DNS is excellent. Different from the low turbulence case, complete burning is achieved before flames reach the rich mixtures and only lean premixed burning mode is present. This is predicted by LES-ODT accurately. Moreover, the magnitude and the location of the peaks are represented in LES-ODT with reasonable accuracy. The Lewis number effects and turbulence condition effects are represented by LES-ODT precisely. Discussions on the details of those effects are included in section 3.7.1 on page 54. Furthermore, results from both LES-ODT cases (a) and (b) are accurate and the LES grid size has negligible effects on LES-ODT model performance.

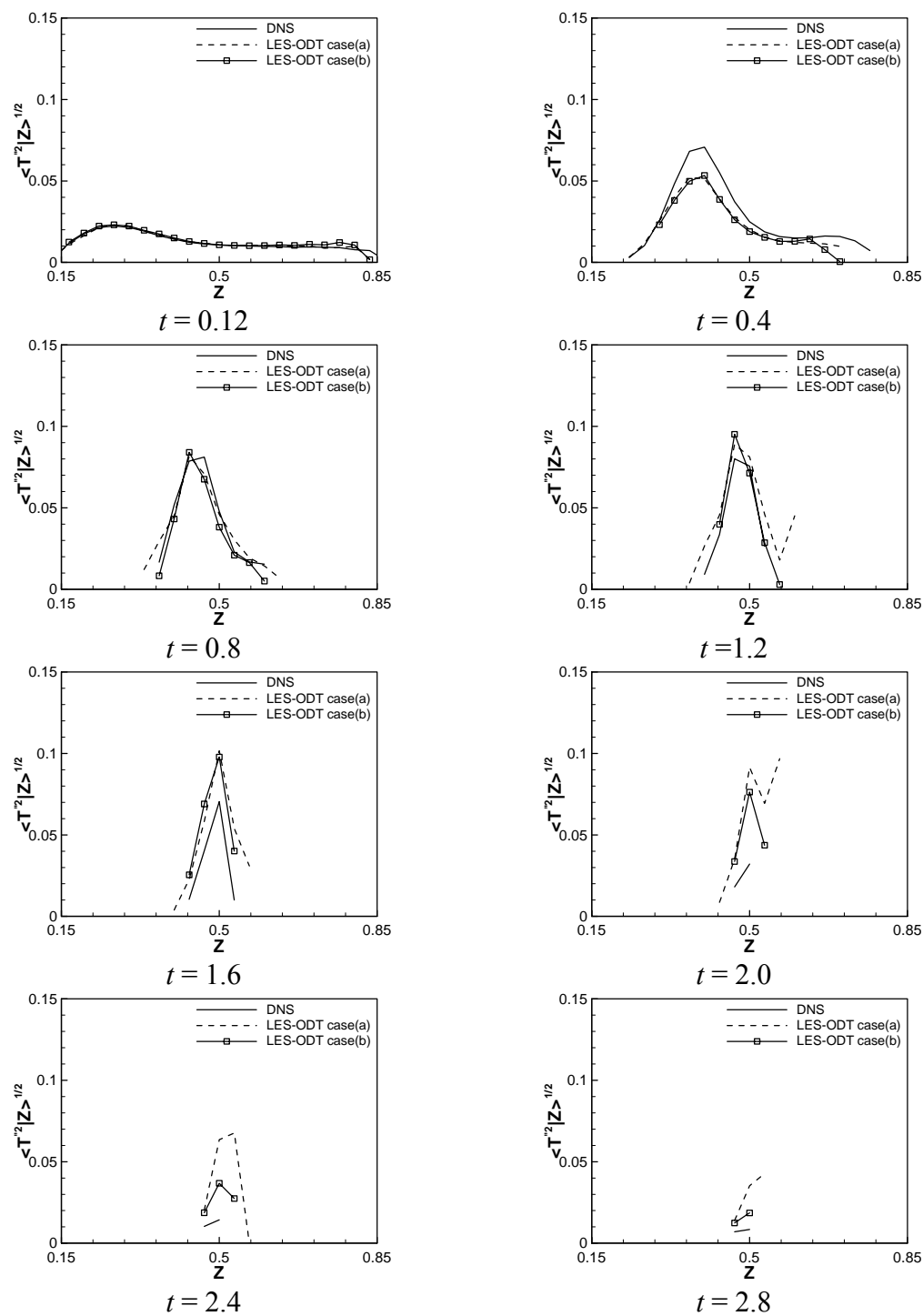


Figure 7-20 Comparison of conditional RMS of the temperature between LES-ODT and DNS at different times for the high turbulence case with $Le = 0.5$



Figure 7-21 Comparison of conditional RMS of the temperature between LES-ODT and DNS at different times for the high turbulence case with $Le = 1.0$

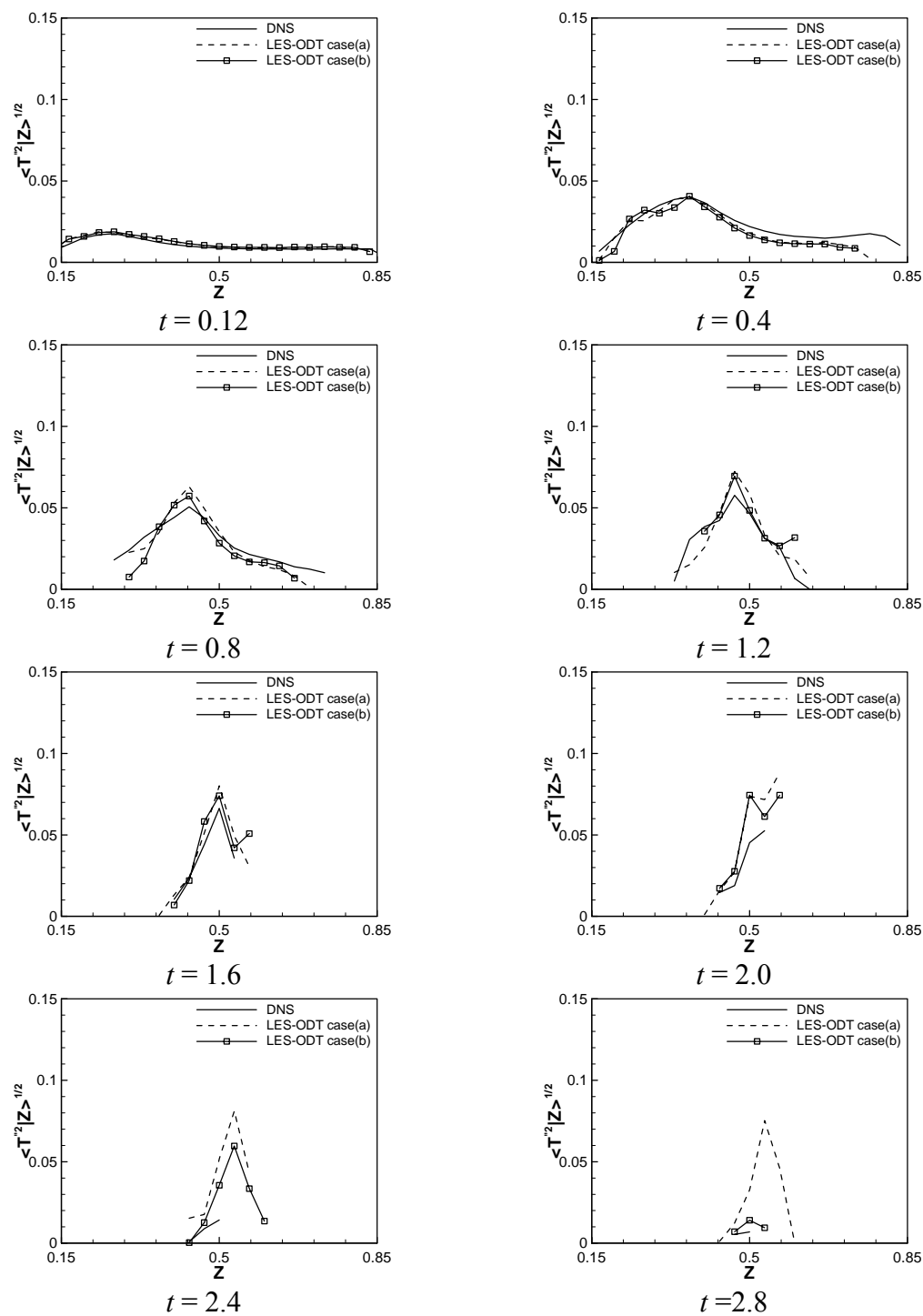


Figure 7-22 Comparison of conditional RMS of the temperature between LES-ODT and DNS at different times for the high turbulence case with $Le = 2.0$

Note that the turbulence intensity is relatively high compared to the low-turbulence simulations, and we have seen already the effects of the turbulence intensity on chemistry. These effects are amplified when we considered higher moments of scalar statistics. This is clearly illustrated by the more pronounced differences between the conditional RMS of the temperature between LES-ODT and DNS at high turbulence intensities. It is possible that additional fine-tuning of the model constants or the SGS stresses and fluxes models can result in improved agreements for higher moments of scalar statistics between LES-ODT and DNS. However, given the fact the overall magnitude of the RMS is small, the difference between LES-ODT and DNS does not impact significantly the positive attributes of the proposed model to address important finite-rate chemistry effects.

7.3.6 Conditional RMS of the Fuel Mass Fraction

Figure 7-23, Figure 7-24, and Figure 7-25 show a comparison of the conditional RMS of the fuel mass fraction between LES-ODT and DNS at high turbulence condition with Lewis numbers equal to 0.5, 1.0, and 2.0, respectively. The fluctuations of the fuel mass fraction are predicted accurately by LES-ODT. Because the results are similar to the conditional RMS of the temperature, the results are included for completeness and readers are referred to section 7.3.5 for detailed discussions.

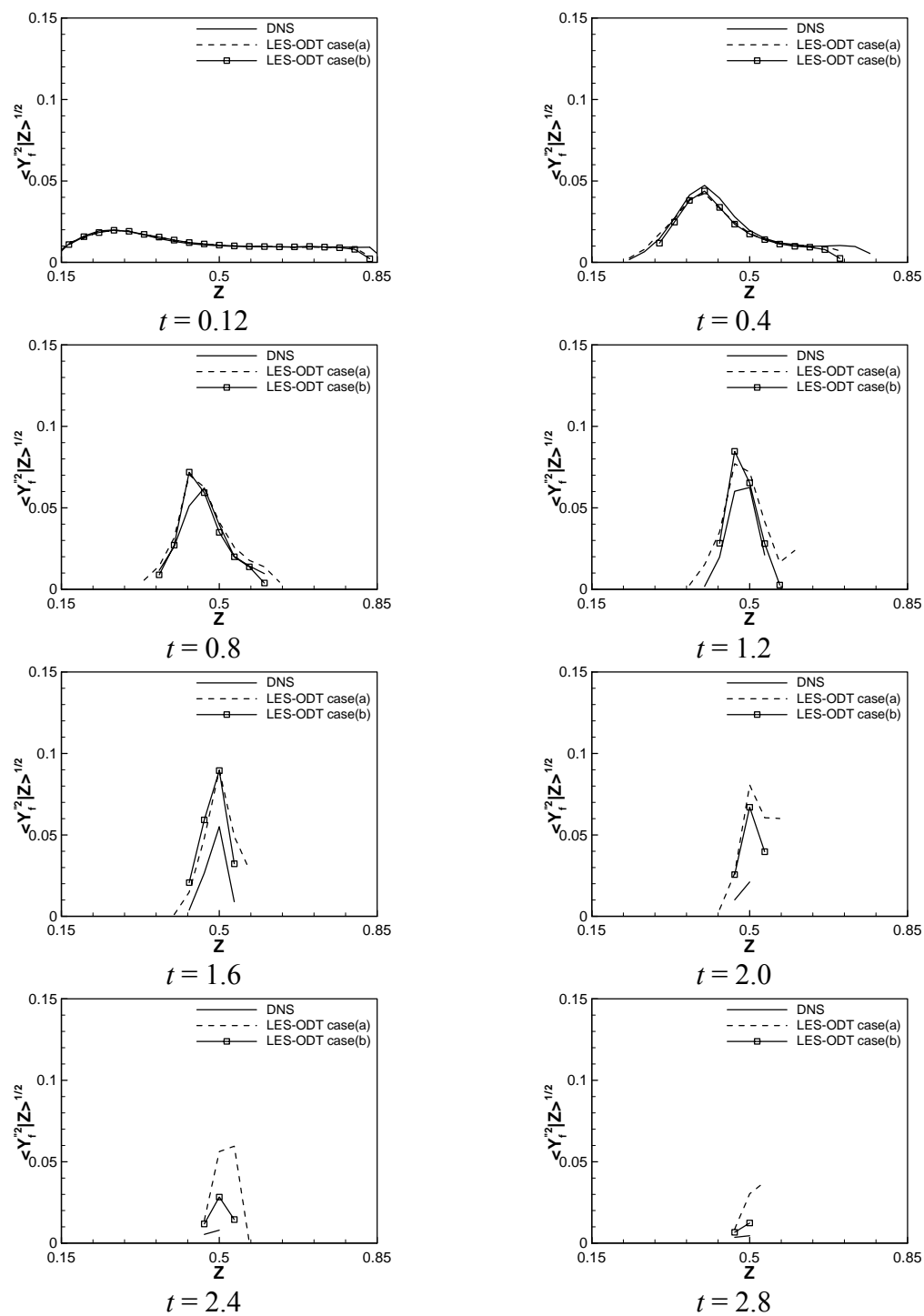


Figure 7-23 Comparison of conditional RMS of the fuel mass fraction between LES-ODT and DNS for the high turbulence case with $Le = 0.5$

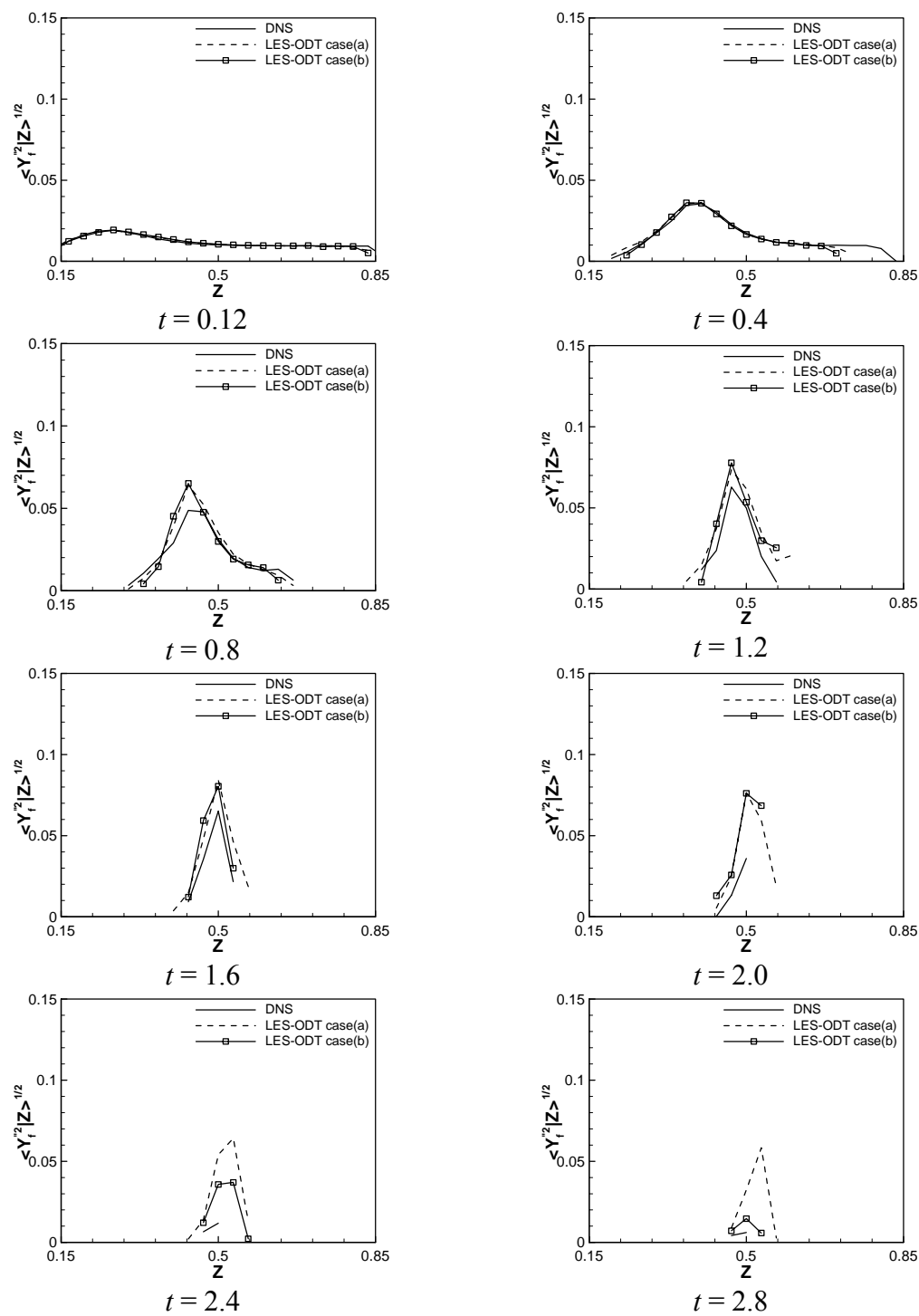


Figure 7-24 Comparison of conditional RMS of the fuel mass fraction between LES-ODT and DNS for the high turbulence case with $Le = 1.0$

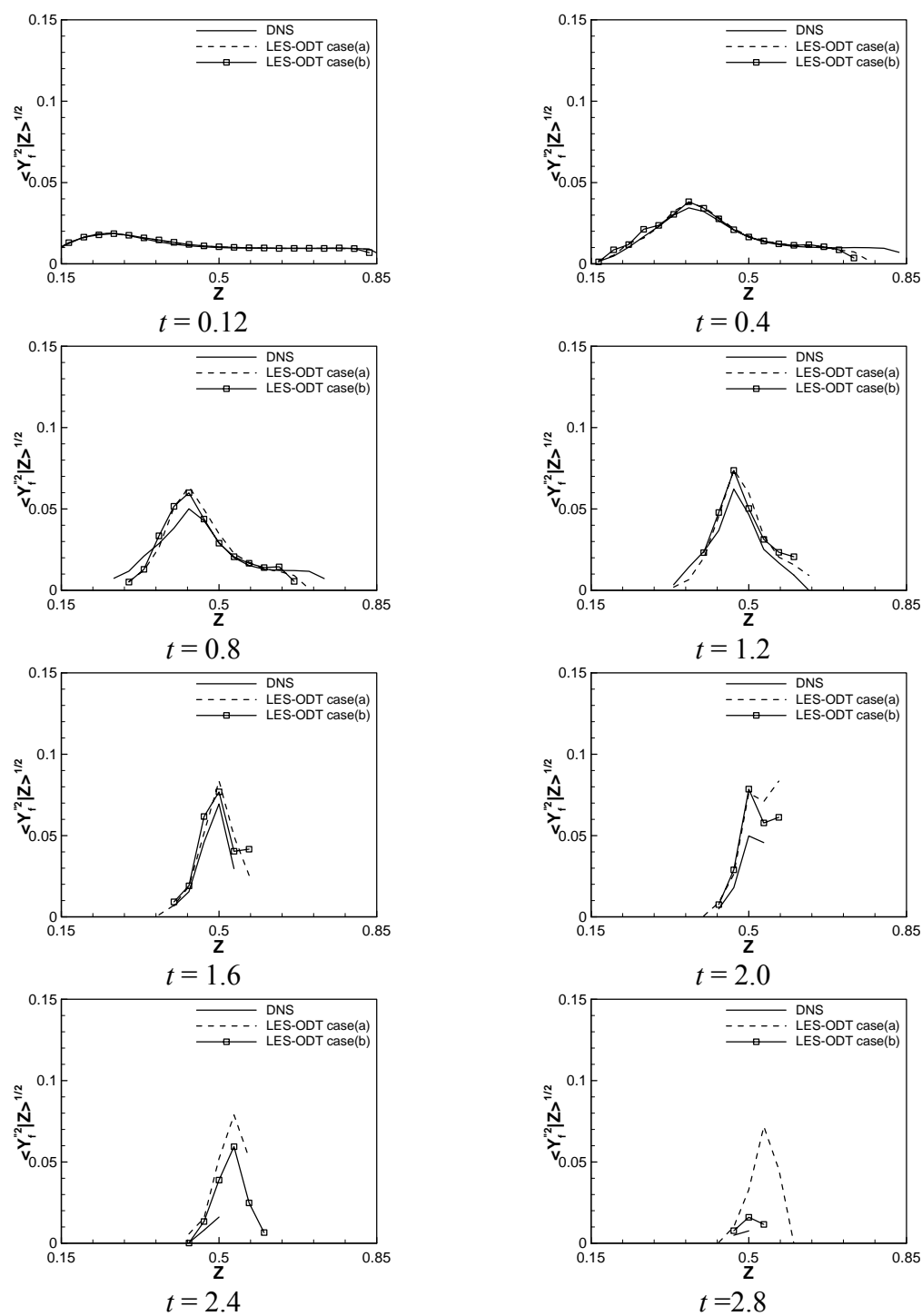


Figure 7-25 Comparison of conditional RMS of the fuel mass fraction between LES-ODT and DNS for the high turbulence case with $Le = 2.0$

7.3.7 Conditional RMS of the Oxidizer Mass Fraction

Figure 7-26, Figure 7-27, and Figure 7-28 show a comparison of the conditional RMS of the oxidizer mass fraction between LES-ODT and DNS at high turbulence condition with Lewis numbers equal to 0.5, 1.0, and 2.0, respectively. The fluctuations of the oxidizer mass fraction are predicted accurately by LES-ODT. Again the results are similar to the conditional RMS of the temperature and readers are referred to section 7.3.5 for detailed discussions.

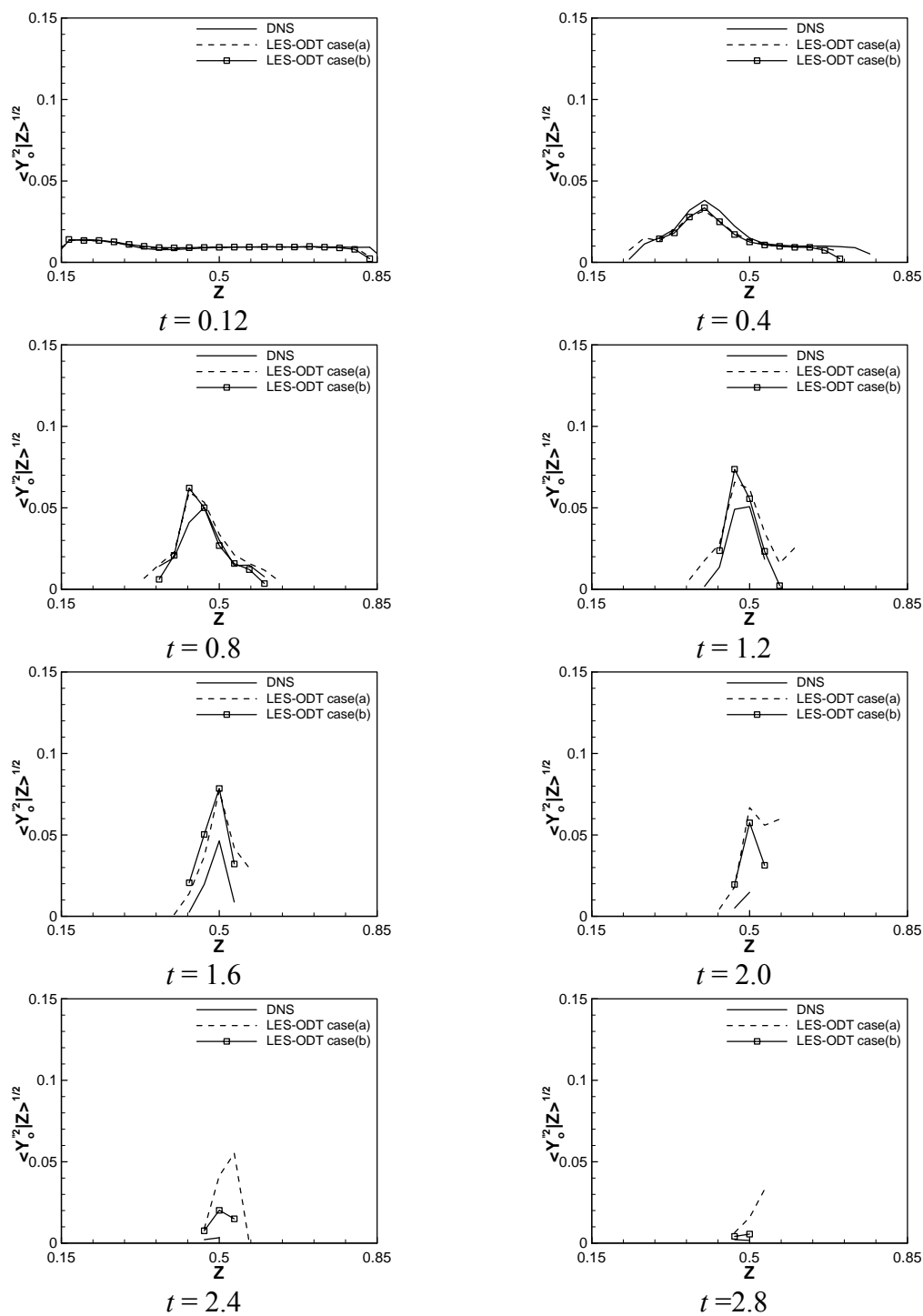


Figure 7-26 Comparison of conditional RMS of the oxidizer mass fraction between LES-ODT and DNS for the high turbulence case with $Le = 0.5$

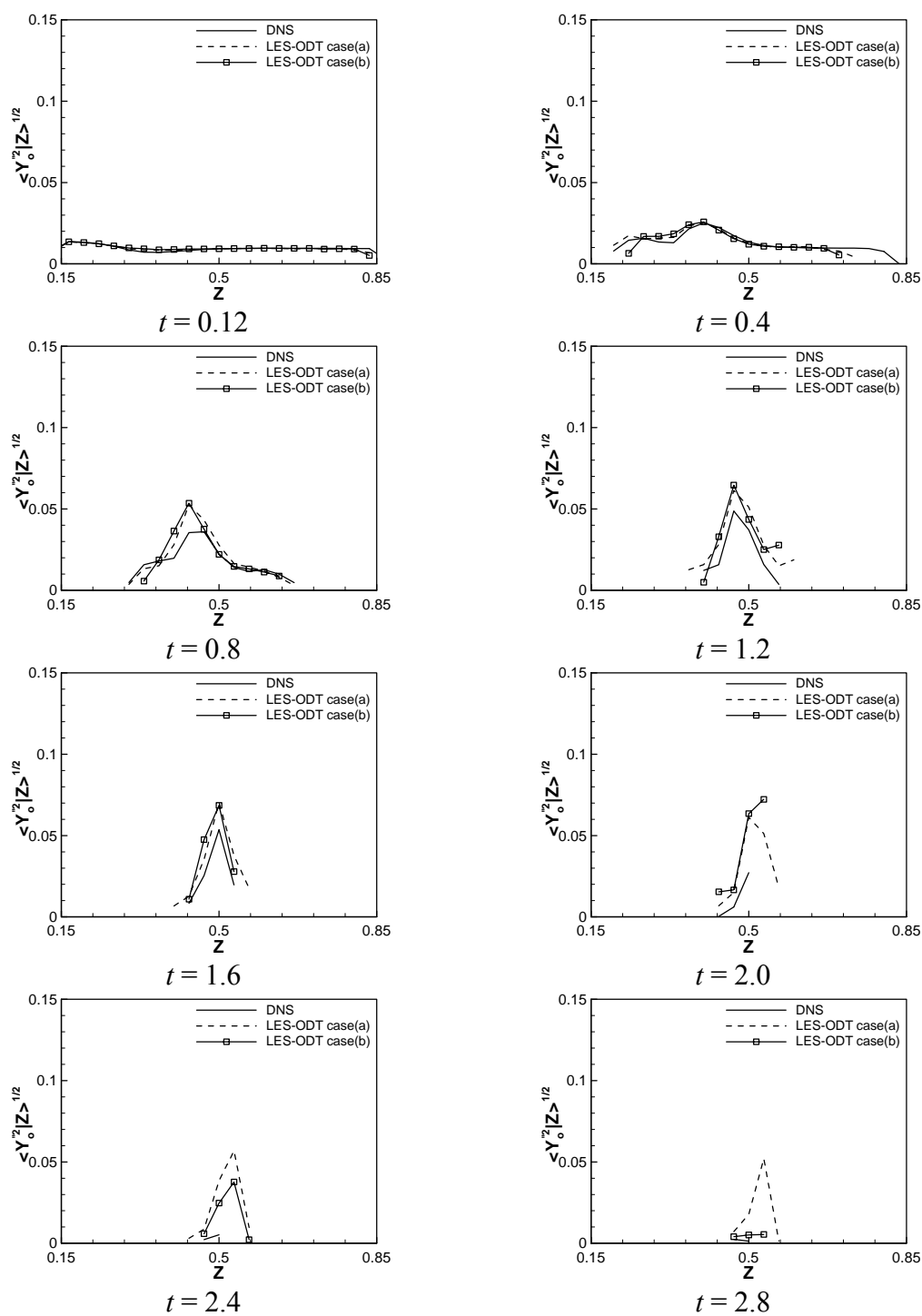


Figure 7-27 Comparison of conditional RMS of the oxidizer mass fraction between LES-ODT and DNS for the high turbulence case with $Le = 1.0$

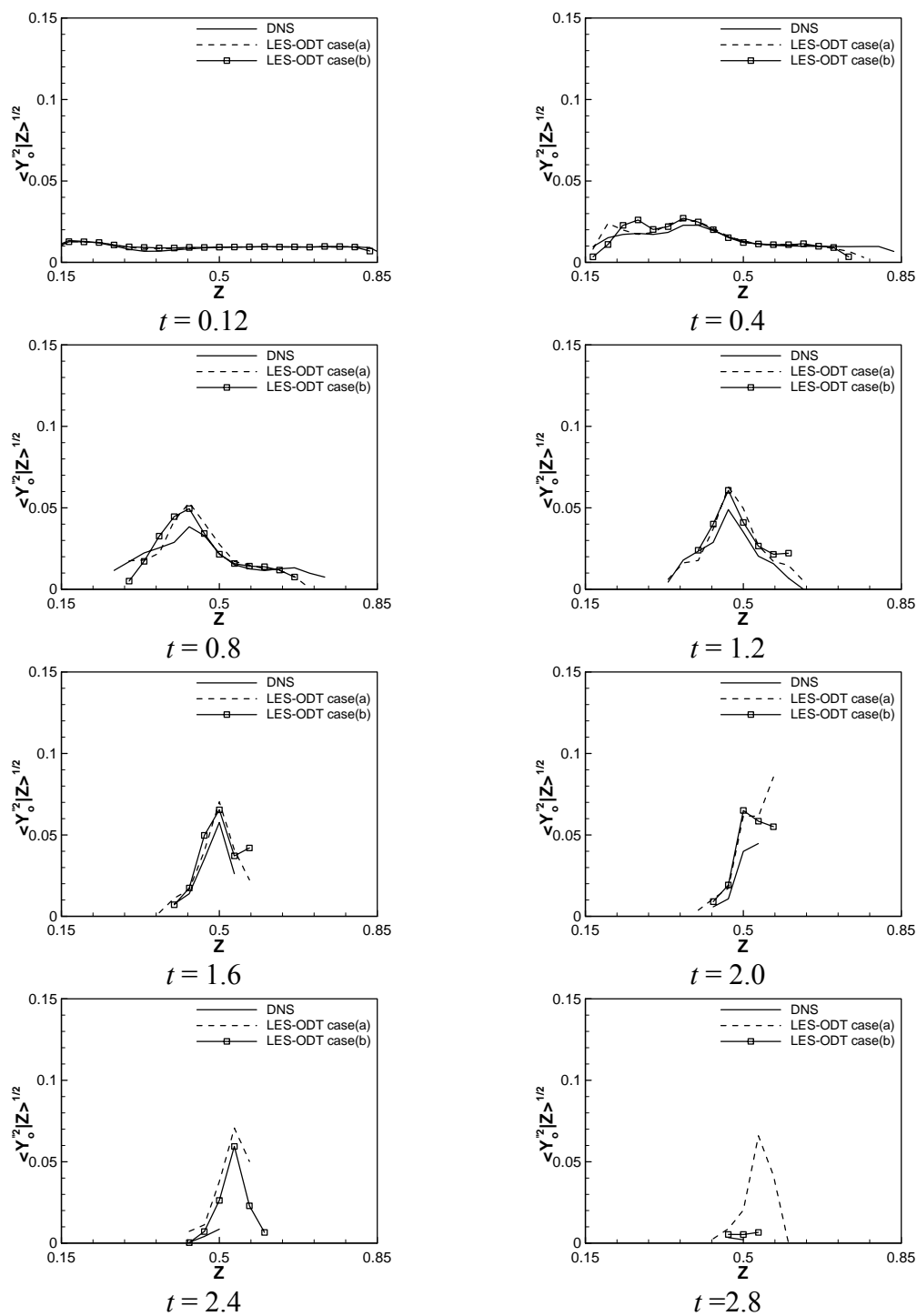


Figure 7-28 Comparison of conditional RMS of the oxidizer mass fraction between LES-ODT and DNS for the high turbulence case with $Le = 2.0$

In conclusion, LES-ODT simulation results provide excellent predictions of the first and second-order conditional statistics in the mixture fraction space during the whole autoignition process at high turbulence conditions. LES-ODT simulation captures not only the onset of ignition and kernel propagation, but also peak values and the locations of the peaks in the conditional statistics as well. Moreover, the turbulence condition effects and Lewis number effects are represented by LES-ODT accurately.

7.4 Conclusions

In this chapter, we have assessed and validated LES-ODT model based on conditional statistics for non-homogenous autoignition in isotropic turbulence. Two LES-ODT simulation cases with different LES spatial resolutions are performed.

Both low and high turbulence conditions are studied and different Lewis number cases for the high turbulence conditions are examined. LES-ODT simulation results show excellent agreement with DNS results at both low and high turbulence conditions. LES-ODT simulation captures not only the onset of ignition, the kernel propagation, the transition of burning modes (low turbulence case), but also the peak values and the locations of the peaks in the conditional statistics as well. Moreover, the turbulence condition effects and Lewis number effects are represented by LES-ODT accurately.

The difference in the mixture fraction range between LES-ODT and DNS indicates that further refinements of the SGS models for SGS stresses can provide additional improvements in the LES-ODT model predictions. The excellent agreement between LES-

ODT and DNS results provides a solid foundation for the model validation. LES-ODT is a very promising model for simulating the turbulent combustion processes.

Chapter 8 Conclusions and Recommendations for Future Work

8.1 Introduction

A new hybrid numerical scheme based on LES and ODT is developed. The development of the model relies on a detailed implementation of the interactions between turbulent mixing and chemical reactions. The formulation of the hybrid scheme is discussed in detail and the validation of the scheme based on traditional direct numerical simulation results is carried out. The major findings and recommendations for future work based on the present study are presented below.

8.2 Conclusions

8.2.1 DNS results

Chapter 3 presents the 3D direct numerical simulation results of non-homogeneous autoignition in isotropic turbulence. This chapter serves as a fundamental basis for testing and validating the new hybrid scheme. It also serves to illustrate a canonical flow that may present challenges for the most common models of LES of turbulent combustion. The initialization of the flow field using von Karman-Pao spectrum is described and the periodic boundary condition is implied. The conditional statistics with respect to one conditioning variable, the mixture fraction, are discussed.

The turbulence intensity plays an important role in the evolution of autoignition in non-homogeneous mixture, since it affects the competition between mixing and chemistry. Three burning modes exist in the low turbulence case but only one burning mode exists in the high turbulence cases. Furthermore, Lewis number effects are studied. These effects contribute to the conditional statistics of reactive scalars in two major aspects. Higher Lewis numbers correspond to lower mass diffusivity compared to the energy transport. This has two consequences. First, the scalar molecular mixing rate is lower, which results in a wider mixture fraction range. Second, because the scalar gradients are higher, the size of the kernels will be smaller. Thus, the heat loss of the kernels is higher, which results in a lower magnitude of the conditional means of the temperature and the reaction rate, and a lower magnitude of conditional RMS of thermo-chemical scalars. Consequently the fuel and the oxidizer are consumed less.

The transition and propagation of flames during the autoignition process in the lean preheated mixtures are present in the conditional statistics. These statistics depart fundamentally from those obtained by using fully segregated mixtures of the fuel and the oxidizer (Mastorakos, 1998 and Sreedhara, 2000). The study further shows that the transient behavior is also present in the second order conditional statistics. Therefore, higher order conditioning may not adequately address the complexity exhibited by the kernel propagation in both the mixture fraction and physical spaces. The applicability to use a second-conditioning variable, the reduced temperature, is also explored. The scatter plots presented in Chapter 3 show that the second conditioning only provides consistent profiles for unity

Lewis number cases regardless of the turbulence conditions. For cases with non-unity Lewis numbers, more conditioning variables may be needed to address the kernel propagation shown in the non-homogeneous autoignition.

8.2.2 LES-ODT Model Formulation

Chapter 4 documents the LES-ODT model formulation and the numerical implementation. The governing equations are provided here, which are not available in other references. The LES governing equations are obtained by applying spatial filtering operations to the instantaneous equations. The ODT formulation includes representing the stochastic stirring events via triplet maps, solving one-dimensional reaction-diffusion transport equations for the molecular diffusion and reaction terms, and constructing schemes for convection. The numerical implementation of LES-ODT is addressed in detail. The stochastic stirring process and the molecular diffusion and reaction processes are implemented similarly as proposed by Kerstein (1999) in ‘Vector-ODT’.

An innovative approach is proposed in the present study to address the turbulent convection, which was not included in the vector ODT formulation by Kerstein (1999, 2001). The convection scheme is characterized by the ‘node convection’ combined with the ‘intra-node relaxation’ or ‘co-linear convection’. The motivation for the ‘node convection’ is to address the limitations faced by the one-dimensional convection along the ODT element and to account the 3D convection. Therefore, the ODT velocity and scalar information at each node, the intersection of three ODT elements in 3D space, is updated to represent the field in

three directions. Each ‘node convection’ event is followed by one ‘intra-node relaxation’ or ‘co-linear convection’ event involving 1D convection at each ODT grid point on each ODT element. The ‘co-linear convection’ accounts for the turbulent transport on ODT 1D element. In both the ‘node convection’ and the ‘co-linear convection’, the TVD scheme is implemented to enforce scalar boundedness. The TVD scheme used here is the second order upwind scheme proposed by Warming and Beam (1975) with the “Superbee” flux limiter of Roe (1985).

8.2.3 LES-ODT Coupling

Chapter 4 also presents the coupling procedure for LES and ODT. Currently, LES only solves the vector field and the Smagorinsky model is used to represent the subgrid stresses. The velocity field solved by LES is interpolated to the ODT field to provide global information on the turbulence field. The solution algorithm to couple LES with ODT temporally and spatially is presented. LES and ODT are coupled at the LES time step temporally. Each ODT process has a much smaller time step compared to the LES time step. The spatial coupling between LES and ODT involves interpolating the velocity from LES grids to ODT grids along each ODT element and adjusting the ODT velocity field by adding a correction from the interpolated value obtained from the LES field and the filtered ODT field. Therefore, LES provides the global information of turbulence for ODT and ODT utilizes this information to represent the interactions of turbulent mixing and chemical reaction at subgrid scales.

8.2.4 LES-ODT Model Validation Using Volume-Averaged Statistics

The first test performed to validate the LES-ODT formulation and implementation is to compare the volume-averaged means and RMS obtained from LES-ODT with that from DNS. We applied LES-ODT to non-homogenous autoignition in isotropic turbulence and initialized the field by interpolating the initial field from DNS to ODT to maintain consistency. Both low and high turbulence conditions are studied. LES-ODT provides very good predictions of the global scalar mixing rate, the global progress of chemistry, the global evolution of the reaction rate and the temperature, and the global consumption rate of the reactants' mass fractions. Moreover, the predictions on global fluctuations of the thermochemical scalars by LES-ODT are excellent. The time for the global progress of the autoignition process at low turbulence conditions is twice as long as at high turbulence conditions, which is captured by LES-ODT successfully. Furthermore, a subtle statistical ignition delay is observed in LES-ODT simulations at high turbulence conditions. The reason attributes to the fact that the number of total ignition kernels is small. Thus, a single failed ignition kernel may have an effect on the total ignition progress. This explanation can be verified by the conditional statistics in which the ignition delay is not present.

8.2.5 LES-ODT Model Validation Using Conditional Statistics

The second test performed for the validation of the LES-ODT formulation and implementation is to compare the conditional statistics obtained from LES-ODT with that from DNS. Two LES-ODT simulation cases with different LES spatial resolutions are

performed. Both low and high turbulence conditions are studied and different Lewis number cases for the high turbulence conditions are examined. LES-ODT simulation results show excellent agreement with DNS results at both low and high turbulence conditions. LES-ODT simulation captures not only the onset of ignition, the kernel propagation, the transition of burning modes (low turbulence case), but also the peak values and the locations of the peaks in the conditional statistics as well. Moreover, the turbulence condition effects and Lewis number effects are represented by LES-ODT accurately. The excellent agreement between LES-ODT and DNS results provides a solid foundation for the model validation. LES-ODT is a very promising model for simulating turbulent combustion processes.

8.3 Recommendations for Future Work

8.3.1 LES SGS Closure

This purpose of this recommendation is for the one-way coupling of LES with ODT, in which LES only provides information to ODT, but is not affected by ODT. In the present study, the Smagorinsky model (1963) is used as a subgrid stress closure model for LES. The turbulence intensity and the Taylor time scale are essentially very high in the high turbulence cases. In the conditional statistical results, the difference in the mixture fraction range between LES-ODT and DNS indicates that the local dissipation of turbulence between LES-ODT and DNS is marginally different and further refinements of the SGS models for SGS stresses can provide additional improvements in the LES-ODT model predictions.

Potentially, the Germano dynamic model, in which the model constant is computed instantaneously based on the flow field, or more complex refinements in the modeling of SGS stresses can be used to refine the closure model for LES subgrid stresses. Ultimately, a direct evaluation of these terms can be achieved using the ODT data.

8.3.2 LES-ODT Coupling

LES provides global velocity information to ODT in the present formulation and this is a one-way coupling from LES to ODT. The coupling between LES and ODT can be improved by integrating the ODT model as a subgrid closure for LES. With this formulation, LES and ODT will be coupled in two directions. ODT can provide detailed information on the turbulence fluctuation, scalar mixing, and chemical reaction by computing the subgrid stresses, fluxes, and the reaction rate term and feed them back to LES. In this way, both the vector and scalar fields can be resolved by LES. The implementation might generate problems because the subgrid closure terms obtained from ODT may contain fluctuations that will cause the mass fractions go beyond the bound and induce instabilities to LES solutions. Furthermore, maintaining the consistency between LES and ODT solutions is another difficulty task to accomplish in the two-way coupling of LES with ODT.

8.3.3 Chemistry Representation

In the present study, we implemented a simple chemistry model in which the chemistry is characterized by the single-step, second-order, and irreversible reaction

mechanism with an Arrhenius dependence on temperature. This is a standard simplification in ignition works, justifiable when the activation energy is high, that the fuel and oxidant concentrations do not change appreciably (Mastorakos *et al.*, 1997b). In the future work, Situ adaptive tabulation of chemistry (e.g. ISAT, Pope and co-workers) can be used for detailed chemistry implementation with reduced computational cost.

8.3.4 Application to Other Types of Flows

In the present study, LES-ODT model is validated for the non-homogeneous autoignition in isotropic turbulence. Future work can address the model validation for more types of flows. Echehki *et al.* (2001) has applied the ODT stand-alone model to simulate the turbulent jet diffusion flames. Implementing and validating the coupled LES-ODT for other types of flows are challenging yet exciting.

References

- Batchelor, G. K., *The theory of homogeneous Turbulence*, Cambridge Science Classics, 1982.
- Bilger, R.W., Advanced laser diagnostics: implications of recent results for advanced combustor models, in *Aerothermodynamics in Combustors*, edited by R.S.L. Lee, J.H. Whitelaw, and T.S. Wang (Springer-Verlag, Heidelberg, 1992).
- Bilger, R. W., Conditional moment closure for turbulent reacting flows, *Phys. Fluids A* **5** (1993) 436.
- Bourlioux, A., Cuenot, B., and Poinso, T., Asymptotic and numerical study of the stabilization of Diffusion Flames by Hot Gas, *Combust. Flame* **120** (2000) 143.
- Caldeira-Pires, A. and Heitor, M. V., Characteristics of turbulent heat transport in nonpremixed jet flames, *Combust. Flame* **124** (2001) 213.
- Cha, C., Kosály, G., and Pitsch, H., Modeling extinction and reignition in turbulent nonpremixed combustion using a doubly-conditioned moment closure approach, *Phys. Fluids* **13** (2001) 3824.
- Chen, J-Y., Challenges in modeling of turbulence-chemistry interactions with large eddy simulations, *Progress in Computational Fluid Dynamics* **4** Nos. 3-5 (2004) 155.
- Chumakov, S., Large-eddy simulation models for subgrid scalar transfer, Master's thesis, Department of Mechanical Engineering, University of Wisconsin-Madison, 2001.
- Deardorff, J. W., Three-dimensional numerical study of the height and mean structure of a heated planetary boundary layer, *Boundary-Layer Meteorol.* **7** (1974) 81.
- Dec, J.E., A conceptual model of DI diesel combustion based on laser-sheet imaging, *SAE Technical Paper No. 97087* (Society of Automotive Engineers, 1997).
- Echekki, T. and Chen, J. H., High-temperature combustion in autoigniting non-homogeneous hydrogen/air mixtures. *Proc. Combust. Inst.* **29** (2002) 2061.
- Echekki, T. and Chen, J. H., Direct numerical simulation of autoignition in non-homogeneous hydrogen-air mixtures, *Combust. Flame* **134** (2003) 169.

Echekki, T., Kerstein, A. R., and Dreeben, T. D., 'One-dimension turbulence' simulation of turbulent jet diffusion flames: model formulation and illustrative applications, *Combust. Flame* **125** (2001) 1083.

Eggenpieler, G. and Menon, S., Large-eddy simulation of pollutant emission in a DOE-HAT combustor, *J. Prop. Power* **20**(6) 2004 1-76.

Fairweather, M. and Woolley, R.M., First-order conditional moment closure modeling of turbulent, non-premixed hydrogen flames. *Combust. Flame* **133** (2003) 393.

Germano, M., Piomelli, U., Moin, P., and Cabot, W. H., A dynamic subgrid-scale eddy viscosity model, *Phys. Fluids A* **3** (1991) 1760.

Goldin, G. M. and Menon, S., A linear eddy model for steady-state turbulent combustion, *Thirty-fourth Aerospace Sciences Meeting* (Reno, NV, 1996) 0519.

Haworth, D. and Jansen, K., Large-eddy simulation on unstructured deforming meshes: towards reciprocating IC engines, *Comput. Fluids* **29** (5) (2000) 493.

Hinze, J.O., *Turbulence*, MacGraw Hill, 1975.

Ihme, M., Cha, C. M., and Pitsch, H., Prediction of local extinction and re-ignition effects in non-premixed turbulent combustion by a flamelet/progress variable approach, *Proc. Combust. Inst.* **30** (2005) 793.

Kempf, A., Sadiki, A., and Janicka, J., Prediction of finite chemistry effects using large eddy simulation, *Proc. Combust. Inst.* **29** (2003) 1979.

Kerstein, A. R., Linear-eddy model of turbulent scalar transport and mixing, *Comb. Sci. and Tech.* **60** (1988) 391.

Kerstein, A. R., Linear-eddy modeling of turbulent transport. II: application to shear layer mixing, *Combust. Flame* **75** (1989) 397.

Kerstein, A. R., Linear-eddy modeling of turbulent transport. Part 3. Mixing and differential molecular diffusion in round jets, *J. Fluid Mech.* **216** (1990) 411.

Kerstein, A. R., Linear-eddy modeling of turbulent transport. Part 6. Microstructure of diffusive scalar mixing fields, *J. Fluid Mech.*, **231** (1991) 361.

Kerstein, A. R., Linear-eddy modeling of turbulent transport. Part 4. Structure of diffusion flames, *Combust. Sci. and Tech.*, **81** (1992a) 75.

Kerstein, A. R., Linear-eddy modeling of turbulent transport. Part 7. Finite-rate chemistry and multi-stream mixing, *J. Fluid Mech.*, **240** (1992b) 289.

Kerstein, A. R., One-dimensional turbulence: model formulation and application to homogeneous turbulence, shear flows, and buoyant stratified flows, *J. Fluid Mech.* **392** (1999a) 277.

Kerstein, A. R., One-dimensional turbulence Part 2. Staircases in double-diffusive convection, *Dyn. Atmos. Oceans* **30** (1999b) 25.

Kerstein, A. R., Ashurst, W. T., Wunsch, S., and Nilsen, V., One-dimensional turbulence: vector formulation and application to free shear flows, *J. Fluid Mech.* **447** (2001) 85.

Kim, S. H., and Huh, K. Y., Application of the elliptic conditional moment closure model to a two-dimensional nonpremixed methanol bluff-body flame. *Combust. Flame* **120** (2000) 75.

Kim, W. W. and Pitsch, H., Conditional filtering method for large eddy simulation of turbulent nonpremixed combustion, *Phys Fluids* **17** (2005) 1.

Klimenko, A. Y., Multicomponent diffusion of various scalars in turbulent flow, *Fluid Dyn.* **25** (1990) 327.

Klimenko, A. Y. and Bilger, R. W., Conditional moment closure for turbulent combustion, *Progress Energy Combust. Sci.* **25** (1999) 595.

Kronenburg, A., Double conditioning of reactive scalar transport equations in turbulent non-premixed flames, *Phys. Fluids* **16** (2004) 2640.

Kronenburg, A., Bilger, R. W., and Kent, J.H., Second-order conditional moment closure for turbulent jet diffusion flames, *Twenty-seventh Symposium (International) on Combustion* (The Combustion Institute, Pittsburgh, 1998) 1097.

Kronenburg, A., and Bilger, R. W., Modelling differential diffusion in turbulent nonpremixed reacting turbulent flow: application to turbulent jet flames. *Combust. Sci. Technol.* **166** (2001) 175.

Kuo, K. K., *Principles of Combustion*, John Wiley and Sons, New York, 1986.

Li, J. D. and Bilger, R. W., Measurement and prediction of the conditional variance equations for second order conditional moment closure, *Phys. Fluids* **11** (1999) 2679.

Mason, S. D., Turbulence Transport in Spatially Developing Reacting Shear Layers, Ph.D. thesis, Department of Mechanical Engineering, University of Wisconsin-Madison, 2000.

Mastorakos, E., Baritaud, T.A., and Poinso, T.J., Numerical simulations of autoignition in turbulent mixing flows. *Combust. Flame* **109** (1997a) 198.

Mastorakos, E., Pires Da Cruz, A., Baritaud, T. A., and Poinso, T. J., A model for the effects of mixing on the autoignition of turbulent flows, *Combust. Sci. Technol.* **125** (1997b) 243.

Mastorakos, E., Bilger, R.W., Second order conditional moment closure for the autoignition of turbulent flows, *Phys. Fluids*. **10** (1998) 1246.

McDermott, R. J., Toward one-dimensional turbulence subgrid closure for large-eddy simulation, Ph. D. Thesis, Department of Chemical Engineering, 2005.

McMurtry, P. A., Gansauge, T. D., Kerstein, A. R., and Krueger, S. K., Linear eddy simulations of mixing in a homogeneous turbulent flow, *Phys. Fluids A* **5** (4) 1993, 1024.

McMurtry, P.A., Menon, S., and Kerstein, A. R., A linear eddy sub-grid model for turbulent reacting flows: application to hydrogen-air combustion, *Twenty-fourth Symposium (International) on Combustion* (The combustion Institute, Pittsburgh, 1992) 271.

Menon, S., McMurtry, P. A., and Kerstein, A. R., A linear eddy mixing model for large-eddy simulation of turbulent combustion, *LES of Complex Engineering and Geophysical Flows* ed B Galperin and S Orszag (Cambridge: Cambridge University Press) 1993.

Moin, P., Advances in large eddy simulation methodology for complex flows, *Int. J. Heat Fluid Flow* **23** (5) 2002 237.

Muradoglu, M., Jenny, P., Pope, S. B., and Caughey, D. A., A consistent hybrid finite-volume/particle method for the PDF equations of turbulent reactive flows, *J. Comput. Phys.* **154** (1999) 342.

Navarro-Martinez, S., Kronenburg, A., and Dimare, F., Conditional moment closure for large eddy simulations, *Flow, Turbulence and Combust.* **75** (2005) 245.

Pierce, C. D. and Moin, P., Progress-variable approach for large eddy simulation and of non-premixed turbulent combustion, *J. Fluid Mech.* **504** (2004) 73.

Pitsch, H., Large-eddy simulation of turbulent combustion, *Annu. Rev. Fluid. Mech.*, **38** (2006) 453.

Pitsch, H., Improved pollutant predictions in large-eddy simulations of turbulent non-premixed combustion by considering scalar dissipation rate fluctuations, *Proc. Combust. Inst.* **29** (2002) 1971.

Pitsch, H. and Ihme, M., An unsteady/flamelet progress variable method for LES of non-premixed turbulent combustion, *AIAA Pap.* (2005) 557.

Pitsch, H. and Steiner, H., Large-eddy simulation of a turbulent piloted methane/air diffusion flame (Sandia flame D), *Phys. Fluids* **12** (10) (2000) 2541.

Poinsot, T., Candel, S., and Trouvé, A., Applications of direct numerical simulation to premixed turbulent combustion, *Prog. Energy Combust. Sci.* **21** (1996) 531.

Poinsot, T. and Veynante, D., *Theoretical and Numerical Combustion*, Edwards, 2001.

Pope, S. B., Computations of turbulent combustion: progress and challenges, *Proc. Combust. Inst.* **23** (1990) 591.

Pope, S. B., *Turbulent Flows*, Cambridge University Press, 2000.

Press, W. H., Teukolsky, S. A., Vetterling, W. T., and Flannery, B. P., *Numerical Recipes in Fortran*, Cambridge University Press, Second edition, Vol. 1, 1996.

Raman, V. and Pitsch, H., Large-eddy simulation of a bluff-body stabilized non-premixed flame using a recursive-refinement procedure, *Combust. Flame* **142** (2005a) 329.

Richardson, L. F., The approximate arithmetical solution by finite differences of physical problems involving differential equations, with an application to the stresses in a masonry dam, *Philos. Trans. R. Soc. London, Ser. A*, **210** (1910) 307.

Roomina, M. R. and Bilger, R., Conditional moment closure (CMC) predictions of a turbulent methane-air jet flame, *Combust. Flame* **125** (2001) 1176.

Ross, S. M., *A course in simulation*, Macmillan, New York, 1990.

Sankaran, V., Porumbel, I., and Menon, S., Large-eddy simulation of single-cup gas-turbine combustor flows, *Thirty-ninth AIAA Joint Propulsion Conference* (2003) 5083.

Schmidt, R. C., Kerstein, A.R., Wunsch, S., and Nilsen, V., Near-wall LES closure based on one-dimensional turbulence modeling, *J. Comput. Phys.*, **186** (2003) 317.

- Smagorinsky, J., General circulation experiments with the primitive equations: I. The basic equations, *Mon. Weather Rev.* **91** (1963) 99.
- Sone, K., Patel, N., and Menon, S., Large-eddy simulation of fuel-air mixing in an internal combustion engine, *Thirty-ninth AIAA Aerospace Sciences Meeting* (2001) 0635.
- Smith, N. S. A., Bilter, R. W., Carter, C. D., Barlow, R. S., and Chen, J.-Y., A comparison of CMC and PDF modeling predictions with experimental nitric oxide LIF/Raman measurements in a turbulent H₂ jet flame, *Combust. Sci. Technol.* **105** (1995) 307.
- Sreedhara, S. and Lakshmisha, K.N., Direct numerical simulation of autoignition in a non-premixed, turbulent medium. *Proc. Combust. Inst.* **28** (2000) 25.
- Swaminathan, N. and Bilger, R. W., Measurement and prediction of the conditional variance in a turbulent reactive-scalar mixing layer, *Phys. Fluids* **5** (1993) 3255.
- Tannehill, J. C., Anderson, D. A., and Pletcher, R. H., *Computational fluid mechanics and heat transfer*, Taylor and Francis, 1997.
- Tap, F. A., Hilbert, R., Thévenin, D., and Veynante, D., A generalized flame surface density modeling approach for the auto-ignition of a turbulent non-premixed system, *Combust. Theo. Model.* **8** (2004) 165.
- Veynante, D., Trouvé, A., Bray, K. N. C., and Mantel, T., Gradient and countergradient diffusion in turbulent premixed flames, *J. Fluid Mech.* **332** (1997) 263.
- Vervisch, L. and Trouvé, A., LES modeling for lifted turbulent jet flames, Center for Turbulent Research Proceedings of the Summer Program, Stanford University/NASA-Ames (1998) 83.
- Wunsch, S. and Kerstein, A. R., A model for layer formulation in stably stratified turbulence, *Phys. Fluids* **13** (2001) 702.
- Zhang, Y. and Haworth, D., A general mass consistency algorithm for hybrid particle/finite-volume PDF methods, *J. Comp. Phys.* **194** (1) (2004) 156.
- Zimberg, M. J., Frankel, S. H., Gore, J. P., and Sivathanu, Y. R., A study of coupled turbulent mixing, soot chemistry, and radiation effects using the linear eddy model, *Combust. Flame* **113** (1998) 454.

Appendices

Appendix A Fractional Method for Solution of DNS Momentum

Equations

A.1 Introduction

The discrete form of the momentum Eq. (2-28) is

$$\frac{\delta u_i}{\delta t} = -\frac{1}{\rho} \frac{\delta p}{\delta x_i} - C_i + D_i, \quad (\text{A-1})$$

where C_i represents the convection term

$$C_i = u_j \frac{\delta u_i}{\delta x_j}, \quad (\text{A-2})$$

and D_i represents the diffusion terms

$$D_i = \frac{1}{\rho Re} \frac{\delta^2 u_i}{\delta x_j \delta x_j} + \frac{1}{3\rho Re} \frac{\delta}{\delta x_i} \left(\frac{\delta u_j}{\delta x_j} \right). \quad (\text{A-3})$$

In Eqs. (A-1) to (A-3), δ denotes the discrete finite-difference derivative operators.

The momentum equation is integrated using the fractional-step method documented in Mason (2000). First, intermediate velocity field is generated by integrating the convection and diffusion terms in the momentum equation. Second, pressure is solved using the Poisson's equation. Third, the new velocity field is obtained by correcting the intermediate velocity vectors using the gradients of pressure.

A.2 Convection and Diffusion Terms Integration

Explicit third-order Runge-Kutta method is used for time integration of the convection and diffusion terms in the momentum Eq. (A-1). Each time step is divided into three sub-steps during the time integration. The equation for integration is derived from Eq. (A-1) without counting the pressure term

$$u_i^* = u_i^{k-1} + \Delta t \left[-\gamma_k (-C_i^{k-1} + D_i^{k-1}) - \zeta_k (-C_i^{k-2} + D_i^{k-2}) \right], \quad (\text{A-4})$$

where $k = 1, 2, 3$ indicates the sub-step, Δt is the overall time step, and u_i^* is the intermediate velocity values at each new sub-step k . The integration coefficients γ and ζ are

$$\begin{array}{lll} \gamma_1 = 8/15 & \gamma_2 = 5/12 & \gamma_3 = 3/4 \\ \zeta_1 = 0 & \zeta_2 = -17/60 & \zeta_3 = -5/12 \end{array}, \quad (\text{A-5})$$

and the integration coefficients obey

$$\sum_{k=1}^3 (\gamma_k + \zeta_k) = 1. \quad (\text{A-6})$$

For each Runge-Kutta sub-step k , the time step dt_k is

$$dt_k = (\gamma_k + \zeta_k) \Delta t, \quad (\text{A-7})$$

where

$$dt_1 = \frac{8}{15} \Delta t \quad dt_2 = \frac{2}{15} \Delta t \quad dt_3 = \frac{1}{3} \Delta t. \quad (\text{A-8})$$

For $k = 1$, C_i^{k-2} and D_i^{k-2} in (A-4) are not needed because $\zeta_1 = 0$. At each sub-step, only two storage locations are needed for each velocity component at each node.

A.3 Poisson Equation for Pressure

The equation used to correct the intermediate velocity field can be derived from Eq. (A-1) by neglecting the convection and diffusion terms. It is as follows

$$u_i^k = u_i^* - \frac{dt_k}{\rho^k} \frac{\delta p^k}{\delta x_i}. \quad (\text{A-9})$$

The continuity equation in discrete form is

$$\frac{\delta \rho^k}{\delta t} + \frac{\delta(\rho^k u_i^k)}{\delta x_i} = 0. \quad (\text{A-10})$$

To ensure that the new velocity field satisfies the continuity Eq. (A-10), Eq. (A-9) is substituted into Eq. (A-10) to obtain the Poisson equation for pressure

$$\frac{\delta}{\delta x_i} \left(\frac{\delta p^k}{\delta x_i} \right) = \frac{1}{dt_k} \left(\frac{\delta \rho^k}{\delta t} + \frac{\delta(\rho^k u_i^*)}{\delta x_i} \right). \quad (\text{A-11})$$

At each Runge-Kutta sub-step during the time integration, pressure in Eq. (A-11) is solved such that the gradients correct the intermediate velocity field by Eq. (A-9) to produce a new velocity field that automatically satisfies the continuity Eq. (A-10). In Eq. (A-11), $\delta \rho^k / \delta t$ for sub-step is approximated as

$$\frac{\delta \rho^1}{\delta t} = \frac{\rho^1 - \rho^0}{dt_1}, \quad (\text{A-12})$$

$$\frac{\delta \rho^2}{\delta t} = \frac{\rho^2 - \rho^0}{dt_1 + dt_2}, \quad (\text{A-13})$$

$$\frac{\delta \rho^3}{\delta t} = \frac{\rho^3 - \rho^0}{\Delta t}. \quad (\text{A-14})$$

In the Poisson Eq. (A-11), the left-hand side is a Laplacian operator constructed from a divergence operator acting on a gradient operator. The numerical operators representing the divergence and gradient used on both sides of Poisson equation should be the same in order to maintain the consistency in solving Poisson equation. This consistency issue is addressed in detail in Mason (2000). Here Eq.(A-11) is solved with complete operator consistency. The iteration scheme to solve the Poisson equation for pressure is Gauss-Seidel coupled with successive over-relaxation (SOR). For detailed information, readers should refer to Mason (2000). During each iteration, the updated pressure is subtracted by the old pressure and the L_2 -norm of the result is compared to the SOR tolerance. The optimum value of the relaxation parameter ω for convergence is found to be 1.1. In order for the code to converge, the Poisson matrix must be ‘diagonally dominant’.

A.4 Velocity Update

When the Poisson Eq. (A-11) is solved and gradients of pressure are obtained, the intermediate velocity field is updated using Eq. (A-9). Because the Poisson equation is derived from the continuity Eq. (A-10), the updated velocity field automatically satisfies the continuity equation.

Appendix B Solution to DNS Energy and Species Equations

B.1 Introduction

The energy and species equations can be written in discrete form as

$$\frac{\delta\theta}{\delta t} = -C + D \pm \omega, \quad (\text{B-1})$$

where θ can be T , Y_F , Y_O . In Eq. (B-1), C denotes the convection terms and D denotes the diffusion terms. The sign preceding the reaction rate term ω is positive for the energy equation ($\theta = T$) and negative for the species equations ($\theta = Y_F$ or Y_O).

B.2 Time Integration

The energy and species equations are integrated in time using a linearly implicit variation of the third-order Runge-Kutta scheme used to integrate the momentum equation. While the convection and the diffusion terms are integrated in the same way as in the momentum equation, the reaction rate term is integrated implicitly for stability due to the fact that it is usually large. Crank-Nicolson scheme is used to integrate the reaction rate term. The form for time integration is

$$\frac{\theta^k - \theta^{k-1}}{\Delta t} = -\gamma_k (-C^{k-1} + D^{k-1}) - \zeta_k (-C^{k-2} + D^{k-2}) \pm \chi_k \omega^k \pm \sigma_k \omega^{k-1}, \quad (\text{B-2})$$

where $k = 1, 2, 3$. The signs preceding the χ_k and σ_k are positive when $\theta = T$ and negative when $\theta = Y_F$ or Y_O . The Runge-Kutta coefficients γ and ζ are from Eq. (A-5). The Crank-Nicolson coefficients χ and σ are from Mason (2000) and are as follows

$$\chi_1 = \sigma_1 = 4/15 \quad \chi_2 = \sigma_2 = 1/15 \quad \chi_3 = \sigma_3 = 1/6, \quad (\text{B-3})$$

where

$$\sum_{k=1}^3 (\chi_k + \sigma_k) = 1. \quad (\text{B-4})$$

B.3 Energy and Species Equations

The unknowns ω^k in Eq. (B-2) can be expanded in terms of ω^{k-1} using first-order terms of Taylor series as follows

$$\omega^k = \omega^{k-1} + \frac{\partial \omega^{k-1}}{\partial T} \frac{\partial T^{k-1}}{\partial t} dt_k + \frac{\partial \omega^{k-1}}{\partial Y_F} \frac{\partial Y_F^{k-1}}{\partial t} dt_k + \frac{\partial \omega^{k-1}}{\partial Y_O} \frac{\partial Y_O^{k-1}}{\partial t} dt_k + \frac{\partial \omega^{k-1}}{\partial \rho} \frac{\partial \rho^{k-1}}{\partial t} dt_k, \quad (\text{B-5})$$

where dt_k is the Runge-Kutta time step from sub-step $k-1$ to sub-step k . The partial time derivatives of T, Y_F, Y_O at $k-1$ are combined with the Runge-Kutta time step to get

$$\omega^k = \omega^{k-1} + \frac{\partial \omega^{k-1}}{\partial T} \Delta T + \frac{\partial \omega^{k-1}}{\partial Y_F} \Delta Y_F + \frac{\partial \omega^{k-1}}{\partial Y_O} \Delta Y_O + \frac{\partial \omega^{k-1}}{\partial \rho} \frac{\partial \rho^{k-1}}{\partial t} dt_k, \quad (\text{B-6})$$

where

$$\Delta T = T^k - T^{k-1} \quad \Delta Y_F = Y_F^k - Y_F^{k-1} \quad \Delta Y_O = Y_O^k - Y_O^{k-1}. \quad (\text{B-7})$$

The linearization of the reaction rate term combined with the implicit Crank-Nicolson scheme constitutes the ‘linearly implicit’ procedure.

Combining Eq. (B-2) with Eq. (B-5), we can get a system of three coupled equations for ΔT , ΔY_F , and Y_O . The matrix form of the equations is

$$\begin{bmatrix} 1 - \Delta t \chi_k \frac{\partial \omega^{k-1}}{\partial T} & - \Delta t \chi_k \frac{\partial \omega^{k-1}}{\partial Y_F} & - \Delta t \chi_k \frac{\partial \omega^{k-1}}{\partial Y_O} \\ - \Delta t \chi_k \frac{\partial \omega^{k-1}}{\partial T} & 1 + \Delta t \chi_k \frac{\partial \omega^{k-1}}{\partial Y_F} & \Delta t \chi_k \frac{\partial \omega^{k-1}}{\partial Y_O} \\ \Delta t \chi_k \frac{\partial \omega^{k-1}}{\partial T} & \Delta t \chi_k \frac{\partial \omega^{k-1}}{\partial Y_F} & 1 + \Delta t \chi_k \frac{\partial \omega^{k-1}}{\partial Y_O} \end{bmatrix} \begin{Bmatrix} \Delta T \\ \Delta Y_F \\ \Delta Y_O \end{Bmatrix} = \begin{Bmatrix} \Delta t (\chi_k + \sigma_k) \omega^{k-1} + \Delta t \chi_k \frac{\partial \omega^{k-1}}{\partial \rho} \frac{\partial \rho^{k-1}}{\partial t} dt_k - \gamma_k (-C_T^{k-1} + D_T^{k-1}) + \varsigma_k (-C_T^{k-2} + D_T^{k-2}) \\ - \Delta t (\chi_k + \sigma_k) \omega^{k-1} + \Delta t \chi_k \frac{\partial \omega^{k-1}}{\partial \rho} \frac{\partial \rho^{k-1}}{\partial t} dt_k - \gamma_k (-C_{Y_F}^{k-1} + D_{Y_F}^{k-1}) + \varsigma_k (-C_{Y_F}^{k-2} + D_{Y_F}^{k-2}) \\ - \Delta t (\chi_k + \sigma_k) \omega^{k-1} + \Delta t \chi_k \frac{\partial \omega^{k-1}}{\partial \rho} \frac{\partial \rho^{k-1}}{\partial t} dt_k - \gamma_k (-C_{Y_O}^{k-1} + D_{Y_O}^{k-1}) + \varsigma_k (-C_{Y_O}^{k-2} + D_{Y_O}^{k-2}) \end{Bmatrix} \quad (\text{B-8})$$

The partial derivatives of the reaction rate term ω are computed from Eq. (2-32). The time derivative of density is computed using Eqs. (A-12)–(A-14). The system of equations can be solved directly by multiplying the column vector on the right-hand side of Eq. (B-8) by the inverse of the coefficient matrix on the left-hand side of Eq. (B-8).